amples G-1 and W-1, 1962.

les éléments en traces dan
7: 149.
Beeson, M.H. and Oxley,
with high-resolution δ-ray detectors.

te—hornblende pairs and in an ortho-
, northern Sierra Nevada, California.

id hornblende from gneisses of south-
elements in coexisting minerals. J.

ics to coexisting minerals of variable
oxene and orthopyroxene—garnet.

groups of igneous rocks. J. Geol., 46:

s of Corona, Elsinore, and San Luis
Am. Mem., 29, 182 pp.
the 18th International Geological

ients — a review of theory and appli-
7: 1209—1264.
s in coexisting hornblendes and bio-

nor elements among some coexisting
93.
y of some igneous rock series. Geo-

y of some igneous rock series, II. Geo-

y of some igneous rock series, III.

on of Fe^{II} and Mg^{II} in coexisting

lements in minerals from rocks of
n. Acta, 16: 57—58.
ion of differentiation trends in igneous

Na, Mn, Cr, Se, and Co in ultramafic

gations in east Greenland, III: The
ssuak, east Greenland. Medd. Grønland,

on of trace elements during strong
f the Skaergaard intrusion, east Green-

for use in geochemistry. Geochim.

Chemical Geology, 17(1976)89—100

EXPERIMENTS ON THE INTERACTION BETWEEN Na_2CO_3—$NaHCO_3$ SOLUTION AND CLINOPTILOLITE TUFF, WITH REFERENCE TO ANALCIMIZATION AROUND KUROKO-TYPE MINERAL DEPOSITS

HIROSHI ABE and MORIHIRO AOKI

Department of Earth Sciences, Miyagi University of Education, Sendai (Japan)

(Received May 12, 1975; revised and accepted October 7, 1975)

ABSTRACT

Abe, H. and Aoki, M., 1976. Experiments on the interaction between Na_2CO_3—$NaHCO_3$ solution and clinoptilolite tuff, with reference to analcimization around Kuroko-type mineral deposits. Chem. Geol., 17: 89—100.

Analcime and albite were synthesized from natural clinoptilolite tuff at 100—300°C and 20—110 kg/cm² with a mixed solution of Na_2CO_3—$NaHCO_3$ in 240-h treatments. A value around pH = 9.0 is required while lower temperatures (150—160°C) are presumed to be conditions suitable for analcimization. The analcime—albite alteration boundary shows dissimilar behaviour due to Na concentration. It was concluded that the formation of analcime zones surrounding Kuroko (Black ore)-type mineral deposits is controlled strongly both by temperature and chemical gradients.

INTRODUCTION

The alteration aureoles enclosing Kuroko (Black ore)-type mineral deposits in Miocene marine acidic pyroclastic sediments show zonal arrangements, both laterally and vertically. These are divided into montmorillonite (outer) and chlorite—sericite (inner) zones. These alteration zones are thought to be related directly to Kuroko mineralization. On the other hand, zeolite alteration zones surrounding the Kuroko deposits are subdivided into clinoptilolite—mordenite, and analcime zones. Iijima (1972, 1974) stated that the analcime zone around the Kuroko deposits was formed by the reaction between clinoptilolite—mordenite-bearing acidic tuff and interstitial solutions containing sodium which migrated from the sericite—chlorite and montmorillonite zones.

In the present study, an attempt was made to estimate the formation temperatures and chemical conditions for analcimization by means of model experiments, in which a specimen of clinoptilolite tuff was subjected to alteration in a Na_2CO_3—$NaHCO_3$ mixed solution.

STARTING MATERIALS

Clinoptilolite tuff (Daijima Formation, Miocene, Locality Tateyamazaki, Oga City, Akita Prefecture, northern Japan) is a whitish-colored, acidic fine-grained rock. Under the microscope, clinoptilolite, quartz, plagioclase, and altered glass were observed, but X-ray diffraction analyses showed no quartz or plagioclase because of their minor contents. X-ray powder-diffraction patterns of the tuff consisted of only clinoptilolite (see Fig. 3 on p. 93). The chemical composition of the tuff is: SiO_2, 62.40; TiO_2, 0.23; Al_2O_3, 11.15; Fe_2O_3, 2.71; FeO, 0.25; MnO, 0.01; CaO, 1.90; MgO, 1.49; Na_2O, 2.17; K_2O, 1.55; $H_2O(+)$, 8.96; and $H_2O(-)$, 6.85; total 99.67 wt.%.

EXPERIMENTS

The clinoptilolite tuff was pulverized in an agate mortar, and 0.5 g of its powder under 250 mesh were used as the starting materials. Hydrothermal treatments were carried out in a test-tube-type autoclave. For the reaction solution in order to examine the reaction under varying pH conditions, treatment was made by fixing the Na concentration in the reaction system at a constant value.

The range of pH values was pH = 8.0—11.2, in a mixed solution of Na_2CO_3–$NaHCO_3$ (0.25-*M* and 0.5-*M* series). The relation between mixed solutions and pH values is shown in Fig. 1. The starting materials with the reaction solution (25 ml) were placed in the autoclave, then heated in the electric furnace at temperatures of 100—300°C, pressures of 20—110 kg/cm², and a reaction time of 10 days. The temperatures and pressures were controlled

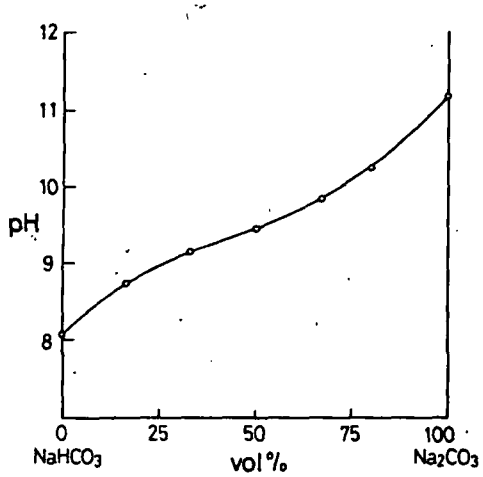

Fig. 1. The pH variation curve of mixing solution of $NaHCO_3$—Na_2CO_3 (0.25-*M* series).

to an accuracy of 0.5% (±
were centrifuged, air-drie
means of both X-ray diffr
electron microscope (Nih
X-ray diffractometry wer

Fig. 2. X-ray diffraction patterns
A = analcime, *Ab* = albite, *Q* = se

to an accuracy of 0.5% (±) and 2% (±), respectively. The reaction products were centrifuged, air-dried at room temperature, and then examined by means of both X-ray diffractometry (Rigaku Denki-4001) and the scanning-electron microscope (Nihon Denshi JSM-U3). The operating conditions of X-ray diffractometry were fixed as follows; Cu—K_α, Ni filter; 30 kV; 15 mA;

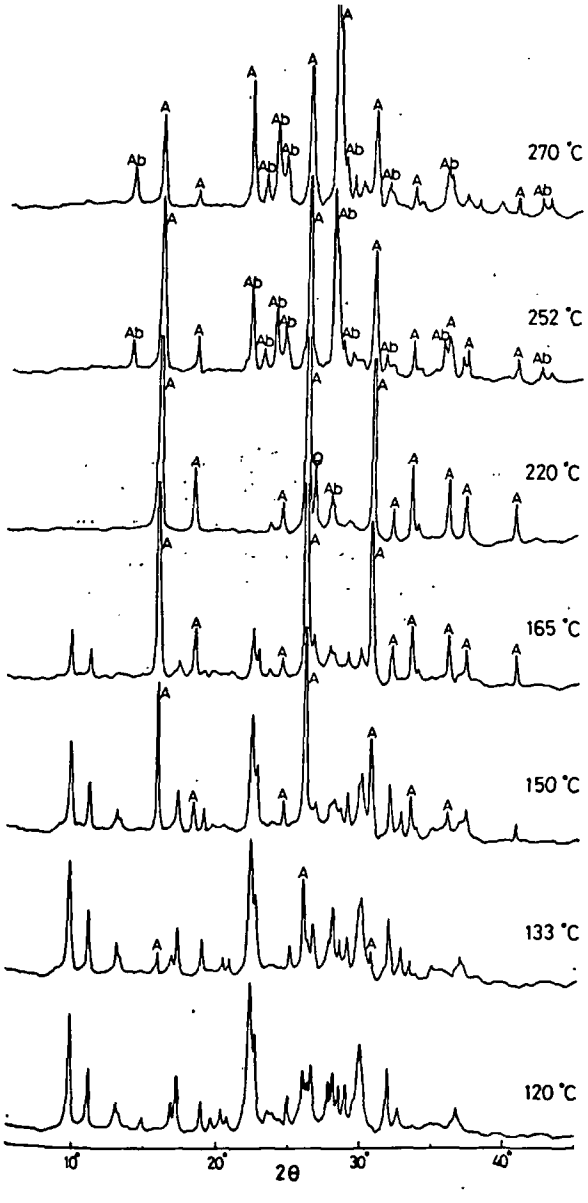

Fig. 2. X-ray diffraction patterns of alteration products at pH = 9.8 (0.25-*M* series). *A* = analcime, *Ab* = albite, *Q* = secondary quartz; others are reflections of clinoptilolite.

glancing angle, 5°; scanning speed, 1°/min; slit divergence, 1°; slit receiving, 0.3; full scale, 500 cps, and time constant, 2.0 sec. The pH values of the residual solutions after hydrothermal treatments were obtained with a Beckmann Zeromatic pH meter.

ALTERATION PROCESSES

X-ray patterns showing the alteration processes in a mixed solution (pH = 9.8) of Na_2CO_3 (0.25 *M*) and $NaHCO_3$ (0.25 *M*) are shown in Fig. 2. When the specimens were treated in the mixed solution (pH = 9.8) at 120—133°C for 10 days, the original clinoptilolite tuff showed no noticeable change. At 150—165°C for 10 days, the reflections of analcime gradually intensified and most of the reflections of clinoptilolite were weakened as shown in Fig. 2. At 220—250°C for 10 days, clinoptilolite was completely decomposed and analcime was in the stable phase. Under these conditions, the reflections of albite were progressively intensified. The reflection of secondary quartz appeared slightly at 220°C. When the specimens were treated at 270—300°C, most of the reflections of analcime were weakened but albite became more stable.

The alteration processes under isothermal (e.g., 150°C) conditions are shown in Fig. 3. At pH values from 8.0 to 8.8 at 150°C for 10 days, the original clinoptilolite tuff showed no remarkable change, but under pH = 9.2—9.8 for 10 days, clinoptilolite was slightly decomposed and the reflections of analcime were gradually intensified. Clinoptilolite was decomposed and analcime was in the stable phase at pH = 11.3 and 150°C for 10 days (Fig. 3).

The results of the alteration processes under the various conditions studied are summarized in Figs. 4 and 5.

The behaviour of pH values showed definite relationships between the initial solution and the residual solution after treatments. The arrow lines in Figs. 4 and 5 show the shifting of pH values from the initial to the residual solution, and the dashed lines the alteration boundaries. The pH values decreased similarly at each temperature in the initial solution with higher values of pH = 10—11 in the analcime field in both the 0.25- and 0.5-*M* series. On the other hand, in the case of the initial solution with lower values of pH = 8.0, the final pH values were observed to increase. At around pH = 8.8 (0.25-*M* series) and pH = 9.0—9.5 (0.5-*M* series) of the initial solutions, no shifting of the pH value in the analcime field was recognized.

FORMATION RANGES OF ANALCIME AND ALBITE

0.25-M series

As shown in Fig. 4, clinoptilolite tuff alters to analcime in the range of pH = 8.0—11.2. However, as the pH values increase, analcimization proceeds

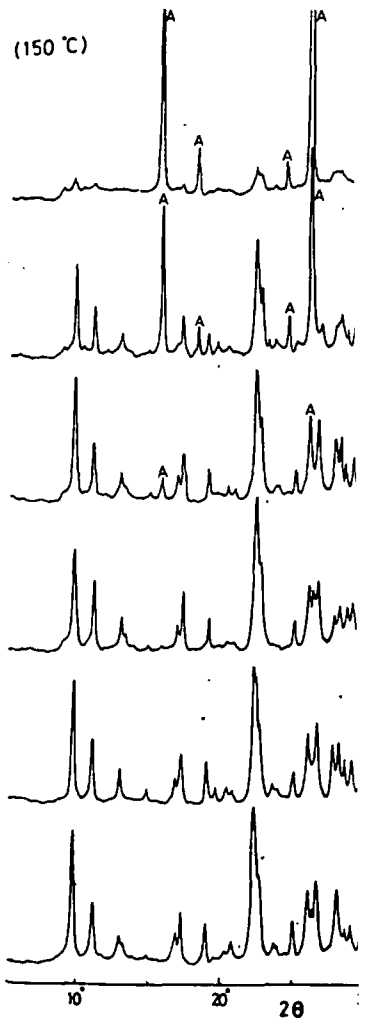

Fig. 3. X-ray diffraction patterns c
series). Starting: clinoptilolite; *A* =

readily at the lower-temperat
ptilolite—analcime was 110°C
broadens at the high-pH side.
mentally are strongly control
Analcime alters secondarily t
alteration temperature betwe
condition was observed on th
about 220°C.

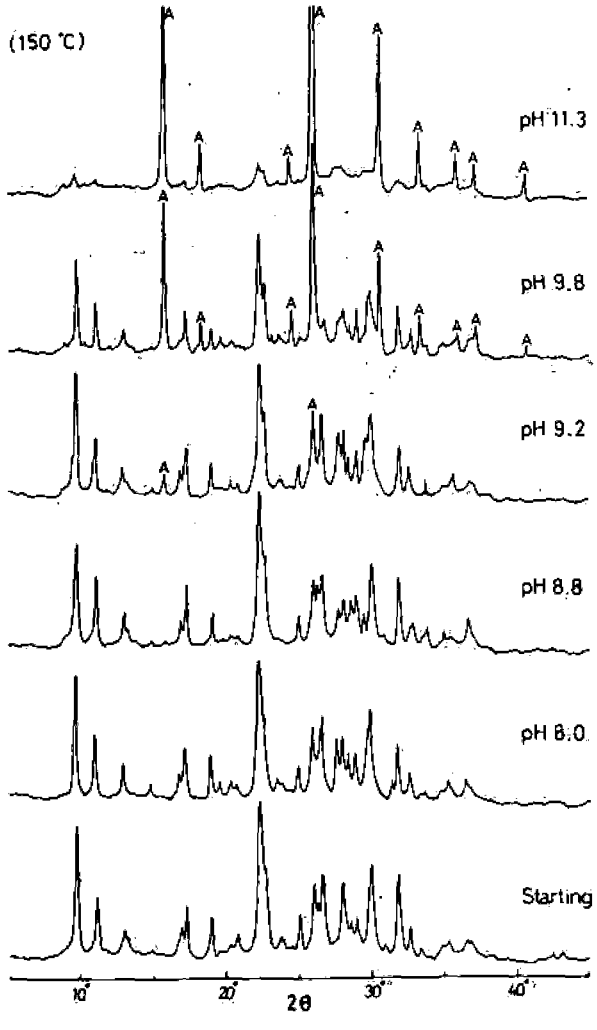

Fig. 3. X-ray diffraction patterns of alteration products at isothermal condition (0.25-*M* series). Starting: clinoptilolite; *A* = analcime.

readily at the lower-temperature side. The alteration temperature for clinoptilolite—analcime was 110°C at pH = 11.2. Consequently, the analcime field broadens at the high-pH side. The synthetic analcime fields obtained experimentally are strongly controlled by both temperature and chemical gradients. Analcime alters secondarily to albite as the temperature rises. As for the alteration temperature between analcime and albite, no effect due to the pH condition was observed on the flat boundary of the reaction relation at about 220°C.

PLATE I

Scanning-electron microphotographs (0.25-*M* series). A. Starting material (clinoptilolite). B. Analcime (180°C, pH = 8.0). C. Analcime (210°C, pH = 8.0). D. Analcime (250°C, pH = 8.0). E and F. Analcime (164°C, pH = 9.2).

PLATE I *(continued)*

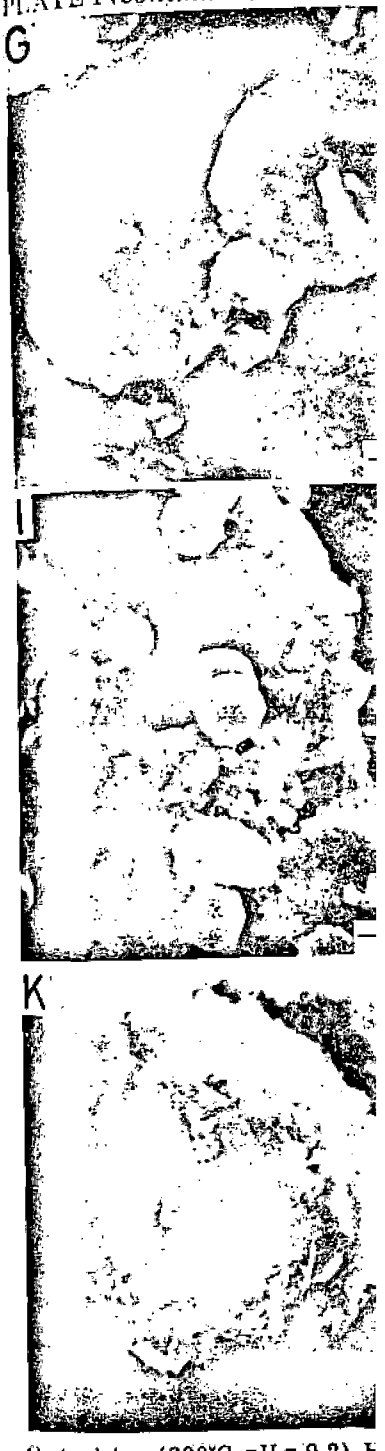

G. Analcime (200°C, pH = 9.2). H
pH = 11.2). K. Analcime and albi

PLATE I (*continued*)

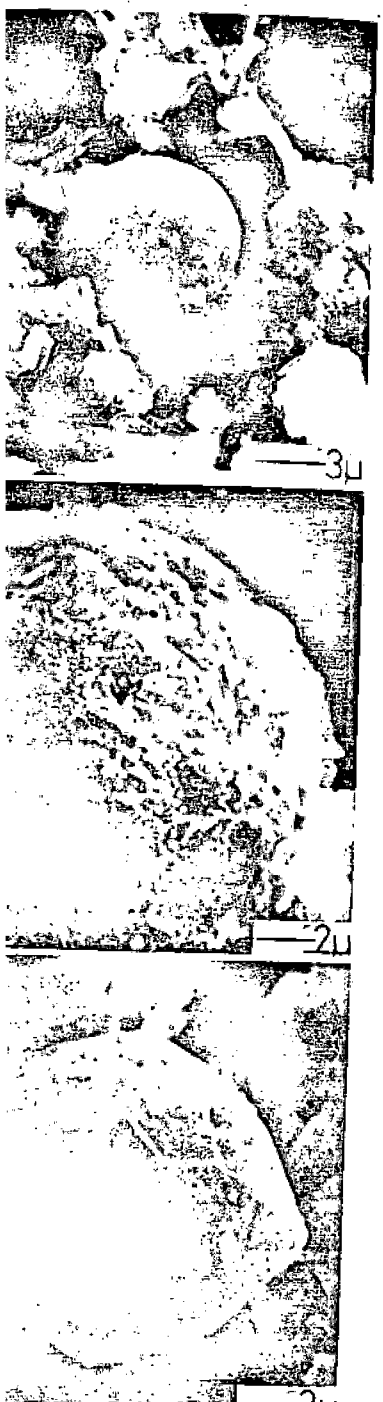

Starting material (clinoptilolite). D. Analcime (250°C, pH =

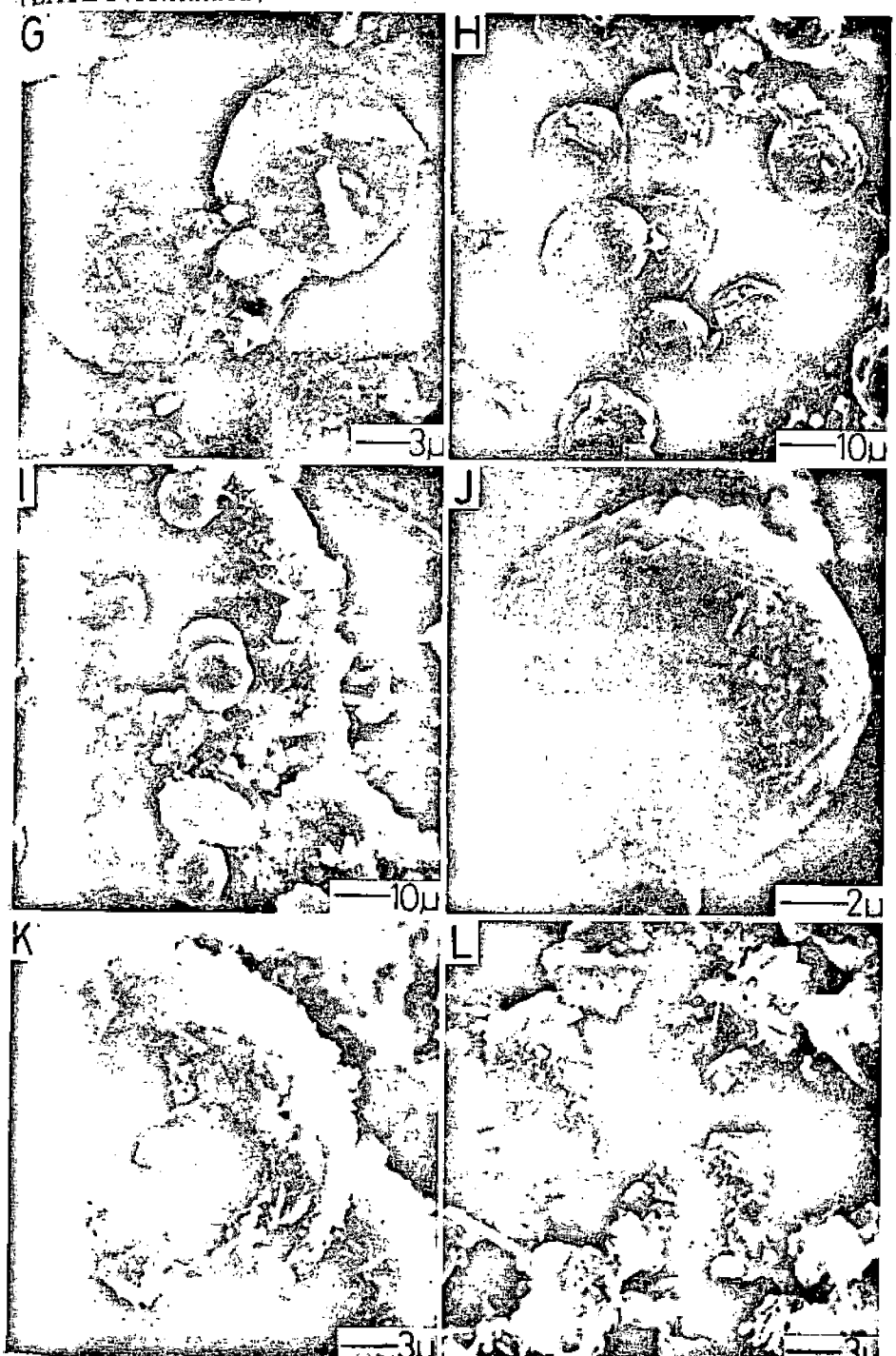

G. Analcime (200°C, pH = 9.2). H. Analcime (120°C, pH = 11.2). I and J. Analcime (219°C, pH = 11.2). K. Analcime and albite (245°C, pH = 11.2). L. Albite (250°C, pH = 11.2).

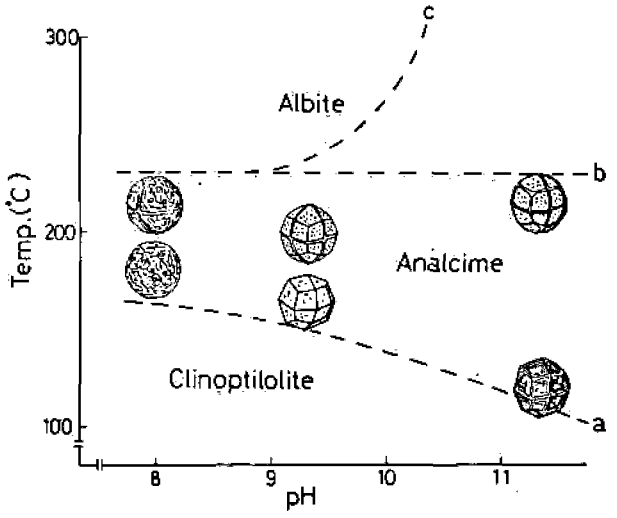

Fig. 6. Schematic diagram for crystal pattern of synthetic analcime.
a = 0.25-*M* and 0.5-*M* series; *b* = 0.25-*M* series, *c* = 0.5-*M* series (cf. Figs. 4 and 5).

tetrahedron shape was formed at the lower temperature. With an increase in temperature, the crystal edge becomes dissolved, resulting in a minor furrow, and, at the same time, crystallization of microlite on the crystal plane begins producing the incomplete crystal plane. The product at pH = 8.0 is an almost spherical crystal, not of euhedral form, even though the condition was the lower-temperature field. A value of around pH = 9.0 and lower temperatures (150—160°C) are presumed to be conditions suitable for analcimization. The difference of Na concentration showed no remarkable influence on the crystal features of the analcime products.

DISCUSSION

Boles (1971) has synthesized analcime from clinoptilolite at 100°C. Höller et al. (1974) mentioned that at low temperature, high concentrations of alkaline solution are necessary, whereas high temperatures require lower concentrations for the formation of zeolites. In the present experiments, when the Na concentration is increased, the alteration boundary of clinoptilolite—analcime showed no noticeable change in either the 0.5-*M* series or the 0.25-*M* series. As to pH values, however, the alteration temperature of clinoptilolite—analcime is higher (155°C) at a lower pH (8.0), and lower (110°C) at a higher pH (11.2).

Many opinions have been expressed on the alteration temperatures for analcime—albite. For alteration, Saha (1959) has proposed a high temperature of 360°C; Coombs et al. (1959) mentioned that 270—290°C was appropriate;

Campbell and Fyfe (1965) st
(1971) pointed out that 150-
experimental results, the alte
a somewhat different behavic
In the 0.25-*M* series, the flat
pH values. In the 0.5-*M* series
a constant alteration tempera
ever, at the higher-pH side (p
not altered to albite at tempe
process for analcime—albite i
ical gradients.

At around pH = 9.0 of the
series) no shifting of the pH
the residual-solution pH valu
commonly measured in extra
Kuroko deposits (Iijima, 197
pH = 9.0(±) showed ideal eut
the scanning-electron microsc
tions are inferred to have pla
crystallization in nature. It is
pH side (around pH = 8.0) m
as a result of the removal of
solution might become more
addition of H^+-ion to the solu

The analcime zone surrour
ply due to diagenesis, but is r
interaction between the cour
rich in Na^+-ion after Kuroko
Ishikawa, 1973; Iijima, 1974
the sericite—chlorite zone wh
fact and the present experim
zone enclosing the Kuroko d
temperature of around 250°C

Honda and Muffler (1970)
fluid are necessary for the fo
zone in nature was formed b
cime is developing in wide ar
areas. Volcanic sediments mi
aqueous environments, if it c
exhalative activities.

ACKNOWLEDGMENTS

The authors express their
University and S. Honda of t

Campbell and Fyfe (1965) stated that 190°C was favorable and Thompson (1971) pointed out that 150—190°C was suitable. As seen from the present experimental results, the alteration temperature for analcime—albite showed a somewhat different behaviour toward the Na concentration and pH value. In the 0.25-*M* series, the flat boundary at about 220°C is irrespective of the pH values. In the 0.5-*M* series at the lower-pH side (pH = 8.0—9.0), it showed a constant alteration temperature of about 220°C for analcime—albite. However, at the higher-pH side (pH = 10.5—11.2) in the 0.5-*M* series, analcime is not altered to albite at temperatures of 250—300°C. Therefore, the alteration process for analcime—albite is controlled strongly by both thermal and chemical gradients.

At around pH = 9.0 of the initial solution (both of the 0.25-*M* and 0.5-*M* series) no shifting of the pH value was recognized compared with the case of the residual-solution pH values. This pH value of around 9.0 is that which is commonly measured in extract water in natural zeolite rocks enclosing Kuroko deposits (Iijima, 1974). The analcime products at 160°C(±) and pH = 9.0(±) showed ideal euhedral crystals of icositetrahedron form under the scanning-electron microscope. These chemical and temperature conditions are inferred to have played a role in controlling hydrothermal analcime crystallization in nature. It is considered that the initial solution at the lower-pH side (around pH = 8.0) might become more alkaline after the treatments as a result of the removal of CO_2. While, at the higher-pH side, the initial solution might become more acidic in the residual solution as a result of the addition of H^+-ion to the solution from the starting materials.

The analcime zone surrounding the Kuroko deposits is not a product simply due to diagenesis, but is rather considered to have been formed by the interaction between the country rock and the alkaline hydrothermal solution rich in Na^+-ion after Kuroko mineralization (Abe et al., 1973; Utada and Ishikawa, 1973; Iijima, 1974; Abe and Aoki, 1975). Albite was observed in the sericite—chlorite zone which enclosed the Kuroko deposits. Taking this fact and the present experimental results into account, the sericite—chlorite zone enclosing the Kuroko deposits is considered to have been formed at the temperature of around 250°C.

Honda and Muffler (1970) stated that elevated temperatures and interstitial fluid are necessary for the formation of hydrothermal zeolites. If the analcime zone in nature was formed by hydrothermal processes, it is assumed that analcime is developing in wide areas, and not only in the Kuroko-mineralization areas. Volcanic sediments might be readily altered to analcime in the Na-rich aqueous environments, if it could be heated by submarine volcanism and/or exhalative activities.

ACKNOWLEDGMENTS

The authors express their thanks to Profs. M. Ichikuni of the Tohoku University and S. Honda of the Akita University for their valuable sugges-

tions. Thanks are also due to Dr. H. Konno of the Tohoku University and Mr. T. Okada of the Government Industrial Research Institute for chemical analyses and electron-microscope observations. Grateful acknowledgment is made to Dr. K. Hatai, Professor Emeritus of the Tohoku University, for reading the manuscript. This study was supported by the grant-in-aid for fundamental scientific research from the Ministry of Education and the Saito Ho-on Kai, Japan.

REFERENCES

Abe, H. and Aoki, M., 1975. Experiments on hydrothermal alteration of mordenite rocks in sodium carbonate solution, with reference to analcimization around Kuroko deposits. Econ. Geol., 70: 770—780.

Abe, H., Aoki, M. and Konno, H., 1973. Synthesis of analcime from volcanic sediments in sodium silicate solution — Experimental studies on the water—rock interaction (I). Contrib. Mineral. Petrol., 42: 81—92.

Boles, J.R., 1971. Synthesis of analcime from natural heulandite and clinoptilolite. Am. Mineral., 56: 1724—1734.

Campbell, A.S. and Fyfe, W.S., 1965. Analcime—albite equilibria. Am. J. Sci., 263: 807—816.

Coombs, D.S., Ellis, A.J., Fyfe, W.S. and Taylor, A.M., 1959. The zeolitic facies, with comments on the interpretation of hydrothermal synthesis. Geochim. Cosmochim. Acta, 17: 53—107.

Höller, H., Wirsching, U. and Fukhuri, M., 1974. Experimente zur Zeolithbildung durch hydrothermale Umwandlung. Zur Entstehung von Chabazit, Phillipsit und Analcim aus den glasigen Bestandteilen der Bims—Staubtuffe des Laacher Vulkangebietes. Contrib. Mineral. Petrol., 46: 49—60.

Honda, S. and Muffler, L.J.P., 1970. Hydrothermal alteration in core from research drill hole Y-1, Upper Geyser Basin, Yellowstone National Park, Wyoming. Am. Mineral., 55: 1714—1737.

Iijima, A., 1972. Argillaceous and zeolitic alteration zones surrounding Kuroko (Black ore) deposits in Odate district of Akita Prefecture. Min. Geol., 22: 1—22 (in Japanese with English abstract).

Iijima, A., 1974. Clay and zeolitic alteration zones surrounding Kuroko deposits in the Hokuroku district, northern Akita, as submarine hydrothermal-diagenetic alteration products. In: S. Ishihara (Editor), Geology of Kuroko Deposits, Min. Geol., Spec. Issue, 6: 267—289.

Saha, P., 1959. Geochemical and X-ray investigation of natural and synthetic analcites. Am. Mineral., 44: 300—313.

Thompson, A.B., 1971. Analcite—albite equilibria at low temperatures. Am. J. Sci., 271: 79—92.

Utada, M. and Ishikawa, T., 1973. Alteration zones surrounding "Kuroko-type" ore deposits in Nishiaizu district — Especially the analcime zone for an indicator of exploration of the ore deposits. Min. Geol., 23: 213—226 (in Japanese with English abstract).

Chemical Geology, 17 (1976) 101—1
© Elsevier Scientific Publishing Co

OCEAN-FLOOR AFFINITY O
OPHIOLITES: GEOCHEMICA

G. FERRARA[1], F. INNOCENTI[2], C

[1] *Laboratorio di Geocronologia, C*
[2] *Istituto di Mineralogia e Petrogra*
[3] *Istituto di Mineralogia e Petrogra*

(Received April 9, 1975; revised am

ABSTRACT

Ferrara, G., Innocenti, F., Ricci, C.
from north Apennine ophiolites:

Elements resistent to alteration a
from metabasalts samples belonging
mined in order to investigate the pri
clearly indicate an ocean-floor affin

INTRODUCTION

The genesis of north Apenni
question: they are considered
duced by crystal settling in lar
formation of peridotites, gabbr
and emplaced on a thinned cor
Lammerer, 1974). Other autho
Fyfe, 1973) consider these opi
sequence constituting the ocea
tectonically emplaced in the A

Useful information on the p
complexes can be obtained by
basaltic rocks. It has been show
Herrmann et al., 1974; Pearce
ferent tectonic environments c
tion of some trace elements. Th
geochemical key to discriminat
margins (ocean-floor basalts), a
ions (island-arc tholeiites, calk

Geochimica et Cosmochimica Acta, 1968, Vol. 32, pp. 853 to 877. Pergamon Press. Printed in Northern Ireland

Evaluation of irreversible reactions in geochemical processes involving minerals and aqueous solutions—I. Thermodynamic relations

HAROLD C. HELGESON
Department of Geology, Northwestern University, Evanston, Illinois

(*Received* 9 *May* 1967; *accepted in revised form* 11 *March* 1968)

Abstract—Application of the thermodynamic principles of chemical petrology and solution chemistry to the study of geochemical processes permits prediction of the consequences of reaction between aqueous solutions of electrolytes and typical igneous, metamorphic, and sedimentary mineral assemblages. A given geochemical process can be represented by a set of reversible and irreversible chemical reactions that corresponds to an array of linear differential equations relating partial equilibrium and nonequilibrium in thermodynamic systems. Simultaneous evaluation of these equations defines the nature and extent of the compositional change and redistribution of species in the aqueous phase, the order of appearance of stable and metastable phases, and the mass transfer resulting from irreversible reactions between the minerals and the aqueous solution.

INTRODUCTION

ALTHOUGH numerous studies of equilibrium in geologic systems have appeared in recent years, few attempts have been made to predict the extent to which components in a system are redistributed by geochemical processes. The principles involved in making such predictions are now well established within the framework of chemical petrology (KORZHINSKII, 1959, 1965; THOMPSON, 1955, 1959; ORVILLE, 1963; ZEN, 1963, 1966), but little has been done to extend KORZHINSKII's (1963. 1964, 1965) efforts to integrate these principles with solution chemistry and apply them quantitatively to specific irreversible processes of geologic interest. This is the object of the present communication, which consists of (1) a summary of thermodynamic relations pertinent to evaluating geochemical processes involving aqueous solutions, and (2) a discussion of the mass transfer, reaction paths, and chemical implications of irreversibility in idealized models of weathering, evaporative concentration, diagenesis, hydrothermal rock alteration, and ore deposition. The first of these topics is considered in the following pages; the second will be presented in a later contribution.

Although irreversible in an overall sense*, any geochemical process can be represented by a succession of partial equilibrium states, each reversible with respect to the next, but all irreversibly related to the initial state of the system. Because the compositional changes resulting from a geochemical process are path dependent functions, they cannot be evaluated by considering only the initial and final states of the system. To predict the mass transfer involved in such a process requires knowledge of (or assumptions about) relative reaction rates and all possible

* That is, the thermodynamic systems involved, together with their surroundings, cannot be restored to their initial states without producing changes in the rest of the universe.

metastable and stable partial equilibrium states that might arise. Because the final observed state may not constitute a stable equilibrium state, and because the system may be partly or completely open with respect to one or more of its components, the alternate paths through which a given overall equilibrium state may be achieved are of particular interest in chemical petrology.

Many geochemical processes arise through reaction of mineral assemblages with an aqueous phase. These reactions are caused by changes in the temperature–pressure environment or by introduction of an aqueous solution with which the mineral assemblage is not initially in equilibrium. The resulting redistribution of components in the system is controlled by the composition of the aqueous solution and the reactant mineral assemblage, and the stable and metastable partial equilibrium states established during the process. To evaluate the effects of these controls in terms of petrology as well as solution chemistry requires a common thermodynamic frame of reference for describing chemical equilibrium in geologic systems.

EQUILIBRIUM CONSIDERATIONS

Compositional representation

Diagrams depicting mineral compositions and compatibilities afford appropriate points of departure for simultaneous consideration of the petrology and solution chemistry of geochemical processes. Diagrams of this kind are portrayed on triangular and orthogonal coordinates in Figs. 1 and 2. Phase relations are depicted in Figs. 1a and 2a for an hypothetical system of q components and three solid phases (ϕ_1, ϕ_2, and ϕ_3) at an unspecified temperature and pressure. Corresponding diagrams are presented in Figs. 1b and 2b for the system Al_2O_3–SiO_2–H_2O at 25°C and one atmosphere. Figures 1 and 2, respectively, provide a general frame of reference and a specific example for the thermodynamic relations discussed below.

Although conventional triangular composition diagrams (Fig. 1) are widely used in petrology in preference to orthogonal plots of mineral compositions and compatibilities (Fig. 2), the orthogonal method of representation has an important geometric advantage over its triangular counterpart. This advantage lies in the fact that the slopes of the tie lines on an orthogonal composition diagram are equal to the negative reciprocals of the slopes of the corresponding field boundaries on a chemical potential diagram (KORZHINSKII, 1959).

Composition and chemical potential

Equilibrium between minerals ϕ_1 and ϕ_2 in Figs. 1a and 2a requires the chemical potential of a given component in each of the phases to be equal. The Gibbs–Duhem equations corresponding to the minerals in this equilibrium state at a given temperature and pressure can be combined to give:

$$n_{\phi_1} \sum_i^q n_{i(\phi_1)}\, d\mu_i = n_{\phi_2} \sum_i^q n_{i(\phi_2)}\, d\mu_i \qquad (1)$$

in which μ_i is the chemical potential of the ith component in the system, n_{ϕ_1} and n_{ϕ_2} represent the number of moles (gram formula weights) of phases ϕ_1 and ϕ_2 in the equilibrium state, and n_i refers to the number of moles of the ith component in one

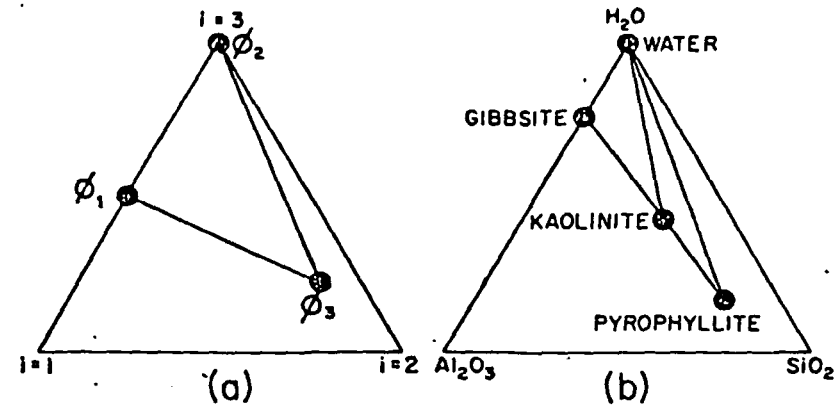

Fig. 1.(a) Schematic compositional projection for an hypothetical system of q components ($i = 1, 2, 3, \ldots q$) and three solid phases (ϕ_1, ϕ_2, and ϕ_3) at a given temperature and pressure. One of the components other than those represented by $i = 1$, $i = 2$, and $i = 3$ is H_2O.

(b) Phase relations in the system Al_2O_3–SiO_2–H_2O at 25°C and one atmosphere. The phase relations and mineral compositions shown in the triangular diagrams above are plotted on orthogonal coordinates in Fig. 2.

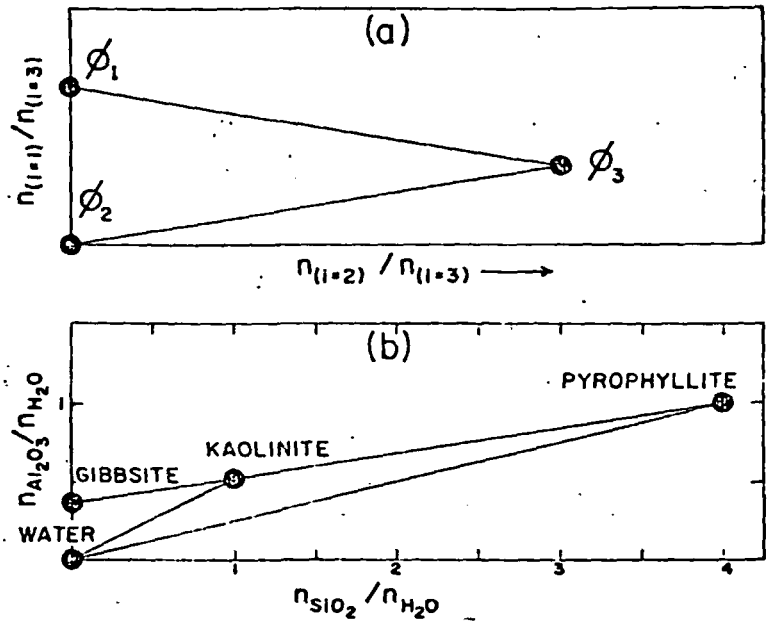

Fig. 2.(a) Schematic compositional projection for an hypothetical system of q components ($i = 1, 2, 3, \ldots q$) and three solid phases (ϕ_1, ϕ_2, and ϕ_3) at a given temperature and pressure. The letter n refers to the number of moles of the subscripted components in the phases. One of the components other than those represented by $i = 1$, $i = 2$, and $i = 3$ is H_2O.

(b) Phase relations in the system Al_2O_3–SiO_2–H_2O at 25°C and one atmosphere. The phase relations and mineral compositions shown in the orthogonal diagrams above are plotted on triangular coordinates in Fig. 1.

mole of the subscripted phase. With the chemical potentials of all components other than those represented by $i = 1$, $i = 2$, and $i = 3$ constant.*

Equation (1) can be written as:

$$\frac{d\mu_1}{d\mu_2} = -\frac{n_{\phi_1}n_{2(\phi_1)} - n_{\phi_2}n_{2(\phi_2)}}{n_{\phi_1}n_{1(\phi_1)} - n_{\phi_2}n_{1(\phi_2)}} - \left(\frac{n_{\phi_1}n_{3(\phi_1)} - n_{\phi_2}n_{3(\phi_2)}}{n_{\phi_1}n_{1(\phi_1)} - n_{\phi_2}n_{1(\phi_2)}}\right)\frac{d\mu_3}{d\mu_2}. \tag{2}$$

If we now specify that

$$n_{\phi_1}n_{3(\phi_1)} = n_{\phi_2}n_{3(\phi_2)}, \tag{3}$$

it follows that the second term on the right side of equation (2) is reduced to zero and we can write

$$\frac{d\mu_1}{d\mu_2} = -\frac{n_{\phi_1}n_{2(\phi_1)} - n_{\phi_2}n_{2(\phi_2)}}{n_{\phi_1}n_{1(\phi_1)} - n_{\phi_2}n_{1(\phi_2)}} = -\frac{(n_{2(\phi_1)}/n_{3(\phi_1)}) - (n_{2(\phi_2)}/n_{3(\phi_2)})}{(n_{1(\phi_1)}/n_{3(\phi_1)}) - (n_{1(\phi_2)}/n_{3(\phi_2)})}. \tag{4}$$

Although the first identity in equation (4) is also true when μ_3 is held constant, the second equality in the expression is valid only when equation (3) is satisfied (or when, by chance, $n_{1(\phi_2)}n_{2(\phi_1)} = n_{1(\phi_1)}n_{2(\phi_2)}$). The constraint provided by equation (3) is applicable when the component represented by $i = 3$ is an inert component in the system. Under these conditions, the chemical potential of the component represented by $i = 3$ is a dependent variable of undefined magnitude that is a function of the equilibrium states in the system.

It can be deduced from equation (4) that equilibrium phase relations in a given system involving an inert component can be portrayed schematically in terms of chemical potential simply by evaluating the slopes of the tie lines on an orthogonal composition diagram such as that in Fig. 2a. To define these relations quantitatively, we need only interpret chemical potential and establish appropriate standard states for the variables of interest.

Interpretation of chemical potential

Activity and chemical potential. The activity of the ith component in the system described by $i = 1, 2, 3, \ldots, q$ at a given temperature and pressure (Figs. 1a and 2a) is related to the chemical potential of the ith component by

$$\mu_i = \left(\frac{\partial G}{\partial n_i}\right)_{P,T,n_k} = \mu_i^0 + RT \ln \frac{f_i}{f_i^0} = \mu_i^0 + RT \ln a_i \tag{5}$$

where μ_i and μ_i^0 are the chemical potentials, and f_i and f_i^0 the fugacities of the ith component in the state of interest and in the standard state respectively, G represents the Gibbs free energy of the system, n_i and a_i refer to the number of moles and activity, respectively, of the ith component, and the subscript k stands for all components other than the ith component in the system. For the components

* The other components may be either inert, that is, their chemical potentials are fixed by other equilibrium conditions in the system (such as μ_{SiO_2} being fixed by equilibrium between quartz, the aqueous phase, and minerals ϕ_1, and ϕ_2), or they may be perfectly mobile with their chemical potentials fixed externally (KORZHINSKII, 1959). In geologic systems, Al_2O_3 and SiO_2 are commonly inert components, but CO_2 and H_2O are often mobile.

represented by $i = 1$ and $i = 2$, the derivatives of equation (5) can be combined to give

$$\frac{d\mu_1}{d\mu_2} = \frac{d \ln f_1}{d \ln f_2} = \frac{d \ln a_1}{d \ln a_2}. \tag{6}$$

Equations (4) and (6) describe relations between composition and the chemical potentials, fugacities, and activities of components in a system without regard to the nature of the components used to describe the system. Oxide components are usually chosen for this purpose, but for systems involving an aqueous phase it is often advantageous to employ the notation used in solution chemistry to describe the state of the system. This can be done within the framework of conventional chemical petrology by first casting the chemical potentials of oxide components other than SiO_2 as activities of ionic species in the aqueous phase.

Components and ionic species. Oxide components can be represented in terms of aqueous species by writing the general chemical reaction

$$M_{\nu_+}O_{\nu_-} + \nu_+ Z_+ H^+ \rightleftarrows \nu_+ M^{Z+} + \frac{\nu_+ Z_+}{2} H_2O \tag{7}$$

in which M represents the cation in the oxide component, O stands for oxygen, H refers to hydrogen, ν_+ and ν_- are the number of moles of the cation and anion, respectively, in one mole of the oxide component, and Z_+ is the charge on the cation. Hydrogen ion is a convenient choice for the reactant in reaction (7) because water is then a product of the reaction and the activity of H_2O can be regarded as unity in many geologic processes.*

The Law of Mass Action for a statement of reaction (7) involving the ith oxide component can be written for a given temperature and pressure as:

$$\frac{a_{M(i)}^{\nu_{+(i)}} a_{H_2O}^{(\nu_{+(i)} Z_{+(i)}/2)}}{a_i a_{H^+}^{(\nu_{+(i)} Z_{+(i)})}} = K \tag{8}$$

in which a denotes the activity of the subscripted species and K is the equilibrium constant for reaction (7). If we assume unit activity of H_2O and take the logarithm of equation (8), we can write

$$\ln a_i = \nu_{+(i)} \ln a_{M(i)}/a_{H^+}^{Z_{+(i)}} - \ln K. \tag{9}$$

The derivatives of equations (5) and (9) can then be combined for the oxide components represented by $i = 1$ and $i = 2$ to give

$$\frac{d\mu_1}{d\mu_2} = \frac{\nu_{+(1)} \, d \ln (a_{M(1)}/a_{H^+}^{Z_{+(1)}})}{\nu_{+(2)} \, d \ln (a_{M(2)}/a_{H^+}^{Z_{+(2)}})}. \tag{10}$$

Equation (10) can be regarded as a "bridge" between solution chemistry and chemical petrology. Together with the other thermodynamic relations discussed

* This is true even when concentrated electrolytes are involved. For example, the activity of H_2O in concentrated sodium chloride solutions ($\leq 3{\cdot}0$ m_{NaCl}) at temperatures up to 270°C varies between 1·0 and 0·9 (Gardner *et al.*, 1963; Helgeson, 1967b, 1968). This variation has an insignificant effect on most geochemical calculations.

above it permits correlation of petrologic observations with the chemistry of aqueous electrolytes.

Summary

The slopes of the field boundaries on chemical potential or logarithmic fugacity diagrams are identical to those on logarithmic activity diagrams cast either in terms of the activities of oxide components (equation 6) or ions in the aqueous phase (equation 10). These slopes are also equal to the negative reciprocals of the slopes of the tie lines on orthogonal composition diagrams. This multiple identity is expressed in equation (11), which is a combination of equations (4), (6) and (10) for two oxide components (represented by $i = 1$ and $i = 2$) in two solid phases (ϕ_1 and ϕ_2) at equilibrium. The conditions specified for the equilibrium state are constant temperature, pressure, and chemical potentials of components other than those for which $i = 1$, $i = 2$, and $i = 3$, where $i = 3$ is an inert component in the system:

$$\frac{\mathrm{d}\mu_1}{\mathrm{d}\mu_2} = \frac{\mathrm{d}\ln f_1}{\mathrm{d}\ln f_2} = \frac{\mathrm{d}\ln a_1}{\mathrm{d}\ln a_2} = \frac{\nu_{+(1)}\,\mathrm{d}\ln\left(a_{\mathrm{M}(1)}/a_{\mathrm{H}^+}^{Z_{+(1)}}\right)}{\nu_{+(2)}\,\mathrm{d}\ln\left(a_{\mathrm{M}(2)}/a_{\mathrm{H}^+}^{Z_{+(2)}}\right)} = -\frac{n_{\phi_1}n_{2(\phi_1)} - n_{\phi_2}n_{2(\phi_2)}}{n_{\phi_1}n_{1(\phi_1)} - n_{\phi_2}n_{1(\phi_2)}}$$

$$= -\frac{n_{2(\phi_1)}/n_{3(\phi_1)} - n_{2(\phi_2)}/n_{3(\phi_2)}}{n_{1(\phi_1)}/n_{3(\phi_1)} - n_{1(\phi_2)}/n_{3(\phi_2)}}. \qquad (11)$$

When the component represented by $i = 3$ is not inert, the last identity in equation (11) becomes an inequality and μ_3 is held constant. Diagrams illustrating phase relations in the systems considered in Figs. 1 and 2 are shown in Fig. 3 in terms of three of the variables in equation (11). The arrows and letter annotations in Fig. 3 are explained in later discussion.

The versatility of diagrams representing alternate interpretations of chemical potential can be demonstrated with the aid of Fig. 3. For example, to aid in solving a particular problem, the variables in equation (11) may be interchanged without obscuring the geometric relation between the chemical potential and composition diagrams for the system under consideration. This has been done in Fig. 3b, where an oxide component is used together with ionic species in the same diagram to describe equilibrium relations in the system Al_2O_3–SiO_2–H_2O at 25°C and one atmosphere. Note that where the activity of H_2O is an externally fixed constant (and therefore H_2O is a perfectly mobile component) in Fig. 3a, it is a variable, implicity specified by any given equilibrium condition (and consequently H_2O is an inert component) in Fig. 3b. In contrast to Fig. 3b, all of the stability fields in Fig. 3a are for the indicated mineral in the presence of an aqueous solution. The positions shown for the field boundaries in Fig. 3 are fixed by equilibrium constants defined in terms of standard states appropriate for the variables involved. Although the minerals in the systems considered in these diagrams do not exhibit solid solubility, the relations discussed above are equally applicable to systems involving solid solutions (HELGESON, 1967b).

Of the several possible interpretations of chemical potential that can be made for the purpose of studying geologic systems, activities of ionic species are the most useful where aqueous solutions are involved. Activity coefficients can be computed

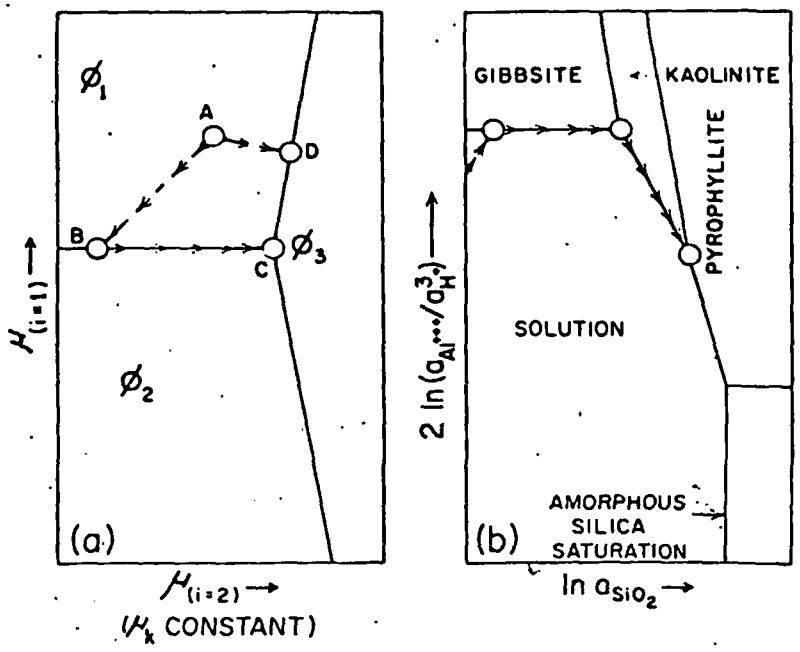

Fig. 3. Schematic chemical potential diagrams for:
(a) The system described by $i = 1, 2, 3, \ldots q$ at a given temperature and pressure (see Fig. 1a and 2a). The subscript k designates all components other than those represented by $i = 1$, $i = 2$, and $i = 3$. The chemical potential of the component designated by $i = 3$ is a dependent variable that is specified implicitly by the equilibrium conditions in the system. One of the components other than those represented by $i = 1$, $i = 2$, and $i = 3$ is H_2O.
(b) The system Al_2O_3–SiO_2–H_2O at 25°C and one atmosphere (see Figs. 1b and 2b) in terms of activities of species in the aqueous phase. For the sake of clarity, quartz saturation has been omitted from the diagram.
The letter annotations in the diagrams represent points on irreversible reaction paths (dashed lines and arrows) followed by an aqueous phase with a specified starting composition reacting with various minerals (see text).

for these species in concentrated (up to 3 molal) electrolyte solutions at temperatures from 25° to 300°C (HELGESON, 1964, 1967b, 1968; HELGESON and JAMES, 1968). Consequently, chemical analysis of aqueous solutions can be made directly applicable to the study of petrologic problems.

IRREVERSIBLE REACTIONS

Equilibrium relations such as those discussed above describe the state of a system before or after a geochemical process has taken place. These relations alone cannot define the chemical reactions or the mass transfer involved in a particular irreversible process that has led to an observed equilibrium state. The additional information required to characterize such a process quantitatively can be illustrated simply by describing the hydrolysis of pyrophyllite with the aid of Fig. 3b.

An example in the system Al_2O_3–SiO_2–H_2O

The paths with arrows in Fig. 3b depict hypothetical changes in the composition of the aqueous phase in the system Al_2O_3–SiO_2–H_2O when pyrophyllite is immersed

in a given amount of pure water and permitted to react at 25°C and one atmosphere. The dissolution process represented in Fig. 3b and discussed below is based on thermodynamic calculations assuming the presence of excess pyrophyllite and solution. Quartz and a number of metastable phases that might appear during the actual dissolution of pyrophyllite are not considered in the following discussion, which represents an idealization of the real process.

Providing for aqueous species that may form to significant degrees, the hydrolysis of pyrophyllite can be written as:

$$Al_2Si_4O_{10}(OH)_2 + (6 - \alpha - 4\beta - \lambda)H^+ + (4 + \alpha + 4\beta)H_2O \rightarrow (2 - \alpha - \beta)Al^{3+} + \alpha Al(OH)^{2+} + \beta Al(OH)_4^- + \lambda H_3SiO_4^- + (4 - \lambda)H_4SiO_4 \quad (12)^*$$

in which α, β, and λ stand for the reaction coefficients of $Al(OH)^{2+}$, $Al(OH)_4^-$, and $H_3SiO_4^-$, respectively. The values of these coefficients depend on the composition of the aqueous solution during the progress of the reaction. Reaction (12) causes the chemical potential of Al_2O_3 and SiO_2 to increase in the aqueous phase; consequently, as the first small amount of pyrophyllite goes into solution, the ratio of the activity of Al^{3+} to the activity of H^+ increases in solution, as does the activity of aqueous silica (Fig. 3b). While the solution is still very dilute, the continued dissolution of pyrophyllite eventually causes the solution to become saturated with respect to gibbsite, and a small amount of gibbsite precipitates from solution. The identity of the mineral with which the solution becomes saturated is determined by the relative sizes of the activity product constants for the phases in the system.

If the equilibrium condition described by:

$$Al^{3+} + 3OH^- \rightleftarrows Al(OH)_{3(gibbsite)} \quad (13)$$

is maintained between gibbsite and the aqueous phase, further reaction of pyrophyllite with the solution causes the removal of aluminum and hydroxyl ions according to

$$\frac{d \ln a_{Al^{3+}}}{d \ln a_{OH^-}} = -3 . \quad (14)$$

The chemical potential of Al_2O_3 in the system is then fixed, and $\log a_{Al^{3+}}/a^3_{H^+}$ remains constant as gibbsite precipitates. In contrast, the activity of H_4SiO_4 continues to increase in solution as gibbsite precipitates until the aqueous phase

* Description of the dissolution process with reaction (12) involves the implicit assumption that all important species in the aqueous phase are included in the reaction as written. Reaction (12) is intended to indicate simply that the total aluminum and silicon in the aqueous phase increases as pyrophyllite dissolves, and that the complexes shown in the reaction may play important roles in the process. The division of species into reactants and products as shown in the reaction does not necessarily correspond to physical reality. The actual changes in the concentrations of the individual species in the aqueous phase may be positive or negative depending on the signs of the respective reaction coefficients. The activities of species such as OH^-, which is not included in the reaction as written, are also affected by the dissolution of pyrophyllite, and these activities must be taken into consideration when calculating the reaction coefficients for reaction (12). Such constraints are discussed further in later pages.

becomes saturated with respect to kaolinite (Fig. 3b). At this point, the gibbsite produced earlier reacts with the pyrophyllite to form kaolinite while the solution composition remains constant. This reaction is

$$Al_2Si_4O_{10}(OH)_2 + 2Al(OH)_3 \rightarrow 2Al_2Si_2O_5(OH)_4. \quad (15)$$

The coefficients in reaction (15) are fixed by the requirement for constant $a_{Al^{3+}}/a_{H^+}{}^3$ and $a_{H_4SiO_4}$ imposed by equilibrium between kaolinite, gibbsite, and solution. After all of the gibbsite is destroyed according to reaction (15), pyrophyllite continues to react with the solution to produce kaolinite (Fig. 3b). As this latter reaction proceeds, $a_{Al^{3+}}/a_{H^+}$ decreases in solution, but the activity of H_4SiO_4 increases. Finally, the reaction ceases when equilibrium is established between kaolinite, pyrophyllite, and solution.

The sequence of events described above involves sequential states of partial equilibrium between the aqueous solution and the successive phases produced along the reaction path as pyrophyllite reacts irreversibly with the aqueous phase. The process results in mass transfer among the phases to an extent defined by the coefficients for the reacting mineral(s), the product minerals, and the aqueous species in the reactions represented by the various segments of the overall reaction path. The nature and extent of this mass transfer, the partial equilibrium states established as the overall irreversible reaction takes place, and the paths followed by the aqueous solution on a chemical potential diagram are all of interest to the geologist. In addition to the thermodynamic data for equilibrium conditions in the system of interest, we need specify only the initial state of the system to define all of these variables quantitatively for geochemical processes in which partial equilibrium is maintained. The equations, reactions, and assumptions involved in making such calculations for the general case are summarized below.

Reaction progress

Selected changes in the composition of an aqueous solution reacting with a given mineral or mineral assemblage can be represented quantitatively on an equilibrium activity diagram if we specify the initial composition of the aqueous phase and calculate the mole transfer involved in the process. The mass of the system and its surroundings is the property that is conserved in irreversible processes, but it is more convenient for most purposes to evaluate chemical reactions in terms of mole transfer. The extent to which a given component in a system is redistributed by a reaction involving an aqueous solution can be described conveniently in terms of a reaction differential, $d\xi$—also called a progress variable (Fitts, 1962), or the degree of advancement or extent of reaction (De Donder, 1920; Prigogine, 1961)—which is defined by:

$$d\xi = \frac{dx_{i,j}}{n'_{i,j}} = \frac{d\bar{x}_\phi}{\bar{n}_\phi} = \frac{dm_s}{\bar{n}_s} \quad (16)$$

in which $x_{i,j}$ is the total number of moles of the ith component in the jth phase in the system ($j = 1, 2, 3, \ldots, l$), $n'_{i,j}$ is the total number of moles of the ith component in the jth phase in the reaction as written, $\bar{x}_\phi$ is the number of moles

per 1000 grams of water of the ϕth reactant or product mineral* in the system ($\phi = 1, 2, 3, \ldots . \Phi$), m_s is the molality of the sth species in the aqueous phase, and $\bar{n}_\phi$ and $\bar{n}_s$ refer to the number of moles per thousand grams of water (reaction coefficient) of the subscripted mineral or aqueous species in the reaction. Where j, ϕ, or s denote products of the reaction, the coefficients $n'_{i,j}$, $\bar{n}_\phi$, and $\bar{n}_s$ are treated as positive numbers, but for reactants these coefficients are negative.

Equation (16) permits calculation of the distribution of components in a system at any given stage of an irreversible reaction. That is, for a given $d\xi$, values of $dx_{i,j}$, or $d\bar{x}_\phi$ and dm_s can be calculated for the reaction as long as numerical values are known for the reaction coefficients, $n'_{i,j}$, or $\bar{n}_\phi$ and $\bar{n}_s$ for all products and reactants. However, to assign numerical values to all of the reaction coefficients we must first take into account all equilibria in the aqueous phase and provide for equilibrium between the aqueous solution and the solid products of the overall irreversible reaction. These partial equilibrium states fix the values of the reaction coefficients at any given stage of reaction progress.

Partial equilibrium

Partial equilibrium describes a state in which a system is in equilibrium with respect to at least one process (or reaction), but out of equilibrium with respect to others (BARTON *et al.*, 1963). Partial equilibrium thus obtains in any part of a system in which the phases are not all mutually incompatible. For example, in a system containing only a single solid phase and an aqueous solution with which it is incompatible, the entire system is in heterogeneous (but not necessarily homogeneous) chemical disequilibrium. However, reaction between the solution and the solid may produce a second solid that is compatible with the solution but not with the original solid phase. Equilibrium then obtains between the second solid phase and the solution, even though the original solid continues to react with the solution. Accordingly, the activity product constant for the product solid phase is satisfied until this phase is either destroyed by later reaction or the overall reaction ceases. When evaluating an irreversible reaction, it is usually safe to assume that homogeneous equilibrium prevails in the aqueous phase involved in the process. Consequently, where any of the reactant or product species in the aqueous solution form complexes, the system is considered to be in partial equilibrium.

An irreversible process that involves a series of successive partial equilibrium states may result in a state of local equilibrium for the system; that is, a state in which no mutually incompatible phases are in contact, even though the system as a whole is not in equilibrium (THOMPSON, 1959). For example, the reaction of pyrophyllite with water discussed above may result in rims of kaolinite completely jacketing the pyrophyllite grains before overall equilibrium is achieved. Reaction will then cease because local equilibrium has been established. When this occurs, the aqueous solution will have a composition consistent with some point along the kaolinite + solution field boundary in Fig. 3b, rather than at the pyrophyllite + kaolinite + solution equilibrium point.

* The compositions of the minerals involved in a given irreversible reaction are specified quantitatively in terms of the oxide components in the system. The subscript ϕ thus refers to a mineral with a specific mole composition.

Partial equilibrium is probably maintained in most geochemical processes. This conclusion is supported by the mineral assemblages commonly found in metamorphic rocks, chemical and mineralogic characteristics of hydrothermal and geothermal systems, and the chemistry of ground waters involved in the weathering process. In geologic systems, partial equilibrium appears to be the rule rather than the exception; consequently, the relative rates at which minerals are produced or destroyed in a given irreversible reaction are defined implicitly for most geochemical processes, and thermodynamic relations for the partial equilibrium states can be used to calculate values of the reaction coefficients in equation (16).

Reaction coefficients

Reaction coefficients for reactant minerals are specified when an irreversible reaction is written.* Consequently, when no product minerals appear in the reaction and no internal equilibria such as the dissociation of complexes in the aqueous phase are involved, the reaction coefficients in equation (16) are independent of the composition of the aqueous phase. Under these conditions, the reaction coefficients (which are negative for reactants and positive for products) are constants defined entirely by mass and charge balance requirements. The conservation of mass and charge is described by

$$\sum_j n'_{i,j} = \sum_s \tilde{n}_s z_s = 0 \tag{17}$$

in which Z_s is the charge on the sth aqueous species.

Where solution equilibria or product minerals are involved in an irreversible reaction, the values of $\tilde{n}_s$ in the reaction change with each increment of reaction progress. Although equation (17) must be satisfied in the process, the values of $\tilde{n}_s$ are no longer defined explicitly by the conservation of mass and charge. For example, in the process described by reaction (12) equilibrium obtains among Al^{3+}, $Al(OH)^{2+}$ $Al(OH)_4^-$, H^+, and OH^- in the aqueous phase. Consequently, the equilibrium concentrations of these species must be considered when calculating the respective values of $\tilde{n}_s$ in reaction (12). On the other hand, because

$$n'_{i,\ \text{aqueous phase}} = \sum_s \nu_{+(i)s}\tilde{n}_s \tag{18}$$

where $\nu_{+(i)s}$ is the total number of moles of the cation in the ith component in the sth species, the total mole transfer in reaction (12) is defined by $n'_{i,\ \text{pyrophyllite}}$.

When product minerals are involved in an irreversible reaction, $n'_{i,j}$, and $\tilde{n}_\phi$ for the products also depend on the composition of the aqueous phase involved in the reaction. The equilibrium solubilities of the product minerals must be satisfied during reaction progress in order to preserve partial equilibrium in the system. In most cases, these solubilities depend on complexing in the aqueous phase. For all irreversible reactions involving partial equilibrium, the reaction coefficients

* In practice, mole transfer calculations are usually carried out relative to one mole of the reactant mineral. Where a group of reactant minerals is present, the reaction coefficient for each mineral is defined relative to one mole of a particular reactant in the group by assigning relative reaction rates to the minerals. The case of multiple reactant minerals is discussed further in later pages.

can be computed from differential equations relating the equilibrium activities of species in solution to the mole transfer resulting from the irreversible reaction.

Constraints imposed by partial equilibrium. The reaction coefficients in an irreversible reaction involving equilibrium between aqueous species or the solution and a product phase can be defined at any given stage of reaction progress by simultaneously evaluating differential equations derived from the Law of Mass Action for the equilibrium states together with mass balance relations for the overall irreversible reaction. The derivation of these equations can be illustrated by using as an example the reaction discussed above in which pyrophyllite reacts with water to produce gibbsite. This particular reaction takes place along the second segment of the reaction path illustrated in Fig. 3b. If we provide for chemical equilibrium among the aqueous species as well as for equilibrium between the solution and gibbsite, we can write the irreversible reaction as

$$\begin{aligned} Al_2Si_4O_{10}(OH)_2 + \bar{n}_{H_2O}H_2O + \bar{n}_{H^+}H^+ \rightarrow \bar{n}_{Al(OH)_3}Al(OH)_3 + \bar{n}_{Al^{3+}}Al^{3+} \\ + \bar{n}_{Al(OH)^{2+}}Al(OH)^{2+} + \bar{n}_{Al(OH)_4^-}Al(OH)_4^- + \bar{n}_{H_3SiO_4^-}H_3SiO_4^- \\ + \bar{n}_{OH^-}OH^- + \bar{n}_{H_4SiO_4}H_4SiO_4, \end{aligned} \quad (19)^*$$

and describe the various equilibria by

$$Al(OH)_{3(gibbsite)} \rightleftarrows Al^{3+} + 3OH^- \quad (20)$$

$$Al(OH)_4^- \rightleftarrows Al^{3+} + 4OH^- \quad (21)$$

$$Al(OH)^{2+} \rightleftarrows Al^{3+} + OH^- \quad (22)$$

$$H_4SiO_4 \rightleftarrows H^+ + H_3SiO_4^- \quad (23)$$

$$H_2O \rightleftarrows H^+ + OH^- \quad (24)$$

for which the statements of the Law of Mass Action appear as (with $a_{H_2O} = a_{gibbsite} = 1$),

$$a_{Al^{3+}}a_{OH^-}^3 = K_1 \quad (25)$$

$$\frac{a_{Al^{3+}}a_{OH^-}^4}{a_{Al(OH)_4^-}} = K_2 \quad (26)$$

$$\frac{a_{Al^{3+}}a_{OH^-}}{a_{Al(OH)^{2+}}} = K_3 \quad (27)$$

$$\frac{a_{H^+}a_{H_3SiO_4^-}}{a_{H_4SiO_4}} = K_4 \quad (28)$$

$$a_{H^+}a_{OH^-} = K_W. \quad (29)$$

* As before in reaction (12), writing the reaction in this way is not meant to imply that the aqueous species shown on the left are actually reactants, or that those on the right are products. The true designation of reactants and products depends on the signs of the reaction coefficients determined from equations (36)–(44). On the other hand, the reaction as written is assumed to include all species that may contribute significantly to the dissolution process.

Taking the derivatives of equations (25)–(29) with respect to the progress variable for reaction (19) and substituting equations (25)–(29) in the resulting expressions yields

$$\frac{da_{Al^{3+}}/d\xi}{a_{Al^{3+}}} + \frac{3da_{OH^-}/d\xi}{a_{OH^-}} = 0 \tag{30}$$

$$\frac{da_{Al^{3+}}/d\xi}{a_{Al^{3+}}} + \frac{4da_{OH^-}/d\xi}{a_{OH^-}} - \frac{da_{Al(OH)_4^-}/d\xi}{a_{Al(OH)_4^-}} = 0 \tag{31}$$

$$\frac{da_{Al^{3+}}/d\xi}{a_{Al^{3+}}} + \frac{da_{OH^-}/d\xi}{a_{OH^-}} - \frac{da_{Al(OH)^{2+}}/d\xi}{a_{Al(OH)^{2+}}} = 0 \tag{32}$$

$$\frac{da_{H^+}/d\xi}{a_{H^+}} + \frac{da_{H_3SiO_4^-}/d\xi}{a_{H_3SiO_4^-}} - \frac{da_{H_4SiO_4}/d\xi}{a_{H_4SiO_4}} = 0 \tag{33}$$

$$\frac{da_{H^+}/d\xi}{a_{H^+}} + \frac{da_{OH^-}/d\xi}{a_{OH^-}} = 0. \tag{34}$$

If we assume that the activity coefficients for the aqueous species are unaffected by the change in solution composition resulting from a given increment of progress in the irreversible reaction,* we can write

$$\bar{n}_s = \frac{dm_s}{d\xi} = \frac{1}{\gamma_s}\frac{da_s}{d\xi}, \tag{35}$$

in which γ_s is the activity coefficient of the sth species. Combining appropriate statements of $a_s = \gamma_s m_s$ and equation (35) with equations (30)–(34) yields

$$\frac{\bar{n}_{Al^{3+}}}{m_{Al^{3+}}} + \frac{3\bar{n}_{OH^-}}{m_{OH^-}} = 0 \tag{36}$$

$$\frac{\bar{n}_{Al^{3+}}}{m_{Al^{3+}}} + \frac{4\bar{n}_{OH^-}}{m_{OH^-}} - \frac{\bar{n}_{Al(OH)_4^-}}{m_{Al(OH)_4^-}} = 0 \tag{37}$$

$$\frac{\bar{n}_{Al^{3+}}}{m_{Al^{3+}}} + \frac{\bar{n}_{OH^-}}{m_{OH^-}} - \frac{\bar{n}_{Al(OH)^{2+}}}{m_{Al(OH)^{2+}}} = 0 \tag{38}$$

$$\frac{\bar{n}_{H^+}}{m_{H^+}} + \frac{\bar{n}_{H_3SiO_4^-}}{m_{H_3SiO_4^-}} - \frac{\bar{n}_{H_4SiO_4}}{m_{H_4SiO_4}} = 0 \tag{39}$$

$$\frac{\bar{n}_{H^+}}{m_{H^+}} + \frac{\bar{n}_{OH^-}}{m_{OH^-}} = 0. \tag{40}$$

* This assumption is valid for most aqueous solutions in geologic systems where the reactant minerals are silicates, sulfides, oxides, carbonates, etc., or for that matter in all cases where the mass transfer between a mineral and an aqueous phase is small compared to the ionic strength of the solution. The total concentration of electrolytes in (and therefore the ionic strength of) an aqueous solution in nature is usually far greater than the mass transfer resulting from a small increment of progress in a given irreversible reaction between the solution and a mineral assemblage. Where dilute water is involved in such reactions, the activity coefficients do not depart significantly from one.

In addition to equations (36)–(40), we can describe relations between the reaction coefficients in reaction (19) by writing the following mass balance equations for the transfer of aluminum, silicon, hydrogen, and oxygen, respectively, relative to *one mole of pyrophyllite*:

$$\bar{n}_{Al^{3+}} + \bar{n}_{Al(OH)^{2+}} + \bar{n}_{Al(OH)_4^-} + \bar{n}_{Al(OH)_3} - 2 = 0 \tag{41}$$

$$\bar{n}_{H_4SiO_4} + \bar{n}_{H_3SiO_4^-} - 4 = 0 \tag{42}$$

$$\bar{n}_{H^+} + 2\bar{n}_{H_2O} + 4\bar{n}_{H_4SiO_4} + 3\bar{n}_{H_3SiO_4^-} + \bar{n}_{Al(OH)^{2+}} + \bar{n}_{OH^-} + 4\bar{n}_{Al(OH)_4^-} + 3\bar{n}_{Al(OH)_3} - 2 = 0 \tag{43}$$

$$\bar{n}_{OH^-} + \bar{n}_{H_2O} + 4\bar{n}_{H_4SiO_4} + 4\bar{n}_{H_3SiO_4^-} + \bar{n}_{Al(OH)^{2+}} + 4\bar{n}_{Al(OH)_4^-} + 3\bar{n}_{Al(OH)_3} - 12 = 0 ; \tag{44}$$

Equations (36)–(44) constitute a set of nine linear equations describing the system along the second segment of the reaction path illustrated in Fig. 3b. Because the reaction coefficients are negative for reactants and positive for products, and because provision has been included for all mass balance relations in the reaction, the requirement for charge balance in equation (17) is implicity met by the combination of equations (36)–(44). The set of nine linear equations involves nine unknown reaction coefficients when the composition of the aqueous phase and the distribution of species in the reacting solution are specified. For a given initial solution, these nine reaction coefficients can be defined numerically by employing matrix algebra to solve the set of linear equations. A similar approach can be used to evaluate any irreversible reaction involving partial equilibrium. For all such reactions, the unknown reaction coefficients can be described by a set of linear differential equations in a nonsingular reaction matrix in which the number of equations equals the number of unknowns. This is demonstrated in the development of equations for the general case summarized below.

Matrix equations in general notation. In a general model of irreversible reactions involving one reacting mineral and an aqueous solution, mass balance equations (e.g. equations 41–44) can be represented by

$$\sum_{\phi_p} \nu_{\varepsilon,\phi_p}\bar{n}_{\phi_p} + \sum_{\zeta} \nu_{\varepsilon,\zeta}\bar{n}_{\zeta} + \sum_{i} \nu_{\varepsilon,i}\bar{n}_i = \nu_{\varepsilon,\phi_r} \tag{45}$$

where ν_{ε,ϕ_p} stands for the number of moles of the εth monatomic ion ($\varepsilon = 1, 2, 3, \ldots \hat{E}$) in one mole of the ϕ_pth product mineral in equilibrium with the solution ($\phi_p = 1, 2, 3, \ldots \Phi_p$), ϕ_r designates the reactant mineral, ζ represents aqueous complexes (except H_2O) for which mass action equations are provided in the calculations

($\phi = 1, 2, 3, \ldots \Phi$), and $\bar{s}$ refers to the remaining species in the aqueous solution ($\bar{s} = 1, 2, 3, \ldots \sigma$). The limit $\hat{\mathrm{E}}$ for the range of ε corresponds to the number of monatomic ions (which equals the number of elements) in the reactant mineral (or minerals in the case of multiple reactants discussed below), and σ is equal to the number of dissociated aqueous species. It follows from these definitions that $\sigma \geq \hat{\mathrm{E}}$. Note that equation (45) has been written relative to one mole of the reactant mineral.

Equilibrium between pure stoichiometric product phases and an aqueous solution can be described for the general case by

$$\sum_i \frac{\nu_{i,\phi_p} \bar{n}_i}{m_i} = 0 . \tag{46}$$

Equation (46) is a general expression of the differential equation derived above (equation 36) from the equilibrium activity product for gibbsite (equation 25). The analogous expression for dissociational reactions in the aqueous phase (e.g. equations 37–39) appears as

$$\sum_i \frac{\nu_{\bar{s},\phi} \bar{n}_i}{m_i} = \frac{\bar{n}_\phi}{m_\phi} . \tag{47}$$

Because the differential equation for the dissociation of H_2O (equation 40) has the form of equation (46), and because H_2O is not included in the designation ϕ, the number of differential equations for activity products is always equal to $\Phi_p + 1$. If provision is included for solid solution in the product phases in the reaction, the corresponding differential equations have the form of equation (47); the activities of the product minerals are then specified in these equations as other than unity. Where equilibrium between a product phase and the aqueous solution is described using H^+ or OH^-, the corresponding equation in the matrix also has the form of equation (47). These modifications are discussed further below. For the moment let us confine our attention to a simple system in which partial equilibrium is maintained and only one mineral is reacting irreversibly with the aqueous phase.

Provided the limit of the range of the subscript ε is set equal to that of the subscript $\bar{s}$ (i.e. $\hat{\mathrm{E}} = \sigma$), equations (45), (46) and (47) define the elements of a matrix in which the number of linear equations equals the number of unknown reaction coefficients for any solution composition and distribution of species. Imposing the constraint that $\hat{\mathrm{E}} = \sigma$ requires the matrix to be square. $\hat{\mathrm{E}}$ will always be equal to σ if only one aqueous species designated as $\bar{s}$ contains a given monatomic ion represented by ε. For example, if provision is not included for the dissociation of H_4SiO_4 in the designation ϕ, then both $H_3SiO_4^-$ and H_4SiO_4 should not be represented in the designation $\bar{s}$; if both are included, σ will be greater than $\hat{\mathrm{E}}$ and the matrix will not be square. The matrix will always be nonsingular, and thus a unique solution can be obtained for the set of equations, as long as all of the equations in the matrix are independent equations.

The matrix equation for the general case involving one reactant mineral can

be written as

$$
\begin{array}{c|c|c|c||c||c|c}
 & \phi_p = 1 \rightarrow \Phi_p + 1 & \text{¢} = 1 \rightarrow \text{Ȼ} & \tilde{s} = 1 \rightarrow \sigma & & & \\
\hline
\varepsilon = 1 \rightarrow \mathcal{E} & \nu_{\varepsilon,\phi_p} & \nu_{\varepsilon,\text{¢}} & \nu_{\varepsilon,\tilde{s}} & \bar{n}_{\phi_p} & & \nu_{\varepsilon,\phi_r} \\
\hline
\phi_p = 1 \rightarrow \Phi_p + 1 & 0 & 0 & \dfrac{\nu_{\tilde{s},\phi_p}}{m_{\tilde{s}}} & \bar{n}_{\text{¢}} & = & 0 \\
\hline
\text{¢} = 1 \rightarrow \text{Ȼ} & 0 & \dfrac{-1}{m_{\text{¢},\text{¢}}} & \dfrac{\nu_{\tilde{s},\text{¢}}}{m_{\tilde{s}}} & \bar{n}_{\tilde{s}} & & 0
\end{array}
\qquad (48)
$$

If we designate the matrix by Γ, the column vector for the unknown reaction coefficients as β, and the column vector for ν_ε in the reactant phase as λ, we can write

$$\beta = \Gamma^{-1}\lambda. \qquad (49)$$

Equation (49) is then the defining equation for evaluation of all reaction coefficients in an irreversible reaction involving one reactant mineral, an unlimited number of product minerals, and an aqueous phase of known composition in which the distribution of species can be calculated at any specified stage of reaction progress. The values of the reaction coefficients computed from equation (49) for a given stage of reaction progress are specified implicitly by the partial equilibrium states of the system. Consequently, the relative rates at which the product minerals are formed as a result of an irreversible reaction are also fixed by the partial equilibrium states. If a given partial equilibrium state is not maintained, the corresponding reaction rate must be defined explicity to determine the reaction coefficient in a manner analogous to that described below for the case of multiple reactants.

Provision for solid solution has not been included in the matrix equation derived above, but solid solution can be taken into account by inserting a coefficient (equal to, in the case of an "ideal" solid solution, the negative reciprocal of the mole fraction of the stoichiometric end member in the product phase) in the appropriate ϕ_p column-row location in equation (48). The species H_2O and the dissociation of H_2O are included in equation (48) as the $\Phi_p + 1$ column and row, respectively, in the matrix. The reaction coefficient for H_2O is thus an unknown, but the activity of H_2O is either specified of taken as unity* in the calculations. Where partial

* See footnote on p. 857.

equilibrium between a product mineral and the aqueous phase is not described by an activity product, but with H^+ as a reactant, a term equal to $-\sum_i (\nu_{i,\phi_p} |Z_{i,\phi_p}|/m_{H^+})$ appears in the appropriate ϕ_p column-row location for the hydrogen ion in equation (48). If the reaction is alternatively written to produce hydroxyl ion, an analogous term appears in the matrix location for that species.

Although equation (48) is written for one reactant mineral, the matrix equation implicitly provides for product phases produced in an early stage of reaction progress that became unstable at some later stage (as in the case of gibbsite along the reaction path in Fig. 3b). When this occurs, the unstable mineral (say that represented by $\phi_p = 1$) becomes a reactant. However, during the reaction of this phase with the original reactant mineral to produce a new mineral, say that for which $\phi_p = 2$, (e.g. the reaction of gibbsite with pyrophyllite to produce kaolinite—Fig. 3b), equilibrium is assumed to obtain between the solution and the phases designated by $\phi_p = 1$ and $\phi_p = 2$. For this reason, no change in the matrix equation is necessary to provide for the reaction of the mineral represented by $\phi_p = 1$; all that is required is to add appropriate terms for the phase for which $\phi_p = 2$. The value of $\bar{n}_{\phi_p = 1}$ determined from the matrix equation will then be negative, and reaction progress will result in changes in the solution composition restricted by the presence of both minerals until the phase designated as $\phi_p = 1$ is completely consumed by the reaction. Reactant phases that are in partial equilibrium with the solution are thus treated in the matrix equation as product phases having negative reaction coefficients. If a possible partial equilibrium state is not maintained, the corresponding reaction coefficient or the relative rate at which the product mineral forms must be specified.

Irreversible reactions between an aqueous solution and two or more phases in a mineral assemblage are not uncommon in geochemical processes. The presence of more than one mineral reacting irreversibly can be taken into account by constructing a matrix equation for the overall reaction. This can be done by specifying one additional constraint for each additional reactant mineral.

Multiple reactants. In cases where more than one reactant mineral, none of which is in equilibrium with the aqueous phase, is involved in an irreversible reaction with an aqueous solution, relative rates for the reaction of the minerals must be specified explicitly to define the reaction coefficients in the overall reaction. This can be stated for the general case by writing

$$\bar{n}_{\phi_r} = \psi_{(\phi_r/\Phi_r)} \bar{n}_{\Phi_r} \tag{50}$$

in which $\psi_{(\phi_r/\Phi_r)}$ represents the reaction rate for the ϕ_rth phase ($\phi_r = 1, 2, 3, \ldots \Phi_r$) relative to that for the Φ_rth phase. The relative reaction rate is defined as

$$\psi_{(\phi_r/\Phi_r)} = \frac{d\xi_{\phi_r}/dt}{d\xi_{\Phi_r}/dt}, \tag{51}$$

in which t refers to time. With the relative reaction rates specified, the reactant phase column vector in equations (48) and (49) can be rewritten for multiple reactant

minerals and represented as

$$\lambda = \begin{vmatrix} \sum_{\phi_r} \psi_{(\phi_r/\Phi_r)}\, \nu_{\epsilon,\phi_r} \\ \hline 0 \\ \hline 0 \end{vmatrix} \tag{52}$$

The summation in equation (52) defines the total amount of the ϵth ion derived from the ϕ_rth reactant phase, relative to one mole of the Φ_rth reactant phase and a single $d\xi$ for the overall irreversible reaction.

Mass transfer calculations

Having defined the initial composition of the system and the initial distribution of the species in the aqueous phase involved in a given irreversible reaction, the mass transfer among the phases resulting from a small increment of progress in the reaction can be calculated from the reaction coefficients derived above. Using the general notation employed in equations (45)–(48), we can write for a small increment of progress in an irreversible reaction*

$$\Delta\bar{x}_{\phi_p} = \bar{x}_{\phi_p} - \bar{x}_{\phi_p}{}^0 = \bar{n}_{\phi_p}\,\Delta\xi \tag{53}$$

and

$$\Delta m_{\epsilon} = m_{\epsilon} - m_{\epsilon}{}^0 = \bar{n}_{\epsilon}\,\Delta\xi \tag{54}$$

and

$$\Delta m_i = m_i - m_i{}^0 = \bar{n}_i\,\Delta\xi \tag{55}$$

in which $\bar{x}_{\phi_p}$ refers to the number of moles per 1000 grams of water of the ϕ_pth phase in the system and the superscript (°) designates an earlier stage in the progress of the reaction. Because irreversible reactions are evaluated relative to one mole of the reactant mineral, $\Delta\bar{x}_{\phi_r} = \Delta\xi$ when only one reactant mineral is present. Where more than one mineral reacts irreversibly, $\psi_{(\phi_r/\Phi_r)}$ is treated as a constant and

$$\Delta\bar{x}_{\phi_r} = \psi_{(\phi_r/\Phi_r)}\,\Delta\xi. \tag{56}$$

For multiple reactant minerals, the mole transfer for each reactant is thus computed relative to $\bar{n}_{\Phi_r} = 1$. The mass transfer resulting from an irreversible reaction can be calculated by multiplying $\Delta\bar{x}_{\phi_p}$, Δm_{ϵ}, Δm_i, and $\Delta\bar{x}_{\phi_r}$ by appropriate molecular or atomic weights.

* Equations (53)–(55) are based on the assumption that the reaction coefficients in a given irreversible reaction are essentially constant for a very small increment of reaction progress; i.e. as $d\xi \to 0$, $\int\bar{n}d\xi \approx n\Delta\xi$. Where partial equilibrium is not involved, $\int\bar{n}d\xi = \bar{n}\Delta\xi$ for all values of $d\xi$. The numerical value chosen for $\Delta\xi$ in the calculations depends on the molalities of the species present in the aqueous phase. In practice, $\Delta\xi$ is usually assigned a value several orders of magnitude smaller than the activity of H^+, OH^-, or the total concentration of the element present in the smallest concentration in the initial solution, whichever is the smallest. See *Note added in proof* p. 876.

The mole transfer calculations discussed above define a new composition of the aqueous phase and a new distribution of species in solution after the first $\Delta\xi$ increment in the progress of the reaction. New values of the reaction coefficients can then be computed from the matrix equation and the calculations repeated. For each stage in the progress of the reaction, an ionic strength ($\bar{I}$) is computed for the aqueous phase from

$$\bar{I} = \tfrac{1}{2} \sum_i Z_i^2 m_i + \tfrac{1}{2} \sum_c Z_c^2 m_c \qquad (57)$$

where Z is the charge on the subscripted species in solution. Activity coefficients are then calculated* from $\bar{I}$ along with activity products for the minerals in the system. The computed activity products are compared with the corresponding activity product constants calculated from thermodynamic data† to determine whether the solution has become saturated with respect to any new phases. When this occurs, the differential equation derived from the activity product expression for the new phase is added to the matrix equation along with a column for the unknown reaction coefficient for the phase. Even if the activity of an aqueous species is fixed by the presence of the new product phase, as is the case when the solution becomes saturated (and partial equilibrium is maintained) with respect to quartz, the matrix will not become singular as long as the new differential equation is an independent equation.

Evaluation of irreversible reactions involving minerals and aqueous solutions invariably requires a model for the internal distribution of species in the aqueous phase. Such models usually give rise to predictions of minimal equilibrium mineral solubilities because provision is rarely included for all complexes that actually form to significant degrees in the aqueous phase. For this reason, mass transfer calculations are often minimal approximations of the actual mass transfer involved in a given geochemical process. An adequate model for the internal distribution of species in the aqueous phase is a prerequisite for computing reliable reaction coefficients and predicting accurately the mass transfer resulting from geologic processes involving aqueous solutions.

The approach described above for evaluating irreversible reactions is general, and it can be modified to provide for the geochemical behavior of any given system. If temperature and/or pressure change during an irreversible reaction, the partial equilibrium states adjust accordingly, but the equations and considerations presented above remain the same. If desired, one or another partial equilibrium state can be ignored in the calculations. For example, it may appear from geologic evidence that a given intermediate product mineral did not form in a geochemical process;

* Activity coefficients can be computed for ions and neutral species in concentrated electrolytes from 25° to 300°C using a variety of methods, most of which involve extensions of the Debye–Hückel equation (Butler, 1964; Cobble, 1964; Helgeson, 1964, 1967b, 1968; Garrels and Christ, 1965; Helgeson and James, 1968).

† Activity product constants for a large number of minerals, and dissociation constants for many aqueous complexes can now be predicted for temperatures from 25° to greater than 300°C without introducing large uncertainties in the calculations (Criss and Cobble, 1964; Cobble, 1964; Sillén and Martell, 1964; Helgeson, 1964, 1967a, b, 1968; Garrels and Christ, 1965; Barnes *et al.*, 1966).

accordingly, provision for that mineral can be omitted from the matrix equation. On the other hand, if the evidence indicates the presence of a mineral such as quartz precipitating from a supersaturated solution, provision for this can be included by specifying the degree of supersaturation. In the absence of partial equilibrium, relative reaction rates can be imposed for the formation or disappearance of product minerals in an analogous manner to that presented above for multiple reactants. Where applicable, the reaction rates can be computed from diffusion coefficients. The validity of assuming that a given partial equilibrium state is maintained in a geochemical process often can be assessed by comparing the mole ratios of minerals in the rock with those predicted on the basis of assuming partial equilibrium. Conversely, when partial equilibrium is not maintained, mole ratios of minerals in rocks can be used to set relative reaction rates for the formation of product minerals when evaluating geochemical processes in the manner described above.

Changes in the activities of aqueous species caused by an irreversible reaction can be represented by reaction paths on equilibrium activity diagrams. These changes are computed in the normal course of evaluating an irreversible reaction in order to detect new partial equilibrium states; plotting the changes as reaction paths provides a geometric illustration of the relative changes in the chemical potentials of the oxide components in a system as an irreversible reaction proceeds toward overall equilibrium.

Reaction paths

As with most peritectic reactions, reaction of natural waters with mineral assemblages in geochemical processes usually leads to changes in the composition of the aqueous phase that are rarely in the direction that one would anticipate solely on the basis of the compositions of the solid reactants and products. This can be demonstrated by deriving an expression of the Gibbs-Duhem equation for the slope of an irreversible reaction path on an equilibrium activity diagram such as that illustrated in Fig. 3b. A derivation of this equation for the general case is summarized below.

Slope equation in general notation. Returning to the notation used in equations (1)–(11), we can write

$$\frac{a_{M(i)}}{\gamma_{M(i)}} = m_{M(i)} \tag{58}$$

and combine this with an appropriate statement of equation (55) to give

$$\frac{a_{M(i)}}{\gamma_{M(i)}} = \frac{a_M{}^0{}_{(i)}}{\gamma_M{}^0{}_{(i)}} + \bar{n}_{M(i)}\,\Delta\xi\,. \tag{59}$$

Because the mass transfer resulting from a small increment of progress in most geochemical reactions is small, we can assume (as before in equation 35) that

$$\gamma_{M(i)} = \gamma_M{}^0{}_{(i)} \tag{60}$$

for a small value of $\Delta\xi$.* Dividing equation (59) by $a_{H^+}^{Z_M(i)}$ then results in

* See footnote on p. 865.

$$\frac{a_{M(i)}}{a_{H^+}^{Z_{+(i)}}} = \frac{a_{M^0(i)} + \bar{n}_{M(i)}\,\gamma_{M(i)}\,\Delta\xi}{a_{H^+}^{Z_{+(i)}}}. \tag{61}$$

Differentiating equation (61) and dividing the resulting expression through by $a_{M(i)}/a_{H^+}^{Z_{+(i)}}$ gives

$$\mathrm{d}\ln\frac{a_{M(i)}}{a_{H^+}^{Z_{+(i)}}} = \frac{a_{H^+}\bar{n}_{M(i)}\gamma_{M(i)}\,\mathrm{d}\xi - Z_{+(i)}\,(a_{M^0(i)} + \bar{n}_{M(i)}\,\gamma_{M(i)}\,\Delta\xi)\,\mathrm{d}a_{H^+}}{a_{M(i)}a_{H^+}}. \tag{62}$$

Combining appropriate statements of equations (55), (58), (60) and (62) for two specific components, rearranging, substituting statements of equations (16) and (58) for the hydrogen ion, and simplifying leads to a differential equation describing the slope of an irreversible reaction path for the aqueous phase on a chemical potential or logarithmic activity diagram. This expression, for the oxide components represented by $i = 1$ and $i = 2$, can be combined with equation (10) and written as

$$\frac{\mathrm{d}\mu_1}{\mathrm{d}\mu_2} = \frac{\mathrm{d}(\nu_{+(1)}\log a_{M(1)}/a_{H^+}^{Z_{+(1)}})}{\mathrm{d}(\nu_{+(2)}\log a_{M(2)}/a_{H^+}^{Z_{+(2)}})} = \frac{\nu_{+(1)}m_{M(2)}(\bar{n}_{M(1)}a_{H^+} - Z_{+(1)}m_{M(1)}\bar{n}_{H^+}\gamma_{H^+})}{\nu_{+(2)}m_{M(1)}(\bar{n}_{M(2)}a_{H^+} - Z_{+(2)}m_{M(2)}\bar{n}_{H^+}\gamma_{H^+})} \tag{63}$$

It can be deduced from equation (63) that when the hydrogen ion is not involved in an irreversible reaction, the slope of the reaction path is described by

$$\frac{\mathrm{d}\mu_1}{\mathrm{d}\mu_2} = \frac{\mathrm{d}(\nu_{+(1)}\log a_{M(1)}/a_{H^+}^{Z_{+(1)}})}{\mathrm{d}(\nu_{+(2)}\log a_{M(2)}/a_{H^+}^{Z_{+(2)}})} = \frac{\nu_{+(1)}\,m_{M(2)}\bar{n}_{M(1)}}{\nu_{+(2)}\,m_{M(1)}\bar{n}_{M(2)}}. \tag{64}$$

Equation (64) is represented in Fig. 3a by path AD, which reflects the change in solution composition as phase ϕ_3 reacts with a solution having an initial composition at point A to produce phase ϕ_1. In the case of path AD, $\bar{n}_{M(1)}$ is negative, hydrogen ion is not involved in the reaction, and $m_{M(1)} \gg m_{M(2)}$ in the initial solution. At point D, equilibrium is established between the solution, phase ϕ_1, and phase ϕ_3.

For a reaction that involves the hydrogen ion as well as an aqueous solution in which the activity of the hydrogen ion is initially small relative to the activities of other reactant species, equation (63) can be abbreviated to

$$\frac{\mathrm{d}\mu_1}{\mathrm{d}\mu_2} = \frac{\mathrm{d}(\nu_{+(1)}\log a_{M(1)}/a_{H^+}^{Z_{+(1)}})}{\mathrm{d}(\nu_{+(2)}\log a_{M(2)}/a_{H^+}^{Z_{+(2)}})} \approx \frac{\nu_{+(1)}Z_{+(1)}}{\nu_{+(2)}Z_{+(2)}}. \tag{65}$$

This relation holds as a close approximation as long as $a_{H^+} \ll a_{M(i)}$ so that $\mathrm{d}\log a_{M(1)}/\mathrm{d}\log a_{M(2)} \approx$ a constant. Equation (65) is represented by path AB in Fig. 3a. In this case, phase ϕ_3 reacts with a solution at point A in which the activity of H^+ is much less than the activity of either M(1) or M(2). This reaction produces phase ϕ_1 and the solution changes composition along AB, which has a 1:1 slope consistent with equation (65). At point B, phase ϕ_2 begins to form along with phase ϕ_1. The composition of the solution then changes along the field boundary BC as long as partial equilibrium obtains between phases ϕ_1, ϕ_2, and the aqueous solution. If the system is closed and phase ϕ_3 is present in excess, continued reaction causes the composition of the solution to reach point C, where overall equilibrium is established between phases ϕ_1, ϕ_2, ϕ_3, and the solution.

It can be deduced from the discussion above that the initial changes in the composition of an aqueous phase involved in a given irreversible reaction are primarily controlled by the initial composition and distribution of species in solution. The species involved in the reaction that are present in the smallest concentrations initially are the species whose concentrations are most affected by the reaction.

Open systems and perfectly mobile components. The reaction paths and sequence of events described above are the same for a closed system as well as one that is open to one or more components. However, the extent to which the various reactions take place and the spatial distribution of the phases produced will be different depending on the relative velocity and rate of flow of the solution compared to the diffusion and reaction rates obtaining in the system. A final overall equilibrium state may not be achieved if the system is open, and the mass transfer may be much larger than that in a closed system. In an open system, the aqueous phase may exit from the rock when its composition is at say, point B in Figure 3a. As a result, the distribution of the product phases will be zoned in the rock, and if the entire amount of phase ϕ_3 present in the original rock is available for reaction, the reactant phase may be completely destroyed in the process. The matrix equations (equations 48 and 49) and the mass transfer calculations discussed above for an irreversible reaction taking place in a closed system can also be applied to a system that is open to one or more of its components. To do so requires provision in the matrix equation for specified activities of the mobile components in the system.

Conservation of inert components

It is often advantageous to balance an irreversible reaction by conserving one or another inert component in the system. The phrase "conserving a component" simply means that all of the mass of the component supplied by the reactant mineral is assumed to go into product minerals rather than the aqueous phase. The chemical potential of the inert component is specified by the partial equilibrium states in the system, and it changes to whatever extent is necessary to maintain these partial equilibrium states as the irreversible reaction proceeds. By conserving the component in the reaction we are simply neglecting the corresponding changes in the mass transfer of the component between the product minerals and the aqueous solution. This mass transfer is often negligible in geochemical processes.

The reaction of K-feldspar with an aqueous phase to produce kaolinite and quartz will serve to illustrate the implications and consequences of conserving an inert component when describing an irreversible process. If we write this reaction as

$$KAlSi_3O_8 + H^+ + 0{\cdot}5H_2O \rightarrow 0{\cdot}5Al_2Si_2O_5(OH)_4 + 2SiO_{2(qtz)} + K^+ \qquad (66)$$

we are assuming that the total concentration of aluminum and silica in the aqueous phase is constant as the reaction proceeds. As indicated above, this is not strictly true because the activities of the aluminum and silica species in the aqueous solution and the solubilities of kaolinite and quartz depend on variables such as a_{H^+} that are changing in the aqueous phase as the reaction proceeds. These changes, which are small compared to the total mass transfer, are manifested in the amounts of kaolinite and quartz produced by the irreversible reaction. When Al_2O_3 and SiO_2 are conserved, as in reaction (66), the mass transfer calculations neglect the amounts

of kaolinite and quartz that must be dissolved by, or precipitated from the aqueous solution to maintain the chemical potentials of Al_2O_3 and SiO_2 at the values required for partial equilibrium as the reaction proceeds. Accordingly, the amounts of kaolinite and quartz that are actually produced in the irreversible process will not correspond exactly to the amounts predicted when Al_2O_3 and SiO_2 are conserved in writing the reaction. The differences are negligible for aluminum (and silica when quartz is present) in most irreversible reactions involving partial equilibrium between silicates and an aqueous phase. Because these differences are usually small, conserving one or more inert components is a convenient method of first approximation for calculating the mass of a product mineral produced in a given geochemical process.

Concluding Remarks

From a mathematical standpoint, evaluating irreversible reactions is considerably easier than carrying out equilibrium calculations for multicomponent systems. Equilibrium models reduce to nonlinear equations that can be evaluated only by invoking indirect and unwieldy analytical methods. In contrast, the differential equations describing an irreversible process are all linear, which makes the calculations amenable to rapid machine computation. A general computer program based on the approach presented above has now been written (by A. Nigrini and T. Mundt). This program makes it possible to analyze geochemical processes of considerable complexity in multicomponent systems involving an aqueous phase and large numbers of silicates, sulfides, oxides, carbonates, and sulfates. Oxidation–reduction reactions, and reactions in which metastable phases participate can also be evaluated. In addition to cases where all partial equilibrium states are maintained, equations are being programmed for processes involving given undersaturation and/or supersaturation states, and systems in which multiple reactant minerals are present. In all cases the initial composition of the system and the relative reaction rates for multiple reactant minerals are specified. The partial equilibrium states are used to define the distribution of species in the aqueous phase. The output routine from the program will eventually include both numerical presentation and graphic display of the results of the computations. In addition, thanks to the efforts of T. H. Brown, the machine will produce appropriate projections of the phase diagrams of interest showing the reaction path for the geochemical process under consideration. With thermodynamic data currently available, calculations can be carried out for a large number of multicomponent systems at temperatures from 25° to 300°C (Helgeson, 1968).

Acknowledgments—It is a pleasure to acknowledge the encouraging support and the many stimulating ideas, helpful suggestions, and critical comments contributed to this study by my colleagues, R. M. Garrels and F. T. Mackenzie.

I am also indebted to C. L. Christ, E-an Zen, H. J. Greenwood and G. M. Anderson for their constructive criticism of the paper in various stages of its development, and to A. Nigrini, T. H. Brown, W. R. James and T. A. Jones for rewarding discussions. The work reported here was supported in part by research funds received from Northwestern University, The Petroleum Research Fund of the American Chemical Society, and NSF Grants GP-4140, GE-9758, GU-1700, and GA-828.

Note added in proof. In practice it may not be feasible (owing to expensive computer time) to take $\Delta\xi$ increments that are small enough to achieve accurate mass transfer calculations using equations (53)-(55), which are equivalent to truncated Taylor's expansions of $\bar{x}_{\phi_p}$, m_ξ, and m_i to linear expressions. To reduce the computer time required, and to achieve a higher degree of accuracy in practical computations, additional expansion terms can be added to equations (53)-(55). For example, quadratic Taylor's expansions appear as

$$\Delta\bar{x}_{\phi_p} = n_{\phi_p}\Delta\xi + \bar{n}_{\phi_p}'\frac{(\Delta\xi)^2}{2!}, \tag{a}$$

$$\Delta m_\xi = \bar{n}_\xi\Delta\xi + \bar{n}_\xi'\frac{(\Delta\xi)^2}{2!}, \tag{b}$$

$$\Delta m_i = \bar{n}_i\Delta\xi + \bar{n}_i'\frac{(\Delta\xi)^2}{2!}, \tag{c}$$

where $\bar{n}_{\phi_p}'$, $\bar{n}_\xi'$, and $\bar{n}_i'$ are the second derivatives of equations (45), (46) and (47), respectively, which appear as

$$\sum_{\phi_p} \nu_{\epsilon,\phi_p}\bar{n}_{\phi_p}' + \sum_{\xi} \nu_{\epsilon,\xi}\bar{n}_\xi' + \sum_{i} \nu_{\epsilon,i}\bar{n}_i' = 0, \tag{d}$$

$$\sum_{i}\frac{\nu_{i,\phi_p}\bar{n}_i'}{m_i} = \sum_{i}\frac{\nu_{i,\phi_p}\bar{n}_i^2}{m_i^2}, \tag{e}$$

$$\sum_{i}\frac{\nu_{i,\xi}\bar{n}_i'}{m_i} - \frac{\bar{n}_\xi'}{m_\xi} = \left(\sum_{i}\frac{\nu_{i,\xi}\bar{n}_i^2}{m_i^2}\right) - \frac{\bar{n}_\xi^2}{m_i^2}. \tag{f}$$

After calculating the reaction coefficients in the manner described in the text, their derivatives can be computed from a matrix equation analogous to equations (48) and (49) in which the last column vector on the right side consists of the terms on the right side of equations (d), (e) and (f).

REFERENCES

BARNES H. L., HELGESON H. C. and ELLIS A. J. (1966) Ionization constants in aqueous solutions. In *Handbook of Physical Constants*, Revised Edition (editor S. P. Clark, Jr.). *Geol. Soc. Amer. Mem.* **97**, 401–414.

BARTON P. L., BETHKE P. M. and TOULMIN P., 3rd (1963) Equilibrium in ore deposits. *Min. Soc. Amer. Spec. Paper* **1**, 171–185.

BUTLER J. N. (1964) *Ionic Equilibrium*. Addison-Wesley.

COBBLE J. W. (1964) The thermodynamic properties of high temperature aqueous solutions. VI. Applications of entropy correspondence to thermodynamics and kinetics. *J. Amer. Chem. Soc.* **86**, 5394–5401.

CRISS C. M. and COBBLE J. W. (1964) The thermodynamic properties of high temperature aqueous solutions. V. The calculations of ionic heat capacities up to 200°. Entropies and heat capacities above 200°. *J. Amer. Chem. Soc.* **86**, 5390–5393.

DE DONDER Th. (1920) *Leçons de Thermodynamique et de Chimie-Phisique*. Gauthier-Villars.

FITTS D. D. (1962) *Nonequilibrium Thermodynamics*. McGraw-Hill.

GARDNER E. R., JONES P. J. and DENORDWALL H. J. (1963) Osmotic coefficients of some aqueous sodium chloride solutions at high temperature. *Trans. Faraday. Soc.* **59**, 1994–2000.

GARRELS R. M. and CHRIST C. L. (1965) *Solutions, Minerals, and Equilibria*. Harper and Row.

HELGESON H. C. (1964) *Complexing and Hydrothermal Ore Deposition*. Pergamon.

HELGESON H. C. (1967a) Thermodynamics of complex dissociation in aqueous solutions at elevated temperatures. *J. Phys. Chem.* **71**, 3121–3136.

HELGESON H. C. (1967b) Solution chemistry and metamorphism. In *Researches in Geochemistry*, (editor P. H. Abelson), Vol. II, pp. 362–404. John Wiley.

HELGESON H. C. (1968) Thermodynamics of hydrothermal systems at elevated temperatures and pressures. *Amer. J. Sci.* in press.

HELGESON H. C. and JAMES W. R. (1968) Activity coefficients in concentrated electrolyte solutions of elevated temperatures, an abstract: *Abstracts of Papers, 155th Natl. Meeting, Amer. Chem. Soc.*, April, 1968, San Francisco, California, S-130.

KORZHINSKII D. S. (1959) *Physicochemical Basis of the Analysis of the Paragenesis of Minerals.* Chapman and Hall.

KORZHINSKII D. S. (1963) Thermodynamic potentials of open systems whose acidity and reduction potential are determined by external conditions. *Dokl. Acad. Sci. U.S.S.R.*, A.G.I. Translation, 152, 175–177.

KORZHINSKII D. S. (1964) An outline of metasomatic processes. *Int. Geol. Rev.* 6, 1713–1734, 1920–1952, 2169–2198.

KORZHINSKII D. S. (1965) The theory of systems with perfectly mobile components and processes of mineral formation. *Amer. J. Sci.* 263, 193–205.

ORVILLE P. M. (1963) Alkali ion exchange between vapor and feldspar phases. *Amer. J. Sci.* 261, 201–237.

PRIGOGINE I. (1961) *Introduction to Thermodynamics of Irreversible Processes*, Second Edition. Interscience.

SILLÉN L. G. and MARTELL A. E. (1964) *Stability Constants of Metal–Ion Complexes.* Special Pub. No. 17., The Chemical Society, London.

THOMPSON J. B., JR. (1955) The thermodynamic basis for the mineral facies concept. *Amer. J. Sci.* 253, 65–103.

THOMPSON J. B., JR. (1959) Local equilibrium in metasomatic processes. In *Researches in Geochemistry*, (editor P. H. Abelson), pp. 427–457. John Wiley.

ZEN E-AN (1963) Components, phases, and criteria of chemical equilibria in rocks. *Amer. J. Sci.* 261, 929–942.

ZEN E-AN (1966) Construction of pressure-temperature diagrams for multicomponent systems after the method of Schreinemakers—A geometric approach. *U. S. Geol. Surv. Bull.* 1225.

Contrib. Mineral. Petrol. 53, 55–60 (1975) – © by Springer-Verlag 1975

Experimental Study of $T-X_{CO_2}$ Boundaries of Metamorphic Zeolite Facies

I. P. Ivanov and L. P. Gurevich

Institute of Experimental Mineralogy, Academy of Sciences of the USSR, Chernogolovka

Abstract. The $T-X_{CO_2}$ conditions of reactions: $Lom = Pr + Mont + Qz + H_2O$ and $Lom + H_2O + CO_2 = Ca + Mont + Qz$ limiting the laumontite stability field that represents the zeolite facies of regional metamorphism have been experimentally studied at $P_s = 1000$ bars. The stability of laumontite has been confirmed at very low carbon dioxide contents in the solution. The boundaries of metamorphic zeolite facies were experimentally and thermodynamically found to be (to a first approximation): temperature range ~200–270° C, maximum total pressure (P_s) up to 2500 bars, maximum carbon dioxide pressure up to 40 bars.

Introduction

The zeolite facies of regional metamorphism is known as the lowest in temperature and pressure. It has been described by Coombs in a work on Triassic volcanic and sedimentary rocks from Southland, New Zealand [1]. He subdivided it into a heulandite subfacies with heulandite and analcite (low grade), and a laumontite subfacies where heulandite is being replaced by laumontite, and intensive albitization of analcite and original rock plagioclases is taking place (higher grade).

Fyfe *et al.* [2] and Winkler [3] consider the zeolite facies as composed of the Coombs' laumontite subfacies only, the heulandite subfacies being diagenetic. However the separation of zeolite facies of regional metamorphism is not universally accepted. Thus, Dobretsov and Sobolev [4] share Eskola's viewpoint that the zeolite associations are formed under hydrothermal conditions, depend on solution compositions and that their chemistry and mineralogy and do not conform to metamorphic facies.

In this paper, we are reporting on results of experimental and thermodynamic studies of mineral equilibria corresponding to the metamorphic zeolite facies, which to our mind will contribute greatly to understanding the problem. The choice of the model system has been influenced by:

1. Petrologic data on regionally altered rocks [1, 4–10] show that analcite, albite, quartz, prehnite, montmorillonite and kaolinite occur in paragenetic associations with heulandite and laumontite.

2. The conditions of the actual zeolite formation [11], experimental data on the wairakite decomposition to calcite + montmorillonite [12], geologic evidence and thermodynamic calculations [13–17] indicate that the Ca-zeolites are ex-

Table 1. Minerals of the system $CaO—Al_2O_3—SiO_2—H_2O—CO_2$

Mineral	Mineral abbreviations	Formula
Heulandite	Heu	$CaAl_2Si_6O_{16} \cdot 6H_2O$
Laumontite	Lom	$CaAl_2Si_4O_{12} \cdot 4H_2O$
Prehnite	Pr	$Ca_2Al_2Si_3O_{10}(OH)_2$
Ca-Montmorillonite	Mont	$Ca_{0.44}Al_{2.23}Si_{3.38}O_{9.09}(OH)_{2.91} \cdot nH_2O$
Kaolinite	Kaol	$Al_2Si_2O_5(OH)_4 \cdot mH_2O$
Quartz	Qz	SiO_2
Calcite	Ca	$CaCO_3$

tremely sensitive to the carbon dioxide in the solution and that they are stable at low CO_2 partial pressures of aqueous solutions. In natural paragenesis, analcite occurs in all associations with heulandite, and albite is found in associations with laumontite ("trans" minerals).

Some Considerations

Thus, the phase equilibria in the system $CaO—Al_2O_3—SiO_2—H_2O—CO_2$ might be used to study, to first approximation, zeolite facies. Table 1 gives the minerals in these equilibria.

We are unable as yet to control the fugacities of two volatile components (H_2O and CO_2) of the system independently and simultaneously. Taking this fact into consideration, we assume temperature (T), total pressure (P_s), fugacity (or partial pressure) of one of the volatile components, and mole contents of CaO, Al_2O_3 and SiO_2, as independent parameters defining phase equilibria in the system. The CO_2 fugacity (f_{CO_2}) should be taken as an independent parameter for H_2O and CO_2, since as it follows from the above, it will markedly influence the stability fields of laumontite and heulandite. This holds also for petrologic conditions where metamorphic solutions are essentially a H_2O+CO_2 mixture without appreciable amounts of any other components. The system under study is possibly open to water and carbon dioxide only and therefore it conforms to mineralogy and chemistry of metamorphic facies.

Topological analysis of the $CaO—Al_2O_3—SiO_2—H_2O—CO_2$ system (with due regard to natural mineral paragenesis) revealed stable reactions, shown in Table 2. Our discussion is confined to the reactions with excess quartz because these reactions more closely correspond to regional metamorphism of volcanic and sedimentary rocks. Divergence from stoichcometric equations of the reactions (1)–(9) prevents some difficulties, because Ca-zeolites (laumontite and heulandite) and clay minerals (Ca-montmorillonite and kaolinite) are minerals of "variable water content". The differential thermal analysis has shown that a temperature rise to within 150–200° resulted in intensive release of "zeolite" water from laumontite and heulandite and of absorbed water from Ca-montmorillonite and kaolinite. Water content of these minerals under hydrothermal conditions (depending on T and P_{H_2O}) has not been studied. In Eqs. (1)–(9) k was assumed to be the variation in zeolitic water content at elevated T and P as

Experimental Study

Table 2. Stable reacti

No. of reactions	R
1	1
2	3
3	L
4	0.
5	0.
6	0.
7	C
8	H
9	C

compared with T
and in kaolinite b
The change in
It is petrologic
T, P_s and f_{CO_2} (of t
are monovariant
function of T and
fluid phase enhan
capsule" technique.
been developed inv
The new method of
An impulsive a
initiation of reacti
defined from the t
(1)–(5), Table 2, we
state at low $T-X_C$
siderable difficulty.

Results

The results are sho
system where X_{CO_2} i
$P=1000$ bars (Fig. 1
(1968) data from 50
mentally studied. Th
The diagram of
field is limited in the
to prehnite + montm
The lower boundary
transition to heuland
is limited by reaction
of clay minerals. Ma
nearly corresponds to
prehnite association i
mineral association i

Table 2. Stable reactions in the system $CaO—Al_2O_3—SiO_2—H_2O—CO_2$ with excess quartz

No. of reactions	Reactions
1	$1.6\,Ca + 0.89\,Mont = Pr + (0.29 + n)H_2O + 1.6\,CO_2$
2	$3.58\,Lom = 1.35\,Pr + 2\,Mont + 3.51\,Qz + (10.06 - 3.58k - 2n)H_2O$
3	$Lom + Ca = Pr + Qz + (3 - k)H_2O + CO_2$
4	$0.6\,Ca + 0.89\,Mont + Qz = Lom + (0.89n + k - 2.72)H_2O + 0.6\,CO_2$
5	$0.88\,Ca + 2.23\,Kaol + 2.3\,Qz = 2\,Mont + (1.55 + 2.23m - 2n)H_2O + 0.88\,CO_2$
6	$0.88\,Lom + 1.35\,Kaol + 0.54\,Qz = 2\,Mont + (3.31 - 0.88k + 1.35m - 2n)H_2O$
7	$Ca + Kaol + 2\,Qz = Lom + (m + k - 2)H_2O + CO_2$
8	$Heu = Lom + 2\,Qz + 2\,H_2O$
9	$Ca + Kaol + 4\,Qz = Heu + (m + k - 4)H_2O + CO_2$

compared with Table 1. Water content in Ca-montmorillonite is denoted by n, and in kaolinite by m, as in Table 1.

The change in values of k, n and m over certain ranges are to be determined.

It is petrologically important first to evaluate external (intensive) parameters T, P_s and f_{CO_2} (of the general form μ_{CO_2}). At P_s = const. all the reactions of Table 2 are monovariant and their equilibria might be (experimentally) studied as a function of T and μ_{CO_2}. Maintaining definite CO_2 mole content (fraction) in the fluid phase enhances the μ_{CO_2} control in experiments carried out by the "big capsule" technique. To obtain more reliable results a new precision technique has been developed involving the introduction of pure carbon dioxide into the system. The new method of dose CO_2 in an Ag capsule by freezing was used [18, 19].

An impulsive ampule shaker was also designed and successfully used for initiation of reactions, which permitted the equilibria to be more accurately defined from the two sides. In our experiments with equilibria of the reactions (1)-(5), Table 2, we found as expected, that these reactions attain equilibrium state at low $T-X_{CO_2}$ values and their experimental identification presents considerable difficulty.

Results

The results are shown on the temperature-mole fraction of CO_2 diagram of the system where X_{CO_2} is the mole fraction in the mixture $H_2O + CO_2$ (fluid phase) at $P = 1000$ bars (Fig. 1). The reaction (8) boundary is an extrapolation of Nitsch's (1968) data from 5000 to 1000 bars. Reactions (7) and (9) have not been experimentally studied. The lines 7 and 9 are as from topological analysis.

The diagram of Fig. 1 shows that at $P = 1000$ bars the laumontite stability field is limited in the upper part by the decomposition reactions (2) of laumontite to prehnite + montmorillonite accompanied by water removal at $T = 260$–$270°$ C. The lower boundary of this field is represented by reaction (8) of laumontite transition to heulandite (hydration reaction) at $T \sim 220°$ C. On the right the field is limited by reactions (4) and (7) of laumontite carbonization with the formation of clay minerals. Maximum CO_2 content in the fluid is 2.0–2.3% (mole) which nearly corresponds to the CO_2 partial pressure $P_{CO_2} = 20$–23 bars. The laumontite-prehnite association is seen to be stable in the upper part and the laumontite-clay-mineral association is stable in the lower zones of this field. Heulandite field

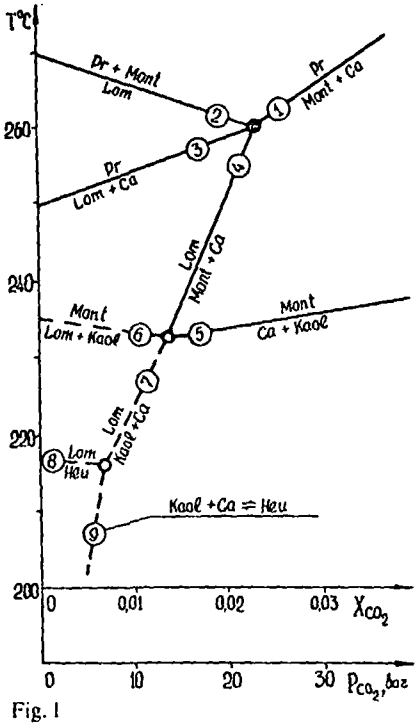

Fig. 1

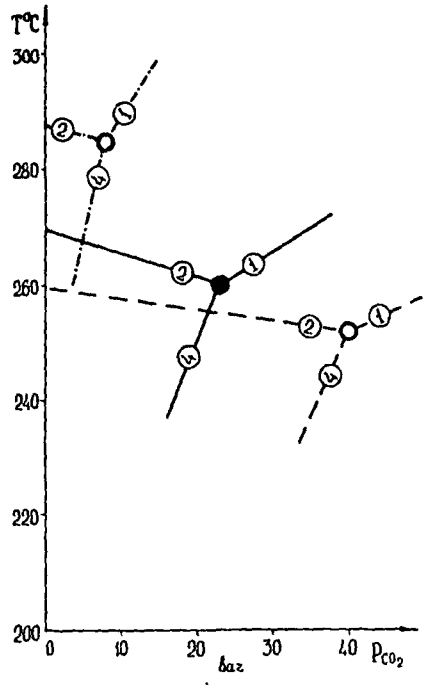

Fig. 2

Fig. 1. The $T-X_{CO_2}$ diagram of stability fields of laumontite, heulandite, prehnite and Ca-montmorillonite in the system $CaO-Al_2O_3-SiO_2-H_2O-CO_2$. Lines 1, 2, 3, 4, 5 – as established by the authors; line 8 – after Nitsch (1968); lines 6, 7 – according to topological construction

Fig. 2. Displacement of the laumontite stability boundaries as a function of P_s. Solid lines – at P_s = 1000 bars; dotted lines – at P_s = 500 bars; dash-dot lines – at P_s = 2500 bars. Numbers of reactions are same as in Fig. 1

bounded by reactions (8) and (9) extends into the temperature region of lower than 200° C, and P_{CO_2} of 10 bars. Lower boundaries of the prehnite reactions (1) and (3) and Ca-montmorillonite reactions (5) and (6) stability fields are also distinctly seen on the diagram. Prehnite and Ca-montmorillonite turned out to be less sensitive to P_{CO_2} changes in the solution. Kaolinite is a lower-temperature mineral than Ca-montmorillonite.

In accordance with Table 2 and Fig. 1, there are two types of stable reactions in this system: net hydration reactions: (2), (6) and (8) and coupled hydration-carbonization reactions: (1), (3), (4), (5), (7) and (9). We have experimentally established that in the temperature range 220–300° C the coupled hydration-carbonization reactions involving laumontite and calcite proceed at fairly high rates. Thus, at P_s = 1000 bars, the reaction (4) rate is comparable with that of the decomposition reaction muscovite = potassium feldspar + corrundum + H_2O in the range 550–650° C. Reaction 5 involving clay minerals and calcite is very sluggish and therefore it should be initiated to attain equilibrium from two sides (kynetic method of "monovariant association"). This is also true for a net hydration reaction and especially for reaction (8).

Experimental Study

The total pr
carbonization h
thermodynamic

$$\lg X_{CO_2} = \frac{-(}{}$$

where X_{CO_2} is th
values; ΔG_T^0 – sta
curve (Fig. 1) for
the reaction; n_{CO}
equation of the re
nents. This expre
and CO_2, and m
(less than 3% mc

We have calcu
laumontite and p
slope of line 2 wa
by the intersectio
dependent change
water content in r
ever, it could be
P_s = 500 bars appr
of higher CO_2 par
field smaller. At
practically "wedge

Summary

1. According to Tu
comprises stable as
reasonable. Isocher
therefore heulandit

Local accumula
solutions on rocks
distinguished withi
clay-laumontite.

2. Associations
stable only at low C
facies are likely to b
pressure $P_s \sim 2500-$
$P_{CO_2} \sim 40-60$ bars. T
be established from i
and of quartz-clay-c

Acknowledgements. T
for useful suggestions an

The total pressure effect on the equilibria of coupled reactions hydration-carbonization has not been studied. It was defined to a first approximation by thermodynamic calculations of a formula:

$$\lg X_{CO_2}=\frac{-(\Delta G_T^0+\Delta V_s P_s+n_{CO_2}\cdot 4.576\cdot T\cdot \lg f^*_{CO_2}+n H_2O\cdot 4.576\cdot T\cdot \lg f^*_{H_2O})}{n_{CO_2}\cdot 4.576\cdot T}$$

where X_{CO_2} is the CO_2 mole fraction in the mixture H_2O+CO_2 at given P_s and T values; ΔG_T^0 – standard free energy of the reaction calculated by the experimental curve (Fig. 1) for T and $P_s=1000$ bars; ΔV_s – the molar volume change of solids in the reaction; n_{CO_2} and n_{H_2O} – stoichiometric coefficients of CO_2 and H_2O in the equation of the reaction; $f^*_{CO_2}$ and $f^*_{H_2O}$ – fugacities of pure CO_2 and H_2O components. This expression does not consider the mixing energy of real gases H_2O and CO_2, and may be used for calculations at low CO_2 contents in the fluid (less than 3% mol.).

We have calculated the equilibria of reactions (1), (2), (3) and (4) bounding the laumontite and prehnite stability fields for $P_s=500$ and 2500 bars (Fig. 2). The slope of line 2 was determined by two points at $X_{CO_2}=0$ and X_{CO_2} as determined by the intersection of lines 1, 3 and 4. Allowances were made for T- and P_{H_2O}-dependent changes in the zeolite-water content in laumontite and in the absorbed-water content in montmorillonite. The values in Fig. 2 are only tentative. However, it could be clearly seen on the diagram that lowering total pressure to $P_s=500$ bars appreciably enlarges the stability field of laumontite into the zone of higher CO_2 partial pressure. Increase in total pressure, in contrast, makes this field smaller. At $P_{CO_2}\sim 50$–60 bars and $P_{H_2O}\sim 2500$ bars the laumontite field practically "wedges out".

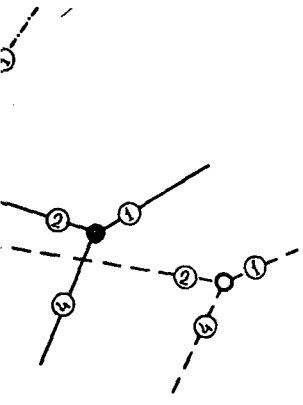

idite, prehnite and Ca-mont-
3, 4, 5 – as established by the
construction

on of P_s. Solid lines – at $P_s=$
bars. Numbers of reactions

rature region of lower
prehnite reactions (1)
tability fields are also
rillonite turned out to
is a lower-temperature

pes of stable reactions
d coupled hydration-
have experimentally
e coupled hydration-
proceed at fairly high
rable with that of the
corrundum + H_2O in
s and calcite is very
rium from two sides
ue for a net hydration

Summary

1. According to Turner and Winkler, the zeolite facies of regional metamorphism comprises stable associations with laumontite only. This theory seems to be most reasonable. Isochemical reactions yielding heulandite are sharply inhibited, and therefore heulandite must be epigenetic.

Local accumulations of heulandite result from the action of hydrothermal solutions on rocks involved in hydrolysis reactions. Two subfacies might be distinguished within the zeolite facies: quartz-prehnite-laumontite and quartz-clay-laumontite.

2. Associations with laumontite have been experimentally verified to be stable only at low CO_2 contents in the fluid. The external parameters of the zeolite facies are likely to be as follows; temperature range 200–270° C; maximum total pressure $P_s\sim 2500$–3000 bars; maximum partial pressure of carbon dioxide $P_{CO_2}\sim 40$–60 bars. The boundary between epigenic zone and zeolite facies could be established from isochemical reactions of transition of heulandite to laumontite and of quartz-clay-carbonate association to associations with laumontite.

Acknowledgements. The authors are grateful to Pr. A. A. Marakushev (Moscow State Universitet) for useful suggestions and comments.

References

1. Coombs, D.S.: The nature and alteration of some Triassic sediments from Southland, New Zealand. Roy. Soc. New Zealand Trans. 82, 65–102 (1954)
2. Fyfe, W.S., Turner, F.J., Verhoogen, J.: Metamorphic reactions and metamorphic facies. Geol. Soc. Am. Mem. 73, – (1958)
3. Winkler, H.J.F.: Abolition of metamorphic facies, introduction of the four divisions of metamorphic stage, and a classification based on isogrades in common rocks. Neues Jahrb. Mineral. Monatsh. 5, 189–284 (1970)
4. Dobretsov, N.L., Sobolev, V.S., Khlestov, V.V.: Intermediate-pressure Metamorphic Facies. [In Russian] Moscow: Nedra Press 1972
5. Coombs, D.S.: Zeolitized tuffs from the Kuttung glacial beds near Seaham. N.S.W. Australian J. Sci., 21, 18–19 (1958)
6. Coombs, D.S.: Lower-grade mineral facies in New Zealand. Report of 22-sess. Norden, 13, 339–351 (1960)
7. Crook, K.A.W.: The Geological Evolution of the Southern Portion of the Tamworth Trough., Ph.D. thesis, Univ. of New England, 1959
8. Packham, G.H., Crook, K.A.: The principle of diagenetic facies and some of its implications. J. Geol. 68, 392–407 (1960)
9. Dickinson, W.K.: Petrology and diagenesis of Jurassic andesitic strata in Central Oregon. Am. J. Sci. 260, 481–500 (1962)
10. Otalora, G.: Zeolites and related minerals in Cretaceous rocks of east-central Puerto-Rico. Am. J. Sci. 262, 726–734 (1964)
11. Ellis, H.J.: The chemistry of some explored geothermal systems. In: Geochemistry of Hydrothermal Ore Deposits (Barnes, ed.), p. 465–574. New York: publisher 1967
12. Liou, J.G.: P—T stabilities of laumontite, wairakite, lawsonite and related minerals in the system $CaAl_2Si_2O_8$—SiO_2—H_2O. J. Petrol. 12, 379–411 (1971)
13. Zen, E-An: Clay mineral-carbonate relations in sedimentary rocks. Am. J. Sci. 257, 29–43 (1959)
14. Zen, E-An: The zeolite facies: an interpretation. Am. J. Sci. 259, 401–409 (1961)
15. Senderov, E.E., Khitarov, N.I.: Zeolites, Synthesis and Formation in Nature. [In Russian]. Moscow: Nauka Press 1970
16. Thompson, A.: P_{CO_2} in low-grade metamorphism. Zeolite, carbonate, clay mineral, prehnite relations in the system CaO—Al_2O_3—SiO_2—H_2O. Contrib. Mineral. Petrol. 33, 145–161 (1971)
17. Ernst, W.G.: CO_2-poor composition of the fluid attending Franciskan and Sanbagawa low-grade metamorphism. Geochim. Cosmochim. Acta. 36, 497–504 (1972)
18. Ivanov, I.P., Gurevich, L.P.: New experimental data on boundaries of the zeolite metamorphic facies. [In Russian], Izv. Acad. Sci. USSR. Geol. Ser. 3, 17–28 (1973)
19. Ivanov, I.P.: Experimental study of mineral equilibria in metamorphic and metasomatic processes. [In Russian], Trudy Inst. Phisiki Tverdogo Tela, Acad. Sci. of USSR, Moscow, 1970
20. Nitsch, K.H.: Die Stabilität von Lawsonit. Naturwissenschaften 55, 388 (1968)

Dr. I.P. Ivanov
Institute of Experimental Mineralogy
Academy of Sciences of USSR
Chernogolovka, Moscow district
USSR

Received May 16, 1975; Accepted June 23, 1975

FLUORINE CHEMISTRY

Edited by

J. H. SIMONS

University of Florida, Gainesville, Florida

VOLUME V

1964

ACADEMIC PRESS · NEW YORK and LONDON

The rare earth oxyfluorides were prepared by Popov and Knudson[554] by treating the fluoride at 800° for about 100 hours with air, nitrogen, ammonia, or hydrogen containing water vapor. LaOF, NdOF, SmOF, EuOF, and GdOF were prepared using air or nitrogen as the carrier gas and CeOF, PrOF, and TbOF using hydrogen. Cerium oxyfluoride was made by Finkelnburg and Stein[225] by baking a mixture of CeO_2 and CeF_2 for 5–30 min at 3000°K. Its crystal structure was studied. Mazza and Jandelli[465] studied the structures of PrOF, NdOF, and SmOF.

XXI. Actinide Metal Fluorides

Thorium tetrafluoride, ThF_4, was prepared by Lipkind and Newton[435] by the reaction of ThH_4 with hydrogen fluoride at 350°. Its vapor pressure in the solid phase from 1055 to 1297°K is given by the equation $\log_{10} P_{atm} = 9.105 - 16{,}860/T$ and in the liquid phase from 1437 to 1595°K by $\log_{10} P_{atm} = 7.940 - 15{,}270/T$, according to Darnell and Keneshea[161]. It is monomeric in the vapor. The X-ray diffractions of its hydrates were reported by D'Eye and Booth[169]. Zachariasen[812] reported the crystal structure of α-K_2ThF_6, α-Na_2ThF_6, $ThOF_2$, $CaThF_6$, $SrThF_6$, $BaThF_6$, $PbThF_6$, ThF_4, and $NaTh_2F_9$. Thoma *et al.*[733c] reported the compound $NaF \cdot BeF_2 \cdot 3ThF_4$ melting at 745°; and Thoma and Carlton[733b] found $3CsF \cdot ThF_4$ melting at 980°, $2CsF \cdot ThF_4$ melting at 869, and $CsF \cdot ThF_4$ melting at 830°.

Protactinium tetrafluoride PaF_4 was prepared by the action of a hydrogen–hydrogen fluoride mixture on protactinium dioxide at 600° by Sellers *et al.*[658]. It is a reddish brown solid that reacts with moist oxygen when heated. It is a starting material for the preparation of the metal. By the action of bromine tri- or pentafluoride on protactinium oxide a volatile compound was formed that may be the pentafluoride or an oxyfluoride. Because of the ability to separate protactinium from thorium with a stream of hydrogen fluoride above 450°, Schulz[636] also assumed a volatile compound of this kind. A complex salt K_2PaF_7 was also reported.

The preparation of uranium trifluoride has been studied in various laboratories. The methods all consist of the reduction of UF_4. Katz and Robinowitch[388] discussed a number of these. Reduction with hydrogen is not very satisfactory but is accomplished at 1000° if the UF_4 is very pure and both water and oxygen are rigorously excluded. Reduction with uranium metal at 1140°C gave a satisfactory product according to Warf[761]. The temperature must not be much higher than this because of the reversal of the reaction. Runnalls[602] found that aluminum could be used at 900° with the formation and volatilization of AlF. At 1200° UF_3 combines with NaF to form Na_2UF_5 according to D'Eye and Martin[171]. Crystallographic data for UF_3 was reported by Staritsky and Douglass[711].

As prepared, uranium trifluoride appears black; but under the microscope the crystals are violet red in color. The melting point is not known, because above 1000° the compound reacts with itself to form the metal and the tetrafluoride. Its crystal structure was discussed by Katz and Robinowitch[388]. It is only slowly affected by most air; but if heated to 900°, it is converted to U_3O_8. Water reacts with it at 100°. Acids react only slowly unless oxidizing. Oxidizing agents react rapidly. Chlorine reacts to form UF_3Cl. It can be reduced to the metal by an excess of calcium.

The details of the preparation of uranium tetrafluoride, UF_4, have been extensively investigated in the various atomic energy programs. These are described at considerable length in the book, "The Chemistry of Uranium"[388]. From aqueous solutions the hydrate $UF_4 \cdot 2.5H_2O$ is precipitated by the addition of fluoride ion usually from hydrofluoric acid to a solution containing U^{4+} ions. The U^{4+} ions are frequently obtained by reduction of a uranate, UO_4^{2-}, or uranyl, UO_2^{2+}, solution by various reducing agents. The material obtained in these ways contains impurities in addition to H_2O. This hydrate can be converted to the monohydrate, $UF_4 \cdot H_2O$, by drying at 100°. At 400° this monohydrate loses water, but the product UF_4 is contaminated by products of both hydrolysis and oxidation. If this dehydration is done under reduced pressure and in the presence of hydrogen fluoride vapor, a purer product results.

Anhydrous UF_4 can be obtained purer, if aqueous solutions are avoided. At 500–750° a mixture of ammonia and hydrogen fluoride will convert UO_3 to UF_4. Uranium trichloride reacts at 450° with hydrogen fluoride to give the tetrafluoride and hydrogen. Uranium oxides with ammonium bifluoride at 700° give UF_4. At 450° NH_4UF_5 is obtained. Uranium tetrachloride reacts with liquid hydrogen fluoride to give a product which appears to be $UF_4 \cdot HF$. Upon heating in a vacuum at 625°, hydrogen fluoride is lost and UF_4 formed. Pure anhydrous UF_4 can be obtained from the pure metal by first converting it to UH_3 with hydrogen at 250° and then treating this with hydrogen fluoride at 200°. Sohoo and Patnaik[704] stated that UF_4 resulted from the reaction of uranium tetraacetate and ammonium bifluoride at 450° under vacuum.

Uranium tetrafluoride is a green crystalline solid only 0.10 gm soluble in a liter of water and rather inert chemically. At elevated temperatures particularly above 600°, UF_4 is converted by water to UO_2. In the presence of oxygen, UO_2F_2 is formed. With elementary fluorine at different temperatures and under different conditions higher fluorides of uranium are formed up to UF_6. These reactions have been very extensively studied as means of preparing UF_6 for the thermal diffusion process of separating the uranium isotopes. Above 250° UF_6 is the principle product. It can

also be obtained by the reaction of UF_4 with CoF_3. Uranium tetrafluoride reacts with dilute acids to give tetravalent uranium salts. Dilute sulfuric acid and silica result in $U(SO_4)_2$ for example. It also will react at 250–500° with $AlCl_3$ to form UCl_4. Oxidizing acids form uranyl ion solutions as do most strong oxidizing agents. Terebaugh *et al.*[732] described ways to obtain U_3O_8 from UF_4. Fusion with ammonium oxalate is one method and treatment at 800 to 850° with superheated steam is another. Robinson[581] reported that above 630° calcium sulfate will react to form U_3O_8 by the reaction $6CaSO_4 + 3UF_4 \xrightarrow{630-730°} 6CaF_2 + U_3O_8 + 2SO_2 + 4SO_3$.

The reaction of uranium tetrafluoride with oxygen at 800° to form UF_6 and UO_2F_2 was apparently first reported by Fried and Davidson[251]. This is a method of obtaining UF_6 without the use of elementary fluorine. A patent to Haimer[292] discloses the same method. Ferris[221,222] showed that some UF_5 results in this reaction, probably from the combination of UF_6 with UF_4; and he studied both the thermodynamics and kinetics of the reaction.

The melting point of UF_4 is 960 ± 5°. It has a vapor pressure of 1.9×10^{-4} mm Hg at 760°. Langer and Blankenship[424a] reported the vapor pressure of liquid UF_4 between 1018 and 1302°K to follow the equation $\log_{10} P_{mm} = 37.086 \pm 0.03 - 16.840 \pm 44T^{-1} - 7.549 \log T$. This gives a boiling point of 1729°K and a ΔS of vaporization = 29.7 e.u. Its crystal structure was discussed by Katz and Rabinowich[388] and its crystallographic data reported by Shanker, Khubchandani, and Padmanabham[665]. The heat capacity of uranium tetrafluoride was determined from 5 to 300°K by Osborne, Westrum, and Lohr[524]. As the measurements below 20° differ considerably from the extrapolation given by Brickwedde, Hoge, and Scott[87] in this temperature range, some changes in the thermodynamic properties result. At 298.16°K $C_p = 27.73 \pm 0.03$ cal per deg per mole, $H^0 - H_0^0 = 5389 \pm 6$ cal per mole, and $S^0 - S_0^0 = 36.13 \pm 0.04$ cal per deg per mole.

Uranium tetrafluoride forms double salts with metal fluorides $NaUF_5$, Na_2UF_6, Na_3UF_6, KUF_5, K_2UF_6, K_3UF_7, $K_2U_2F_9$, and KU_6F_{25} are mentioned and crystal properties studied. Some of them exist in several crystal forms. Thoma *et al.*[733c] reported the compound $NaF \cdot BeF_2 \cdot 3UF_4$ which melted at 548°. Harris[304a] studied the crystal structure of Rb_3UF_3 and [304b] RbU_6F_{25} which he found isomorphous with KU_6F_{25} and KTh_6F_{25}.

The intermediate uranium fluorides αUF_5, βUF_5, U_2F_9, and U_4F_{17} are mentioned in Volume I of "Fluorine Chemistry" and discussed in detail in "The Chemistry of Uranium"[388], and also in two books of the United States Atomic Energy Commission[713] and in individual reports such as the one of Argon *et al.*[3]. There are very few additional recent studies of them.

Uranium hexafluoride, UF_6, can be made by the action of elementary fluorine on the metal or any of its compounds. It was first prepared in this way using either the metal or its carbide. Because of the importance of producing large quantities of the compound for the atomic energy program, many methods were devised for producing it using less elementary fluorine or none and also avoiding the use of the pure metal. The fluorination of the tetrafluoride by either F_2 or CoF_3 is one such method. In this reaction the pentafluoride is first produced, if the reaction temperature is less than 250°; and the hexafluorine results from its further fluorination. Uranium oxide, U_3O_8, reacts with fluorine at 360° or at 300°, if mixed with carbon. Hydrogen fluoride reacts at 500° with U_3O_8 to form UO_2F_2 and UF_4. This mixture produces UF_6 on further fluorination.

It has been mentioned above that UF_4 reacts with oxygen to form UF_6 and UO_2F_2. With hydrogen fluoride UCl_5 can be converted to UF_5, at 175° UF_5 is converted into U_2F_5 and UF_6, and above 200° U_2F_9 goes to UF_4 and UF_6. By the following reactions,

$$12UCl_5 + 6OHF \rightarrow 12UF_5 + 6OHCl$$

$$12UF_5 \xrightarrow{175°} 4U_2F_9 + 4UF_6$$

$$4U_2F_9 \xrightarrow{200°} 6UF_4 + 2UF_6$$

$$6UF_4 + 3O_2 \rightarrow 3UO_2F_2 + 3UF_6$$

$$12UCl_5 + 6OHF + 3O_2 \rightarrow 9UF_6 + 3UO_2F_2 + 6OHCl$$

three-fourths of the uranium in the pentachloride can be converted to UF_6 without the use of elementary fluorine. It is also reported by Rosen[598] that UCl_6 reacts with hydrogen fluoride at 60 to 150° to produce UF_6.

Uranium hexafluoride is a very reactive chemical. It reacts with water readily to produce UO_2F_2 and hydrogen fluoride. This reaction has been studied by Googin[275]. It also reacts with glass or quartz, particularly in the presence of water or hydrogen fluoride. Hydrogen fluoride is equivalent to water for this reaction, as it produces water from silica. As all glass has water on its surface and as hydrogen fluoride is a common impurity in UF_6, glass or quartz vessels cannot usually be used to contain it. If the UF_6 is freed from HF and the glass thoroughly dried, the action is slower; and it can be still further reduced by adding dry KF or NaF as shown by Grosse[281]. These salts combine with both HF and H_2O. They also add to SiF_4 so that they remove reacting molecules. Copper, nickel, and aluminum are satisfactory material for equipment for handling UF_6.

Uranium hexafluoride does not react with oxygen, nitrogen, chlorine, or bromine gases. It dissolves in liquid chlorine and bromine and can react with carbon dioxide. It dissolves without reaction in liquid fluorocarbons.

It reacts with hydrogen above 400° but only complex products are produced, and the reaction gives evidence of being one having a large energy of activation. Hydrocarbons and other organic compounds will reduce it at room temperature but SO_2 does not at 150°. Johns *et al.*[272] found that ammonia reacts rapidly at −80° to reduce it to a mixture of products one of which is NH_4UF_5. Hydrogen bromide at 80° and hydrogen chloride at 300° reduce it to UF_4 and hydrogen fluoride with the formation of the free halogen. At 500° UF_6 reacts with UO_2 to form UO_2F_2 and UF_4 according to Rampy[561]. In a study of the freezing solubilities of the UF_6—HF system. Rutledge, Jarry, and Davis[604] concluded that no complex compound exists between these two substances. Grosse[281] affirms that no combination occurs between sodium or potassium fluoride and uranium hexafluoride in the absence of hydrogen fluoride and that the combination contains only one mole per mole of hydrogen fluoride, when it is present. He also states that $KF \cdot HF$ does not react with UF_6. Other workers find the complex $UF_6 \cdot 3NaF$ to be formed. Martin, Albers, and Dust[457] reported this compound, Massoth and Hensel[460] studied the kinetics of the reaction even as low as 24°, and Cathers, Bennett, and Jolley[116] measured the vapor pressure of UF_6 from the complex and agreed with Martin, Albers, and Dust[457] that between 200 and 450°, $UF_6 \cdot 3NaF \rightarrow UF_5 \cdot NaF + 2NaF + 0.5F_2$ and above 450°, $UF_5 \cdot NaF \rightarrow UF_4 \cdot NaF + 0.5F_2$. Worthington[805] also found that NaF and UF_6 combined at 80–130° to form Na_3UF_9 which at 150° and low pressure gives Na_3UF_7 and F_2. Rüdorff and Leuther[601] reported Na_3UF_8 by treatment of Na_3UF_7 with F_2 at 390–400°. In copper at 410° NaF and UF_6 resulted. Martin, Albers, and Dust[457] reported that UF_6 also combines below 100° with AgF, KF, and RbF as well as NaF to form UF_6—3AgF, $UF_6 \cdot 3NaF$, $2UF_6 \cdot 3KF$, and $UF_6 \cdot 2RbF$(?).

The physical properties of uranium hexafluoride have been extensively studied. For a thorough treatment the various reports of the atomic energy commissions, authorities, and conferences, should be consulted, for example, the survey by De Witt[168a]. The melting point is given as 64.052°C. Oliver, Milton, and Grisard[520] determined its vapor pressure and critical constants. The vapor pressure of the solid (0 to 64°) was found to be represented by the equation $\log_{10} P_{mm} = 6.38363 + 0.0075377t - 942.76/(t + 183.416)$. Similarly the vapor pressure of the liquid from 64 to 116° is $\log_{10} P_{mm} = 6.99464 - 1126.288/(t + 221.963)$ and above 116°, $\log_{10} P_{mm} = 7.69069 - 1683.165/(t + 302.148)$. The critical temperature = 230.2 ± 0.2° and the critical pressure = 45.5 ± 0.5 atm. Triple point = 64.02 ± 0.05°. ΔH at triple point = 6.82 kcal per mole. The heat of sublimation at 25° = 11.80 kcal per mole and at 56.54° and one atmosphere = 11.50 kcal per mole. The heat of fusion at the triple point is

4.58 kcal per mole. As
energy of formation
$H - H_0 = 9865.0$
$S - S_0 = 125.59 - 20.$
UF_6, $H - H_0 = 598$
$S - S_0 = -50.33 +$
precision of the above is
$0.003968T^2 + 320,680$
$0.007935T + 160,340$
$\rho = 3.630 - 5.805 \times 1$
The viscosity, $\epsilon \times 10^4$
surface tension in dynes
at 90° = 14.3 ± 0.3, a
essentially zero. The di
molar polarization was
31.034 by Magnuson[44

The crystal structur
and Stroupe[331]. Thes
molecular structure as
structure would satisf
measurements of Bauer
the Raman spectrum b
by Gaunt[254], and by
by Burke, Smith, and
structure not only for
ReF_6, OSF_6, IrF_6, Np
stock and Malm[765] g
diffraction measuremen

The crystal structu
determined by Zacha
$\alpha KLaUF_6$, UF_3, SrUF

Uranium forms co
atom is attached to the
Warf and Baenzigen[7
first of these, $UClF_3$,
proportionates to UCl_4
is stable below 100°C.
of UF_3 and the haloge
CCl_4 in the liquid pha

Uranyl fluoride, U
questionable dihydrate
in hydrofluoric acid.

4.58 kcal per mole. As reported by Katz and Rabinowich[388], the free energy of formation $\Delta F_{298°K} = -485$ kcal per mole. For solid UF_6, $H - H_0 = 9865.0 - 20.082T + 0.080790T^2 - 1{,}047{,}920T^{-1}$, $S - S_0 = 125.59 - 20.082 \ln T + 0.1612T - 523{,}960T^{-2}$. For liquid UF_6, $H - H_0 = 5986.6 + 17.954T + 0.032514T^2 - 666{,}990T^{-1}$, $S - S_0 = -50.33 + 17.954 \ln T + 0.065028T - 333{,}490T^{-2}$. The precision of the above is $\pm 0.01\%$. For gaseous UF_6 $H = 8460 + 32.43T + 0.003968T^2 + 320{,}680T^{-2}$ cal per mole. $S_{(1\ atm)} = 74.69 \log T + 0.007935T + 160{,}340T^{-2} - 98.05$ e.u. The density of liquid UF_6, $\rho = 3.630 - 5.805 \times 10^{-3}(t - t_f) - 1.36 \times 10^{-5}(t - t_f)^2$, $t_f = 64.052°C$. The viscosity, $\epsilon \times 10^4$ poises $= 1.67 - 0.0044t$, t in °C, $\pm 2\%$. The surface tension in dynes per cm at 70° = 16.8 ± 0.3, at 80° = 15.6 ± 0.3, at 90° = 14.3 ± 0.3, and at 100° = 13.1 ± 0.3. The dipole moment is essentially zero. The dielectric constant of the liquid at 65° = 2.18. The molar polarization was given as 27 ± 0.3 by Smyth and Hannay[702] and 31.034 by Magnuson[445].

The crystal structure of uranium hexafluoride was reported by Hoard and Stroupe[331]. These measurements are not critical in regard to the molecular structure as either a totally symmetrical or an unsymmetrical structure would satisfy the measurements. The electron diffraction measurements of Bauer[53] indicated an unsymmetrical structure, although the Raman spectrum by Claassen, Weinstock, and Malm[125], the infrared by Gaunt[254], and by Hawkins, Mattraw, and Carpenter[309], and both by Burke, Smith, and Nielsen[100] strongly favor a totally symmetrical structure not only for UF_6 but also for MoF_6, WF_6, SF_6, SeF_6, TeF_6, ReF_6, OSF_6, IrF_6, NpF_6, and PuF_6. Using a symmetrical model Weinstock and Malm[765] gave 1.994A as the U—F distance from electron diffraction measurements.

The crystal structures of a number of uranium compound were determined by Zachariasen[813]. These include αK_2UF_6, αNa_2UF_6, $\alpha KLaUF_6$, UF_3, $SrUF_6$, $BaUF_6$, $PbUF_6$, UF_4, K_3UF_7, and U_2F_9.

Uranium forms compounds in which more than one kind of halogen atom is attached to the fluorine atom. In the tetravalent uranium fluorides Warf and Baenzigen[761] found $UClF_3$, UCl_2F_2, $UBrF_3$, UIF_3. The first of these, $UClF_3$, is stable but cannot be volatilized. UCl_2F_2 disproportionates to UCl_4 and UF_4, $UBrF_3$ is stable below 450°, and UIF_3 is stable below 100°C. The first and last two were made by the reaction of UF_3 and the halogen; UCl_2F_2 was made by the reaction of UO_2F_2 and CCl_4 in the liquid phase under pressure at 130°.

Uranyl fluoride, UO_2F_2, as the mono hydrate, $UO_2F_2 \cdot H_2O$, or a questionable dihydrate can be obtained by dissolving a uranium oxide in hydrofluoric acid. The anhydrous compound can be prepared by

treating UO_3 with HF at 350 to 500° or by the action of fluorine with a uranium oxide at 350°. It is also one of the products of the oxidation with oxygen of UF_4 to form UF_6. It is hydroscopic and significantly soluble in water, 67.3wt% at 35°. Its aqueous solutions do not attack glass. It does not melt but decomposes on heating above 300°. At 850 to 900° UF_4 and F_2 or UF_6 are formed. Ellis and Forrest[200a] reported that at 150° UO_2F_2 reacts with ClF_3 to produce UF_6, ClO_2F, Cl_2, O_2, and F_2. It can be reduced with hydrogen at 600° to UO_2 and HF. It forms many complex salts such as $NaF \cdot UO_2F_2$, $3KF \cdot UO_2F_2$, $3NH_4F \cdot UO_2F_2$, $3KF \cdot 2UO_2F_2$, $5KF \cdot 2UO_2F_2$, and $2CsF \cdot UO_2F_2$. Solutions of these salts appear to form insoluble per compounds upon the addition of hydrogen peroxide. These compounds decompose at 100°. The preparation of $K_3UO_2F_5$, $(NH_4)_3UO_2F_5$, and $Cs_2UO_2F_4$ were given by Dieke and Duncan[173], the crystal structure of $K_3UO_2F_5$ by Zachariasen[813], and that of $K_5(UO_2)_2F_9$ by Staritzky, Cromer, and Walker[710].

Neptunium trifluoride, NpF_3, is a purple hexagonal crystalline compound having a heat of formation of -360 ± 2 kcal per mole, according to Cunningham and Hindman[156]. It was prepared by treating the dioxide with hydrogen and hydrogen fluoride at 500°. It was reduced to the metal at 1300° by reaction with barium as shown by Westrum and Eyring[775]. It can be obtained from the tetrafluoride by reaction with H_2 and HF at elevated temperatures according to Fried and Davidson[248]. Its crystal structure and also that of NpF_4, NpF_6, and KNp_2F_9 were studied by Zachariasen[814].

Naptunium tetrafluoride, NpF_4, is a light green monoclinic crystalline substance with a heat of formation of -428 ± 3 kcal per mole. It was made from the trifluoride by reaction at 500° with oxygen and hydrogen fluoride[156]. It can also be made by the reaction between NpO_2 and HF at 400 to 700° according to Fried and Davidson[249]. $Np(OH)_4$ can also be used.

Neptunium pentafluoride is not reported as having been prepared.

Neptunium hexafluoride, NpF_6, is a white orthorhombic crystalline compound with a heat of formation for the gas of -463 ± 3 kcal per mole[156]. It was prepared by the action of F_2 on either NpF_3 or NpF_4. Malm, Weinstock, and Weaver[452] gave detailed directions for its preparation and purification. They studied the infrared spectrum and concluded the molecule to be symmetrical. Raman spectrum cannot be taken as the compound is sensitive to photochemical decomposition. Weinstock, Weaver, and Malm[767] stated the vapor pressure of the solid from 0 to 55.10° followed the equation $\log_{10} P_{mm} = 18.48130 - 2.6690 \log T - 2892.0/T$ and that of the liquid from 55.10° to 76.86° $\log_{10} P = 0.01023 + 2.5826 \log T - 1191.1/T$. The boiling point = 55.18°, the triple point = 55.10° at 758.
mole, and ΔS of fusio
infrared spectrum was

Neptunium dioxydi
hydrogen fluoride on
NH_4NpF_5 and KNp_2F_9

Plutonium trifluoric
at 1425 ± 3°C with a h
heat of fusion of abou
It was prepared from r
$Pu(NO_3)_4 \cdot xH_2O$, or I
hydrogen at 550 to 600°
acid to aqueous solutic
water at 70° and at 30(
oxygen it is converted t
and Davidson[250]. It rea
Its vapor pressure was
the solid, 120–144°K, l
and for the liquid, 1440–
53)/T from which ΔH of
The vapor pressure of
ningham[112]. Westrum
1425 ± 3°, and gave the
$\log_{10} P_{mm} = 38.920 - 2$
tion at 1400° of 89 kca
properties of PuF_3 an
by Dawson *et al.*[163] and
trifluoride with calcium
Grison[16].

Plutonium tetrafluoric
a melting point estimate
-424 ± 4 kcal per mole.
vapor pressure of PuF_4 b
$10{,}040T^{-1}$. They state th
which may be PuF_5, an
follow the equation log P
treatment of the dioxide w
according to Cunningham
by treatment either with
oxygen at 600°. It does n
Fried and Davidson[250], b
$PuF_4 \cdot 2.5H_2O$. Its reducti

point = 55.10° at 758.0 mm of Hg, and the ΔH of fusion = 4198 cal per mole, and ΔS of fusion = 12.79. The Np—F distance = 1.981A. The infrared spectrum was reported by Malm, Weinstock, and Claassen[451].

Neptunium dioxydifluoride, NpO_2F_2, was prepared by the action of hydrogen fluoride on $NaNpO_2Ac_3$ at 300–325°. The complex salts NH_4NpF_5 and KNp_2F_9 were also reported[156].

Plutonium trifluoride, PuF_3, is a hexagonal crystalline solid melting at 1425 ± 3°C with a heat of formation of −375 ± 1 kcal per mole and a heat of fusion of about 13 kcal per mole according to Cunningham[154]. It was prepared from most plutonium compounds such as PuO_2, PuF_4, $Pu(NO_3)_4 \cdot xH_2O$, or $PuO_2(NO_3)_2 \cdot xH_2O$ with hydrogen fluoride and hydrogen at 550 to 600°. It may also be prepared by adding hydrofluoric acid to aqueous solutions containing Pu(III) ions. It hydrolyzes with water at 70° and at 300° is converted to the dioxide. At 600° with dry oxygen it is converted to the tetrafluoride and dioxide according to Fried and Davidson[250]. It reacts with fluorine at 200° to give the tetrafluoride. Its vapor pressure was determined by Phipps *et al.*[550]. They give for the solid, 120–144°K, $\log_{10} P_{mm} = 12.468 \pm 0.074 - (21{,}120 \pm 100)/T$ and for the liquid, 1440–1770°, $\log_{10} P_{mm} = 11.273 \pm 0.034 - (19{,}399 \pm 53)/T$ from which ΔH of vaporization of the liquid is 105.9 kcal per mole. The vapor pressure of PuF_3 was also measured by Carniglia and Cunningham[112]. Westrum and Wallman[777] determined the melting point, 1425 ± 3°, and gave the dissociation pressure, represented by the equation $\log_{10} P_{mm} = 38.920 - 24{,}917/T - 7.5513 \log T$; and a heat of sublimation at 1400° of 89 kcal per mole. The preparation and some of the properties of PuF_3 and PuF_4 were treated in considerable detail by Dawson *et al.*[163] and the preparation of the metal by reduction of the trifluoride with calcium was mentioned by Anselin, Faugeras, and Grison[16].

Plutonium tetrafluoride, PuF_4, is a monoclinic crystalline solid with a melting point estimated to be 1310°K and a heat of formation of −424 ± 4 kcal per mole. Mandleberg and Davies[453a] determined the vapor pressure of PuF_4 between 700 and 1200°K. $\text{Log}_{10} P_{mm} = 5.58 - 10{,}040T^{-1}$. They state that above 1200° a more volatile species occurs, which may be PuF_5, and leaving PuF_3. The pressures above 1200°F follow the equation $\log P_{mm} = 36.1 - 54{,}180T^{-1}$. It is prepared by the treatment of the dioxide with hydrogen fluoride and oxygen at 550 to 600° according to Cunningham[154]. It can also be obtained from the trifluoride by treatment either with fluorine at 200° or with hydrogen fluoride and oxygen at 600°. It does not react with oxygen up to 900° according to Fried and Davidson[250], but does decompose at 1000°. It forms a hydrate, $PuF_4 \cdot 2.5H_2O$. Its reduction to the metal is discussed by Fried *et al.*[252].

It can be fluorinated at temperatures above 100° by elementary fluorine to the hexafluoride; but the rate becomes significant only above 400° according to Steindler, Steidl, and Steunenberg[715]. The crystal structures of PuOF, PuF_3, and PuF_4 were given by Zachariasen[812].

Plutonium oxyfluoride, PuOF, has a tetragonal structure and a melting point above 1635°C. It was obtained by heating PuF_3 to a very high temperature. Its crystal structure was given by Zachariasen[817].

Complex salts of tetravalent plutonium were described by Anderson[10]. They were made by adding a solution of a soluble tetravalent plutonium salt to a solution of a fluoride. $NaPuF_5$, $KPuF_5$, $RbPuF_5$, and $CsPu_2F_9 \cdot 3H_2O$ have been identified and the crystal structures determined by Zachariasen[817].

A pentafluoride of plutonium has not been identified.

Plutonium hexafluoride was first obtained by Florin[234]. Its preparation and properties were described by Florin, Tannenbaum, and Lemon[235]. It was prepared by treating PuO_2, PuF_3, or PuF_4 with elementary fluorine. In this reaction Pu_4F_{17} which is isomerphous with U_4F_{17}, is also formed according to Madleberg, *et al.*[454]. It is an extremely powerful fluorinating agent, even reacting with BrF_3 to form BrF_5. This is a reaction beyond the fluorinating capabilities of UF_6, as was shown by Weinstock, and Malm[764]. The physical properties of PuF_6 were reported by Weinstock, Weaver, and Malm[767]. Its triple point is 51.59°, and between 0 and 51.59° its vapor pressure can be represented by the equation, $\log P_{mm} = 0.39024 + 3.4990 \log T - 2095.0/T$. For the liquid between 51.59 and 77.17°, $\log P_{mm} = 12.14545 - 1.5340 \log T - 1807.5/T$. The boiling point is 62.16°, the pressure at the triple point is 533.0 mm of Hg; its heat of fusion is 4456 cal per mole, and its entropy of fusion is 13.72 cal per mole per deg. The plutonium–fluorine distance in the molecule was given by Weinstock and Malm[765] as 1.969A. Its infrared spectra was discussed by Hawkins, Mattraw, and Sabol[310] and by Malm and Weinstock[451].

Plutonyl fluoride, $PuO_2F_2 \cdot xH_2O$, can be precipitated as a white gelatinous substance from a mixture of methanol and concentrated hydrofluoric acid according to Anderson[11]. It was also discussed by Alenchikova *et al.*[8].

Americium trifluoride, AmF_3, was made by Fried[247] by treating the hydroxide with a mixture of hydrogen fluoride and oxygen at 600–750°. It is pink and isomorphous with the trifluorides of uranium, neptunium, and plutonium. It failed to form the tetrafluoride at 500–700°, when treated with elementary fluorine. By reduction of the trifluoride at 1100° with barium the metal was prepared by Westrum and Eyring[774]. The vapor pressure of AmF_3 was determined by Carniglia[111]. He found

between 1120 and 147
gave the melting poin
95.0 kcal per mole an
of the compound w
The crystal structure
Dauben[731].

Americium tetrafl
fluorination of Am(III
at 500°. $KAmF_5$ was
The vapor pressure o
as following the equa
$\times 10^3/T$. The ΔH of
49.8 kcal per mole and

Curium trifluoride
hydrofluoric acid to a
reduced to the metal
Crane, and Cunningha

Curium tetrafluori
with fluorine at 400°
mined.

1. Adams, R. M., and
2. Afaf, M., (1950). *Pr*
3. Agron, P. A., Grenh
Comm. MD. D.C.–15
4. Abearn, A. J., and H
5. Akishin, P. A., and
6. Akishin, P. A., Spir
30, 951.
7. Akishin, P. A., Spir
Zhur. Fiz. Khim. 30,
8. Alenchikova, I. F., Z
and Chebotarev, N.
9. Altman, D., and Fa
10. Anderson, H. H. (19
11. Anderson, H. H. (19
12. Anderson, R., Schni
Chem. **56**, 473.
13. Anderson, T. H., an
14. Anderson, W. E., Sh
15. Andrychuk, D. (1950
15a. Angelov, I. I., and
Inst. Khim. Reaktivo
16. Anselin, F., Faugeras
17. Appel, R., and Eisen

between 1120 and 1470°K, $\log_{10} P_{mm} = 36.880 - 24{,}650/T - 7.046 \log T$, gave the melting point as 1700°K, and gave for sublimation $\Delta H_{1273°K} = 95.0$ kcal per mole and $\Delta H_0 = 112.8$ kcal per mole. The vapor pressure of the compound was also given by Carniglia and Cunningham[112]. The crystal structure was studied by Zachariasen and by Templeton and Dauben[731].

Americium tetrafluoride, AmF_4, was prepared by Asprey[20] by the fluorination of $Am^{(III)}$, as AmF_3, $Am^{(IV)}$, as AmO_2, or $Am^{(V)}$ compounds at 500°. $KAmF_5$ was also formed, but no evidence was found for AmF_5. The vapor pressure of AmF_4 was given by Yakovlev and Kosyakov[809] as following the equation, $\log P_{mm} = 7.727 \pm 0.093 - (10.886 \pm 0.065) \times 10^3/T$. The ΔH of sublimation in the temperature range 383–640° is 49.8 kcal per mole and $S_{850} = 22.2$.

Curium trifluoride, CmF_3, was made by precipitating it by adding hydrofluoric acid to a nitric acid solution of curium(III) ion. It can be reduced to the metal at 1275° with barium vapor according to Wallman, Crane, and Cunningham[758].

Curium tetrafluoride, CmF_4, was made by fluorinating the trifluoride with fluorine at 400° by Asprey *et al.*[21] and its crystal properties determined.

References

1. Adams, R. M., and Katz, J. J. (1956). *J. Opt. Soc. Am.* **46**, 895.
2. Afaf, M., (1950). *Proc. Phys. Soc. (London)* **63A**, 544.
3. Agron, P. A., Grenhall, A., Kunin, R., and Weller, S. (1948). *U.S. Atomic Energy Comm. MD. D.C.*–1588.
4. Ahearn, A. J., and Hannay, N. B. (1953). *J. Chem. Phys.* **21**, 119.
5. Akishin, P. A., and Spiridonov, V. P. (1957). *Kristallografiya* **2**, 475.
6. Akishin, P. A., Spiridonov, V. P., and Naumov, V. A. (1956). *Zhur. Fiz. Khim.* **30**, 951.
7. Akishin, P. A., Spiridonov, V. P., Naumov, V. A., and Rambidi, N. G. (1956). *Zhur. Fiz. Khim.* **30**, 155.
8. Alenchikova, J. F., Zaitseva, L. L., Lipis, L. V., Nikololaev, N. S., Fomin, V. V., and Chebotarev, N. T. (1958). *Zhur. Neorg. Khim.* **3**, 951.
9. Altman, D., and Farber, M. (1953). *J. Chem. Phys.* **21**, 1118.
10. Anderson, H. H. (1949). *Natl. Nuclear Energy Ser., Div. IV* **14B**, Pt. I, 775.
11. Anderson, H. H. (1949). *Natl. Nuclear Energy Ser., Div. IV* **14B**, Pt. I, 825.
12. Anderson, R., Schnizlein, J. G., Toole, R. C., and O'Brien, T. D. (1952). *J. Phys. Chem.* **56**, 473.
13. Anderson, T. H., and Lingafelter, E. C. (1951). *Acta Cryst.* **4**, 181.
14. Anderson, W. E., Sheridan, J., and Gordy, W. (1951). *Phys. Rev.* **81**, 819.
15. Andrychuk, D. (1950). *J. Chem. Phys.* **18**, 288, (1951). *Can. J. Phys.* **29**, 151.
15a. Angelov, I. I., and Khainson, S. I. (1959). *Trudy Vsesoyuz. Nauch-Issledovatol Inst. Khim. Reaktivov* **25**, 19.
16. Anselin, F., Faugeras, P., and Grison, E. (1956). Compt. rend. *Acad. Sci.* **242**, 1996.
17. Appel, R., and Eisenhauer, G., (1958). *Angew. Chem.* **70**, 742.

Chemical Geology, 17(1976)125—133

FLUORINE AND CHLORINE GEOCHEMISTRY OF KIMBERLITES

D.K. PAUL, F. BUCKLEY and P.H. NIXON

Department of Earth Sciences, University of Leeds, Leeds (Great Britain)

(Received July 3, 1975; accepted for publication October 9, 1975)

ABSTRACT

Paul, D.K., Buckley, F. and Nixon, P.H., 1976. Fluorine and chlorine geochemistry of kimberlites. Chem. Geol., 17: 125—133.

Abundances of fluorine and chlorine in thirty-two kimberlites and six ultrabasic inclusions from India, Greenland and Africa have been determined and shown to be held by apatite (mainly F) and phlogopite (mainly Cl). Compared with other ultrabasic rocks, kimberlites show higher level of fluorine. Secondary alteration depletes chlorine more than fluorine. In the Indian kimberlites, the variation of element abundance is related to geographical regions. A significant positive correlation exists between F and P and a fractionation index suggesting that the halogens, especially F, represent differing degrees of evolution of the kimberlitic magma. This possibly reflects regional variation in levels of "incompatible" elements within the mantle dependent upon cratonic ages.

INTRODUCTION

Kimberlite is a Mg-silicate rock, derived from great depth, which during irruption, has incorporated a variety of mantle and crustal xenoliths and undergone reaction with its own volatile constituents. The main products representing hydration ("serpentinisation") and carbonate formation are implicit in most kimberlite chemical analyses, but of other volatiles that are likely to be present, e.g., fluorine and chlorine, virtually nothing is known.

These volatile constituents comprise part of the "incompatible" suite of elements that have been enriched in the mantle during kimberlite formation (Harris and Middlemost, 1969). The main volatile, H_2O, has given rise to a series of hydrated Mg-bearing silicates including vermiculite, saponite, talc, serpentine, phlogopite, chlorite, montmorillonite, and nontronite which are products of both magmatic alteration and weathering (Kresten, 1973). CO_2, as carbonates of Ca and Mg, has been similarly redistributed. It is not known the extent to which F and Cl are remobilised, although Stueber et al., (1968) have shown that, in ultrabasic rocks, these elements vary according to mode of occurrence and degree of secondary alteration.

Our objective is to determine the main mineral carriers of F and Cl, in

kimberlites and to assess the amount of secondary redistribution of these elements and, most importantly, to investigate whether the variation of these elements can be ascribed to an evolutionary trend in kimberlites as, for example, in basaltic and andesitic magmas (Anderson, 1975). The relationship with host mantle, represented by six ultrabasic xenoliths from southern Africa (none has been found in the Indian kimberlites) is also investigated since this is relatively volatile-free.

MATERIAL STUDIED

Over half the specimens analysed (Table I) are from Indian kimberlite pipes (Paul et al., 1975a). These can be divided in two groups; those from central and south India. The central Indian samples are serpentinised (fresh olivine is absent) and agglomeratic. The colour ranges from yellowish grey at the surface (e.g. MG 11) where secondary calcite is abundant to greyish green at depth. Phenocrysts of phlogopite up to 0.5 cm across are often present.

The south Indian samples, especially those from the Wajrakarur pipe 2, are dark grey, hard and show a conchoidal fracture similar to the "hardebank" of southern Africa. The degree of serpentinisation is less than in the central Indian occurrences and fresh olivine megacrysts are often present. Minor phlogopite is present in the matrix at Lattavaram. Kimberlite from the Hinota pipe is soft, friable and very altered.

In contrast, PGH 1 from Greenland is exceptionally fresh, greenish black with abundant megacrysts of ilmenite, olivine and garnet. JA 3, also from Greenland, is greenish brown, hard but carbonated rock. Among the Zambian samples, AK 1 is a medium-grained rock with abundant calcite and phlogopite. Phenocrysts of olivine are completely altered to serpentine. Ilmenite occurs both in the groundmass and in phenocrysts. Sample K 5 is soft, friable and highly altered kimberlite with about 29% CO_2 (Hawkes, 1974).

The kimberlite dyke from Marakabei, Lesotho, which has also been described as a carbonatite (Dawson, 1967) consists of altered subhedra of olivine and mica in a highly calcitic groundmass (Ferguson et al., 1973). Dark blue-grey hardebank (tough kimberlite) from Monastery Mine, South Africa, constitutes the main diamond-bearing "quarry type" with abundant olivine and ilmenite inclusions (Whitelock, 1973). A much paler "East End" variety consists of calcite-rimmed serpentine pseudomorphs after olivine and with groundmass phlogopite.

Two phlogopite megacrysts from Monastery Mine which were analysed are pale bronze-brown subhedral crystals 4—5 cm across (illustrated by Whitelock, 1973). Another analysed sample forms grains up to 0.5 cm across in kimberlite from the Majhgawan pipe, central India.

The ultrabasic inclusions are mainly garnet lherzolites and include varieties derived from different levels within the upper mantle and from three geographical points within the Kaapvaal (South Africa) craton. They have also

suffered varying degrees of ma
accretion (Nixon and Boyd, in
indication of the range of F an
of kimberlite activity.

Analytical procedure

The method used for these
and Johns (1967) as modified
made using a Hilger and Watts

In the determination of chl
10 min after mixing to obviate
to occur over the period 15—3

The determination of fluori
Cyanine R, commercial sample
to be of variable and often low
according to their procedure. I
tive constituent, it was found
in the original papers. A conce
found to give reasonable sensit
0—60 μg/50 ml.

The precision of the analyti
nations carried out on one of
of the work. The results produ
0.018 for fluorine. In the case
fluorine will be less due to the

The accuracy of the proced
sample GSP-1. Results of 0.32
published values of 0.320% F

RESULTS

The variation in fluorine an
(Table I) is related to their geo
two geochemical provinces ea
mean F and Cl abundances of
0.023% and those of the south
respectively.

There is a significant positiv
suggesting that fluorine is con
is illustrated in the linear plot
separation of the two kimberl
tween P_2O_5 and Cl even withi
there is a positive correlation

suffered varying degrees of magmatic depletion and incompatible element accretion (Nixon and Boyd, in press). The six samples were chosen to give an indication of the range of F and Cl values in the upper mantle in the region of kimberlite activity.

Analytical procedure

The method used for these determinations was essentially that of Huang and Johns (1967) as modified by Sen Gupta (1968). The measurements were made using a Hilger and Watts "Uvispek" spectrophotometer.

In the determination of chloride, absorbance measurements were taken 10 min after mixing to obviate the increase (approx. 5%) which was found to occur over the period 15—30 min after mixing.

The determination of fluoride requires the use of the dye Solochrome Cyanine R, commercial samples of which were shown by Dixon et al. (1970) to be of variable and often low quality. The dye used in this work was purified according to their procedure. Due to the increased concentration of the active constituent, it was found necessary to reduce the amount from that given in the original papers. A concentration of 1.0 g/l (instead of 1.8 g/l) was found to give reasonable sensitivity and a linear calibration over the range 0—60 μg/50 ml.

The precision of the analytical procedure was tested by repeated determinations carried out on one of the samples (MG-6) throughout the duration of the work. The results produced a value of $2\sigma = 0.003\%$ for chlorine, and 0.018 for fluorine. In the case of the ultrabasic inclusions, the 2σ value for fluorine will be less due to the larger weights and aliquots used.

The accuracy of the procedure was checked using the USGS standard sample GSP-1. Results of 0.326% F and 0.030% Cl are comparable with the published values of 0.320% F and 0.030% Cl (Flanagan, 1973).

RESULTS

The variation in fluorine and chlorine contents of the Indian kimberlites (Table I) is related to their geographical distribution and this emphasises the two geochemical provinces earlier outlined by Paul et al. (1975a). Thus, the mean F and Cl abundances of the central Indian kimberlites are 0.492% and 0.023% and those of the south Indian kimberlites are 0.182% and 0.017%, respectively.

There is a significant positive correlation between P_2O_5 and F ($r = 0.96$) suggesting that fluorine is contained in apatite (cf. Roegge et al. (1974)). This is illustrated in the linear plot in Fig. 1 which also shows the geographical separation of the two kimberlite groups. There is no such relationship between P_2O_5 and Cl even within a single pipe. Paul et al. (1975b) showed that there is a positive correlation between the fractionation index 1/3 SiO_2 +

TABLE I

Fluorine and chlorine abundances in kimberlites and ultrabasic inclusions

No.	Sample location	F (wt.%)	Cl (wt.%)	F/Cl
Kimberlite — Central India:				
MG 21	quarry sample, depth 9 m, Majhgawan	0.367	0.036	10.1
MG 11	weathered quarry sample, depth 12 m, Majhgawan	0.337	0.007	48.1
MG 6	quarry sample, depth 19 m, Majhgawan	0.409	0.035	11.7
MG 25	quarry sample, depth 20 m, Majhgawan	0.421	0.034	12.2
MG 40	quarry sample, depth 20 m, Majhgawan	0.435	0.030	14.5
MG 50	quarry sample, depth 20 m, Majhgawan	0.503	0.033	15.2
UG 11A	underground samples from a depth of 100 m, Majhgawan pipe	0.473	0.041	11.7
UG 84		0.521	0.017	30.7
UG 136		0.473	0.037	12.8
UG 191		0.477	0.020	23.9
HV 4/1	bore-hole sample (30.8 m), Hinota	0.487	0.006	81.2
HV 4/2	bore-hole sample (49.2 m), Hinota	0.726	0.013	55.9
HV 4/4	bore-hole sample (80.8 m), Hinota	0.749	0.006	124.8
HV 4/6	bore-hole sample (88.9 m), Hinota	0.512	0.009	56.9
Kimberlite — South India:				
WK 1/1	surface sample, Wajrakarur	0.231	(0.001)	—
WK 2/5	surface samples, 3.2 km east of Wajrakarur	0.209	(0.001)	—
WK 2/6		0.115	0.004	28.8
WK 2/7		0.213	0.014	15.2
WK 2/9		0.269	(0.001)	—
LM 3/4	surface samples, 1 km east of Lattavaram	0.258	0.042	6.1
LM 3/5		0.096	0.074	1.3
LM 4/6	surface samples, 1.6 km east of Lattavaram	0.021	0.010	2.1
LM 4/9		0.225	0.008	28.1
Kimberlite — Southern Africa and Greenland:				
AK 1	north Luangwa, Zambia	0.200	0.005	40.0
K 5	Kufue Hook, Zambia	0.122	(0.001)	—
PHN 2522	kimberlite dyke, Marakabei, Lesotho	0.349	0.010	34.9
PHN 2643	hardebank, quarry type, Monastery, South Africa	0.173	0.007	24.7
PHN 2644	East End kimberlite, Monastery, South Africa	0.112	0.003	37.3
PHN 1867	East End kimberlite, Monastery, South Africa	0.075	0.007	10.7
PHN 2655	soft kimberlite, Monastery, South Africa	0.128	(0.001)	—
PGH 1	Holsteinsborg, Greenland	0.068	0.011	6.2
JA 3	Nigardlikasik, Greenland	0.118	0.073	1.6
Phlogopite from kimberlite				
MG PH	phenocrysts, Majhgawan pipe, central India	1.239	(0.003)	413.0
PHN 2648A	4—5 cm megacrysts, Monastery Mine, South Africa	0.446	0.045	9.9
PHN 2648C		0.440	0.048	9.2

TABLE I (*continued*)

No.	Sample location
Ultrabasic inclusions from kimb	
PHN 2765	highly sheared n South Africa
PHN 2766/6	highly sheared n South Africa
PHN 2838	highly sheared n Lesotho
PHN 2839	highly sheared n Lesotho
PHN 2654	harzburgite, Mo
PHN 2771	phlogopite—clin Monastery, Sou
USGS-GSP-1	international ref

Figures in parenthesis are approxi

$K_2O - MgO - FeO - CaO$ and correlation ($r = 0.95$) also exi

The group of kimberlites f ities to those of southern Ind Fluorine greatly outweighs Cl samples particularly in the ca The average level of P_2O_5 of s (Gurney and Ebrahim, 1973)

Kimberlitic phlogopites we major carriers of halogens (cf (Table I) confirms this in sou must be present in micas of n in Table I (and JA 3 from Gr probably apatite — must be p phlogopites compared with n However, several generations there may be compositional

There is some evidence tha kimberlite from Majhgwan pi Hinota (Table I). Other possi mite (McGetchin et al., 1970 graphic examination.

Variations of F and Cl in t geneities in the mantle that v of the order of F, 0.024% an from Lesotho, phlogopite is results.

abasic inclusions

	F (wt.%)	Cl (wt.%)	F/Cl
	0.367	0.036	10.1
	0.337	0.007	48.1
n	0.409	0.035	11.7
n	0.421	0.034	12.3
n	0.435	0.030	14.5
n	0.503	0.033	15.2
	0.473	0.041	11.5
	0.521	0.017	30.7
	0.473	0.037	12.8
	0.477	0.020	23.9
	0.487	0.006	81.2
	0.726	0.013	55.9
	0.749	0.006	124.8
	0.512	0.009	56.9
	0.231	(0.001)	–
	0.209	(0.001)	–
	0.115	0.004	28.8
	0.213	0.014	15.2
	0.269	(0.001)	–
ıram	0.258	0.042	6.1
	0.096	0.074	1.3
	0.021	0.010	2.1
	0.225	0.008	28.1
	0.200	0.005	40.0
	0.122	(0.001)	–
	0.349	0.010	34.9
	0.173	0.007	24.7
	0.112	0.003	37.3
	0.075	0.007	10.7
frica	0.128	(0.001)	–
	0.068	0.011	6.2
	0.118	0.073	1.6
l India	1.239	(0.003)	413.0
,	0.446	0.045	9.9
	0.440	0.048	9.2

TABLE I (*continued*)

No.	Sample location	F (wt.%)	Cl (wt.%)	F/Cl
	Ultrabasic inclusions from kimberlite:			
PHN 2765	highly sheared nodule, Bultfontein, South Africa	0.013	0.021	0.6
PHN 2766/6	highly sheared nodule, Bultfontein, South Africa	0.023	0.010	2.3
PHN 2838	highly sheared nodule, Thaba Putsoa, Lesotho	0.007	(0.001)	–
PHN 2839	highly sheared nodule, Thaba Putsoa, Lesotho	0.004	(0.001)	–
PHN 2654	harzburgite, Monastery, South Africa	0.025	0.002	12.5
PHN 2771	phlogopite—clinopyroxene-rich nodule, Monastery, South Africa	0.072	0.002	36.0
USGS-GSP-1	international reference sample	0.326	0.030	10.9

Figures in parenthesis are approximate, measured values of which are less than 2σ.

$K_2O - MgO - FeO - CaO$ and Ce/Yb ratios of Indian kimberlites. A positive correlation ($r = 0.95$) also exists between this index and fluorine (Fig. 1).

The group of kimberlites from southern Africa and Greenland show similarities to those of southern India in absolute abundances of F and Cl (Table I). Fluorine greatly outweighs Cl, though this is not marked in the two Greenland samples particularly in the carbonated kimberlite JA3 in which Cl = 0.073%. The average level of P_2O_5 of southern African kimberlites is less than 1% (Gurney and Ebrahim, 1973) as in south India.

Kimberlitic phlogopites were analysed as it was thought that they could be major carriers of halogens (cf. Correns, 1956). Their relatively high Cl content (Table I) confirms this in southern African kimberlites but a higher Cl content must be present in micas of many of the Indian kimberlites than is indicated in Table I (and JA 3 from Greenland) or another Cl bearing mineral — most probably apatite — must be present. Fluorine is not significantly higher in the phlogopites compared with most of the analysed whole-rock kimberlites. However, several generations of phlogopite are present in kimberlites and there may be compositional differences between these.

There is some evidence that Cl is less abundant in altered rocks, e.g. altered kimberlite from Majhgwan pipe (MG 11) and the altered specimens from Hinota (Table I). Other possible halogen bearing minerals e.g. titanoclinohumite (McGetchin et al., 1970) and amphibole were not observed during petrographic examination.

Variations of F and Cl in the ultrabasic nodules illustrate large inhomogeneities in the mantle that will be discussed elsewhere but mean values are of the order of F, 0.024% and Cl, 0.006%. With the exception of the nodules from Lesotho, phlogopite is present and is thought to account for the higher results.

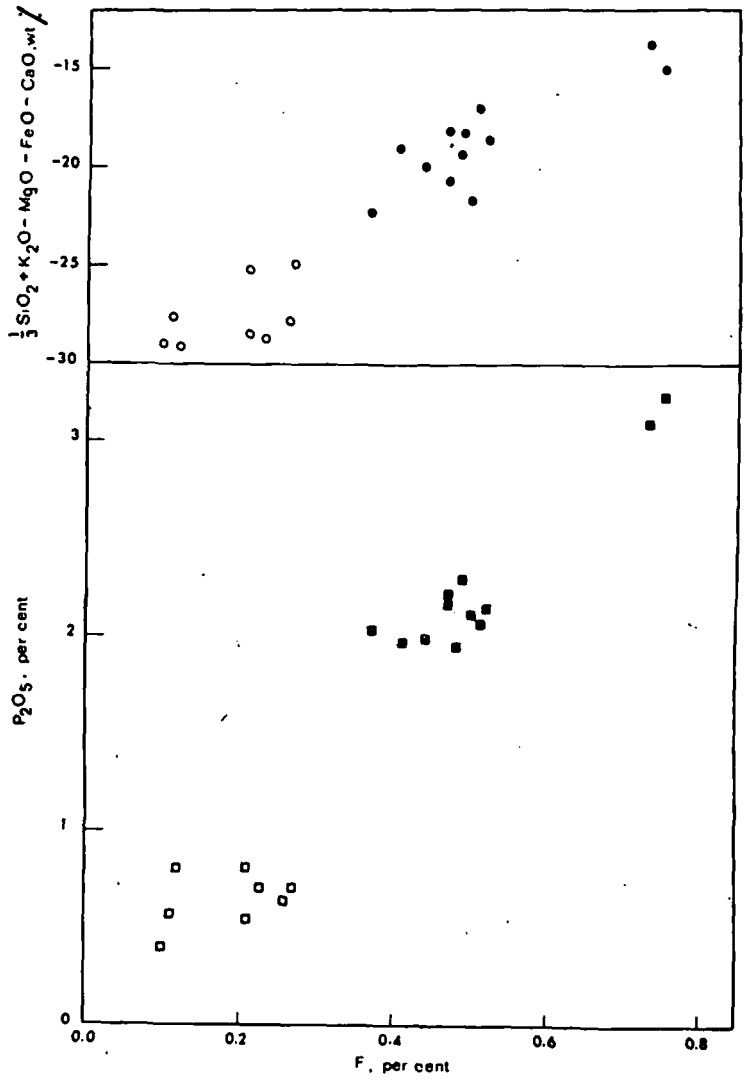

Fig. 1. Plot of 1/3 SiO_2 + K_2O – MgO – FeO – CaO (wt.%) and P_2O_5 (wt.%) against F (wt.%), for Indian kimberlites. Open symbols are kimberlites from south India and closed symbols are those from central India (see Paul et al., 1975b).

Overall, F is much lower than in kimberlites. The difference is less marked in the case of Cl and, with the exception of the central Indian kimberlites, is about the same concentration (Table I). This is reflected in the lower F/Cl ratios in the nodules compared with the kimberlites (*Note*, nodule PHN 2765, Table I, has Cl > F.) This suggests that there has been little or no kimberlite magma contamination of the nodules.

DISCUSSION AND CONCLUSIONS

The enrichment factor in kimb
in which it formed ranges from 7
(up to 50 if the nodule data is ex
However, these figures are ove
chemical variations within the m
and local variations within kimb
magmatic alteration and weather
(F, Cl) and phlogopite (Cl). The
little affected by these processes
samples, central India and soft a
South Africa (Table I). Stormer
secondary depletion in altered b
Variation of volatiles could al
gation, whether as explosive ven
intrusions, but major difference
magma evolution. The phospho
considered as an indicator for th
Anderson and Greenland, 1969)
phase is low and it, thus, enters
links F with P as an element bel
A comparison of the halogen
(Table II) shows that F is invari
is subject to greater enrichment

TABLE II

Fluorine and chlorine mean abundan

Rock type	
Kimberlite (excluding central Indian occurrences)	
Kimberlites, central India	
Ultrabasic inclusions in kimberlite	
Ultrabasic rocks (alpine type)	
Carbonatite	
Basalt	
Chondrite (carbonaceous)	

DISCUSSION AND CONCLUSIONS

The enrichment factor in kimberlitic fluorine compared with host mantle in which it formed ranges from 7 to 33 for the southern African examples (up to 50 if the nodule data is extended to central India).

However, these figures are oversimplified because there are large regional chemical variations within the mantle (Table I; Nixon and Boyd, in press) and local variations within kimberlite. The latter could arise from post-magmatic alteration and weathering of the main carrier minerals; apatite (F, Cl) and phlogopite (Cl). The present evidence suggests that fluorine is little affected by these processes but that chlorine could be e.g. in the Hinota samples, central India and soft altered kimberlite from Monastery Mine, South Africa (Table I). Stormer and Carmichael (1971) have observed similar secondary depletion in altered biotites.

Variation of volatiles could also arise from the mode of kimberlite propagation, whether as explosive vent (pipe) extrusions or as quiet, sealed, dyke intrusions, but major differences probably represent degrees of kimberlite magma evolution. The phosphorus content of a crystallising magma has been considered as an indicator for the degree of crystallisation (Henderson, 1968; Anderson and Greenland, 1969) because its concentration in the cumulus phase is low and it, thus, enters the liquid phase preferentially. Our evidence links F with P as an element behaving in a similar manner.

A comparison of the halogen contents in kimberlites with other rocks (Table II) shows that F is invariably more abundant than Cl. Furthermore, F is subject to greater enrichment than Cl in kimberlite compared to chondrites.

TABLE II

Fluorine and chlorine mean abundances and ratios in some major rock types

Rock type	F (wt.%)	Cl (wt.%)	F/Cl	Reference
Kimberlite (excluding central Indian occurrences)	0.165	0.015	11.0	this paper
Kimberlites, central India	0.492	0.023	21.4	this paper
Ultrabasic inclusions in kimberlite	0.024	0.006	4.0	this paper
Ultrabasic rocks (alpine type)	0.0088	0.0019	4.6	Stueber et al. (1968)
Carbonatite	0.81	—	—	Heinrich (1966)
Basalt	0.04	0.006	6.7	Taylor (1964)
Chondrite (carbonaceous)	0.0405	0.028	1.4	Reed and Allen (1966); Fisher (1963)

0.8

id P_2O_5 (wt.%) against F
from south India and closed

difference is less marked
ral Indian kimberlites, is
cted in the lower F/Cl
(Note, nodule PHN 2765,
n little or no kimberlite

Ultrabasic rocks and basalts on the other hand have similar or lower levels than chondrites. Conventional differentiation processes such as partial melting and crystal fractionation would appear to have no marked effect on F and Cl distribution. Only by extreme differentiation as in zone refining (Harris, 1957) is a great degree of enrichment observed, i.e., in kimberlites and carbonatites (Table II) and then only with F. The same mechanism has little apparent effect on Cl concentration but this may be a reflection of the greater aqueous solubility and dispersal of Cl from silicate—carbonate magmas.

We attribute regional grouping of the chemical data, particularly in central and south India, to kimberlite development in the mantle where zone refining had been operative for varying lengths of time dependent upon cratonic ages.

ACKNOWLEDGEMENTS

We thank Prof. P.G. Harris for the benefit of discussion at various stages of the work. The kimberlite samples from Greenland and Zambia were kindly donated by Drs. B. Windley, J.R. Andrews and Mr. A.L. Hawkes. The work was made possible through financial support from the Natural Environment Research Council. One of us (D.K. Paul) is indebted to the Director General, Geological Survey of India for permission to work on the project.

REFERENCES

Anderson, A.T., 1975. Some basaltic and andesitic gases. Rev. Geophys. Space Phys., 13: 37—55.

Anderson, A.T. and Greenland, L.P., 1969. Phosphorus fractionation diagram as a quantitative indicator of crystallisation differentiation of basaltic liquids. Geochim. Cosmochim. Acta, 33: 493—505.

Boyd, F.R. and Nixon, P.H., 1972. Ultramafic nodules from the Thaba Putsoa kimberlite pipe. Carnegie Inst. Washington, Yearb., 71: 362—373.

Correns, C.W., 1956. The geochemistry of the halogens. In: L.H. Ahrens, S.K. Runcorn and H.C. Urey (Editors), Physics and Chemistry of the Earth, 1 Pergamon, London, pp. 181—233.

Dawson, J.B., 1962. Basutoland kimberlites. Bull. Geol. Soc. Am., 73: 545—560.

Dawson, J.B., 1967. A review of the geology of the kimberlite. In: P.J. Wyllie (Editor), Ultramafic and Related Rocks, Wiley, New York, N.Y., pp. 241—251.

Dixon, E.J., Grisley, L.M. and Sawyer, R., 1970. The purification of Solochrome Cyanine R. Analyst (London), 95: 945—949.

Ferguson, J., Danchin, R.V. and Nixon, P.H., 1973. Fenitization associated with kimberlite magmas. In: P.H. Nixon (Editor), Lesotho Kimberlites, Lesotho National Development Corporation, Maseru, pp. 207—213.

Fisher, D.E., 1963. The fluorine content of some chondritic meteorites. J. Geophys. Res., 68: 6331.

Flanagan, F.J., 1973. 1972 values for international geochemical reference samples. Geochim. Cosmochim. Acta, 37: 1189—1200.

Gurney, J.J. and Ebrahim, S., 1973. Chemical composition of Lesotho kimberlites. In: P.H. Nixon (Editor), Lesotho Kimberlites, Lesotho National Development Corporation, Maseru, pp. 280—284.

Harris, P.G., 1957. Zone refining a
Acta, 12: 195—208.
Harris, P.G. and Middlemost, E.A.
Hawkes, A.L., 1974. Ilmenites fro
Leeds, Leeds (unpublished).
Heinrich, E.W.M., 1966. The Geol
555 pp.
Henderson, P., 1968. The distribu
formation of some basic layere
Huang, W.H. and Johns, W.D., 19
rine in silicate rocks by a rapid
508—515.
Kresten, P., 1973. Differential the
Lesotho Kimberlites, Lesotho I
269—279.
McGetchin, T.R., Silver, L.T. and
mineralogical site for water in t
Nixon, P.H. and Boyd, F.R., in pr
nodules from Southern Africa.
Paul, D.K., Rex, D.C. and Harris,
Indian kimberlites. Geol. Soc.
Paul, D.K., Potts, P.J., Gibson, I.L
Indian kimberlite. Earth Planet
Reed, G.W. and Allen, R.O., 1966
30: 633—643.
Roegge, J.S., Logsdon, M.J., Your
1974. Halogens in apatites fron
229—240.
Sen Gupta, J.G., 1968. Determina
and stony meteorites. Anal. Ch
Stormer, J.C. and Carmichael, I.S.
biotite: a potential igneous geo
Stueber, A.M., Huang, W.H. and J
ultramafic rocks. Geochim. Cos
Taylor, S.R., 1964. Abundance of
table. Geochim. Cosmochim. A
Whitelock, T.K., 1973. The Monas
Lesotho Kimberlites, Lesotho N
214—218.

Harris, P.G., 1957. Zone refining and the origin of potassic basalts. Geochim. Cosmochim. Acta, 12: 195—208.
Harris, P.G. and Middlemost, E.A., 1969. The evolution of kimberlites. Lithos, 3: 77—88.
Hawkes, A.L., 1974. Ilmenites from Zambian Kimberlites. M.Sc. Thesis, University of Leeds, Leeds (unpublished).
Heinrich, E.W.M., 1966. The Geology of Carbonatites. Rand McNally, Chicago, Ill., 555 pp.
Henderson, P., 1968. The distribution of phosphorus in the early and middle stages of formation of some basic layered intrusions. Geochim. Cosmochim. Acta, 32: 897—911.
Huang, W.H. and Johns, W.D., 1967. Simultaneous determinations of fluorine and chlorine in silicate rocks by a rapid spectrophotometric method. Anal. Chim. Acta, 37: 508—515.
Kresten, P., 1973. Differential thermal analysis of kimberlites. In: P.H. Nixon (Editor), Lesotho Kimberlites, Lesotho National Development Corporation, Maseru, pp. 269—279.
McGetchin, T.R., Silver, L.T. and Chodos, A.A., 1970. Titanoclinohumite: A possible mineralogical site for water in the upper mantle. J. Geophys. Res., 75: 255—259.
Nixon, P.H. and Boyd, F.R., in press. Mantle evolution based on studies of kimberlite nodules from Southern Africa. XVIII Annu. Rep., Res. Inst. Afr. Geol., Univ. of Leeds.
Paul, D.K., Rex, D.C. and Harris, P.G., 1975a. Chemical characteristics and K—Ar ages of Indian kimberlites. Geol. Soc. Am. Bull., 86: 364—366.
Paul, D.K., Potts, P.J., Gibson, I.L. and Harris, P.G., 1975b. Rare earth abundances in Indian kimberlite. Earth Planet. Sci. Lett., 25: 151—158.
Reed, G.W. and Allen, R.O., 1966. Halogens in chondrites. Geochim. Cosmochim. Acta, 30: 633—643.
Roegge, J.S., Logsdon, M.J., Young, H.S., Barr, H.N., Borscsik, M. and Holland, H.D., 1974. Halogens in apatites from the Providencia area, Mexico. Econ. Geol., 69: 229—240.
Sen Gupta, J.G., 1968. Determination of fluorine in silicate and phosphate rocks, micas and stony meteorites. Anal. Chim. Acta, 42: 119—125.
Stormer, J.C. and Carmichael, I.S.E., 1971. Fluorine—hydroxyl exchange in apatite and biotite: a potential igneous geothermometer. Contrib. Mineral. Petrol., 31: 121——131.
Stueber, A.M., Huang, W.H. and Johns, W.D., 1968. Chlorine and fluorine abundances in ultramafic rocks. Geochim. Cosmochim. Acta, 32: 353—358.
Taylor, S.R., 1964. Abundance of chemical elements in the continental crust: a new table. Geochim. Cosmochim. Acta, 28: 1273—1285.
Whitelock, T.K., 1973. The Monastery Mine kimberlite pipe. In: P.H. Nixon (Editor), Lesotho Kimberlites, Lesotho National Development Corporation, Maseru, pp. 214—218.

alline phase of $K_2Si_4O_9$
:) have synthesized
ave triclinic symmet-
und Z = 2. With thes
s value is compared t
he wadeite-type phase
e converts to a glass
$_4O_9$ in air is probably
Goranson and Kracek

action being:

The volume change
te-type phase is 35 %
ably an intermediate
h there has been very
$5iSi_3O_9$ in nature, the
occur in some part of

esearch Fund from the

Chem. 7, 408–17.
6.

Chem. Japan, 34, 103–8.
143 (ed. AHRENS *et al.*,

7, 241–51.

961. Геохимия (*Geok-*

MINERALOGICAL MAGAZINE, DECEMBER 1975, VOL. 40, PP. 405–14

Fluorine and chlorine in peralkaline liquids and the need for magma generation in an open system

D. K. BAILEY

Department of Geology, University of Reading, Reading, RG6 2AB

AND R. MACDONALD

Department of Environmental Sciences, University of Lancaster, Bailrigg, Lancaster

SUMMARY. Fluorine, chlorine, zinc, niobium, zirconium, yttrium, and rubidium have been determined on fifteen obsidians from Eburru volcano (Kenya Rift Valley), spanning the range from pantellkritic trachyte to pantellerite. All pairs of elements show positive correlation coefficients, ranging between 0·769 and 0·998, but with most values better than 0·900. In spite of some very high correlations, only two of the twenty-one best-fit lines pass near the origin of the Cartesian coordinates. Linear distributions are found *within* two separate groups of elements: F, Zr, Rb; and Cl, Nb, Yt. Zn behaves in general as a member of the second group but seems to be subject to an additional variation. When an element from the fluorine group is plotted against one from the chlorine group the resulting pattern is non-linear. Therefore, although the elements in both groups would generally be considered 'residual' (partition coefficients between crystals and liquid approaching zero) there are clearly detectable differences in their variation, and hence their behaviour.

Major-element variations in the obsidians are such that a vapour (fluid) phase would be needed to account for any magma evolution. The trace-element patterns are also impossible by closed-system crystal fractionation and suggest that this fluid may have been rich in halogens, with the metallic elements forming preferred 'complexes' with either F or Cl. The F–Zr–Rb 'complex' also varies quite independently of the important major oxides (e.g. Al_2O_3) in the rocks. In the case of Rb this is but one aspect of a more significant anomaly, in which there is no sign of any influence of alkali feldspar (which partitions Rb) in the variation. This is remarkable because trachytes and rhyolites have normative $ab+or > 50$ %, and any evolutionary process *controlled* by crystal ⇌ liquid interactions must be dominated by the melting or crystallization of alkali feldspar. The results on the Eburru obsidians show that *if they are an evolutionary series* then *either*, the process was not crystal ⇌ liquid controlled, *or* that any such process has been overriden (or buffered) by other processes that have superimposed the observed trace-element patterns. In the latter event, the buffering phase may have been a halogen-bearing vapour.

The same considerations must apply to other pantellerite provinces where Rb appears to have behaved as a 'residual' element.

In recent years we have compiled all the available data on oversaturated peralkaline obsidians (Macdonald and Bailey, 1973) and set in train an analytical programme on all new samples that we have been able to obtain. Our own field sampling has been focused on the Nakuru–Naivasha region of Kenya, the topographic culmination of the East African rift, where there is an unparalleled development of Quaternary–Recent peralkaline volcanoes. In the trachyte to pantellerite composition range it had been demonstrated previously that the obsidians from different volcanoes showed systematic variations in major-element chemistry, but these variations were not consistent with

a fractional-crystallization model involving the observed phenocryst phases (Macdonald *et al.*, 1970). The best development of pantellerite magmatism is found in the Eburru volcano (Sutherland, 1971) just north-west of Lake Naivasha. Trace-element analyses of some of Sutherland's samples by Weaver *et al.* (1972) were used (with data from five other volcanoes) to argue that the relationships between trachytes and pantellerites are most reasonably explained by fractional crystallization. Subsequent examination has revealed, however, that the 'Eburru' specimens used by Weaver *et al.* were a mixed population (Bailey *et al.*, 1975).

Since 1970 we have collected and analysed obsidians from Eburru, which span the composition range from quartz-trachyte to pantellerite, and the major-element variation within this one volcanic pile cannot be explained by fractional crystallization of the phenocryst phases. The major-element evidence on quenched liquids is thus in direct conflict with the conclusions reached through the trace elements by Weaver *et al.* (1972). Trace-element analyses of our own Eburru samples form part of the long-term study of peralkaline obsidians, and they are now sufficiently far advanced to demonstrate that fractional crystallization *cannot* explain the variations. This demonstration, however, is only a subsidiary aim of the present article—our chief concern is to describe some unexpected relationships (especially involving halogens) which may provide some real clues to the secrets of this magmatism.

We shall look at a small group of trace elements (F, Cl, Zn, Nb, Zr, Yt, and Rb), which includes the two (Nb and Zr) considered most significant by Weaver *et al.* (1972). Our population is fifteen obsidians from quartz-trachyte to rhyolite: we are unable to include any basalts because we are restricting our study to glasses (quenched liquids). Actually, there are no contemporaneous basalts in the Eburru pile, although there is a Recent basalt field in the lowlands just to the north. We believe it would be begging the question to include these basalts with the Eburru magmatism until we have evidence other than geographic proximity to indicate that the two may be cogenetic (this problem is currently being studied by A. W. H. Bowhill, University of Reading: see also Bailey *et al.*, 1975, fig. 1). Correlations among the selected trace elements are moderately to strongly positive, whereas their correlations with major elements are generally poor. Although the major element ranges in the population are small (e.g. SiO_2 range from 66·2 to 72·0 per cent) the trace element ranges are large (e.g. Zr range from 1038 to 3058 ppm). Samples with essentially identical major-element chemistry show widely different trace-element levels, and the impossibility of reconciling these facts with simple fractional crystallization has been noted elsewhere (Bailey, 1973).

Trace-element relations. The limits, means, and concentration factors are listed in Table I. Trace-element values, sample points, rock names, and age relations are given in the Appendix.

The absence of basic rocks, with very low levels of the selected trace elements, is not a serious drawback to correlation analysis because in the case of the strongly concentrated elements, F, Zr, and Rb, the obsidian values span two-thirds of the possible range from the maximum observed down to zero. The results of the correlation analysis are given in matrix form in Table II.

TABLE I. *Limits, means, c*

Minimum (m)	
Maximum (M)	
Mean	
Standard Deviatio	
Maximum concentration factor (M/m)	

TABLE II. *Correlation m*
are positive). Plus or minu
major-axis equation: Till,
the 95 % confidence limit

	F	Cl
F	1·000	
Cl	0·862(+)	1·00
Zn	0·769(+)	0·87
Nb	0·955(+)	0·94
Zr	0·994(0)	0·87
Yt	0·932(+)	0·95
Rb	0·996(−)	0·85

Imp

The central tenet of t
as propounded by Weav
elements will be unable
concentrated in the resi
cess dominated by cryst
to be proven, but for th
the prime example of a
melts (and insolubility i
'volatile effects'; and
(Weaver *et al.*, 1972).
ferentiation than the m
are, of course, compou
reconcile the claim wit
now cannot find suppo

Weaver *et al.* (1972
graphical plots of each

TABLE I. *Limits, means, and concentration factors in 15 obsidians from Eburru, Kenya. Values in ppm*

	F	Cl	Zn	Nb	Zr	Yt	Rb
Minimum (m)	2910	2090	333	230	1038	195	131
Maximum (M)	7800	4290	537	542	3058	410	417
Mean	4900	3300	457	388	1910	307	252
Standard Deviation	1660	630	58	96	671	63	98
Maximum concentration factor (M/m)	2·68	2·05	1·61	2·36	2·95	2·10	3·18

TABLE II. *Correlation matrix for trace elements in the Eburru obsidians (all coefficients are positive). Plus or minus indicates the sign of the intercept of the best-fit line (reduced major-axis equation: Till, 1973) on the axis of the second variable in those cases where the 95 % confidence limits do not include the origin. Zero indicates that the origin falls within the 95 % confidence limits*

	F	Cl	Zn	Nb	Zr	Yt	Rb
F	1·000						
Cl	0·862(+)	1·000					
Zn	0·769(+)	0·879(+)	1·000				
Nb	0·955(+)	0·943(−)	0·909(−)	1·000			
Zr	0·994(0)	0·876(−)	0·817(−)	0·972(−)	1·000		
Yt	0·932(+)	0·954(0)	0·928(−)	0·995(+)	0·951(+)	1·000	
Rb	0·996(−)	0·853(−)	0·790(−)	0·959(−)	0·998(−)	0·937(−)	1·000

Implications of the trace-element distributions

The central tenet of the trace-element argument with respect to magma evolution, as propounded by Weaver *et al.* (1972), is that in a series of peralkaline liquids certain elements will be unable to enter the crystallizing phases, and will become progressively concentrated in the residual liquids. This assumes that the liquids are related by a process dominated by crystal ⇌ liquid interactions: we would claim that this itself needs to be proven, but for the moment let us examine the rest of the case. Zr is chosen as the prime example of a residual element because of: its high solubility in peralkaline melts (and insolubility in the major crystalline phases); its impassiveness to late-stage 'volatile effects'; and its abundance and high-precision determination by XRF (Weaver *et al.*, 1972). Consequently Zr is claimed to be a more useful index of differentiation than the more commonly used major-element indices. More assumptions are, of course, compounded in this claim. In the case of the Eburru rocks we cannot reconcile the claim with the major-element patterns (Bailey, 1973) and, moreover, we now cannot find support for it in our trace-element data.

Weaver *et al.* (1972) state that in the six volcanic centres they have tested the graphical plots of each of the elements Ce, La, Nb, and Rb against Zr are linear, and

project through the origin. They deduce from this (assuming that Zr is the archetype residual element) that the other four elements also have bulk distribution-coefficients (element concentration in combined crystal phases/concentration in liquid) close to zero. Compared with their data on Eburru (kindly provided by S. D. Weaver) our

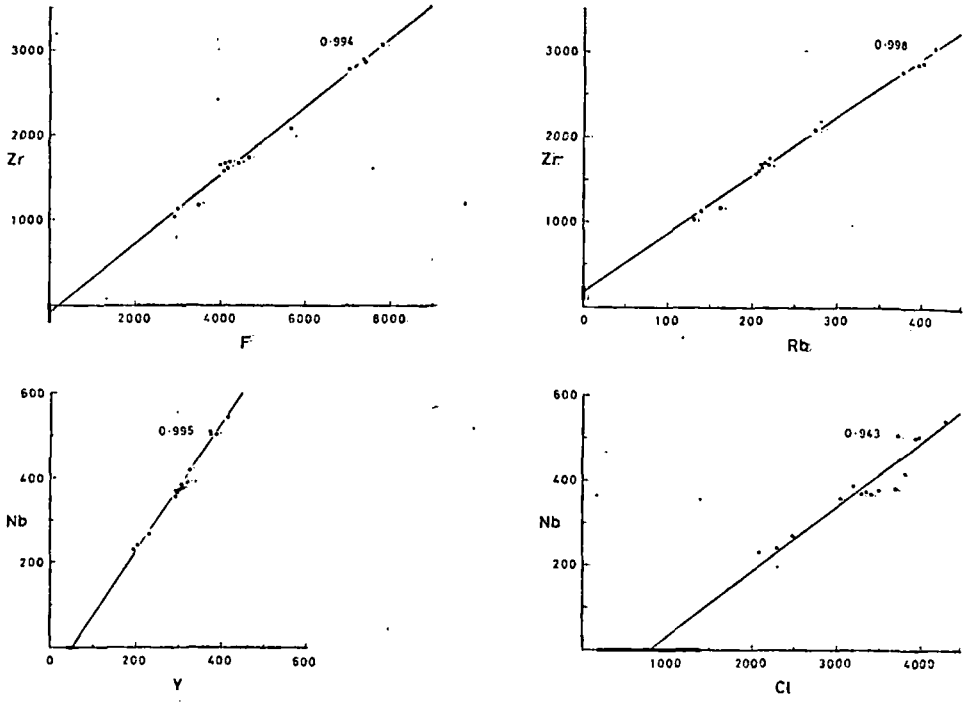

FIG. 1. Four examples of linear correlations of element pairs in the Eburru obsidians (solid circles). In every case the line is the computed reduced major-axis line and the heavy bar on the axis shows the 95 % confidence limits on the intercept. All values in ppm.

obsidian analyses show far less 'noise', more systematic variations, and higher correlation coefficients throughout. Our distribution patterns are quite different. Many are not linear, and most do not project through the origin. The latter are shown in Table II by plus and minus signs, to indicate the sign of the intercept on the axis of the second variable when the first variable reaches zero. Only those pairs of variables with a correlation coefficient better than 0·990 appear to be convincingly linear; these four are examined first.

Fluorine, zirconium, and rubidium. These three elements are the most strongly correlated, each pair providing a linear plot, two of which are shown in fig. 1.

In the case of F and Zr the calculated best-fit line passes close to the origin, which falls within the 95 % confidence limits. Assuming that Zr is the archetype residual element, then F too would have a bulk distribution coefficient close to zero, and constant throughout the series. The consistent behaviour of F would also indicate that the

population of obsidians is
tests confirm the findings o
conspicuous effects of devit

The correlation of Rb wi
element. The line misses th
to zero. If this distribution i
then Zr must be fractionate
throughout the lava series.
then the *system must be op*
crystallization model, then
Zr: if a fractional-melting n
Zr as the liquid volume inc
way, Rb has to move in c
system if Zr is behaving as a
ment. The same deduction
the precision, could have be
the concentration factors ir

In fact, the covariance o
shown in this range of obsi
more dramatic, because il
were generated by fraction
tion about two-thirds of th
crystals would have to be a
(based on normative *ab*+*or*
hytes) and the partition coef
between alkali feldspar and
be greater than zero. Relev
coefficients are available fro
Hedge (1970) for alkali fel
crysts and glassy matrices fi
line volcanics. They give valu
partition coefficients in eleve
rocks, ranging from 0·25 to
separated phenocrysts and g
Samples 4 and 11*b*). Deterr
spars and glass from two Eb
of 0·41 and 0·31, respectivel
D. A. Bungard). Taking th
feldspars/peralkaline-liquids
which 70 % of the separati
distribution coefficient for F
show the curve that would
distribution coefficients for
calculated from a starting-po

population of obsidians is free of vagarious late-stage volatile losses, because our tests confirm the findings of Noble *et al.* (1967) that fluorine-loss is one of the most conspicuous effects of devitrification in this sort of lava.

The correlation of Rb with Zr, however, destroys the primacy of Zr as a residual element. The line misses the origin, making a positive intercept on Zr when Rb runs to zero. If this distribution is generated by crystal ⇌ liquid relations in a closed system then Zr must be fractionated (at a constant distribution coefficient) in the solid phases throughout the lava series. If Zr is held to have a distribution coefficient close to zero then the *system must be open to Rb*. Because, if the data are fitted to a fractional-crystallization model, then Rb increases in the residual liquids at a greater rate than Zr: if a fractional-melting model is adopted then the level of Rb must fall faster than Zr as the liquid volume increases. Either way, Rb has to move in or out of the system if Zr is behaving as a residual element. The same deduction, but without the precision, could have been made from the concentration factors in Table I.

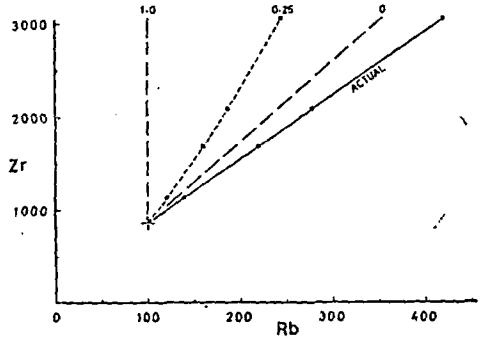

FIG. 2. Showing the difference between the actual array line for Rb *v.* Zr and that expected by fractional crystallization if the bulk distribution coefficient for Rb is finite whilst that for Zr is zero. In the latter case, taking a starting concentration of 100 ppm Rb, the points should lie between the broken lines 0 and 1·0 (if there is to be any concentration of Rb). The line 0·25 represents a reasonable case calculated on the basis of four-stage fractionation (solid squares) at intervals defined by Zr concentrations (solid circles) in the actual array.

In fact, the covariance of Rb and Zr shown in this range of obsidians is even more dramatic, because if the liquids were generated by fractional crystallization about two-thirds of the separating crystals would have to be alkali feldspar (based on normative *ab*+*or* in the trachytes) and the partition coefficient for Rb between alkali feldspar and liquid must be greater than zero. Relevant partition coefficients are available from Noble and Hedge (1970) for alkali feldspar phenocrysts and glassy matrices from peralkaline volcanics. They give values for the Rb partition coefficients in eleven peralkaline rocks, ranging from 0·25 to 0·45. Two of these determinations were made directly on separated phenocrysts and glass, giving values of 0·32 and 0·38 (1970, p. 235, Table, Samples 4 and 11*b*). Determinations of Rb have also been made on separated feldspars and glass from two Eburru rocks (PCO 134 and 135) giving partition coefficients of 0·41 and 0·31, respectively (Geochemistry Unit, Reading: analysts S. A. Malik and D. A. Bungard). Taking the average partition coefficient for Rb of 0·35 for alkali-feldspars/peralkaline-liquids, fractional crystallization (from a trachytic parent) in which 70 % of the separating crystals were alkali feldspar would result in a *bulk distribution coefficient* for Rb of 0·25. Fig. 2 is a graphical plot for Rb *v.* Zr to show the curve that would be generated by fractional crystallization when the bulk distribution coefficients for Rb and Zr are 0·25 and zero, respectively. The curve is calculated from a starting-point at 100 ppm Rb on the *actual* line and is developed by

four successive crystal crops at stages marked by *actual* Zr contents in the Eburru rocks. The highest calculated Rb value on the 'fractionation' curve is 244 ppm, which is only a little more than half the actual value (417 ppm) for the same Zr content. It is glaringly obvious from fig. 2 that either Zr is *not* a reliable index of differentiation, or fractional crystallization *cannot* account for the covariance of Rb and Zr, or *both*. All evidence available to us favours the third conclusion!

Niobium, yttrium, and chlorine. There is good correlation between Nb and Yt; the plot, shown in fig. 1, is linear within the limits of experimental error, with a narrow 95 % confidence band. The calculated line does not pass through the origin. If it were assumed that crystal fractionation controls the series, and Nb has a distribution coefficient close to zero, the sample array might be explained by Yt having a significantly higher distribution coefficient. The only phase that might be separating throughout the whole series is alkali feldspar, which would not normally be suspected of fractionating Yt with respect to Nb. Furthermore, neither Nb nor Yt shows a simple linear relation with Zr, which adds further complications to the model.

Nb and Yt both show reasonably linear correlations with Cl. The graphical plot for Nb *v.* Cl, shown in fig. 1, reveals a high positive intercept of the computed line on the Cl axis. This has the same implications for fractional crystallization as the Nb *v.* Yt array. It should be noted that if a fractional-melting evolution model is applied to these data, and Nb is taken to have a distribution coefficient of zero, then the system must be open to the ingress of Yt and Cl.

Yt *v.* Cl gives a similar pattern to Nb *v.* Cl but the line runs through the origin (within the 95 % confidence band).

Non-linear patterns, and covariance with fluorine and chlorine. Examination of the correlation matrix (Table II) shows that in addition to the four coefficients better than 0·990, there are a further ten better than 0·900. Nb and Zr are the best of this group with a coefficient of 0·972. But when graphical plots of these pairs of variables are made it emerges that many of these correlation coefficients are not lower (i.e. $< 0{\cdot}990$) due to random deviations from the line (as might be argued, for instance, for Nb *v* Cl, fig. 1). The lower coefficients for many pairs of elements result from *patterned*, but *non-linear* arrays of points. Examples are depicted in fig. 3, in which it may be seen that each computed best-fit line has been achieved by balancing a cluster of points in the middle of the array against points at the extremities. These are certainly not random patterns. The most obvious case is F *v.* Cl, with a relatively low correlation coefficient of 0·862, where a better description of the array would be an inflected line. The fact that this pattern is matched by Nb *v.* Zr, elements of a completely different kind, determined by a completely different method, must rule out the possibility that the arrangement is fortuitous. Fig. 3 confirms what was implicit from fig. 1 and the earlier discussion, namely, that Zr varies linearly with F (and Rb), that Nb varies linearly with Cl (and Yt), but between these groups of elements there is a marked inflection in the pattern of distribution. The complexity of the element covariances within these two groups, coupled with this additional complication of the relationships between the groups, rules out any rational *closed-system* (isochemical) evolutionary model. Such a conclusion is entirely consonant with those reached earlier on the

basis of major-element v
and trace elements (Bail
Before considering al
Eburru obsidians, the a
needs comment (fig. 3).

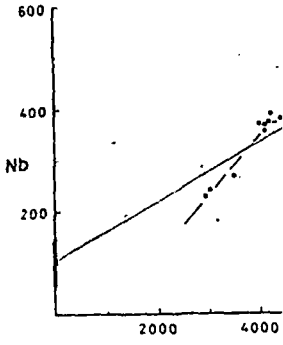

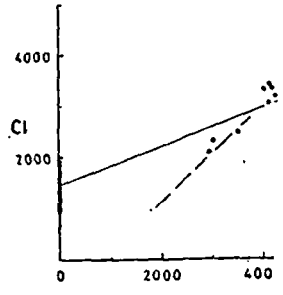

FIG. 3. Four examples of n
and heavy bars as in fig. 1.
case. In the Zn *v.* Zr plot

Secondly, the limiting
good agreement. Third
Eburru samples, are no
method, because the s
sidians from the Naiva
prepared, and analyse
anomaly in the Eburru
best-fit line in fig. 3 is
for F and Cl)—the imp
Zn concentration supe

basis of major-element variations (Macdonald *et al.*, 1970) and comparisons of major and trace elements (Bailey, 1973).

Before considering alternative explanations for the chemical variations in the Eburru obsidians, the anomalously high, and seemingly erratic, zinc distribution needs comment (fig. 3). Firstly, Zn can be determined with high precision by XRF.

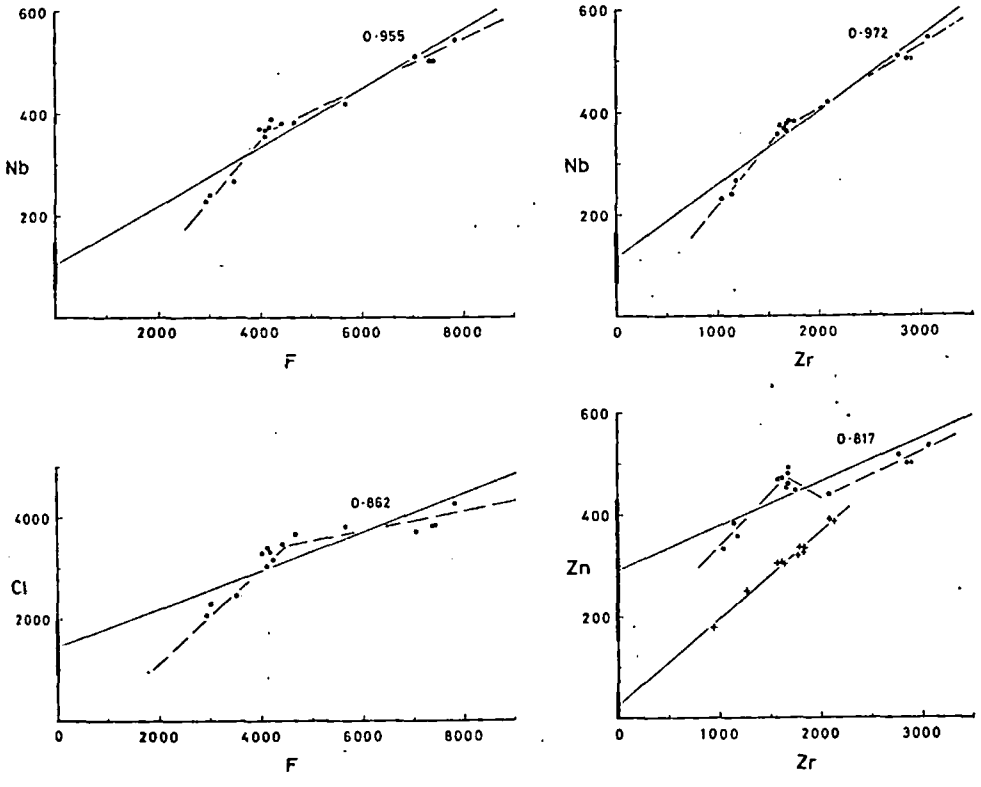

FIG. 3. Four examples of non-linear arrays in the Eburru obsidians. Solid circles, continuous lines, and heavy bars as in fig. 1. The broken lines represent preferred descriptions of the variation in each case. In the Zn *v.* Zr plot the plus signs are comendite obsidians from the Naivasha volcanic area (see text).

Secondly, the limiting Zn values in fig. 3 were checked by atomic absorption, with good agreement. Thirdly, the high levels, and the variability, of the Zn values in the Eburru samples, are not due to vagaries of sampling, sample preparation, or analytical method, because the second data set (plus signs) in fig. 3 represent comendite obsidians from the Naivasha volcanic area, just south of Eburru. These were collected, prepared, and analysed with the Eburru samples, so we are seeing a genuine Zn anomaly in the Eburru rocks. Fourthly, the broad scatter of the Zn values about the best-fit line in fig. 3 is confirmed by later results on other samples (not yet analysed for F and Cl)—the impression given by this pattern is of a second-order fluctuation in Zn concentration superimposed on a main trend indicated by the line. The general

form of the Zn distribution, when plotted against Zr, resembles that of Yt, Nb, and Cl against Zr, except that the general high levels of Zn are more obvious. Indeed, Zn shows its strongest correlations with Yt, Nb, and Cl, in that order (see Table II) so that similar factors, either at source or during magma generation, or both, have presumably influenced all four elements, but to different degrees. At present we have no evidence to suggest possible causes of the second-order fluctuations in the Zn pattern.

As a final point it should be noted that inflected patterns similar to those among the trace elements (shown in fig. 3) also emerge when some major elements (and their functions) are plotted against Zr. Examples are Al_2O_3, TiO_2, and agpaitic index $(Mol(Na_2O+K_2O)/Al_2O_3)$.

An open-system model

In our earlier paper on the major-element patterns in the range pantelleritic trachyte to pantellerite (Macdonald *et al.*, 1970) we had to conclude that *if the rocks were an evolutionary series* a phase now missing from the rocks must have played a major part in the evolutionary process. The Eburru obsidians fall into the previously defined major-element patterns and the same conclusion applies. Furthermore, the trace-element patterns are now found to be incompatible with closed-system evolution. We concluded from the earlier major-element studies that if the rocks had been generated by a series of melting episodes then a separate vapour (fluid) phase had contributed Na (and possibly Si and Fe) to successive silicate liquids. Our reasons for preferring a fractional-melting model were given in that account (Macdonald *et al.*, 1970): a further reason in the Eburru rocks is that the chemical variations do not seem to fit any regular pattern in the development of the volcano. It would be premature to try to elaborate this model much further until all our data are in, but some additional conclusions from the present trace-element distributions are in order.

It is clear that a simple fractional-melting model could not generate most of the observed trace-element patterns. For instance, most of the correlation lines do not pass through the origin, which would be the first requirement for 'residual' elements. In such cases, where the correlation is linear (fig. 1) the line could be interpreted as a product of simple mixing, but the true picture must be more complex because some patterns are inflected (fig. 3). The most significant feature is the affinity of Zr and Rb with F, and the *separate* affinity of Nb, Yt, and Zn with Cl: judging by the inflected variation patterns between these two groups they would seem to have some degree of independence throughout the rock series. One possibility is that the metallic elements form preferred complexes with either fluorine or chlorine, and the partitioning of these complexes between vapour (fluid) and silicate melt varies with the melting conditions (e.g. relative volumes of melt to vapour, variations in melt or vapour compositions, temperature, and pressure). We are investigating this and other possibilities by: further analyses of Eburru rocks and extracted gases; experimental determination of melting, crystallization, and volatile exsolution; and by studies of obsidian suites from other volcanoes.

Another remarkable feature of the Eburru rocks is the Rb variation, which shows no recognizable contribution from alkali feldspars in contact with the melt (yet

alkali-feldspar phenocrysts
Rb (and Zr and F) is accep
this vapour is paramount.
major element such as Al gi
and F also suggests that th
factor other than those tha

Finally, one general point
It is commonly argued by
centrations of Zr that disti
the solubility of Zr in per
zircon during crystallizatio
centrations of F and Cl t
other oversaturated magm
in our samples exposes this
and petrochemists to criti
magma evolution.

Acknowledgements. Wet cher
Bungard; XRF analyses for
indebted, too, to Dr. A. Park
putations, and to Dr. R. T
operation. A. Parker, J. E. Th
comments on the first draft.

Bailey (D. K.), 1973. *Journ..g*
—— Weaver (S. D.), and Sut
Macdonald (R.) and Bailey
—— —— and Sutherland (D
Noble (D. C.) and Hedge (C.
Parker (A.) (unpubl.). *Geol. J*
Sutherland (D. S.), 1971. *Jo*
Thomas (J. E.), Bungard (D.
Till (R.), 1973. *Area* (*Inst. of*
Weaver (S. D.), Sceal (J. S. C

[*Manuscript received 21 Augus*

alkali-feldspar phenocrysts are normal). If a coexisting vapour phase contributing Rb (and Zr and F) is accepted, the Rb patterns in the rocks suggest that the effect of this vapour is paramount. It is as if the melts were buffered for Rb. The fact that a key major element such as Al gives inflected variation patterns when plotted against Zr, Rb, and F also suggests that the concentrations of these elements are controlled by some factor other than those that determine the major-element distributions in the magmas.

Finally, one general point may be made concerning F and Cl in peralkaline magmas. It is commonly argued by advocates of fractional crystallization, that the high concentrations of Zr that distinguish peralkaline from subaluminous magmas are due to the solubility of Zr in peralkaline melts, and their consequent failure to precipitate zircon during crystallization. But how, then, is it possible to account for the high concentrations of F and Cl that equally distinguish these same peralkaline melts from other oversaturated magmas? We believe that the very high correlation of Zr and F in our samples exposes this as an artificial dilemma, and we appeal to fellow petrologists and petrochemists to critically reappraise some of the time-honoured concepts of magma evolution.

Acknowledgements. Wet chemical analyses for F and Cl were made by S. A. Malik and D. A. Bungard; XRF analyses for Zn, Nb, Zr, Yt, and Rb by G. J. Smith and N. I. Tarrant. We are indebted, too, to Dr. A. Parker who set up the XRF routines, calibration methods, and computations, and to Dr. R. Till and Mrs. J. Webber for the correlation programme and its operation. A. Parker, J. E. Thomas, and R. Till improved the final manuscript by their valuable comments on the first draft.

REFERENCES

BAILEY (D. K.), 1973. *Journ. geol. Soc. Proc.* 129, 649.
—— WEAVER (S. D.), and SUTHERLAND (D. S.), 1975. *Contr. Min. Petr.* 50, 47–8.
MACDONALD (R.) and BAILEY (D. K.), 1973. *U.S. Geol. Surv. Prof. Paper*, 440N–1.
—— —— and SUTHERLAND (D. S.), 1970. *Journ. Petrology*, 11, 507–17.
NOBLE (D. C.) and HEDGE (C. E.), 1970. *Contr. Min. Petr.* 29, 234–41.
PARKER (A.) (unpubl.). *Geol. Dept. Univ. of Reading.*
SUTHERLAND (D. S.), 1971. *Journ. geol. Soc. Proc.* 127, 417.
THOMAS (J. E.), BUNGARD (D. A.), and MALIK (S. A.), 1975. *Univ. Reading Geol. Reports*, 6.
TILL (R.), 1973. *Area (Inst. of Brit. Geographers)*, 5, 303–8.
WEAVER (S. D.), SCEAL (J. S. C.), and GIBSON (I. L.), 1972. *Contr. Min. Petr.*, 36, 181–94.

[*Manuscript received 21 August 1974; revised 5 June 1975*]

MINERALOGICAL MAGAZINE, DECEMBER 1975, VOL. 40, PP. 405–14

Fluorine and chlorine in peralkaline liquids and the need for magma generation in an open system

D. K. BAILEY

Department of Geology, University of Reading, Reading, RG6 2AB

AND R. MACDONALD

Department of Environmental Sciences, University of Lancaster, Bailrigg, Lancaster

SUMMARY. Fluorine, chlorine, zinc, niobium, zirconium, yttrium, and rubidium have been determined on fifteen obsidians from Eburru volcano (Kenya Rift Valley), spanning the range from pantellcritic trachyte to pantellerite. All pairs of elements show positive correlation coefficients, ranging between 0·769 and 0·998, but with most values better than 0·900. In spite of some very high correlations, only two of the twenty-one best-fit lines pass near the origin of the Cartesian coordinates. Linear distributions are found *within* two separate groups of elements: F, Zr, Rb; and Cl, Nb, Yt. Zn behaves in general as a member of the second group but seems to be subject to an additional variation. When an element from the fluorine group is plotted against one from the chlorine group the resulting pattern is non-linear. Therefore, although the elements in both groups would generally be considered 'residual' (partition coefficients between crystals and liquid approaching zero) there are clearly detectable differences in their variation, and hence their behaviour.

Major-element variations in the obsidians are such that a vapour (fluid) phase would be needed to account for any magma evolution. The trace-element patterns are also impossible by closed-system crystal fractionation and suggest that this fluid may have been rich in halogens, with the metallic elements forming preferred 'complexes' with either F or Cl. The F–Zr–Rb 'complex' also varies quite independently of the important major oxides (e.g. Al_2O_3) in the rocks. In the case of Rb this is but one aspect of a more significant anomaly, in which there is no sign of any influence of alkali feldspar (which partitions Rb) in the variation. This is remarkable because trachytes and rhyolites have normative $ab+or > 50$ %, and any evolutionary process *controlled* by crystal ⇌ liquid interactions must be dominated by the melting or crystallization of alkali feldspar. The results on the Eburru obsidians show that *if they are an evolutionary series* then *either*, the process was not crystal ⇌ liquid controlled, *or* that any such process has been overriden (or buffered) by other processes that have superimposed the observed trace-element patterns. In the latter event, the buffering phase may have been a halogen-bearing vapour.

The same considerations must apply to other pantellerite provinces where Rb appears to have behaved as a 'residual' element.

In recent years we have compiled all the available data on oversaturated peralkaline obsidians (Macdonald and Bailey, 1973) and set in train an analytical programme on all new samples that we have been able to obtain. Our own field sampling has been focused on the Nakuru–Naivasha region of Kenya, the topographic culmination of the East African rift, where there is an unparalleled development of Quaternary–Recent peralkaline volcanoes. In the trachyte to pantellerite composition range it had been demonstrated previously that the obsidians from different volcanoes showed systematic variations in major-element chemistry, but these variations were not consistent with

a fractional-crystallization model involving the observed phenocryst phases (Macdonald *et al.*, 1970). The best development of pantellerite magmatism is found in the Eburru volcano (Sutherland, 1971) just north-west of Lake Naivasha. Trace-element analyses of some of Sutherland's samples by Weaver *et al.* (1972) were used (with data from five other volcanoes) to argue that the relationships between trachytes and pantellerites are most reasonably explained by fractional crystallization. Subsequent examination has revealed, however, that the 'Eburru' specimens used by Weaver *et al.* were a mixed population (Bailey *et al.*, 1975).

Since 1970 we have collected and analysed obsidians from Eburru, which span the composition range from quartz-trachyte to pantellerite, and the major-element variation within this one volcanic pile cannot be explained by fractional crystallization of the phenocryst phases. The major-element evidence on quenched liquids is thus in direct conflict with the conclusions reached through the trace elements by Weaver *et al.* (1972). Trace-element analyses of our own Eburru samples form part of the long-term study of peralkaline obsidians, and they are now sufficiently far advanced to demonstrate that fractional crystallization *cannot* explain the variations. This demonstration, however, is only a subsidiary aim of the present article—our chief concern is to describe some unexpected relationships (especially involving halogens) which may provide some real clues to the secrets of this magmatism.

We shall look at a small group of trace elements (F, Cl, Zn, Nb, Zr, Yt, and Rb), which includes the two (Nb and Zr) considered most significant by Weaver *et al.* (1972). Our population is fifteen obsidians from quartz-trachyte to rhyolite: we are unable to include any basalts because we are restricting our study to glasses (quenched liquids). Actually, there are no contemporaneous basalts in the Eburru pile, although there is a Recent basalt field in the lowlands just to the north. We believe it would be begging the question to include these basalts with the Eburru magmatism until we have evidence other than geographic proximity to indicate that the two may be cogenetic (this problem is currently being studied by A. W. H. Bowhill, University of Reading: see also Bailey *et al.*, 1975, fig. 1). Correlations among the selected trace elements are moderately to strongly positive, whereas their correlations with major elements are generally poor. Although the major element ranges in the population are small (e.g. SiO_2 range from 66·2 to 72·0 per cent) the trace element ranges are large (e.g. Zr range from 1038 to 3058 ppm). Samples with essentially identical major-element chemistry show widely different trace-element levels, and the impossibility of reconciling these facts with simple fractional crystallization has been noted elsewhere (Bailey, 1973).

Trace-element relations. The limits, means, and concentration factors are listed in Table I. Trace-element values, sample points, rock names, and age relations are given in the Appendix.

The absence of basic rocks, with very low levels of the selected trace elements, is not a serious drawback to correlation analysis because in the case of the strongly concentrated elements, F, Zr, and Rb, the obsidian values span two-thirds of the possible range from the maximum observed down to zero. The results of the correlation analysis are given in matrix form in Table II.

TABLE I. *Limits, means, c*

Minimum (m)	
Maximum (M)	
Mean	
Standard Deviatio	
Maximum concentration factor (M/m)	

TABLE II. *Correlation m*
are positive). Plus or minu
major-axis equation: Till,
the 95 % confidence limit

	F	Cl
F	1·000	
Cl	0·862(+)	1·00
Zn	0·769(+)	0·87
Nb	0·955(+)	0·94
Zr	0·994(0)	0·87
Yt	0·932(+)	0·95
Rb	0·996(−)	0·85

Imp

The central tenet of t
as propounded by Weav
elements will be unable
concentrated in the resic
cess dominated by cryst
to be proven, but for th
the prime example of a
melts (and insolubility i
'volatile effects'; and
(Weaver *et al.*, 1972). (
ferentiation than the m
are, of course, compou
reconcile the claim with
now cannot find suppo

Weaver *et al.* (1972
graphical plots of each

TABLE I. *Limits, means, and concentration factors in 15 obsidians from Eburru, Kenya. Values in ppm*

	F	Cl	Zn	Nb	Zr	Yt	Rb
Minimum (m)	2910	2090	333	230	1038	195	131
Maximum (M)	7800	4290	537	542	3058	410	417
Mean	4900	3300	457	388	1910	307	252
Standard Deviation	1660	630	58	96	671	63	98
Maximum concentration factor (M/m)	2·68	2·05	1·61	2·36	2·95	2·10	3·18

TABLE II. *Correlation matrix for trace elements in the Eburru obsidians (all coefficients are positive). Plus or minus indicates the sign of the intercept of the best-fit line (reduced major-axis equation: Till, 1973) on the axis of the second variable in those cases where the 95 % confidence limits do not include the origin. Zero indicates that the origin falls within the 95 % confidence limits*

	F	Cl	Zn	Nb	Zr	Yt	Rb
F	1·000						
Cl	0·862(+)	1·000					
Zn	0·769(+)	0·879(+)	1·000				
Nb	0·955(+)	0·943(−)	0·909(−)	1·000			
Zr	0·994(0)	0·876(−)	0·817(−)	0·972(−)	1·000		
Yt	0·932(+)	0·954(0)	0·928(−)	0·995(+)	0·951(+)	1·000	
Rb	0·996(−)	0·853(−)	0·790(−)	0·959(−)	0·998(−)	0·937(−)	1·000

Implications of the trace-element distributions

The central tenet of the trace-element argument with respect to magma evolution, as propounded by Weaver *et al.* (1972), is that in a series of peralkaline liquids certain elements will be unable to enter the crystallizing phases, and will become progressively concentrated in the residual liquids. This assumes that the liquids are related by a process dominated by crystal ⇌ liquid interactions: we would claim that this itself needs to be proven, but for the moment let us examine the rest of the case. Zr is chosen as the prime example of a residual element because of: its high solubility in peralkaline melts (and insolubility in the major crystalline phases); its impassiveness to late-stage 'volatile effects'; and its abundance and high-precision determination by XRF (Weaver *et al.*, 1972). Consequently Zr is claimed to be a more useful index of differentiation than the more commonly used major-element indices. More assumptions are, of course, compounded in this claim. In the case of the Eburru rocks we cannot reconcile the claim with the major-element patterns (Bailey, 1973) and, moreover, we now cannot find support for it in our trace-element data.

Weaver *et al.* (1972) state that in the six volcanic centres they have tested the graphical plots of each of the elements Ce, La, Nb, and Rb against Zr are linear, and

project through the origin. They deduce from this (assuming that Zr is the archetype residual element) that the other four elements also have bulk distribution-coefficients (element concentration in combined crystal phases/concentration in liquid) close to zero. Compared with their data on Eburru (kindly provided by S. D. Weaver) our

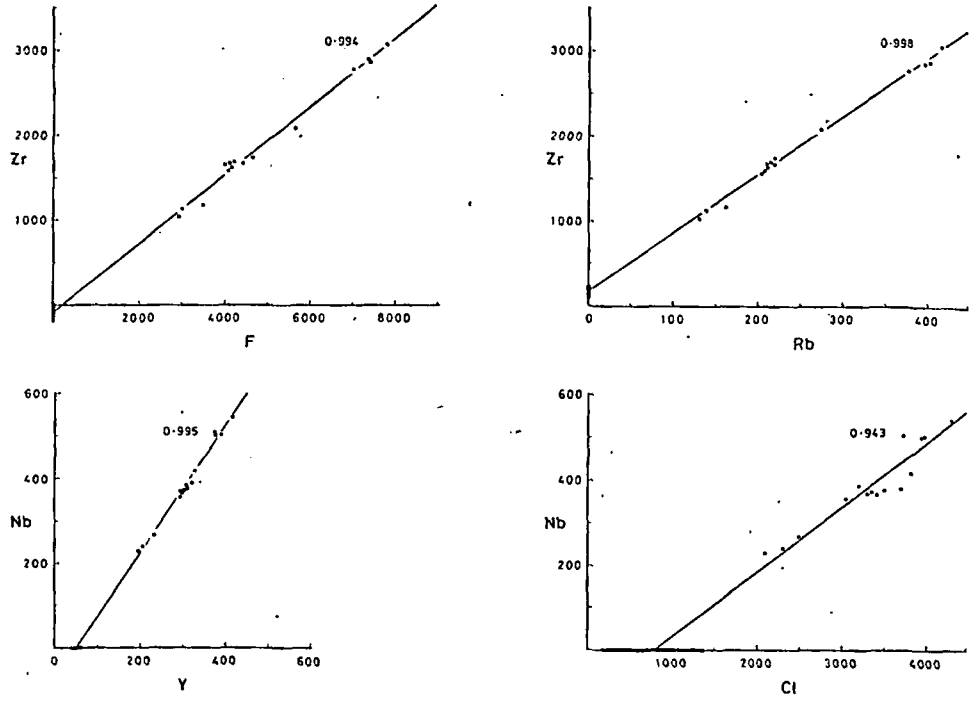

FIG. 1. Four examples of linear correlations of element pairs in the Eburru obsidians (solid circles). In every case the line is the computed reduced major-axis line and the heavy bar on the axis shows the 95 % confidence limits on the intercept. All values in ppm.

obsidian analyses show far less 'noise', more systematic variations, and higher correlation coefficients throughout. Our distribution patterns are quite different. Many are not linear, and most do not project through the origin. The latter are shown in Table II by plus and minus signs, to indicate the sign of the intercept on the axis of the second variable when the first variable reaches zero. Only those pairs of variables with a correlation coefficient better than 0·990 appear to be convincingly linear; these four are examined first.

Fluorine, zirconium, and rubidium. These three elements are the most strongly correlated, each pair providing a linear plot, two of which are shown in fig. 1.

In the case of F and Zr the calculated best-fit line passes close to the origin, which falls within the 95 % confidence limits. Assuming that Zr is the archetype residual element, then F too would have a bulk distribution coefficient close to zero, and constant throughout the series. The consistent behaviour of F would also indicate that the

population of obsidians is
tests confirm the findings o
conspicuous effects of devit

The correlation of Rb w
element. The line misses th
to zero. If this distribution i
then Zr must be fractionate
throughout the lava series.
then the *system must be op*
crystallization model, then
Zr: if a fractional-melting n
Zr as the liquid volume inc
way, Rb has to move in c
system if Zr is behaving as a
ment: The same deduction
the precision, could have be
the concentration factors ir

In fact, the covariance o
shown in this range of obsi
more dramatic, because il
were generated by fraction
tion about two-thirds of th
crystals would have to be a
(based on normative *ab*+*or*
hytes) and the partition coef
between alkali feldspar and
be greater than zero. Relev
coefficients are available fro
Hedge (1970) for alkali fel
crysts and glassy matrices fi
line volcanics. They give valu
partition coefficients in eleve
rocks, ranging from 0·25 to
separated phenocrysts and g
Samples 4 and 11*b*). Deterr
spars and glass from two Eb
of 0·41 and 0·31, respectively
D. A. Bungard). Taking the
feldspars/peralkaline-liquids
which 70 % of the separati
distribution coefficient for I
show the curve that would
distribution coefficients for
calculated from a starting-pc

population of obsidians is free of vagarious late-stage volatile losses, because our tests confirm the findings of Noble *et al.* (1967) that fluorine-loss is one of the most conspicuous effects of devitrification in this sort of lava.

The correlation of Rb with Zr, however, destroys the primacy of Zr as a residual element. The line misses the origin, making a positive intercept on Zr when Rb runs to zero. If this distribution is generated by crystal ⇌ liquid relations in a closed system then Zr must be fractionated (at a constant distribution coefficient) in the solid phases throughout the lava series. If Zr is held to have a distribution coefficient close to zero then the *system must be open to Rb*. Because, if the data are fitted to a fractional-crystallization model, then Rb increases in the residual liquids at a greater rate than Zr: if a fractional-melting model is adopted then the level of Rb must fall faster than Zr as the liquid volume increases. Either way, Rb has to move in or out of the system if Zr is behaving as a residual element. The same deduction, but without the precision, could have been made from the concentration factors in Table I.

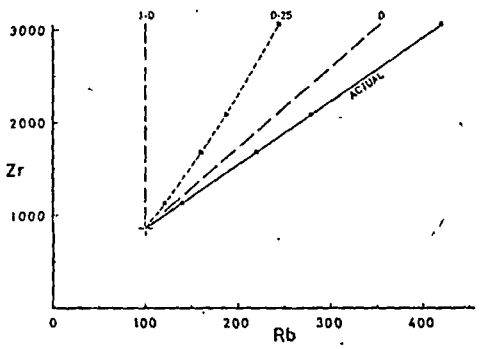

FIG. 2. Showing the difference between the actual array line for Rb *v.* Zr and that expected by fractional crystallization if the bulk distribution coefficient for Rb is finite whilst that for Zr is zero. In the latter case, taking a starting concentration of 100 ppm Rb, the points should lie between the broken lines 0 and 1·0 (if there is to be any concentration of Rb). The line 0·25 represents a reasonable case calculated on the basis of four-stage fractionation (solid squares) at intervals defined by Zr concentrations (solid circles) in the actual array.

In fact, the covariance of Rb and Zr shown in this range of obsidians is even more dramatic, because if the liquids were generated by fractional crystallization about two-thirds of the separating crystals would have to be alkali feldspar (based on normative *ab*+*or* in the trachytes) and the partition coefficient for Rb between alkali feldspar and liquid must be greater than zero. Relevant partition coefficients are available from Noble and Hedge (1970) for alkali feldspar phenocrysts and glassy matrices from peralkaline volcanics. They give values for the Rb partition coefficients in eleven peralkaline rocks, ranging from 0·25 to 0·45. Two of these determinations were made directly on separated phenocrysts and glass, giving values of 0·32 and 0·38 (1970, p. 235, Table, Samples 4 and 11*b*). Determinations of Rb have also been made on separated feldspars and glass from two Eburru rocks (PCO 134 and 135) giving partition coefficients of 0·41 and 0·31, respectively (Geochemistry Unit, Reading: analysts S. A. Malik and D. A. Bungard). Taking the average partition coefficient for Rb of 0·35 for alkali-feldspars/peralkaline-liquids, fractional crystallization (from a trachytic parent) in which 70 % of the separating crystals were alkali feldspar would result in a *bulk distribution coefficient* for Rb of 0·25. Fig. 2 is a graphical plot for Rb *v.* Zr to show the curve that would be generated by fractional crystallization when the bulk distribution coefficients for Rb and Zr are 0·25 and zero, respectively. The curve is calculated from a starting-point at 100 ppm Rb on the *actual* line and is developed by

four successive crystal crops at stages marked by *actual* Zr contents in the Eburru rocks. The highest calculated Rb value on the 'fractionation' curve is 244 ppm, which is only a little more than half the actual value (417 ppm) for the same Zr content. It is glaringly obvious from fig. 2 that either Zr is *not* a reliable index of differentiation, or fractional crystallization *cannot* account for the covariance of Rb and Zr, or *both*. All evidence available to us favours the third conclusion!

Niobium, yttrium, and chlorine. There is good correlation between Nb and Yt; the plot, shown in fig. 1, is linear within the limits of experimental error, with a narrow 95 % confidence band. The calculated line does not pass through the origin. If it were assumed that crystal fractionation controls the series, and Nb has a distribution coefficient close to zero, the sample array might be explained by Yt having a significantly higher distribution coefficient. The only phase that might be separating throughout the whole series is alkali feldspar, which would not normally be suspected of fractionating Yt with respect to Nb. Furthermore, neither Nb nor Yt shows a simple linear relation with Zr, which adds further complications to the model.

Nb and Yt both show reasonably linear correlations with Cl. The graphical plot for Nb *v.* Cl, shown in fig. 1, reveals a high positive intercept of the computed line on the Cl axis. This has the same implications for fractional crystallization as the Nb *v.* Yt array. It should be noted that if a fractional-melting evolution model is applied to these data, and Nb is taken to have a distribution coefficient of zero, then the system must be open to the ingress of Yt and Cl.

Yt *v.* Cl gives a similar pattern to Nb *v.* Cl but the line runs through the origin (within the 95 % confidence band).

Non-linear patterns, and covariance with fluorine and chlorine. Examination of the correlation matrix (Table II) shows that in addition to the four coefficients better than 0·990, there are a further ten better than 0·900. Nb and Zr are the best of this group with a coefficient of 0·972. But when graphical plots of these pairs of variables are made it emerges that many of these correlation coefficients are not lower (*i.e.* $< 0{\cdot}990$) due to random deviations from the line (as might be argued, for instance, for Nb *v* Cl, fig. 1). The lower coefficients for many pairs of elements result from *patterned*, but *non-linear* arrays of points. Examples are depicted in fig. 3, in which it may be seen that each computed best-fit line has been achieved by balancing a cluster of points in the middle of the array against points at the extremities. These are certainly not random patterns. The most obvious case is F *v.* Cl, with a relatively low correlation coefficient of 0·862, where a better description of the array would be an inflected line. The fact that this pattern is matched by Nb *v.* Zr, elements of a completely different kind, determined by a completely different method, must rule out the possibility that the arrangement is fortuitous. Fig. 3 confirms what was implicit from fig. 1 and the earlier discussion, namely, that Zr varies linearly with F (and Rb), that Nb varies linearly with Cl (and Yt), but between these groups of elements there is a marked inflection in the pattern of distribution. The complexity of the element covariances within these two groups, coupled with this additional complication of the relationships between the groups, rules out any rational *closed-system* (isochemical) evolutionary model. Such a conclusion is entirely consonant with those reached earlier on the

basis of major-element va
and trace elements (Baile

Before considering alt
Eburru obsidians, the a
needs comment (fig. 3).

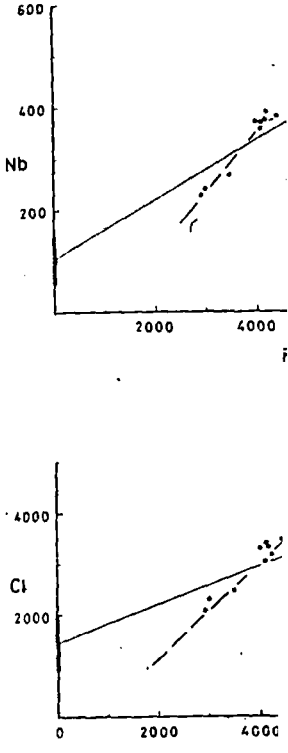

FIG. 3. Four examples of n
and heavy bars as in fig. 1.
case. In the Zn *v.* Zr plot t

Secondly, the limiting
good agreement. Thirdl
Eburru samples, are not
method, because the s
sidians from the Naiva
prepared, and analyse
anomaly in the Eburru
best-fit line in fig. 3 is
for F and Cl)—the imp
Zn concentration supe

basis of major-element variations (Macdonald *et al.*, 1970) and comparisons of major and trace elements (Bailey, 1973).

Before considering alternative explanations for the chemical variations in the Eburru obsidians, the anomalously high, and seemingly erratic, zinc distribution needs comment (fig. 3). Firstly, Zn can be determined with high precision by XRF.

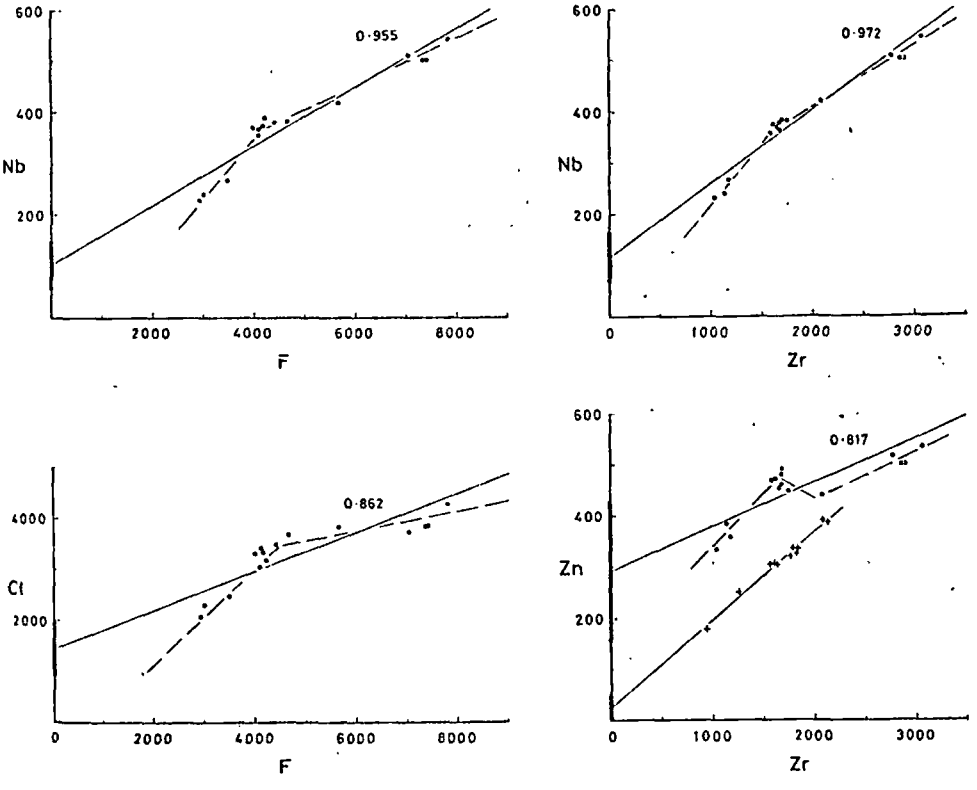

FIG. 3. Four examples of non-linear arrays in the Eburru obsidians. Solid circles, continuous lines, and heavy bars as in fig. 1. The broken lines represent preferred descriptions of the variation in each case. In the Zn *v.* Zr plot the plus signs are comendite obsidians from the Naivasha volcanic area (see text).

Secondly, the limiting Zn values in fig. 3 were checked by atomic absorption, with good agreement. Thirdly, the high levels, and the variability, of the Zn values in the Eburru samples, are not due to vagaries of sampling, sample preparation, or analytical method, because the second data set (plus signs) in fig. 3 represent comendite obsidians from the Naivasha volcanic area, just south of Eburru. These were collected, prepared, and analysed with the Eburru samples, so we are seeing a genuine Zn anomaly in the Eburru rocks. Fourthly, the broad scatter of the Zn values about the best-fit line in fig. 3 is confirmed by later results on other samples (not yet analysed for F and Cl)—the impression given by this pattern is of a second-order fluctuation in Zn concentration superimposed on a main trend indicated by the line. The general

form of the Zn distribution, when plotted against Zr, resembles that of Yt, Nb, and Cl against Zr, except that the general high levels of Zn are more obvious. Indeed, Zn shows its strongest correlations with Yt, Nb, and Cl, in that order (see Table II) so that similar factors, either at source or during magma generation, or both, have presumably influenced all four elements, but to *different degrees*. At present we have no evidence to suggest possible causes of the second-order fluctuations in the Zn pattern.

As a final point it should be noted that inflected patterns similar to those among the trace elements (shown in fig. 3) also emerge when some major elements (and their functions) are plotted against Zr. Examples are Al_2O_3, TiO_2, and agpaitic index $(Mol(Na_2O+K_2O)/Al_2O_3)$.

An open-system model

In our earlier paper on the major-element patterns in the range pantelleritic trachyte to pantellerite (Macdonald *et al.*, 1970) we had to conclude that *if the rocks were an evolutionary series* a phase now missing from the rocks must have played a major part in the evolutionary process. The Eburru obsidians fall into the previously defined major-element patterns and the same conclusion applies. Furthermore, the trace-element patterns are now found to be incompatible with closed-system evolution. We concluded from the earlier major-element studies that if the rocks had been generated by a series of melting episodes then a separate vapour (fluid) phase had contributed Na (and possibly Si and Fe) to successive silicate liquids. Our reasons for preferring a fractional-melting model were given in that account (Macdonald *et al.*, 1970): a further reason in the Eburru rocks is that the chemical variations do not seem to fit any regular pattern in the development of the volcano. It would be premature to try to elaborate this model much further until all our data are in, but some additional conclusions from the present trace-element distributions are in order.

It is clear that a simple fractional-melting model could not generate most of the observed trace-element patterns. For instance, most of the correlation lines do not pass through the origin, which would be the first requirement for 'residual' elements. In such cases, where the correlation is linear (fig. 1) the line could be interpreted as a product of simple mixing, but the true picture must be more complex because some patterns are inflected (fig. 3). The most significant feature is the affinity of Zr and Rb with F, and the *separate* affinity of Nb, Yt, and Zn with Cl: judging by the inflected variation patterns between these two groups they would seem to have some degree of independence throughout the rock series. One possibility is that the metallic elements form preferred complexes with either fluorine or chlorine, and the partitioning of these complexes between vapour (fluid) and silicate melt varies with the melting conditions (e.g. relative volumes of melt to vapour, variations in melt or vapour compositions, temperature, and pressure). We are investigating this and other possibilities by: further analyses of Eburru rocks and extracted gases; experimental determination of melting, crystallization, and volatile exsolution; and by studies of obsidian suites from other volcanoes.

Another remarkable feature of the Eburru rocks is the Rb variation, which shows no recognizable contribution from alkali feldspars in contact with the melt (yet

alkali-feldspar phenocrysts
Rb (and Zr and F) is accept
this vapour is paramount. *I*
major element such as Al giv
and F also suggests that th
factor other than those that

Finally, one general point
It is commonly argued by
centrations of Zr that distu
the solubility of Zr in per
zircon during crystallizatio
centrations of F and Cl th
other oversaturated magma
in our samples exposes this
and petrochemists to criti
magma evolution.

Acknowledgements. Wet chen
Bungard; XRF analyses for Z
indebted, too, to Dr. A. Park
putations, and to Dr. R. Ti
operation. A. Parker, J. E. Th
comments on the first draft.

Bailey (D. K.), 1973. *Journ. g*
—— Weaver (S. D.), and Sut
Macdonald (R.) and Bailey (
—— —— and Sutherland (D
Noble (D. C.) and Hedge (G.
Parker (A.) (unpubl.). *Geol. L*
Sutherland (D. S.), 1971. *Jou*
Thomas (J. E.), Bungard (D.
Till (R.), 1973. *Area (Inst. of*
Weaver (S. D.), Sceal (J. S. C

[*Manuscript received 21 Augus*

alkali-feldspar phenocrysts are normal). If a coexisting vapour phase contributing Rb (and Zr and F) is accepted, the Rb patterns in the rocks suggest that the effect of this vapour is paramount. It is as if the melts were buffered for Rb. The fact that a key major element such as Al gives inflected variation patterns when plotted against Zr, Rb, and F also suggests that the concentrations of these elements are controlled by some factor other than those that determine the major-element distributions in the magmas.

Finally, one general point may be made concerning F and Cl in peralkaline magmas. It is commonly argued by advocates of fractional crystallization, that the high concentrations of Zr that distinguish peralkaline from subaluminous magmas are due to the solubility of Zr in peralkaline melts, and their consequent failure to precipitate zircon during crystallization. But how, then, is it possible to account for the high concentrations of F and Cl that equally distinguish these same peralkaline melts from other oversaturated magmas? We believe that the very high correlation of Zr and F in our samples exposes this as an artificial dilemma, and we appeal to fellow petrologists and petrochemists to critically reappraise some of the time-honoured concepts of magma evolution.

Acknowledgements. Wet chemical analyses for F and Cl were made by S. A. Malik and D. A. Bungard; XRF analyses for Zn, Nb, Zr, Yt, and Rb by G. J. Smith and N. I. Tarrant. We are indebted, too, to Dr. A. Parker who set up the XRF routines, calibration methods, and computations, and to Dr. R. Till and Mrs. J. Webber for the correlation programme and its operation. A. Parker, J. E. Thomas, and R. Till improved the final manuscript by their valuable comments on the first draft.

REFERENCES

BAILEY (D. K.), 1973. *Journ. geol. Soc. Proc.* **129**, 649.
—— WEAVER (S. D.), and SUTHERLAND (D. S.), 1975. *Contr. Min. Petr.* **50**, 47–8.
MACDONALD (R.) and BAILEY (D. K.), 1973. *U.S. Geol. Surv. Prof. Paper*, 440N–1.
—— —— and SUTHERLAND (D. S.), 1970. *Journ. Petrology*, **11**, 507–17.
NOBLE (D. C.) and HEDGE (C. E.), 1970. *Contr. Min. Petr.* **29**, 234–41.
PARKER (A.) (unpubl.). *Geol. Dept. Univ. of Reading.*
SUTHERLAND (D. S.), 1971. *Journ. geol. Soc. Proc.* **127**, 417.
THOMAS (J. E.), BUNGARD (D. A.), and MALIK (S. A.), 1975. *Univ. Reading Geol. Reports*, **6**.
TILL (R.), 1973. *Area (Inst. of Brit. Geographers)*, **5**, 303–8.
WEAVER (S. D.), SCEAL (J. S. C.), and GIBSON (I. L.), 1972. *Contr. Min. Petr.*, **36**, 181–94.

[*Manuscript received 21 August 1974; revised 5 June 1975*]

MINERALOGICAL MAGAZINE, DECEMBER 1975, VOL. 40, PP. 405–14

Fluorine and chlorine in peralkaline liquids and the need for magma generation in an open system

D. K. BAILEY

Department of Geology, University of Reading, Reading, RG6 2AB

AND R. MACDONALD

Department of Environmental Sciences, University of Lancaster, Bailrigg, Lancaster

SUMMARY. Fluorine, chlorine, zinc, niobium, zirconium, yttrium, and rubidium have been determined on fifteen obsidians from Eburru volcano (Kenya Rift Valley), spanning the range from pantelleritic trachyte to pantellerite. All pairs of elements show positive correlation coefficients, ranging between 0·769 and 0·998, but with most values better than 0·900. In spite of some very high correlations, only two of the twenty-one best-fit lines pass near the origin of the Cartesian coordinates. Linear distributions are found *within* two separate groups of elements: F, Zr, Rb; and Cl, Nb, Yt. Zn behaves in general as a member of the second group but seems to be subject to an additional variation. When an element from the fluorine group is plotted against one from the chlorine group the resulting pattern is non-linear. Therefore, although the elements in both groups would generally be considered 'residual' (partition coefficients between crystals and liquid approaching zero) there are clearly detectable differences in their variation, and hence their behaviour.

Major-element variations in the obsidians are such that a vapour (fluid) phase would be needed to account for any magma evolution. The trace-element patterns are also impossible by closed-system crystal fractionation and suggest that this fluid may have been rich in halogens, with the metallic elements forming preferred 'complexes' with either F or Cl. The F–Zr–Rb 'complex' also varies quite independently of the important major oxides (e.g. Al_2O_3) in the rocks. In the case of Rb this is but one aspect of a more significant anomaly, in which there is no sign of any influence of alkali feldspar (which partitions Rb) in the variation. This is remarkable because trachytes and rhyolites have normative $ab+or > 50$ %, and any evolutionary process *controlled* by crystal ⇌ liquid interactions must be dominated by the melting or crystallization of alkali feldspar. The results on the Eburru obsidians show that *if they are an evolutionary series* then *either*, the process was not crystal ⇌ liquid controlled, *or* that any such process has been overriden (or buffered) by other processes that have superimposed the observed trace-element patterns. In the latter event, the buffering phase may have been a halogen-bearing vapour.

The same considerations must apply to other pantellerite provinces where Rb appears to have behaved as a 'residual' element.

In recent years we have compiled all the available data on oversaturated peralkaline obsidians (Macdonald and Bailey, 1973) and set in train an analytical programme on all new samples that we have been able to obtain. Our own field sampling has been focused on the Nakuru–Naivasha region of Kenya, the topographic culmination of the East African rift, where there is an unparalleled development of Quaternary–Recent peralkaline volcanoes. In the trachyte to pantellerite composition range it had been demonstrated previously that the obsidians from different volcanoes showed systematic variations in major-element chemistry, but these variations were not consistent with

a fractional-crystallization model involving the observed phenocryst phases (Macdonald *et al.*, 1970). The best development of pantellerite magmatism is found in the Eburru volcano (Sutherland, 1971) just north-west of Lake Naivasha. Trace-element analyses of some of Sutherland's samples by Weaver *et al.* (1972) were used (with data from five other volcanoes) to argue that the relationships between trachytes and pantellerites are most reasonably explained by fractional crystallization. Subsequent examination has revealed, however, that the 'Eburru' specimens used by Weaver *et al.* were a mixed population (Bailey *et al.*, 1975).

Since 1970 we have collected and analysed obsidians from Eburru, which span the composition range from quartz-trachyte to pantellerite, and the major-element variation within this one volcanic pile cannot be explained by fractional crystallization of the phenocryst phases. The major-element evidence on quenched liquids is thus in direct conflict with the conclusions reached through the trace elements by Weaver *et al.* (1972). Trace-element analyses of our own Eburru samples form part of the long-term study of peralkaline obsidians, and they are now sufficiently far advanced to demonstrate that fractional crystallization *cannot* explain the variations. This demonstration, however, is only a subsidiary aim of the present article—our chief concern is to describe some unexpected relationships (especially involving halogens) which may provide some real clues to the secrets of this magmatism.

We shall look at a small group of trace elements (F, Cl, Zn, Nb, Zr, Yt, and Rb), which includes the two (Nb and Zr) considered most significant by Weaver *et al.* (1972). Our population is fifteen obsidians from quartz-trachyte to rhyolite: we are unable to include any basalts because we are restricting our study to glasses (quenched liquids). Actually, there are no contemporaneous basalts in the Eburru pile, although there is a Recent basalt field in the lowlands just to the north. We believe it would be begging the question to include these basalts with the Eburru magmatism until we have evidence other than geographic proximity to indicate that the two may be cogenetic (this problem is currently being studied by A. W. H. Bowhill, University of Reading: see also Bailey *et al.*, 1975, fig. 1). Correlations among the selected trace elements are moderately to strongly positive, whereas their correlations with major elements are generally poor. Although the major element ranges in the population are small (e.g. SiO_2 range from 66·2 to 72·0 per cent) the trace element ranges are large (e.g. Zr range from 1038 to 3058 ppm). Samples with essentially identical major-element chemistry show widely different trace-element levels, and the impossibility of reconciling these facts with simple fractional crystallization has been noted elsewhere (Bailey, 1973).

Trace-element relations. The limits, means, and concentration factors are listed in Table I. Trace-element values, sample points, rock names, and age relations are given in the Appendix.

The absence of basic rocks, with very low levels of the selected trace elements, is not a serious drawback to correlation analysis because in the case of the strongly concentrated elements, F, Zr, and Rb, the obsidian values span two-thirds of the possible range from the maximum observed down to zero. The results of the correlation analysis are given in matrix form in Table II.

TABLE I. *Limits, means, and concentration factors in 15 obsidians from Eburru, Kenya. Values in ppm*

	F	Cl	Zn	Nb	Zr	Yt	Rb
Minimum (m)	2910	2090	333	230	1038	195	131
Maximum (M)	7800	4290	537	542	3058	410	417
Mean	4900	3300	457	388	1910	307	252
Standard Deviation	1660	630	58	96	671	63	98
Maximum concentration factor (M/m)	2·68	2·05	1·61	2·36	2·95	2·10	3·18

TABLE II. *Correlation matrix for trace elements in the Eburru obsidians (all coefficients are positive). Plus or minus indicates the sign of the intercept of the best-fit line (reduced major-axis equation: Till, 1973) on the axis of the second variable in those cases where the 95 % confidence limits do not include the origin. Zero indicates that the origin falls within the 95 % confidence limits*

	F	Cl	Zn	Nb	Zr	Yt	Rb
F	1·000						
Cl	0·862(+)	1·000					
Zn	0·769(+)	0·879(+)	1·000				
Nb	0·955(+)	0·943(−)	0·909(−)	1·000			
Zr	0·994(0)	0·876(−)	0·817(−)	0·972(−)	1·000		
Yt	0·932(+)	0·954(0)	0·928(−)	0·995(+)	0·951(+)	1·000	
Rb	0·996(−)	0·853(−)	0·795(−)	0·959(−)	0·998(−)	0·937(−)	1·000

Implications of the trace-element distributions

The central tenet of the trace-element argument with respect to magma evolution, as propounded by Weaver *et al.* (1972), is that in a series of peralkaline liquids certain elements will be unable to enter the crystallizing phases, and will become progressively concentrated in the residual liquids. This assumes that the liquids are related by a process dominated by crystal ⇌ liquid interactions: we would claim that this itself needs to be proven, but for the moment let us examine the rest of the case. Zr is chosen as the prime example of a residual element because of: its high solubility in peralkaline melts (and insolubility in the major crystalline phases); its impassiveness to late-stage 'volatile effects'; and its abundance and high-precision determination by XRF (Weaver *et al.*, 1972). Consequently Zr is claimed to be a more useful index of differentiation than the more commonly used major-element indices. More assumptions are, of course, compounded in this claim. In the case of the Eburru rocks we cannot reconcile the claim with the major-element patterns (Bailey, 1973) and, moreover, we now cannot find support for it in our trace-element data.

Weaver *et al.* (1972) state that in the six volcanic centres they have tested the graphical plots of each of the elements Ce, La, Nb, and Rb against Zr are linear, and

project through the origin. They deduce from this (assuming that Zr is the archetype residual element) that the other four elements also have bulk distribution-coefficients (element concentration in combined crystal phases/concentration in liquid) close to zero. Compared with their data on Eburru (kindly provided by S. D. Weaver) our

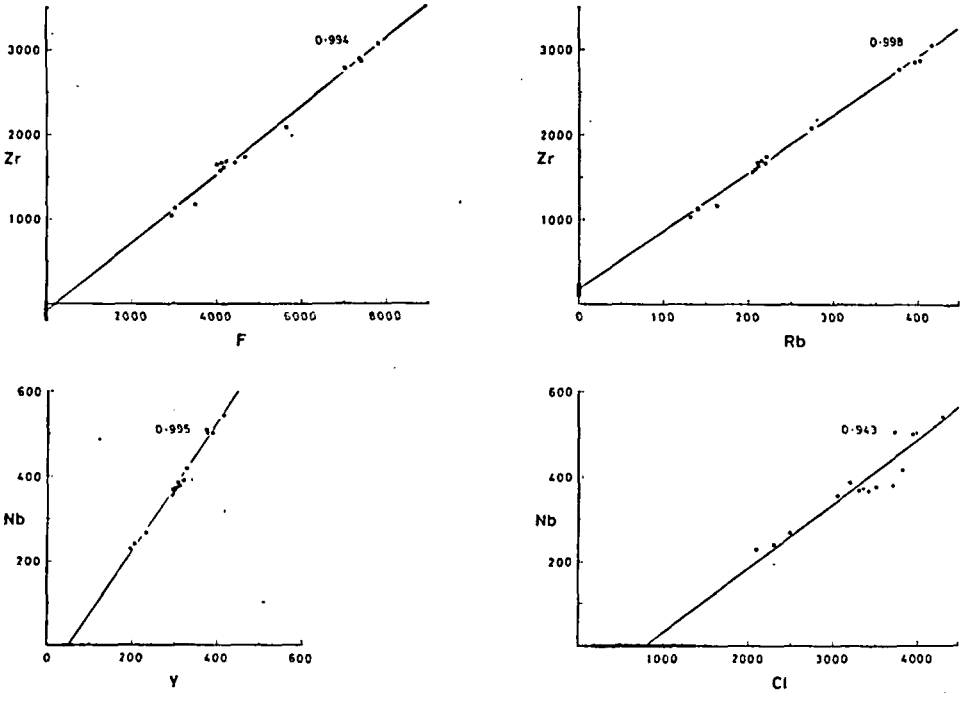

FIG. 1. Four examples of linear correlations of element pairs in the Eburru obsidians (solid circles). In every case the line is the computed reduced major-axis line and the heavy bar on the axis shows the 95 % confidence limits on the intercept. All values in ppm.

obsidian analyses show far less 'noise', more systematic variations, and higher correlation coefficients throughout. Our distribution patterns are quite different. Many are not linear, and most do not project through the origin. The latter are shown in Table II by plus and minus signs, to indicate the sign of the intercept on the axis of the second variable when the first variable reaches zero. Only those pairs of variables with a correlation coefficient better than 0·990 appear to be convincingly linear; these four are examined first.

Fluorine, zirconium, and rubidium. These three elements are the most strongly correlated, each pair providing a linear plot, two of which are shown in fig. 1.

In the case of F and Zr the calculated best-fit line passes close to the origin, which falls within the 95 % confidence limits. Assuming that Zr is the archetype residual element, then F too would have a bulk distribution coefficient close to zero, and constant throughout the series. The consistent behaviour of F would also indicate that the

population of obsidians is free of vagarious late-stage volatile losses, because our tests confirm the findings of Noble *et al.* (1967) that fluorine-loss is one of the most conspicuous effects of devitrification in this sort of lava.

The correlation of Rb with Zr, however, destroys the primacy of Zr as a residual element. The line misses the origin, making a positive intercept on Zr when Rb runs to zero. If this distribution is generated by crystal ⇌ liquid relations in a closed system then Zr must be fractionated (at a constant distribution coefficient) in the solid phases throughout the lava series. If Zr is held to have a distribution coefficient close to zero then the *system must be open to Rb*. Because, if the data are fitted to a fractional-crystallization model, then Rb increases in the residual liquids at a greater rate than Zr: if a fractional-melting model is adopted then the level of Rb must fall faster than Zr as the liquid volume increases. Either way, Rb has to move in or out of the system if Zr is behaving as a residual element. The same deduction, but without the precision, could have been made from the concentration factors in Table I.

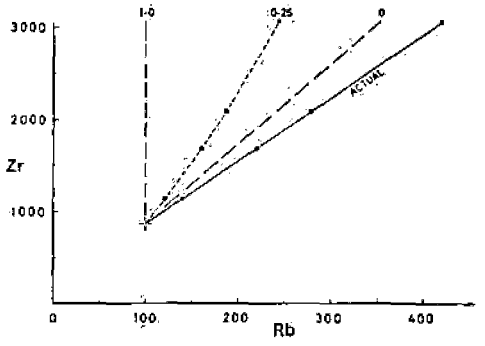

FIG. 2. Showing the difference between the actual array line for Rb *v.* Zr and that expected by fractional crystallization if the bulk distribution coefficient for Rb is finite whilst that for Zr is zero. In the latter case, taking a starting concentration of 100 ppm Rb, the points should lie between the broken lines 0 and 1·0 (if there is to be any concentration of Rb). The line 0·25 represents a reasonable case calculated on the basis of four-stage fractionation (solid squares) at intervals defined by Zr concentrations (solid circles) in the actual array.

In fact, the covariance of Rb and Zr shown in this range of obsidians is even more dramatic, because if the liquids were generated by fractional crystallization about two-thirds of the separating crystals would have to be alkali feldspar (based on normative *ab*+*or* in the trachytes) and the partition coefficient for Rb between alkali feldspar and liquid must be greater than zero. Relevant partition coefficients are available from Noble and Hedge (1970) for alkali feldspar phenocrysts and glassy matrices from peralkaline volcanics. They give values for the Rb partition coefficients in eleven peralkaline rocks, ranging from 0·25 to 0·45. Two of these determinations were made directly on separated phenocrysts and glass, giving values of 0·32 and 0·38 (1970, p. 235, Table, Samples 4 and 11*b*). Determinations of Rb have also been made on separated feldspars and glass from two Eburru rocks (PCO 134 and 135) giving partition coefficients of 0·41 and 0·31, respectively (Geochemistry Unit, Reading: analysts S. A. Malik and D. A. Bungard). Taking the average partition coefficient for Rb of 0·35 for alkali-feldspars/peralkaline-liquids, fractional crystallization (from a trachytic parent) in which 70 % of the separating crystals were alkali feldspar would result in a *bulk distribution coefficient* for Rb of 0·25. Fig. 2 is a graphical plot for Rb *v.* Zr to show the curve that would be generated by fractional crystallization when the bulk distribution coefficients for Rb and Zr are 0·25 and zero, respectively. The curve is calculated from a starting-point at 100 ppm Rb on the *actual* line and is developed by

four successive crystal crops at stages marked by *actual* Zr contents in the Eburru rocks. The highest calculated Rb value on the 'fractionation' curve is 244 ppm, which is only a little more than half the actual value (417 ppm) for the same Zr content. It is glaringly obvious from fig. 2 that either Zr is *not* a reliable index of differentiation, or fractional crystallization *cannot* account for the covariance of Rb and Zr, or *both*. All evidence available to us favours the third conclusion!

Niobium, yttrium, and chlorine. There is good correlation between Nb and Yt; the plot, shown in fig. 1, is linear within the limits of experimental error, with a narrow 95 % confidence band. The calculated line does not pass through the origin. If it were assumed that crystal fractionation controls the series, and Nb has a distribution coefficient close to zero, the sample array might be explained by Yt having a significantly higher distribution coefficient. The only phase that might be separating throughout the whole series is alkali feldspar, which would not normally be suspected of fractionating Yt with respect to Nb. Furthermore, neither Nb nor Yt shows a simple linear relation with Zr, which adds further complications to the model.

Nb and Yt both show reasonably linear correlations with Cl. The graphical plot for Nb *v.* Cl, shown in fig. 1, reveals a high positive intercept of the computed line on the Cl axis. This has the same implications for fractional crystallization as the Nb *v.* Yt array. It should be noted that if a fractional-melting evolution model is applied to these data, and Nb is taken to have a distribution coefficient of zero, then the system must be open to the ingress of Yt and Cl.

Yt *v.* Cl gives a similar pattern to Nb *v.* Cl but the line runs through the origin (within the 95 % confidence band).

Non-linear patterns, and covariance with fluorine and chlorine. Examination of the correlation matrix (Table II) shows that in addition to the four coefficients better than 0·990, there are a further ten better than 0·900. Nb and Zr are the best of this group with a coefficient of 0·972. But when graphical plots of these pairs of variables are made it emerges that many of these correlation coefficients are not lower (i.e. $< 0{\cdot}990$) due to random deviations from the line (as might be argued, for instance, for Nb *v* Cl, fig. 1). The lower coefficients for many pairs of elements result from *patterned*, but *non-linear* arrays of points. Examples are depicted in fig. 3, in which it may be seen that each computed best-fit line has been achieved by balancing a cluster of points in the middle of the array against points at the extremities. These are certainly not random patterns. The most obvious case is F *v.* Cl, with a relatively low correlation coefficient of 0·862, where a better description of the array would be an inflected line. The fact that this pattern is matched by Nb *v.* Zr, elements of a completely different kind, determined by a completely different method, must rule out the possibility that the arrangement is fortuitous. Fig. 3 confirms what was implicit from fig. 1 and the earlier discussion, namely, that Zr varies linearly with F (and Rb), that Nb varies linearly with Cl (and Yt), but between these groups of elements there is a marked inflection in the pattern of distribution. The complexity of the element covariances within these two groups, coupled with this additional complication of the relationships between the groups, rules out any rational *closed-system* (isochemical) evolutionary model. Such a conclusion is entirely consonant with those reached earlier on the

basis of major-e
and trace eleme
Before consid
Eburru obsidia
needs comment

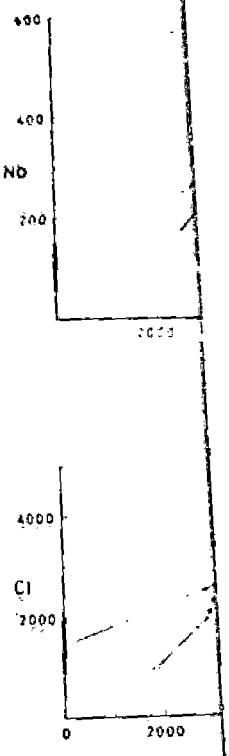

FIG. 3. Four example
and heavy bars as in fi
case. In the Zn *v.* Zr

Secondly, the limit
good agreement. T
Eburru samples, ar
method, because t
sidians from the N
prepared, and ana
anomaly in the Eb
best-fit line in fig.
for F and Cl)—the
Zn concentration

basis of major-element variations (Macdonald *et al.*, 1970) and comparisons of major and trace elements (Bailey, 1973).

Before considering alternative explanations for the chemical variations in the Eburru obsidians, the anomalously high, and seemingly erratic, zinc distribution needs comment (fig. 3). Firstly, Zn can be determined with high precision by XRF.

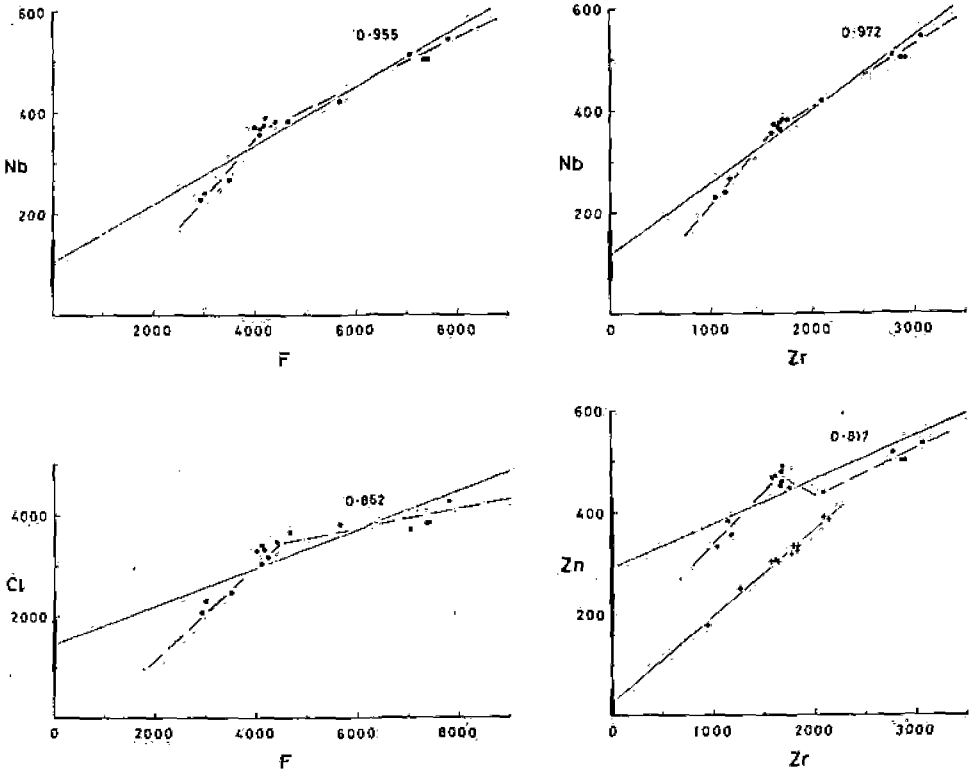

FIG. 3. Four examples of non-linear arrays in the Eburru obsidians. Solid circles, continuous lines, and heavy bars as in fig. 1. The broken lines represent preferred descriptions of the variation in each case. In the Zn *v.* Zr plot the plus signs are comendite obsidians from the Naivasha volcanic area (see text).

Secondly, the limiting Zn values in fig. 3 were checked by atomic absorption, with good agreement. Thirdly, the high levels, and the variability, of the Zn values in the Eburru samples, are not due to vagaries of sampling, sample preparation, or analytical method, because the second data set (plus signs) in fig. 3 represent comendite obsidians from the Naivasha volcanic area, just south of Eburru. These were collected, prepared, and analysed with the Eburru samples, so we are seeing a genuine Zn anomaly in the Eburru rocks. Fourthly, the broad scatter of the Zn values about the best-fit line in fig. 3 is confirmed by later results on other samples (not yet analysed for F and Cl)—the impression given by this pattern is of a second-order fluctuation in Zn concentration superimposed on a main trend indicated by the line. The general

form of the Zn distribution, when plotted against Zr, resembles that of Yt, Nb, and Cl against Zr, except that the general high levels of Zn are more obvious. Indeed, Zn shows its strongest correlations with Yt, Nb, and Cl, in that order (see Table II) so that similar factors, either at source or during magma generation, or both, have presumably influenced all four elements, but to different degrees. At present we have no evidence to suggest possible causes of the second-order fluctuations in the Zn pattern.

As a final point it should be noted that inflected patterns similar to those among the trace elements (shown in fig. 3) also emerge when some major elements (and their functions) are plotted against Zr. Examples are Al_2O_3, TiO_2, and agpaitic index ($Mol(Na_2O+K_2O)/Al_2O_3$).

An open-system model

In our earlier paper on the major-element patterns in the range pantelleritic trachyte to pantellerite (Macdonald *et al.*, 1970) we had to conclude that *if the rocks were an evolutionary series* a phase now missing from the rocks must have played a major part in the evolutionary process. The Eburru obsidians fall into the previously defined major-element patterns and the same conclusion applies. Furthermore, the trace-element patterns are now found to be incompatible with closed-system evolution. We concluded from the earlier major-element studies that if the rocks had been generated by a series of melting episodes then a separate vapour (fluid) phase had contributed Na (and possibly Si and Fe) to successive silicate liquids. Our reasons for preferring a fractional-melting model were given in that account (Macdonald *et al.*, 1970): a further reason in the Eburru rocks is that the chemical variations do not seem to fit any regular pattern in the development of the volcano. It would be premature to try to elaborate this model much further until all our data are in, but some additional conclusions from the present trace-element distributions are in order.

It is clear that a simple fractional-melting model could not generate most of the observed trace-element patterns. For instance, most of the correlation lines do not pass through the origin, which would be the first requirement for 'residual' elements. In such cases, where the correlation is linear (fig. 1) the line could be interpreted as a product of simple mixing, but the true picture must be more complex because some patterns are inflected (fig. 3). The most significant feature is the affinity of Zr and Rb with F, and the *separate* affinity of Nb, Yt, and Zn with Cl: judging by the inflected variation patterns between these two groups they would seem to have some degree of independence throughout the rock series. One possibility is that the metallic elements form preferred complexes with either fluorine or chlorine, and the partitioning of these complexes between vapour (fluid) and silicate melt varies with the melting conditions (e.g. relative volumes of melt to vapour, variations in melt or vapour compositions, temperature, and pressure). We are investigating this and other possibilities by: further analyses of Eburru rocks and extracted gases; experimental determination of melting, crystallization, and volatile exsolution; and by studies of obsidian suites from other volcanoes.

Another remarkable feature of the Eburru rocks is the Rb variation, which shows no recognizable contribution from alkali feldspars in contact with the melt (yet

alkali-feldspar phenocrysts are normal). If a coexisting vapour phase contributing Rb (and Zr and F) is accepted, the Rb patterns in the rocks suggest that the effect of this vapour is paramount. It is as if the melts were buffered for Rb. The fact that a key major element such as Al gives inflected variation patterns when plotted against Zr, Rb, and F also suggests that the concentrations of these elements are controlled by some factor other than those that determine the major-element distributions in the magmas.

Finally, one general point may be made concerning F and Cl in peralkaline magmas. It is commonly argued by advocates of fractional crystallization, that the high concentrations of Zr that distinguish peralkaline from subaluminous magmas are due to the solubility of Zr in peralkaline melts, and their consequent failure to precipitate zircon during crystallization. But how, then, is it possible to account for the high concentrations of F and Cl that equally distinguish these same peralkaline melts from other oversaturated magmas? We believe that the very high correlation of Zr and F in our samples exposes this as an artificial dilemma, and we appeal to fellow petrologists and petrochemists to critically reappraise some of the time-honoured concepts of magma evolution.

Acknowledgements. Wet chemical analyses for F and Cl were made by S. A. Malik and D. A. Bungard; XRF analyses for Zn, Nb, Zr, Yt, and Rb by G. J. Smith and N. J. Tarrant. We are indebted, too, to Dr. A. Parker who set up the XRF routines, calibration methods, and computations, and to Dr. R. Till and Mrs. J. Webber for the correlation programme and its operation. A. Parker, J. E. Thomas, and R. Till improved the final manuscript by their valuable comments on the first draft.

REFERENCES

Bailey (D. K.), 1973. *Journ. geol. Soc. Proc.* **129**, 649.
—— Weaver (S. D.), and Sutherland (D. S.), 1975. *Contr. Min. Petr.* **50**, 47–8.
Macdonald (R.) and Bailey (D. K.), 1973. *U.S. Geol. Surv. Prof. Paper*, 440N–1.
—— —— and Sutherland (D. S.), 1970. *Journ. Petrology*, **11**, 507–17.
Noble (D. C.) and Hedge (C. E.), 1970. *Contr. Min. Petr.* **29**, 234–41.
Parker (A.) (unpubl.). *Geol. Dept. Univ. of Reading.*
Sutherland (D. S.), 1971. *Journ. geol. Soc. Proc.* **127**, 417.
Thomas (J. E.), Bungard (D. A.), and Malik (S. A.), 1975. *Univ. Reading Geol. Reports*, **6**.
Till (R.), 1973. *Area (Inst. of Brit. Geographers)*, **5**, 393–8.
Weaver (S. D.), Sceal (J. S. C.), and Gibson (I. L.), 1972. *Contr. Min. Petr.*, **36**, 181–94.

[*Manuscript received 21 August 1974; revised 5 June 1975*]

APPENDIX. *Trace-element values (ppm) in 15 Eburru obsidians*

Sample	F	Cl	Zn	Nb	Zr	Yt	Rb	Co-ordinates	Age group
PCO082	4000	3300	454	370	1653	294	212	AK 966 332	c
PCO083	4100	3400	467	367	1664	296	211	AK 956 323	c
PCO084	3000	2300	384	240	1137	203	139	AK 971 329	b–c
PCO129	4650	3680	448	381	1748	305	220	AK 943 297	d
PCO130	4200	3190	491	389	1697	318	213	AK 933 363	b
PCO131	7020	3710	519	508	2776	371	377	BK 001 398	a–b
PCO132	4400	3480	480	379	1679	305	218	AK 950 279	d
PCO133	4150	3330	472	372	1608	300	208	AK 954 295	d
PCO134	5630	3810	440	419	2091	324	273	AK 965 242	d
PCO135	4090	3040	469	357	1593	292	206	AK 974 229	a?
PCO161	7390	3930	501	502	2865	383	397	BK 037 323	a
PCO162	7370	3930	503	502	2880	375	402	BK 039 329	a
PCO163	7800	4290	537	542	3058	410	417	BK 022 263	a
PCO164	3480	2480	359	269	1168	230	162	AK 910 362	b
PCO165	2910	2090	333	230	1038	195	131	AK 905 374	b

Methods: F and Cl; determined colorimetrically (Thomas *et al.*, 1975). Zn, Nb, Zr, Yt, Rb; determined by XRF (Parker, unpub.), using U.S.G.S. Standard Rocks (G2, GSP1, AGV1, PCC1, DTS1, BCR1) for calibration.

Co-ordinates. 1000 m Universal Transverse Mercator Grid Clarke 1880 (Modified) Spheroid. Grid Zone Designation 37 M. The 100 000 m Sq Identification is given by the prefix letters: easting and northing by the final six digits. As used on Survey of Kenya maps.

Age groups: a–d: oldest–youngest. Broad groupings only are possible because many flows do not overlap to give precise relationships.

Rock descriptions. The suffix (P) signifies rare feldspar phenocrysts: in such rocks there are usually abundant microphenocrysts. Full modal data will be published later, with the major element analyses.

PCO082 See Macdonald and Bailey (1973), Anal. 82.
PCO083 See Macdonald and Bailey (1973), Anal. 83.
PCO084 See Macdonald and Bailey (1973), Anal. 84.
PCO129 Obsidian
PCO130 Obsidian (P)
PCO131 Obsidian
PCO132 Obsidian
PCO133 Obsidian
PCO134 Glassy lava with abundant phenocrysts of feldspar, quartz, and aenigmatite, and rare clinopyroxene.
PCO135 Glassy lava with phenocrysts of feldspar, aenigmatite, and clinopyroxene.
PCO161 Obsidian
PCO162 Obsidian
PCO163 Obsidian. Same locality as Anal. 89, Macdonald and Bailey (1973).
PCO164 Obsidian (P)
PCO165 Obsidian (P)

Reprinted from
Economic Geology
Vol. 69, 1974, pp. 1328–1334

The FeS Content of Sphalerite Along the Chalcopyrite-Pyrite-Bornite Sulfur Fugacity Buffer

GERALD K. CZAMANSKE

Abstract

Concentrations of 0.19 ± 0.02 and 0.55 ± 0.08 mole percent FeS have been measured in sphalerite crystallized at 1 kbar in equilibrium with the chalcopyrite-pyrite-bornite sulfur fugacity buffer at temperatures of 271° and 395°C, respectively. These data yield a relationship of $\log C = -1353/T + 1.77$, where C is measured in mole percent FeS, T is in °K, and the pressure is 1 kb. The effect of pressure on C is evaluated. Henceforth, indications of equilibrium or disequilibrium crystallization and estimates of temperature of formation may be made for the assemblage sphalerite-chalcopyrite-pyrite-bornite at temperatures in the range 150° to 450°C.

The composition of bornite in equilibrium with chalcopyrite and pyrite is found to be $Cu_{5.24}Fe_{0.86}S_{4.00}$ at 271°C and $Cu_{5.02}Fe_{0.93}S_{4.00}$ at 395°C. At these temperatures chalcopyrite and pyrite in the buffer assemblage do not deviate measurably from stoichiometry. Bornite and chalcopyrite are found to incorporate 0.03 to 0.18 and 0.00 to 0.43 atomic percent Zn in the range 197° to 503°C.

Introduction

MUCH experimental effort has been devoted to determining the FeS content of sphalerite in equilibrium with the assemblage pyrite-pyrrhotite, with a view toward developing an ore geothermometer. Papers representative of this effort include Scott and Barnes (1971), Boorman, Sutherland, and Chernyshev (1971), Chernyshev and Anfilogov (1968), Boorman (1967), and Kullerud (1953), as well as the more general paper of Barton and Toulmin (1966). Unfortunately, the results of these studies indicate that between 550° and 300°C, a temperature range of much interest to students of ore formation, sphalerite composition is constant at 20.7 ± 0.6 mole percent FeS (Scott and Barnes, 1971) and is thus not useful as a geothermometer. Concentration of attention on sphalerite compositions along the pyrite-pyrrhotite solvus reflects the tacit assumption that sulfur fugacities during ore formation frequently correspond to those of pyrite-pyrrhotite equilibrium.

Associations of sphalerite with the assemblage chalcopyrite-pyrite-bornite (hereafter referred to often as cpy-py-bn) are less common, principally because that assemblage is stable only at sulfur fugacities that are higher than those typical of most ore environments (Holland, 1965; Barton, 1970). Barton and Toulmin (1964, 1966) and Yui and Czamanske (1971) recognized that the FeS content of sphalerite from the assemblage sphalerite-chalcopyrite-pyrite-bornite is a potentially useful geothermometer. Barton and Toulmin (1966, fig. 17), in particular, presented data that suggested that the relative variation of the FeS content of ZnS along the cpy-py-bn, f_{S_2} buffer might be greater than that anticipated for variation in FeS content along the pyrite-pyrrhotite, f_{S_2} buffer. On the basis of an analysis of sphalerite in a cpy-py-bn assemblage from the Iimori mine, Japan, and relations set forth by Barton and Toulmin (1966), Yui and Czamanske (1971) estimated that the Iimori ore formed at a temperature below 300°C.

Because the pertinent relationships presented by Barton and Toulmin (1966) are based on extrapolated rather than direct experimental data, they are uncertain, particularly in regard to the choice of the Henry's law constant, which relates the activity of FeS to the mole fraction of FeS in sphalerite. Therefore, the studies reported here were carried out in order to place these relationships on a firmer experimental footing.

Experimental Procedures

To promote reactions involving sphalerite at the relatively low experimental temperatures of interest for this system, experimentation in hydrothermal solutions is essential. Previous experience (see, e.g., Czamanske and Rye, 1974; or Scott and Barnes, 1971) has demonstrated that equilibration with extensive recrystallization can be obtained in NH_4Cl and NH_4I solutions by applying a thermal gradient of about 5°C over the 10 cm length of the platinum sample tubes.

Sulfide phases for reaction were prepared from high-purity elements by reaction at elevated temperatures in evacuated silica tubes. Synthesized in

TABLE 1. FeS Contents of Sphalerites Crystallized in Association with Chalcopyrite-Pyrite-Bornite Over the Temperature Range 197° to 400°C

Experiment Number	Crystallization Temperature, °C	Duration of Run, Days	Solution Composition[1]	Mole Percent FeS in Starting ZnS	Mole Percent FeS in Product ZnS
176	197 ± 3	615	Sat. NH_4Cl	0.00	0.12 ± 0.03
145	272 ± 3	220	Sat. NH_4Cl	0.00	0.20 ± 0.03
202	272 ± 3	195	Sat. NH_4I	0.00	0.10 ± 0.04
237	271 ± 3	85	Sat. NH_4Cl	0.00	0.21 ± 0.04
238[2]	271 ± 3	85	Sat. NH_4Cl	1.00	0.18 ± 0.03
239	271 ± 3	85	Sat. NH_4Cl	2.00	0.19 ± 0.02
108[3]	400 ± 5	165	1N NH_4Cl	0.00	0.95 ± 0.12
179	396 ± 4	160	Sat. NH_4Cl	0.00	0.65 ± 0.05
180	396 ± 4	160	Sat. NH_4Cl	40.00	0.80 ± 0.07
227	395 ± 4	99	Sat. NH_4Cl	0.00	0.49 ± 0.06
228	395 ± 4	99	Sat. NH_4Cl	1.00	0.47 ± 0.04
229	395 + 4	99	Sat. NH_4Cl	5.00	0.49 ± 0.06
261	394 ± 4	193	1N NH_4Cl	0.00	0.64 ± 0.07
262	394 ± 4	193	1N NH_4Cl	1.00	0.52 ± 0.06
263	394 ± 4	193	Sat. NH_4Cl	0.00	0.62 ± 0.10
264	394 ± 4	193	Sat. NH_4Cl	1.00	0.64 ± 0.05
265	394 ± 4	193	NH_4I	0.00	0.49 ± 0.05
266	394 ± 4	193	NH_4I	1.00	0.52 ± 0.05

[1] Sat. indicates solution saturated at 25°C. Concentration of NH_4I in runs 265 and 266 was 7.7 gm/10 ml.
[2] Runs with consecutive numbers and identical run duration are from same reaction vessel.
[3] Run carried out in cold-seal vessel and contained PbS.

this way were: a series of (Zn,Fe)S solid solutions; FeS_2; and an intimate, fine-grained buffer mixture containing roughly equal portions by weight of $CuFeS_2$, FeS_2, and Cu_5FeS_4. Consumption of the FeS_2 component of the buffer mixture was common in early experiments, so experiments reported in Table 1 typically used 300 mg of the cpy-py-bn mixture, 75 mg of additional FeS_2, and 50 to 75 mg of (Zn,Fe)S. Runs were started with compositions of (Zn,Fe)S that bracketed anticipated equilibrium compositions, so that equilibrium was approached from both directions.

Reactants and solutions (Table 1) were loaded into 8 mm O.D. platinum tubes, which were flushed with hydrogen and flame-welded while partly immersed in ice water. Groups of six sample tubes were placed into medium-sized (22.9 cm × 6.4 cm) pressure vessels with modified Bridgman-type seals. Vessels were lowered into vertical, gradient furnaces, such that nutrient and buffer phases settled to the lower (hotter) end of the platinum tube and crystallization products formed at the upper (cooler) end of the tube. All experiments were conducted at 1 kb pressure to promote solution transport via a relatively dense medium. Temperature uncertainties reported in Table 1 include calibration of the thermocouple and recorder, short- and long-term furnace fluctuations, and an estimated correction for separation of thermocouple and sample (see Czamanske and Rye, 1974). Runs were quenched by plunging the vessels at pressure into a bucket filled with ice and water. Quenches to room temperature took several minutes, and some (Cu,Fe)-sulfide exsolution textures may have resulted from the relatively slow quench. No reaction between the sulfides and the platinum tube was noted.

Crystallization products were analyzed with an ARL EMX-SM electron microprobe using an accelerating voltage of 15 KV and a specimen current of 2×10^{-8} amperes on brass. Lines analyzed and crystals used for each element are as follows: Cu, Fe, and Zn, Kα, LiF; and S, Kα, ADP. Standards used were: chemically analyzed, stoichiometric bornite from Butte, Montana, and chalcopyrite from O'okiep, Namaqualand, South Africa; synthetic ZnS containing 0.00, 1.00, 2.00, and 5.00 mole percent FeS; synthetic $CuFeS_2$ containing 0.50 weight percent Zn; synethetic FeS containing 2.00 weight percent Cu; and a synthetic bornite of composition $Cu_{5.44}Fe_{0.82}S_{4.00}$. Reported analyses of sphalerites represent 10-second counts at 30 to 60 discrete points on 5 to 10 homogeneous grains; for (Cu,Fe)-sulfide phases 8 to 20 points were analyzed. All analyses reported are based on direct comparison of counting rates for unknowns and standards of similar composition, with appropriate corrections for background and instrument drift calculated by hand. For analyses of sulfides, it is very important to use either a rigorous, theoretical correction scheme, or a low acceleration voltage (Desborough et al., 1971), or close standards. For example, at 15 KV using Cu_5FeS_4 as a standard, 38.2 rather than 34.9 weight percent S was obtained for $CuFeS_2$ by direct comparison of count rates.

Many of the (Cu,Fe)-sulfide products displayed exsolution textures, apparently related to quenching

TABLE 2. Compositions (in atomic percent) of Bornite Crystallized at 197°, 271°, and 395°C in Association with Stoichiometric Chalcopyrite and Pyrite

Experiment Number	Cu	Fe	S
197°C			
176T[1]	50.0[2]	9.9[2]	40.1[2]
271°C			
147T[3]	50.2	8.3	41.5
$202A_1$	58.7	4.7	36.6
$202A_2$	51.4	8.7	39.9
237T	51.9	8.5	39.6
238A	52.1	8.3	39.6
238T	51.9	8.5	39.6
239A	52.0	8.4	39.6
239T	52.2	8.5	39.3
Average composition $202A_2$ – 239T, $Cu_{5.24}Fe_{.86}S_4$			
395°C			
108T	49.9	9.5	40.6
179T	49.2	9.9	40.9
180T	49.1	10.0	40.9
228S	50.8	9.0	40.2
228T	50.7	9.3	40.0
229A	50.6	9.6	39.9
229T	50.7	9.2	40.1
261T	50.3	9.4	40.3
263T	50.6	9.2	40.2
264T	50.7	9.1	40.1
265T	50.1	9.4	40.4
266T	50.0	9.5	40.5
Average composition 228S – 266T, $Cu_{5.02}Fe_{.93}S_4$			

[1] Letters designate material as: T—transported; S—source; A—annealed.
[2] Calculated standard deviations representative for all data presented are Cu ± 0.5, Fe ± 0.2, and S ± 0.6.
[3] Poor material for analysis.

(Brett, 1946), which made difficult the precise determination of bulk phase compositions at the temperatures of experimentation. To obtain more homogeneous products, several samples from each temperaure were annealed at identical temperatures in small-diameter silica tubes for which much superior quenches were obtained. Analyses of these homogeneous products are in good agreement with "bulk" analyses for the more coarsely exsolved products obtained by using a defocussed beam and many points of analyses.

Results

Although experiments were carried out at nominal temperatures of 200°, 275°, 400°, and 500°C, the most extensive and reliable results were obtained at 271° and 395°C. All results except those for 500°C are summarized in Tables 1 and 2. Certain results are considered of greater significance than others, and the data will be considered in detail. Experiment numbers reflect the sequence of experiments. Results are reported in mole or atomic percent, and uncertainties are given as one standard deviation, based on microprobe counting statistics.

FeS content of ZnS

Sphalerite compositions are the principal focus of this study. The single experiment at 197°C is not given weight in the derived equation; the measured FeS content of 0.12 ± 0.03 mole percent compares with the value 0.08 calculated from 271° and 395° data.

Experiments 237, 238, and 239 were planned to locate a point at ~275°C and are in good agreement. The average composition for these sphalerites of 0.19 ± 0.02 mole percent FeS also agrees with the result of earlier experiment 145, but differs from the result of experiment 202 (0.10 mole percent FeS), which used a solution saturated in NH_4I at 25°C as the transporting agent. Although Czamanske and Rye (1974) have shown that NH_4I can have a different effect than NH_4Cl on solution-mineral equilibria, experiments 265 and 266 suggest that this factor is not operative in the present system. Failure of pyrite to be reactive in the system is the preferred explanation for the low FeS content of the 202 sphalerite.

Twelve experiments in the temperature range 394° to 400°C produced sphalerite crystals up to 500μ in size that were compositionally homogeneous as determined by microprobe analysis. On the basis of 10 of these experiments, 0.55 ± 0.08 mole percent FeS is accepted for the composition of sphalerite in equilibrium with cpy-py-bn at 395°C, 1 kb. Results of experiments 108 and 180 can be explained only by assuming that equilibrium among the four mineral phases did not prevail, e.g., supersaturation in FeS_2 could be the reason. The homogeneity of crystals from these runs indicates that aberrant conditions were sustained throughout the runs.

Data for the 500°C experiments are presented in only a fragmentary way, as no consistent picture emerges from them. Apparently because of tie-line switches and possible metastability in the Cu-Fe-S, buffering system (Barton, 1973; Cabri, 1973) sphalerites with FeS contents ranging from 1.07 to 3.77 mole percent have been produced at 500°C. Two experiments produced two distinct, coexisting sphalerite compositions, each represented by 4 to 7 homogeneous grains to 900μ in size. As a partial explanation for the 500°C results, P. B. Barton (written commun., 1973) suggests that Zn may enter the intermediate solid solution (iss), and stabilize it, so that the cpy + iss + py field persists down to, or below, 500°C rather than disappearing below 532°C (see fig. 6, Barton, 1973). Analyses of the (Cu,Fe)-sulfide products support this interpretation by indicating coexistence of iss ($Cu_{1.26}Fe_{0.94}S_{2.00}$) and stoichiometric chalcopyrite in two runs, as well as the incorporation of significant Zn in chalcopyrite at

503°C (Table 3). Considerable additional study will be required to clarify relationships in the Cu-Fe-Zn-S system in the temperature range 450° to 535°C.

(Cu,Fe)-sulfide compositions

Determination of compositions of product (Cu,Fe)-sulfide phases has been an integral aspect of the present study. At 197°, 271°, and 395°C chalcopyrite is homogeneous and stoichiometric within the uncertainty of microprobe analysis, with the qualification that Fe contents are typically 0.1 to 0.2 mole percent low because of Zn substitution (Table 3). On the other hand, bornite produced at 271° and 395°C is not stoichiometric (Table 2) but has a composition along the bornite-digenite join. Bornite crystals to 250μ produced at 197°C are compositionally near stoichiometric bornite. Inasmuch as Yund and Kullerud (1966) present only schematic relationships below 500°C, these analyses presently constitute the only published data for compositions of bornite in equilibrium with chalcopyrite and pyrite at low temperature.

The nonstoichiometric bornites display exsolution textures developed during quenching. Textures of the 271°C bornites strongly resemble the "basket weave" texture of figure 5 in Brett (1966), whereas those of the 395°C bornites appear as a fine, regular cell-work with bornite cells two or three times as long as they are wide arranged in parallel chains and separated by thin films of digenite. (Brett mentions development of a dominant orientation in one of his experiments on this join). This texture was excellently developed during an otherwise unsatisfactory polishing attempt employing Fe_2O_3 suspended in chromic acid (Cameron and Van Rensburg, 1965).

Phase relations along the diagenite-bornite join, as presented by Yund and Kullerud (1960, fig. 47), are apparently related to two results of (Cu,Fe)-sulfide analysis: (1) experiment 202 at 272°C produced two phases compositionally near the limits of the digenite-bornite solvus shown by Yund and Kullerud; (2) the composition of bornite produced at 197°C in experiment 176 is stoichiometric, or nearly so, in contrast to the distinctly nonstoichiometric bornites produced at 271° and 395°C. The phase relations shown by Yund and Kullerud suggest this result to be reasonable. Differences in composition between these phases produced at 197° and 272°C and those predicted from Yund and Kullerud, figure 47, may relate to equilibration with chalcopyrite and pyrite in the present study.

"Bulk" compositions (averages of repetitive measurements with a defocussed beam) of (Cu,Fe)-sulfide grains from the 500°C experiments typically plot at the FeS_2-rich limit of the bornite solid solution field and the Cu_2S-rich limit of intermediate solid solution field, as defined for 500°C by Yund and Kullerud (1966). Grains with bulk compositions at the limit of the bornite solid solution field show incipient development of a chalcopyrite exsolution texture similar to that shown by Brett (1964, fig. 8) Grains of former, intermediate solid solution show dramatic exsolution of chalcopyrite in bornite, quite like the "basket-weave" texture shown by Brett (fig. 3). Average, bulk compositions are $Cu_{4.76}Fe_{1.09}S_{4.00}$ and $Cu_{1.26}Fe_{0.94}S_{2.00}$. Two runs produced stoichiometric chalcopyrite in association with intermediate solid solution, suggesting, as noted earlier, that Zn alters the phase relationships of Cu-Fe-S. One run produced stoichiometric chalcopyrite in association with a phase intermediate in composition to bornite and idaite, i.e., $Cu_{46.6}Fe_{8.4}S_{45.1}$ (atomic proportions). S. Yui (oral commun., 1973) has produced phases of similar composition, apparently metastably, in the course of a detailed study of idaite.

Table 3. Zinc Contents (in atomic percent) of Hydrothermal Bornite and Chalcopyrite Crystallized in Association with Pyrite and Sphalerite

T, °C	Bornite	Chalcopyrite
197	0.05 (1)	0.04 (1)
271	0.13–0.18, 0.16 (2)[1]	0.00–0.05, 0.02 (4)
395	0.03–0.12, 0.09 (5)	0.05–0.13, 0.09 (7)
503	0.11 (1)	0.33–0.43, 0.38 (4)

[1] Sequence of values: range of concentrations measured, average concentration, number of samples analyzed.

Representative product phases were checked for extraneous elements at the 0.01 mole percent level: sphalerite and pyrite for Cu; pyrite, chalcopyrite, and bornite for Zn. No Cu or Zn were detected in pyrite and no Cu was found in sphalerite. Determinations of Zn in chalcopyrite (no data for iss compositions are reported) and bornite are summarized in Table 3. The data show a distinct increase in the Zn content of chalcopyrite as a function of temperature but suggest that the Zn content of bornite is relatively constant at 0.08 to 0.16 mole percent under the conditions of experimentation.

Discussion

Critical analysis of the sphalerite compositional data is complicated by the fact that minor discrepancies exist among thermodynamic data for the Fe-S and Cu-Fe-S systems. As a frame of reference for discussion, Figure 1 has been constructed as follows: (1) The three equilibrium univariant curves other than chalcopyrite $\rightleftarrows$ bornite + pyrite, as well as the contouring of the pyrrhotite field, have been taken from Scott and Barnes (1971, fig. 2) with modest extension of the isopleths for sphalerite compositions

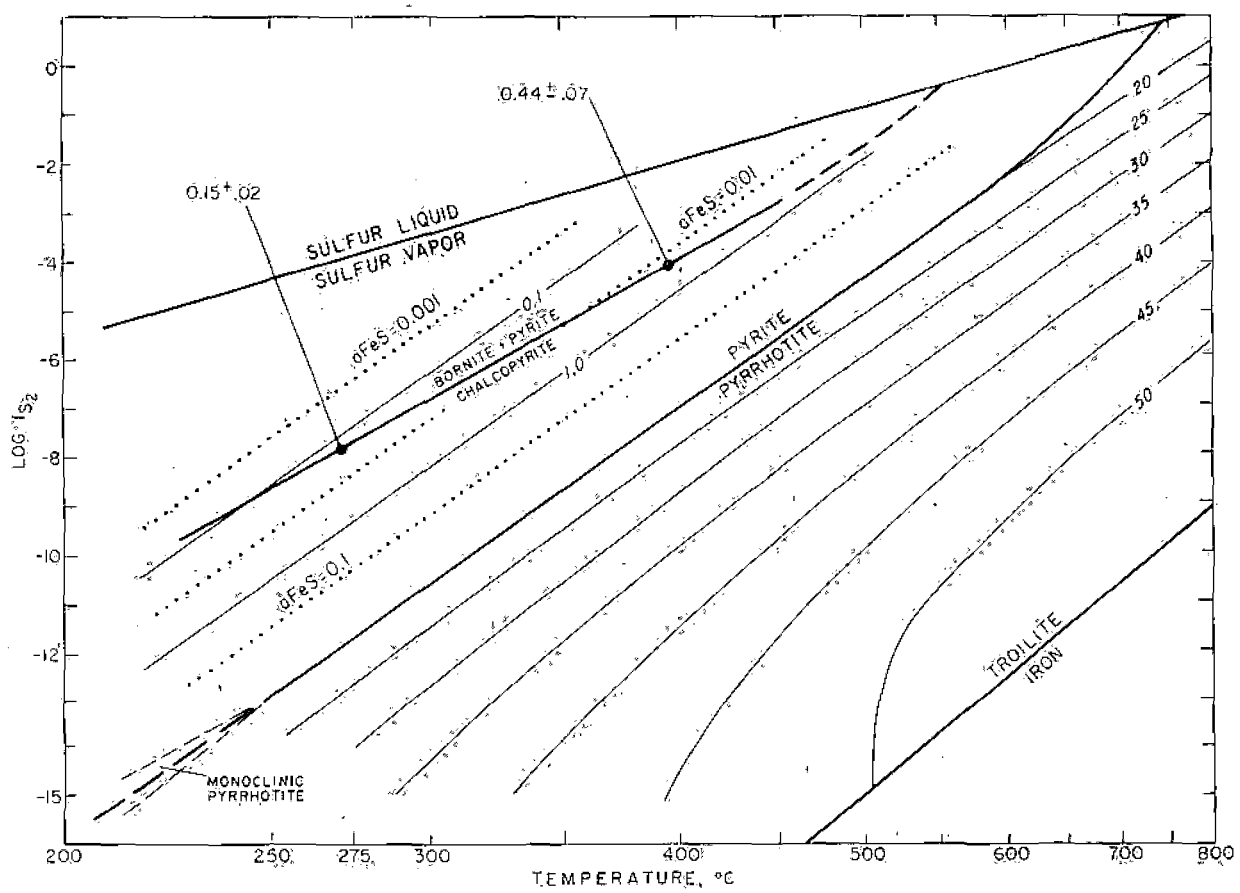

FIG. 1. Relationships between the composition of sphalerite in mole percent FeS (light, solid lines) and pertinent univariant equilibria, as a function of fugacity of sulfur and temperature at 1 bar. Several isopleths for a_{FeS} in the area of interest are shown as dotted lines. Measured values for mole percent FeS in sphalerite at 271° and 395°C have been corrected for the pressure change from 1 kbar to 1 bar and are indicated. Methods of compilation discussed in text.

in the pyrrhotite field, based on their equation (2). The Scott-Barnes univariant curve for pyrite $\rightleftarrows$ pyrrhotite has been chosen over that of Toulmin and Barton (1964) for three reasons: a) with the study of Toulmin and Barton in hand, Scott and Barnes located a univariant curve which is consistent, within stated error limits, with both sets of data; b) independent studies by Giletti et al. (1968) and Schneeberg (1973) have each supported the slightly flatter curve (in log f_{S_2}-1/T space) of Scott and Barnes; and c) data from the present study relate better to the Scott-Barnes univariant curve. (2) The univariant curve for the reaction chalcopyrite + $S_2 \rightleftarrows$ bornite + pyrite has been located on the basis of the electrochemical measurements of Schneeberg (1973), which fit the equation $\log f_{S_2} = 12.560 - 1.1067 \times 10^4(1/T)$. Schneeberg's univariant curve was selected because it is based on more extensive and inherently more precise data than the univariant curve of Barton and Toulmin (1964); the two univariant curves are parallel and that of Barton and Toulmin lies at values of f_{S_2} only 0.2 log unit lower. (3) Isopleths for a_{FeS} within the pyrite field have been located as follows: a) at 475°C, the approximate crossover point of the Toulmin-Barton and Scott-Barnes pyrite-pyrrhotite univariant curves, a_{FeS} has been calculated from the relation $2FeS + S_2 \rightleftarrows 2FeS_2$, using the expression $\Delta G° = -70{,}740 + 69.04T$ (Barton and Skinner, 1967, table 7.2). Based on the calculated spacings, isopleths were constructed parallel to the Scott-Barnes univariant curve. This procedure is not entirely arbitrary because the constancy of the iron content of sphalerite in equilibrium with pyrite and pyrrhotite, from 250° to 550°C, strongly suggests that the isopleths of FeS activity in the pyrite field must parallel the pyrite-pyrrhotite univariant curve. (Minor inaccuracies that may exist because a free energy expression has not been derived for the Scott-Barnes univariant curve are considered to be well within the overall uncertainties of this treatment.) (4) A Henry's law constant of 2.5 for sphalerite of low FeS content is obtained from Barton and Toulmin (1966) by drawing a straight line through the origin

of their figure 14 tangent to their array of data. Based on this value, sphalerite compositional points were located at 475°C from the calculated a_{FeS} values. Compositional isopleths were constructed parallel to the a_{FeS} isopleths (and to the pyrite-pyrrhotite univariant curve) as required for a Henry's law constant insensitive to composition and temperature. (5) A field for monoclinic pyrrhotite has been shown schematically below its apparent upper stability limit at 248°C (Kissin and Scott, 1972). (6) The two data points representing the results of this study (see Table 1) have been pressure corrected to 1 bar (see below) and have been placed on the chalcopyrite $\rightleftarrows$ bornite + pyrite univariant curve of Schneeberg (1973) at 271° and 395°C.

The effect of pressure upon sphalerite composition has received attention from Barton and Toulmin (1964), Scott and Barnes (1971), and Scott (1973). Along the pyrite-pyrrhotite univariant curve, increased pressure markedly decreases N_{FeS}^{sph} at constant temperature. In contrast, along the chalcopyrite $\rightleftarrows$ bornite + pyrite univariant curve, increased pressure increases N_{FeS}^{sph} slightly at constant temperature. Using the molar volume data of Robie et al. (1966) for bornite and pyrite, Hall and Stewart (1973) for chalcopyrite, and Barton and Toulmin (1966) for $\bar{V}_{FeS}$sph, ΔV_r is calculated to be $\simeq -0.5$ cal/bar for the reaction $5CuFeS_2 \rightleftarrows Cu_5FeS_4 + 2FeS_2 + [FeS]_{(in\ sphalerite)}$. It can be shown that

$$-\Delta V_r dP = 2\,RT\,d\ln(a_{FeS}).$$

Assuming that ΔV_r is constant, partial integration gives the desired equation,

$$-\Delta V_r (P_2 - P_1) = 2.303\,RT\,[\log(a_{FeS})_{P_2} - \log(a_{FeS})_{P_1}]$$

At 1 bar (the pressure for which the framework of Figure 1 is constructed), a_{FeS} will be ~80 percent of its value at 1 kb, the pressure of experimentation. Values for the mole fraction of FeS in sphalerite at 1 bar are therefore estimated at 0.15 ± 0.02 (271°C) and 0.44 ± 0.07 (395°C); these values fit quite well into the framework of existing data (Fig. 1). Because $a_{FeS} = (\gamma_{FeS}^{sph})\ (N_{FeS}^{sph})$, where γ_{FeS}^{sph} represents the Henry's law constant and N_{FeS}^{sph} the mole fraction of FeS in ZnS, another way of considering the new data is to derive the Henry's law constant which relates the measured N_{FeS}^{sph} values to the contoured a_{FeS} values. The calculated values of 2.5 ± 0.3 and 2.6 ± 0.4 for 271° and 395°C, respectively, are in good agreement with the data of Barton and Toulmin (1966, Fig. 14) for γ_{FeS}^{sph} at low FeS contents.

Scott (1973) found that calculation of the pressure effect on sphalerite composition along the pyrite-pyrrhotite solvus did not agree with measurement unless volume changes in the coexisting phases as a function of temperature and pressure were considered. Sphalerite compositions measured in this study agree reasonably with existing data when uncorrected for pressure, and well when pressure corrected; however, it seems advisable to apply corrections to high pressure with caution.

It is appropriate to discuss the implications of the present study for the sphalerite from the Iimori mine, Japan, studied by Yui and Czamanske (1971), as this is at present the only known application of data from the Cu-Fe-Zn-S system to geothermometry. Reanalysis of the Iimori sphalerite during the course of the present study suggests that 0.053 ± 0.009 mole percent FeS is probably a better measure of its FeS content than the value 0.044 ± 0.009 given by Yui and Czamanske (1971). According to the present study, 0.053 mole percent FeS in ZnS should correspond to a formation temperature of ~170°C, if the sphalerite is in equilibrium with cpy-py-bn at 1 kb. Although this temperature appears low in comparison with published estimates of conditions during ore formation (see Yui and Czamanske, 1971), some students of Sanbagawa metamorphism will find it quite realistic (Yui, oral commun., 1973). The possible effect of pressure on the calculated temperature is marked for the Iimori sphalerite because pressures of 5–7 kb have been postulated during formation of the Iimori ore. This pressure correction would call for even lower temperatures of equilibration.

Acknowledgments

Critical reviews by G. M. Anderson, P. B. Barton, Jr., L. J. Cabri, J. T. Nash, and S. D. Scott have materially improved the clarity and content of this manuscript, and I have profited from numerous stimulating discussions with C. L. Christ.

U. S. Geological Survey
345 Middlefield Road
Menlo Park, California 94025
February 28, May 7, 1974

REFERENCES

Barton, P. B., Jr., 1970, Sulfide petrology: Mineralog. Soc. America Spec. Paper 3, 187–198.

—— 1973, Solid solutions in the system Cu-Fe-S: Part 1: The Cu-S and CuFe-S joins: Econ. Geol., v. 68, p. 455–465.

—— and Skinner, B. J., 1967, Sulfide mineral stabilities, *in* Barnes, H. L., ed., Geochemistry and hydrothermal ore deposits: New York, Holt, Rinehart and Winston, p. 236–333.

Barton, P. B., Jr., and Toulmin, P., III, 1964, Experimental determination of the reaction chalcopyrite + sulfur = pyrite + bornite from 350° to 500°C: Econ. Geol., v. 59, p. 747–752.

—— 1966, Phase relations involving sphalerite in the Fe-Zn-S system: Econ. Geol., v. 61, p. 815–849.

Boorman, R. S., 1967, Sobsolidus studies in the ZnS-FeS-FeS_2 system: Econ. Geol., v. 62, p. 614–631.
—— Sutherland, J. K., and Chernyshev, L. V., 1971, New data on the sphalerite-pyrrhotite-pyrite solvus: Econ. Geol., v. 66, p. 670–673.
Brett, R., 1964, Experimental data from the system Cu-Fe-S and their bearing on exsolution textures in ores: Econ. Geol., v. 59, p. 1241–1269.
Cabri, L. J., 1973, New data on phase relations in the Cu-Fe-S system: Econ. Geol., v. 68, p. 443–454.
Cameron, E. N., and Van Rensburg, W. C. J., 1965, Chemical-mechanical polishing of ores: Econ. Geol., v. 60, p. 630–632.
Chernyshev, L. V., and Anfilogov, V. N., 1967, Subsolidus phase relations in the ZnS-FeS-FeS_2 system: Econ. Geol., v. 63, p. 841–844.
Czamanske, G. K., and Rye, R. O., 1974, Experimentally determined sulfur isotope fractionations between sphalerite and galena in the temperature range 600° to 275°C: Econ. Geol., v. 69, p. 17–25.
Desborough, G. A., Heidel, R. H., and Czamanske, G. K., 1971, Improved electron microprobe analysis at low operating voltage: II. Sulfur: Am. Mineralogist, v. 56, p. 2136–2141.
Giletti, B. J., Yund, R. A., and Lin, T. J., 1968, Sulfur vapor pressure of pyrite-pyrrhotite [abs.]: Econ. Geol., v. 63, p. 702.
Hall, S. R., and Stewart, J. M., 1973, The crystal structure refinement of chalcopyrite, $CuFeS_2$: Acta Crystallographica, B29, p. 579–585.
Holland, H. D., 1965, Some applications of thermochemical data to problems of ore deposits II. Mineral assemblages and the composition of ore-forming fluids: Econ. Geol., v. 60, p. 1101–1166.
Kissin, S. A., and Scott, S. D., 1972, Phase relations of intermediate pyrrhotite [abs.]: Geol. Soc. America Abstracts with Programs for 1972, p. 562, also in Econ. Geol., v. 67, p. 1007.
Kullerud, G., 1953, The FeS-ZnS system, a geological thermometer: Norsk. geol. tidsskr., v. 32, p. 61–147.
Robie, R. A., Bethke, P. M., Toulmin, M. S., and Edwards, J. L., 1966, X-ray crystallographic data, densities, and molar volumes of minerals, *in* Clark, S. P., Jr., ed., Handbook of physical constants, rev. ed.: Geol. Soc. America Mem. 97, p. 27–73.
Schneeberg, E. P., 1973, Sulfur fugacity measurements with the electrochemical cell $Ag|AgI|Ag_{2+x}S, f_{S_2}$: Econ. Geol., v. 68, p. 507–517.
Scott, S. D., 1973, Experimental calibration of the sphalerite geobarometer: Econ. Geol., v. 68, p. 466–474.
—— and Barnes, H. L., 1971, Sphalerite geothermometry and geobarometry: Econ. Geol., v. 66, p. 653–669.
Toulmin, P., III and Barton, P. B., Jr., 1964, A thermodynamic study of pyrite and pyrrhotite: Geochim. et Cosmochim. Acta., v. 28, p. 641–671.
Yui, S., and Czamanske, G. K., 1971, Iron content of sphalerite from the Iimori mine, Japan: Soc. Mining Geologists Japan, Spec. Issue 3, p. 277–279.
Yund, R. A., and Kullerud, G., 1960, The Cu-Fe-S system: Carnegie Inst. Washington Yearbook 59, p. 111–114.
—— 1966, Thermal stability of assemblages in the Cu-Fe-S system: Jour. Petrology, v. 7, p. 454–488.

THE AMERICAN MINERALOGIST, VOL. 56, JANUARY-FEBRUARY, 1971

THE FREE ENERGY OF SODALITE AND THE BEHAVIOR OF CHLORIDE, FLUORIDE AND SULFATE IN SILICATE MAGMAS

J. C. STORMER, JR. AND I. S. E. CARMICHAEL, *University of California, Berkeley, California 94720*

ABSTRACT

The Gibbs free energy of formation for sodalite, $Na_4Al_3Si_3O_{12}Cl$, calculated from published data on its decomposition to nepheline and NaCl is:

T (deg. K)	1000	1100	1200	1300	1400
ΔG_f (K cal/gfw)	−1305.8	−1273.5	−1239.6	−1199.9	−1160.2

Sodalite stability is strongly controlled by silica activity. At high temperatures it will be found only in magmas whose silica activities are near or below the nepheline-albite equilibrium. At lower temperatures its stability field expands and it will be stable at higher silica activities, and will therefore precede nepheline in the crystallization sequence of phonolitic trachytes. If f_{Cl_2} is not more than 10^8 greater than f_{F_2}, villiaumite (NaF) or fluorite and nepheline will take the place of sodalite. ΔG°_f for nosean ($Na_8Al_6Si_6O_{24}[SO_4]$) has also been estimated, and it similarly can precede nepheline in the crystallization order of phonolitic trachytes. The ratio of f_{SO_2}/f_{Cl_2} of nosean coexisting with sodalite has been calculated for various temperatures and f_{O_2}. The stability of sulphate (nosean) rather than sulphide minerals is controlled not only by f_{O_2}, but also by silica activity and peralkalinity.

Values of f_{Cl_2} calculated from the sodalite-bearing trachytes of Mt. Suswa, Kenya, vary from $10^{-13.4}$ at 1400°K to $10^{-22.5}$ at 1000°K, and the upper limits of f_{F_2} vary from 10^{-23} to 10^{-35} atmospheres. Estimated fugacities of HCl and SO_2 are several orders of magnitude lower than the partial pressures of the same components in fumarolic gases of a hypersthene-dacite, as is to be expected. Siliceous magmas rich in Cl will generate a fluid phase rich in Cl which is expelled as crystallization proceeds. Magmas of lower silica activities (trachytes, leucite-basanites) will retain their Cl or SO_2, as sodalite or nosean are stable.

INTRODUCTION

With the exception of volcanic gases, the fugitive components in silicate magmas are not conveniently studied, and only analyses of quenched natural liquids provide any approach to their distribution and concentration. However, if during the crystallization of a silicate magma, the presence of a halogen induces a particular mineral to precipitate, then with the necessary thermodynamic data on that mineral, we can calculate a parameter (an intensive variable) which can characterize the behavior of the particular fugitive component. For example, the occurrence of sodalite in lavas can be used as a clue to the behavior of Cl, or nosean or hauyne can be used for SO_3.

As the data for sodalite are more reliable, in this paper we consider Cl and its contrasting behavior with F in silicate magmas. As an indication of the concentration of Cl in various igneous rock types, several average values are given in Table 1. Granite and basalt, comprising the vast

TABLE 1. CHLORIDE ABUNDANCES IN SOME IGNEOUS ROCKS

Rock Description	Percent Cl
Average Igenous Rocks	
Granite (Taylor, 1964)	0.02
Basalt (Taylor, 1964)	0.006
Phonolite (Nockolds, 1954)	0.23
Pantellerites	
Pantelleria (Carmichael, 1962)	
glassy (av. of 6)	0.56
microcrystalline	0.04
Comendites	
New Zealand (Nicholls and Carmichael, 1968)	
glassy (av. of 5)	0.24
microcrystalline (av. of 2)	0.02
Phonolites	
Mt. Suswa, Kenya (Nash *et al.*, 1969)	
glassy (av. of 2)	0.17
crystalline (av. of 7)	0.21
Leucite Tephrites and Basanites	
Vesuvius	
Savelli, 1967 (av. of 21)	0.48
Carmichael, 1971 (av. of 4)	0.46

majority of crustal igneous rocks, have less than 0.02 percent Cl; however one variety of acid lava, the peralkaline glassy pantellerites and comendites contain more than ten times as much Cl (Table I), but the low Cl contents of their crystalline counterparts show that Cl is expelled during crystallization. However, in peralkaline sodic trachytes the precipitation of sodalite retains Cl, so that the glassy and crystalline varieties of these lavas contain comparable amounts (Table I). In the holocrystalline and potassic leucite-basanites of Vesuvius, the occurrence of sodalite in the groundmass similarly retains a high concentration of Cl (Table I). It seems clear that the key to the retention of Cl in a crystalline lava lies in the stability or precipitation of sodalite, and in its absence, Cl will be expelled as part of the fluid phase.

This fluid phase, particularly in magmas with a high silica activity (Carmichael *et al.*, 1970) is rich in NaCl (Roedder and Coombs, 1967), a common component of volcanic sublimates (White and Waring, 1963). The work of Roedder and Coombs (1967) coupled with the experiments of Van Groos and Wyllie (1969) have indicated that a Cl-rich fluid phase

is immiscible with silicate liquids. Thus the generation of a Cl-rich fluid is the alternative in magmas with high silica activities to the crystallization of sodalite in magmas with lower silica activities; both may initially contain comparable amounts of Cl (Table I).

The Free Energy ($\Delta G°_f$) of Sodalite

The data published by Wellman (1969) on the vapor pressure of NaCl over decomposing sodalite, provides a basis for the calculation of the free energy of sodalite. These data were obtained by determining the temperature of precipitation of halite from the gas evolved by decomposing sodalite to nepheline and NaCl vapor in an evacuated quartz tube placed in a gradient furnace. Two slightly different methods of calculation can be used to determine a value for the free energy of sodalite.

One may assume the equilibrium of sodalite, nepheline and gas at the temperature of the sodalite. The equilibrium of the two predominant sodium chloride polymers, NaCl and Na_2Cl_2, in the gas can be calculated, and the free energies of nepheline and the gas summed to obtain the sodalite free energy.

$$NaCl_{(gas)} + 3\underset{\text{(nepheline)}}{NaAlSiO_4} = \underset{\text{(sodalite)}}{Na_4Al_3Si_3O_{12}Cl} \qquad \Delta G = 0 \qquad (1)$$

$$\Delta G°_{(NaCl\ gas)} + 3\Delta G°_{(nepheline)} - RT \ln f_{NaCl} = \Delta G°_{(sodalite)}$$

(where f = fugacity of NaCl species) (1a)

Alternatively one may assume that the sodalite and the nepheline at a higher temperature (T_1) are in equilibrium with pure halite at a lower temperature (T_2) through the medium of the gas:

$$NaCl_{(halite,T_2)} + 3NaAlSiO_{4(nepheline,T_1)} = Na_4Al_3Si_3O_{12}Cl_{(sodalite,T_1)} \quad (2)$$

$$\Delta G°_{(halite,T_2)} + 3\Delta G°_{(nepheline,T_1)} = \Delta G°_{(sodalite,T_1)} \qquad (2a)$$

The calculated values of free energy are shown in Figure 1. The agreement between both sets of calculations is quite good.

In the discussion which follows, we have assumed that all liquids and solids mix ideally, so that $a_{(activity)} = X_{(mol.\ fraction)}$. We are also concerned with components in a liquid rather than species.

Sodalite Stability and Silica Activity

As sodalite is found only in silica-undersaturated rocks, and never in quartz-bearing assemblages, its stability is obviously strongly influenced by silica activity (Carmichael *et al.*, 1970). Using the reaction (3) below, the effect of varying silica activity on the stability of sodalite can be calculated. At the same time the effect of varying the activity of NaCl in

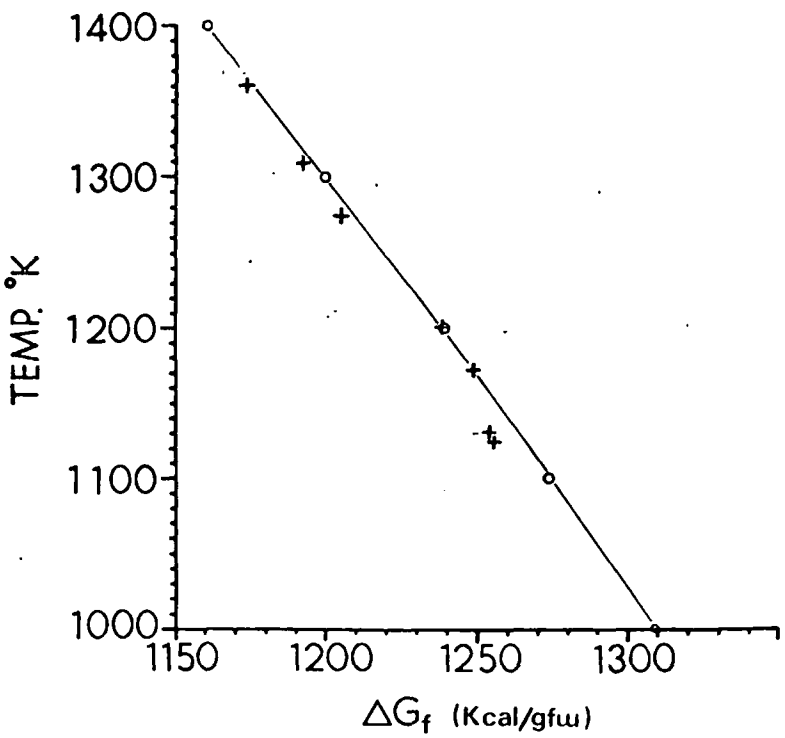

FIG. 1. The free energy of formation of sodalite ($Na_4Al_3Si_3O_{12}Cl$) calculated from measurements of the vapor pressure of NaCl over decomposing sodalite (Wellman, 1969). Calculations using reaction 1 shown as circles, reaction 2 as crosses.

the liquid, a_{NaCl}^{liquid}, which can be taken as a measure of Cl concentration, together with the effect of changing the composition of the coexisting feldspar, can be shown (assuming sodalite remains stoichiometric or nearly so).

$$\underset{\text{sodalite}}{Na_4Al_3Si_3O_{12}Cl} + 6\underset{\text{liquid}}{SiO_2} = \underset{\text{liquid}}{NaCl} + 3\underset{\text{albite}}{NaAlSi_3O_8} \qquad (3)$$

$$\log a_{SiO_2}^{liquid} = \frac{1}{6}\left[\frac{\Delta G^\circ}{2.303\ RT} + \log a_{NaCl}^{liquid} + 3 \log a_{NaAlSi_3O_8}^{feldspar}\right] \qquad (3a)$$

In Figure 2, the limit of the stability field of sodalite is shown at two temperatures. If the coexisting feldspar is pure albite ($a_{NaAlSi_3O_8}^{feldspar} = 1$), then sodalite is stable at higher silica activities than those defined by the reaction

$$NaAlSiO_4 + 2SiO_2 = NaAlSi_3O_8 \qquad (4)$$

in a typical phonolite assemblage (Carmichael *et al.*, 1970). The curves in

Figure 2 indicate that sodalite will co-precipitate with feldspar in trachytic liquids *before* they become sufficiently poor in silica to precipitate nepheline; this sequence of crystallization is particularly well displayed in the Mt. Suswa phonolitic trachytes (Nash *et al.*, 1969). However if the coexisting feldspar is not pure albite, then the precipitation of sodalite will be delayed at both temperatures (Fig. 2), until silica activity is lower than under the corresponding conditions of pure feldspar. The calculated data shown in Figure 2 may be emphasised in a different way; the lower the crystallization temperature, the more likely sodalite is to precede nepheline in the order of crystallization of a trachytic magma whose residual liquid is changing in composition so as to eventually crystallize nepheline. The greater the activity of NaCl or concentration of Cl in the trachyte magnia, the greater will this precedence of sodalite be in comparison to nepheline (Fig. 2).

In a paper on silica activity in igneous rocks, Carmichael *et al.* (1970) suggested that the thermodynamic data for leucite are likely to be wrong, and that the variation in a_{SiO_2} with temperature defined by the reaction

$$\underset{\text{leucite}}{KAlSi_2O_6} + \underset{\text{liquid}}{SiO_2} = \underset{\text{feldspar}}{KAlSi_3O_8} \qquad (5)$$

should be at higher values of a_{SiO_2} than the corresponding curve for the nepheline-albite assemblage. This conclusion is not invalidated by the occurrence of sodalite in the crystalline groundmass of the Vesuvius leucite-basanites (Carmichael, unpublished work). In these, leucite, plagioclase (An_{56}), sodalite and phlogopite coexist, an assemblage which in view of the calculated stability of sodalite (Fig. 2) could well have a higher silica activity than the analogous nepheline-albite assemblage.

In magmas with high silica activities, namely rhyolites and siliceous trachytes, the Cl component, represented as NaCl (Fig. 2) will presumably form an immiscible fluid phase if the results of Van Groos and Wyllie (1969) in the immiscibility of liquid NaCl in $NaAlSi_3O_8$ liquid are applicable to siliceous magmas.

Sodalite Stability and Fluorine Fugacity

One of the intriguing contrasts between chlorine and fluorine in igneous rocks is seen in the absence of a fluoride analogue of sodalite. Villiaumite (NaF) and nepheline are the stable equivalent association, and although very rare in nature, they do occur (Stormer and Carmichael, 1970). Another example of the separation of these two halides is found in the groundmass assemblage of the Vesuvius leucite-basanites (Carmichael, 1971a) there, as noted above, sodalite is associated with chloride-poor fluorphlogopite.

1400°K

1000°K

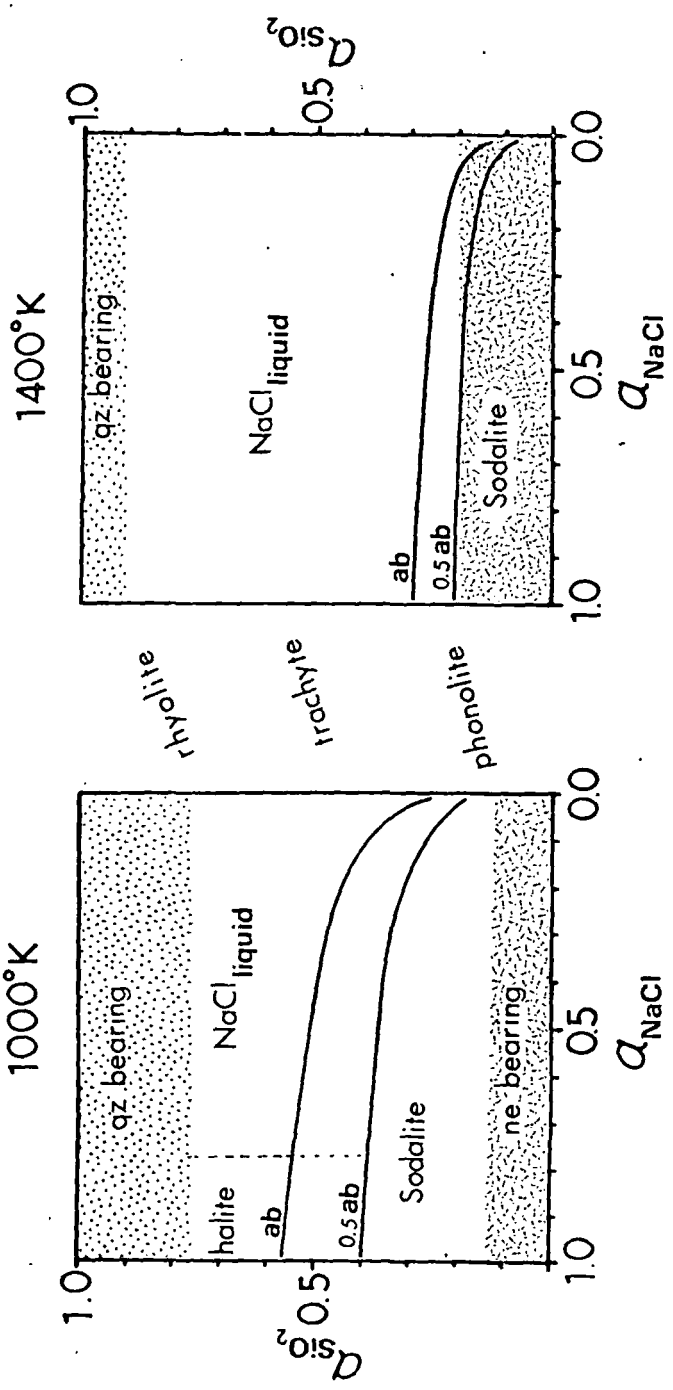

FIG. 2. The stability field of sodalite at 1000°K (727°C) and 1400°K (1127°C) as calculated by reaction 3. Sodalite will be stable at silica and NaCl activities below the curves; the upper curve is for pure albite, the lower for an activity of 9.5 albite in coexisting feldspar. The standard state for SiO_2 has been taken as silica glass (cf. Carmichael *et al.*, 1970). The lower boundary of the shaded area labeled "quartz bearing" is defined by the activity of silica glass in equilibrium with crystalline quartz. Below this line quartz will not be stable. Rhyolitic magmas will have silica activities near this boundary. The upper boundary of the shaded area labeled "ne bearing" is defined by the activity of silica in equilibrium with nepheline and albite. Above this line nepheline will not be stable; below it an albite-rich feldspar will not be stable. Phonolitic magmas will have silica activities near this value. Trachytic magmas will have intermediate values of silica activity. Liquid NaCl was similarly chosen as the standard state for sodium chloride. Therefore at temperatures below the melting temperature of halite, crystalline halite will be in equilibrium with NaCl liquid at activities less than one. The activity of liquid NaCl in equilibrium with halite is shown at 1000°K (727°C) by the dashed boundary. Magmas having activities of liquid NaCl on this boundary, and silica activities above the sodalite stability field would contain crystalline halite. No natural example of such a magma has been reported.

It is possible to calculate limits of the ratio of the fugacities of F to Cl (f_{F_2}/f_{Cl_2}) for rocks which contain sodalite. In the following reaction

$$2Na_4Al_3Si_3O_{12}Cl + F_2 = 2NaF + 6NaAlSiO_4 + Cl_2 \quad (6)$$

$$\log f_{F_2}/f_{Cl_2} = \frac{\Delta G^\circ}{2.303\ RT} + 6 \log a^{\text{nepheline}}_{NaAlSiO_4} \quad (6a)$$

the ratio f_{F_2}/f_{Cl_2} is approximately $10^{-8.4}$ over the temperature range 1000°–1400°K for the equilibrium assemblage sodalite, nepheline and villiaumite. If water is present as a component in reaction (6) then HF and HCl will be the predominant halide species, and, as hydrolysis of fluorine is the more complete, the corresponding fugacity ratios f_{HF}/f_{HCl} vary between $10^{4.8}$ and $10^{2.4}$ over the same temperature range (1000–1400°K). It is therefore possible to calculate the *upper* limit of the two fugacity ratios f_{F_2}/f_{Cl_2} and f_{HF}/f_{HCl} for natural assemblages of sodalite and nepheline. The calculated fugacity ratios are not greatly changed if reaction (6) is modified to include albite (7), provided that the silica activity is appropriately low:

$$\underset{\text{sodalite}}{2Na_4Al_3Si_3O_{12}Cl} + \underset{\text{liquid}}{12SiO_2} + F_2 = \underset{\text{villiaumite}}{2NaF} + \underset{\text{albite}}{6NaAlSi_3O_8} + Cl_2 \quad (7)$$

Stormer and Carmichael (1970) have shown that villiaumite in reaction (7) will be replaced by fluorite if the anorthite component of the feldspar exceeds about 10 mole percent. Fluorite and nepheline will then take the place of sodalite at the expense of anorthite as indicated in the reaction below

$$\underset{\text{sodalite}}{2Na_4Al_3Si_3O_{12}Cl} + \underset{\text{anorthite}}{CaAl_2Si_2O_8} + F_2 = \underset{\text{fluorite}}{CaF_2} + \underset{\text{nepheline}}{8NaAlSiO_4} + Cl_2 \quad (8)$$

and

$$\log f_{F_2}/f_{Cl_2} = \frac{\Delta G^\circ}{2.303\ RT} + 8 \log a^{\text{nepheline}}_{NaAlSiO_4} - \log a^{\text{feldspar}}_{CaAl_2SiO_8} \quad (8a)$$

In Figure 3, we have plotted the results for the two reactions (6) and (8) at 1200°K. Using the data on the Vesuvius leucite-basanites where sodalite coexists with An_{56} in the groundmass, the calculated stability curve of sodalite in Figure 3 indicates a *maximum* value of f_{F_2}/f_{Cl_2} of about 10^{-9} at 927°C for these lavas. Savelli (1967) has given an average value of 2700 ppm F and 4800 ppm Cl for the Vesuvius lavas, which correspond to a concentration ratio of 0.56 or $10^{-0.25}$.

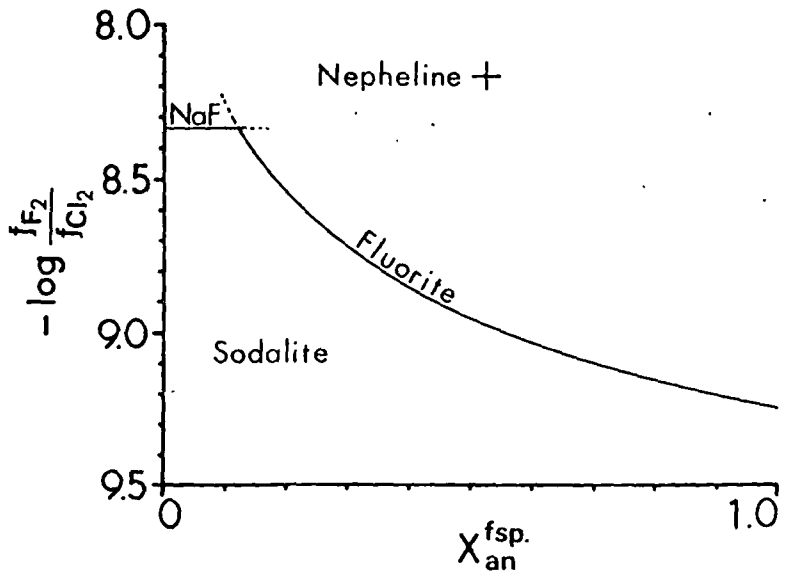

FIG. 3. The stability field of sodalite as limited by high ratios of fluorine to chlorine at 1200°K (927°C); see reactions 7 and 8 in text. If a feldspar containing more than 10 mole percent anorthite coexists with sodalite, fluorite plus nepheline will take the place of sodalite, the ratio of fluorine to chlorine falling with increasing anorthite. If a feldspar with more than 10 mole percent anorthite is not present villiaumite and nepheline will take the place of sodalite. These relationships remain essentially the same over the temperature range 1000°K (727°C)–1400°K (1127°C).

NOSEAN AND SULPHATE ACTIVITY

In order to estimate the free energy of nosean (ΔG°_f), we can assume that over the temperature range of interest, the sum of the free energies of nepheline and thenardite (Na_2SO_4) are equal to that of nosean in an analogous way to the discussion of sodalite. In other words, it can be assumed that ΔG of the following reaction is zero

$$\underset{\text{thenardite}}{Na_2SO_4} + 2\underset{\text{sodalite}}{Na_4AlSi_3O_{12}Cl} = 2\underset{\text{halite}}{NaCl} + \underset{\text{nosean}}{Na_8Al_6Si_6O_{24}(SO_4)} \quad (9)$$

Then

$$\Delta G^\circ_{f\,(\text{nosean})} = 2\Delta G^\circ_{f\,(\text{sodalite})} + \Delta G^\circ_{f\,(\text{thenardite})} - 2\Delta G^\circ_{f\,(\text{halite})} \quad (9a)$$

Since nosean can be produced from sodalite, and sodalite from nosean, in a flux of the appropriate sodium salt (Pauling, 1930), this assumption may not be far wrong.

Using the estimated values of ΔG°_f for nosean, it is possible to calculate

the stability of nosean at various temperatures as a function of silica activity and Na_2SO_4 activity using the reaction:

$$\underset{\text{nosean}}{Na_8Al_6Si_6O_{24}(SO_4)} + 12\underset{\text{liquid}}{SiO_2} = \underset{\text{liquid}}{Na_2SO_4} + 6\underset{\text{albite}}{NaAlSi_3O_8} \qquad (10)$$

The calculated curves are almost identical[1] to those for sodalite plotted in Figure 2, and indicate that nosean can precede nepheline in the order of crystallization of a trachytic magma whose residual liquid will eventually precipitate nepheline. Both the experimental results of Taylor (1967) on the system nosean-albite-orthoclase, and observations on the Wolf Rock nosean phonolite (Tilley, 1959) indicate that nosean may precede nepheline in magmas crystallizing feldspar.

Peteghem and Burley (1963) and Tomisaka and Eugster (1968) have investigated the sodalite-nosean join. There is a large miscibility gap, and both solids show limited solid solution. However there is substantial disagreement between the two sets of results on the extent of solid solution in the two phases. Analyses of natural sodalite and nosean (Deer *et al.*, 1963; Taylor, 1967) suggest that there is considerably more solid solution of the chloride component in nosean than of the sulphate component in sodalite. If the extent of the mutual solid solution in the nosean-sodalite series is assumed to be minimal at magmatic temperatures, then the following reaction can be used to calculate the limiting fugacity ratio f_{SO_2}/f_{Cl_2} for nosean or sodalite. It is also assumed that SO_2 is the predominant sulphur-oxygen species at magmatic temperatures (Heald *et al.*, 1963).

$$2\underset{\text{sodalite}}{Na_4Al_3Si_3O_{12}Cl} + SO_2 + O_2 = \underset{\text{nosean}}{Na_8Al_6Si_6O_{24}(SO_4)} + Cl_2 \qquad (11)$$

$$\log f_{SO_2}/f_{Cl_2} = \frac{\Delta G^\circ}{2.303\,RT} - \log f_{O_2} - 2\log a^{\text{sodalite}}_{Na_4Al_3Si_3O_{12}Cl} + \log a^{\text{nosean}}_{Na_8Al_6Si_6O_{24}(SO_4)} \qquad (11a)$$

The variations of the fugacity ratio f_{SO_2}/f_{Cl_2} with temperature and f_{O_2} has been plotted in Figure 4 assuming unit activity of nosean and sodalite. Each curve represents the f_{SO_2}/f_{Cl_2} ratio for the coexistence of nosean and

[1] It may appear that the stability fields of nosean and sodalite in terms of the activities of silica, albite and sodium salt (reactions (3) and (10) Fig. 2) are necessarily identical because of the assumptions used to estimate the free energy of nosean. However, the standard state of the sodium salt in equation (3) was the pure liquid, whereas that used to estimate the free energy of nosean was the crystalline solid. As a result the stability field of nosean in terms of these variables will differ from that of sodalite by an amount determined by the difference in the solid-liquid transition energies of Na_2SO_4 and NaCl. This difference is in fact negligibly small; at 1000°K it would be represented by an increase of about 0.01 in the silica activity.

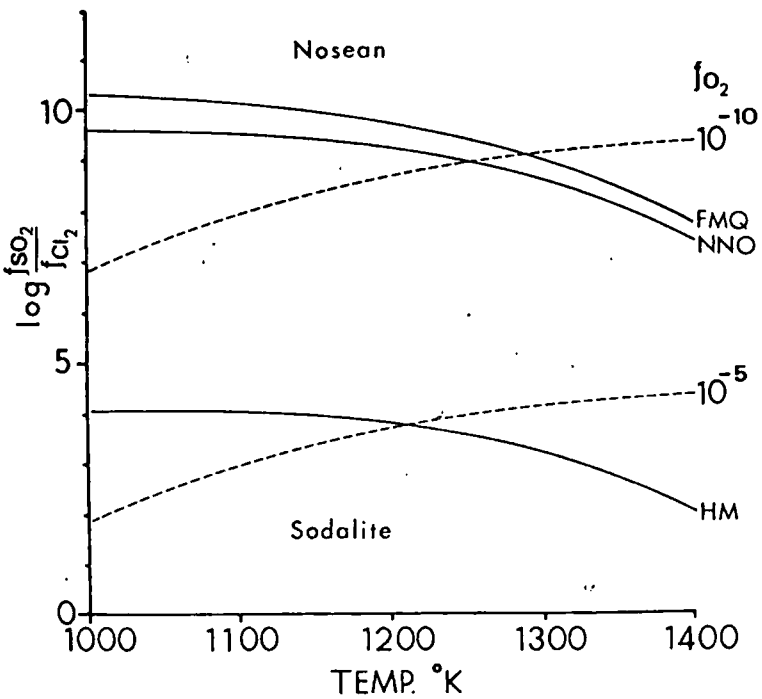

FIG. 4. Reaction 11, equilibrium between nosean and sodalite, plotted in terms of the ratio of SO_2 to Cl_2 and temperature for several oxygen fugacities. Dashed curves for constant oxygen fugacities. Solid curves for oxygen fugacities buffered by the following assemblages: FMQ, fayalite-magnetite-quartz; NNO, nickel-nickel oxide; HM, hematite-magnetite.

sodalite for particular oxygen-fugacity conditions. Thus nosean in equilibrium with hematite and magnetite would have a minimum value of f_{SO_2}/f_{Cl_2} of 10^2 to 10^4 over the temperature range of Figure 4.

NOSEAN AND OXYGEN FUGACITY

The presence of sulphate sulphur in a magma rather than sulphide sulphur is often thought to require an unusually high f_{O_2}, or at least values higher than those normally associated with sulphide minerals (Skinner and Peck, 1969, 319). But the association of nosean with olivine and titaniferous magnetite in alkali olivine-basalt bombs in Quaternary cinder cones of northeastern New Mexico (Baldwin and Muehlberger, 1958; Stormer, 1970) shows that unless either of the ferromagnesian minerals have extreme composition, the oxygen fugacity will not differ greatly from any other olivine-basalt, or from that in equilibrium with the synthetic fayalite-magnetite-quartz assemblage (Carmichael and Nicholls, 1967). The more common paragenesis of nosean, or perhaps of hauyne, a

calcium-bearing sulphate variety, is in olivine-free lavas, for example, the etindites of West Africa (Tilley, 1953; Carmichael, unpublished work), where noscanhauyne solid solutions occur with titan-augite, titaniferous magnetite and perovskite. In some salic lavas, nosean or hauyne may occur with melanite, augite titaniferous magnetite and leucite. In both parageneses, the absence of olivine could be suggestive of a higher f_{O_2}.

Perhaps the problem of the occurrence of sulphate rather than sulphide can be illustrated by the following reaction, a plausible representation of a nosean paragenesis

$$\underset{\text{nosean}}{Na_8Al_6Si_6O_{24}(SO_4)} + \underset{\text{magnetite}}{Fe_3O_4} + \underset{\text{liquid}}{16SiO_2} = \underset{\text{pyrrhotite}}{FeS} + \underset{\text{acmite}}{2NaFeSi_2O_6} + \underset{\text{albite}}{6NaAlSi_3O_8} + 2O_2 \quad (12)$$

A cursory inspection shows that if silica activity falls, the reaction will run to the left, despite f_{O_2} remaining constant. This reaction illustrates an essential point: the occurrence of sulphate rather than sulphide need not require an unusually high f_{O_2}, because it is also controlled by the overall composition of the silicate magma. In this example, low silica activity and a large component of acmite in the coexisting pyroxene would promote the crystallization of nosean. Sulphate minerals are therefore to low silica activity peralkaline magmas what sulphide minerals are to high silica activity magmas; even though f_{O_2} may be constant (at comparable T), witness the occurrence of olivine and titaniferous magnetite.

Calculation of Fugitive Fugacities in Igneous Assemblages

The volatile constituents of a magma as we have seen are often lost in the later stages of crystallization. However, thermodynamic data can be used to recalculate the activities or fugacities from analyses of the mineral phases whose presence and composition was controlled by, or controlled, them.

The sodalite-bearing trachytic lavas of Mt. Suswa, Kenya, have been studied by Nash *et al.* (1969) and analyses of the mineral phases are available. The fugacity of chlorine in one lava (W158) can be calculated using the following reaction:

$$2NaFeSi_2O_6 + 6NaAlSiO_4 + Cl_2 = 2Na_4Al_3Si_3O_{12}Cl + 4SiO_2 + \tfrac{2}{3}Fe_3O_4 + \tfrac{2}{3}O_2 \quad (13)$$

$$\log f_{Cl_2} = \frac{\Delta G^\circ}{2.303\,RT} + 2\log a^{\text{sodalite}}_{Na_4Al_3Si_3O_{12}Cl} + 4\log a_{SiO_2} + \tfrac{2}{3}\log a^{\text{magnetite}}_{Fe_3O_4} + \tfrac{2}{3}\log f_{O_2} - 2\log a^{\text{pyroxene}}_{NaFeSi_2O_6} - 6\log a^{\text{nepheline}}_{NaAlSiO_4} \quad (13a)$$

The activity of silica is calculated from the data for nepheline and feldspar (Carmichael, *et al.*, 1970; Nash *et al.*, 1969). Activity coefficients for nepheline obtained from the data of Perchuck and Ryabchikov (1968) were used although they do not take the excess silica component into account. In the absence of any better information the activities of the other components were assumed to be equal to their mole fractions in the respective mineral phases.

The fugacity of chlorine has been calculated and plotted in Figure 5 as a function of temperature, assuming that all the phases in reaction (9) coexist at a given temperature. In all probability they coexist only for a limited range of temperature, which unfortunately is not known. As neither villiaumite nor noscan are present, only the *upper* limits of the fugacities of F_2 and SO_2 for the observed mineral assemblage can be calculated using reactions (8a) and (11a), and they are plotted in Figure 5. In order to facilitate comparison with analysed volcanic gases, it was assumed that the fugacity of water in the lava was 1 atm and the approximate fugacity of HCl calculated. Also shown in Figure 5 are the partial pressures of HCl and SO_2 derived from analyses of fumarolic gases associated with the extrusion of a hypersthene dacite dome at Showa-Shinzan, Japan (White and Waring, 1963). The Showa-Shinzan data was selected because of the completeness of the analyses and the appropriateness of the temperature range. HCl and SO_2 in these analyses are not unusually high when compared with other data. A hypersthene dacite such as this will, of course, have a much higher silica activity than the phonolites with which it is being compared, and will no doubt generate and expel a fluid phase rich in Cl as crystallization proceeds. It is not surprising therefore that the fugacity of HCl, and also SO_2, is so much higher at Showa-Shinzan than the values calculated for Mt. Suswa lavas. The most striking feature of Figure 5 is the very low volatile pressure (equal to fugacity at 1 atm H_2O) required to stabilize sodalite in trachyte lavas (*cf.* Nash *et al.*, 1969). It is obvious that sodalite may be unstable only in a very thin zone of the flow crust (Nash *et al.*, 1969). It is also apparent that high activities of chlorine are not necessarily characteristic of sodalite-bearing undersaturated magmas in spite of the high chloride contents of such rocks. Other chemical parameters, particularly silica activity, are the controlling factors in the behavior of chloride in magmas and its distribution in rocks. Relatively silicic magmas may be expected to show a rising activity of chlorine and higher fugacities of HCl upon crystallization, even though the chloride content of the resulting rock is very low. Conversely, silica-undersaturated peralkaline magmas will precipitate sodalite and retain their chloride in the rock. The occurrence of sodalite or any other halide or sulfate mineral in a rock is not necessarily indicative of unusual activity of that component in the parent magma.

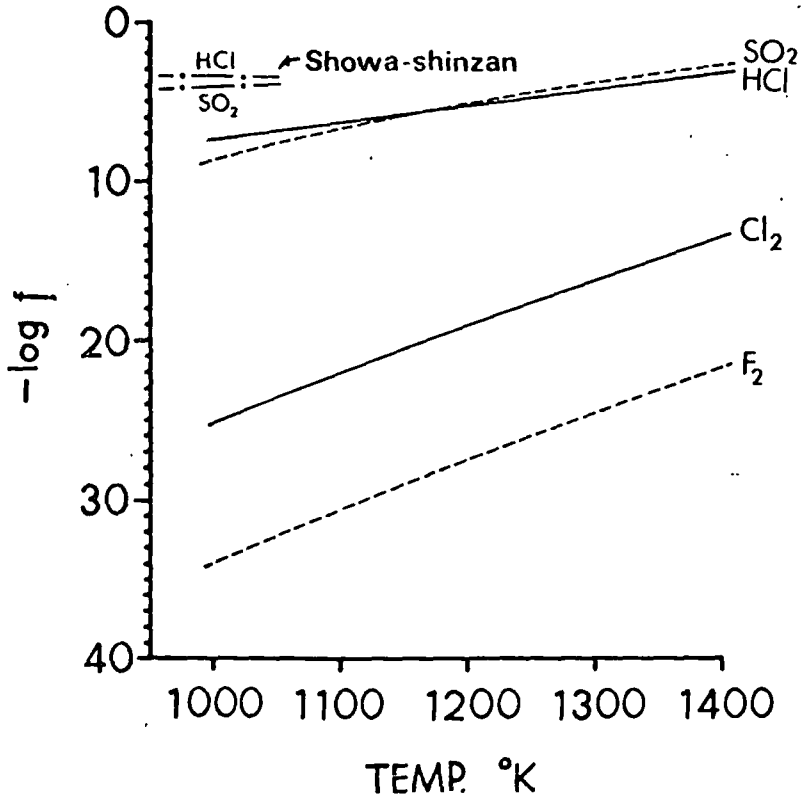

FIG. 5. Fugacities of certain volatile components calculated for one lava of Mt. Suswa, Kenya between 727°C (1000°K) and 1127°C (1400°K). The fugacities of Cl_2 and HCl calculated by reaction 13 (see text). Upper limits of the fugacities of F_2 and SO_2 were determined by reactions 8a and 11a. Partial pressures of HCl and SO_2 in analysed fumarolic gases from a hypersthene dacite at Showa-Shinzan, Japan are also shown.

Quantitative definition of the role halogens and other fugitive components play in the genesis and differentiation of magmas require this type of thermodynamic investigation, which will indicate more clearly than has previously been possible the behavior of volatiles in magmatic liquids.

THERMODYNAMIC DATA

Sodalite ($Na_4Al_3Si_3O_{12}Cl$)—calculated from Wellman's (1969) data.

$T°$ (°K)	1000	1100	1200	1300	1400	
ΔG_f (Kcal/gfw)	−1305.8	−1273.5	−1239.6	−1199.9	−1160.2	all ±3.0

Nosean ($Na_8Al_6Si_6O_{24}(SO_4)$—estimated this paper.

T (°K)	1000	1100	1200	1300	1400

ΔG_f, (Kcal/gfw)	−2695.0	−2624.2	−2550.5	−2468.3	−2386.0	all ±3.0 (numerical errors)

Acmite ($NaFeSi_2O_6$)—estimated by Nicholls and Carmichael (1969)

NaCl and HF (liquid and gaseous)—JANAF Thermochemical Tables

All other data—Robie and Waldbaum (1968)

ACKNOWLEDGEMENTS

NSF has materially supported much of this research (GA-1541). Dr. Wellman kindly supplied some additional information on his vapor pressure measurements.

REFERENCES

BALDWIN, B., AND W. R. MUEHLBERGER (1959) Geologic studies of Union County, New Mexico. *N. Mex. Bur. Mines Bull.* **63**, 171 p.

CARMICHAEL, I. S. E. (1962) Pantelleritic liquids and their phenocrysts. *Mineral Mag.* **33**, 86–113.

——— AND NICHOLLS (1967) Iron-titanium oxides and oxygen fugacities in volcanic rocks. *J. Geophys. Res.* **72**, 4665–4687.

———, ——— AND A. L. SMITH (1970) Silica activity in igneous rocks. *Amer. Mineral.* **55**, 246–263.

DEER, W. A., R. A. HOWIE, AND J. ZUSSMAN (1962) *Rock-Forming Minerals, Vol. 4*, Wiley, New York.

JANAF Thermochemical Tables. Dow Chemical Co., Dow Chemical Co. Midland, Michigan (1960–1962).

HEALD, E. F., J. J. NAUGHTON, AND I. L. BARNES (1963) The chemistry of volcanic gasses. *J. Geophys. Res.* **68**, 539–557.

JOHANNSEN, A. (1939) *A Descriptive Petrography of the Igneous Rocks, IV*. University of Chicago Press, Chicago.

KOSTER VAN GROOS, A. F., AND P. J. WYLLIE (1968) Melting relationships in the system $NaAlSi_2O_8$-NaF-H_2O to 4 kilobars pressure. *J. Geol.* **76**, 50–70.

———, AND ——— (1969) Melting relationships in the system $NaAlSi_2O_8$-NaCl-H_2O at one kilobar pressure with petrological applications. *J. Geol.* **77**, 581–605.

LIN, S. B., AND B. J. BURLEY (1969) The system CaF_2-$CaMgSi_2O_6$. *Can. J. Earth Sci.* **6**, 269–280.

NASH, W. P., I. S. E. CARMICHAEL, AND R. W. JOHNSON (1969) The mineralogy and petrology of Mount Suswa, Kenya. *J. Petrology* **10**, 409–439.

NICHOLLS, J., AND I. S. E. CARMICHAEL (1969), Peralkaline acid liquids: a petrological study. *Contrib. Mineral. Petrology* **20**, 268–294.

PERCHUCK, L. L., AND I. D. RYABCHIKOV (1968) Mineral equilibria in the system nepheline-alkali feldspar-plagioclase and their petrological significance. *J. Petrology* **9**, 123–167.

PAULING, L. (1930) The structure of sodalite and helvite. *Z. Kristallogr.* **74**, 213–225.

PETEGHEM, J. K. VAN, AND B. J. BURLEY (1962) Studies on solid solution between sodalite, nosean and haüyne. *Can. Mineral.* **7**, 808–813.

ROBIE, R. A., AND D. R. WALDBAUM (1968) Thermodynamic properties of minerals and related substances at 298.15°K (25°C) and one atmosphere (1.013 bars) pressure and at higher temperature. *U. S. Geol. Surv. Bull.* 1259.

ROEDDER, E. (1968) Studies of fluid inclusions. II: Freezing data and their interpretation. *Econ. Geol.* **58**, 167–211.

——— AND D. S. COOMBS (1967) Immiscibility in granitic melts, indicated by fluid inclusions in ejected granitic blocks from Ascension Island. *J. Petrology* 8, 415–417.

SAVELLI, C. (1967) The problem of rock assimilation by Somma-Vesuvius magma. I. Composition of Somma and Vesuvius lavas. *Contrib. Mineral. Petrology* 16, 328–353.

SKINNER, B. J., AND D. L. PECK (1969) An immiscible sulfide melt from Hawaii. *Econ. Geol. Mono.* 4, 310–322.

STORMER, J. C., JR., AND I. S. E. CARMICHAEL (1970) Villiaumite and the occurrence of fluoride minerals in igneous rocks. *Amer. Mineral.* 55, 126–134.

TAYLOR, D. (1967a) The sodalite group of minerals. *Contrib. Mineral. Petrology* 16, 172–188.

——— (1967b) Ph.D. thesis, Univ. of Manchester.

TAYLOR, S. R. (1964), Abundance of chemical elements in the continental crust. *Geochim. Cosmochim. Acta* 28, 1280–1281.

TILLEY, C. E. (1953) The nephelinite of Etinde, Cameroons, West Africa. *Geol. Mag.* 90, 145–151.

——— (1959) A note on the nosean phonolite of the Wolf Rock, Cornwall. *Geol. Mag.* 96, 503–504.

TOMISAKA, T., AND H. P. EUGSTER (1968) Synthesis of the sodalite group and subsolidus equilibria in the sodalite-nosean system. *J. Mineral. Soc. Jap.* 5, 249–275.

WELLMAN, T. R. (1969) The vapor pressure of NaCl over decomposing sodalite. *Geochim. Cosmochim. Acta* 33, 1302–1303.

——— (1970) The stability of sodalite in a synthetic syenite plus aqueous chloride fluid system. *J. Petrology* 11, 49–71.

WHITE, D. E., AND G. A. WARING (1963) Volcanic emanations. *U. S. Geol. Surv. Prof. Pap.* 440-K.

Manuscript received, June 24, 1970; accepted for publication, July 23, 1970.

Chemical Geology, 19 (1977) 1—42

FLUORINE IN GRANITIC ROCKS AND MELTS: A REVIEW*[1]

J.C. BAILEY

Institute for Petrology, University of Copenhagen, Copenhagen (Denmark)[*2]

(Received October 8, 1975; revised and accepted April 13, 1976)

ABSTRACT

Bailey, J.C., 1977. Fluorine in granitic rocks and melts: A review. Chem. Geol., 19: 1—42.

Proposed average fluorine contents for granite (about 800 ppm) have limited value as contents range from tens of ppm to several per cent and vary greatly within and between different granite types. F may be either concentrated or released by both alkaline and calc-alkaline series. Enhanced contents occur in alkalic varieties, late hypabyssal stocks, some roof zones and margins, autometasomatized granites, and reach a maximum in Li—F granites and ongonite dykes, and in alkali granite pegmatites. F-rich fluid inclusions from the Volhynia pegmatites, Ukraine, fuse to granitic melts and evolve continuously into hydrothermal solutions. The lowest F contents occur in migmatites, and in gases from acid igneous volcanoes.

Mineralogically, 30—90% of the F in calc-alkaline granites is usually located in biotite, with lesser amounts in hornblende, muscovite, quartz and accessories. However, accessory minerals — apatite, sphene, fluorite, microlite, pyrochlore, topaz, tourmaline, bastnäsite, amblygonite, spodumene, cryolite, etc. — occasionally contribute more than 50% of the F notably in F-rich magmatic and metasomatic roof-zone granites (apogranites). Geothermometry based on F/OH ratios of biotite seems invalid for granitic series. The stability of Li-micas, topaz and cryolite is briefly presented.

In granite melts F^- replaces O^{2-} forming Si—F bonds or it links with Na^+ and other network modifiers. It partitions into magma rather than the vapour phase, but increasing degassing occurs in the more siliceous, less alkaline, magmas. Addition of HF lowers the freezing point of granite magmas (by 36—110° C), delays the onset of crystallization, and promotes quartz, topaz and feldspars above biotite in the order of crystallization. F increases the solubility of H_2O in melts and with alkali silicates may cause complete transition to hydrothermal solutions especially at higher pressures. F-rich melts may show immiscible separation into a fluoridic alkaline melt and a polymerized silicate melt.

Deviations from the generally monotonous relation of F: Li: Sn in granites are found in stanniferous and Li—F granites, and in greisen. F-rich apogranites are economically interesting for Ta, Rb, Cs and Be; F-rich pegmatites for Li, Rb and Cs; and albitized riebeckite granites for Zr, Nb and REE. Fluorite deposits stem from granites, particularly alkalic granites, but are usually well separated in space. Cryolite is intimately associated with autometasomatized alkali granite stocks and pegmatites.

*[1] A contribution to the International Geological Correlation Programme, *Metallization Associated with Acid Magmas.*

*[2] Address: Institute for Petrology, University of Copenhagen, Øster Voldgade 5—7, DK-1350 Copenhagen K, Denmark.

INTRODUCTION

The fluorine chemistry of granitic materials is relevant to:

(1) Assessing the role of volatiles in petrogenesis: by initiating melting and prolonging crystallization, influencing the composition and crystallization sequence of melts, their structure, viscosity and uptake of water and alkalis, and by introducing phenomena of immiscibility and element redistribution by volatiles.

(2) Geothermometry via the F/OH ratios of micas, apatite and topaz.

(3) Economic prospecting in granitic terrains, since F is associated with Sn—W—Mo and REE—Zr—Ta—Be deposits, with Li—Rb—Cs pegmatites, rare-metal greisens and albitized granites and is ultimately responsible for fluorite and cryolite deposits.

Following the pioneer work of Shepherd (1940), major analytical surveys of F geochemistry were provided by Koritnig (1951), Seraphim (1951) and Kokubu (1956), while important compilations appeared in the works of Correns (1956), Fleischer and Robinson (1963), and Allmann and Koritnig (1972).

No attempt has been made in this paper to compile every F analysis on granitic materials. Instead emphasis is placed on articles interpreting the behaviour of F in different granitic processes and environments, its experimental behaviour in melts, crystals and fluids, and on already existing compilations.

Geochemical analysis for F has speeded up in recent years. A variety of colorimetric techniques are now supplemented by spectrographic, microprobe and specific ion electrode analysis. Commercial X-ray spectrometers should soon permit trace-element determinations.

Nevertheless F continues to be a "difficult" element to analyse in many laboratories, especially towards the lower levels (< 0.1%) found in many granitic materials. The present review largely overcomes this uncertainty by emphasising reputable, modern publications, and by giving averages or repeated examples where possible. When in doubt about the quality of the quoted data, the reader should consult the original publication.

Examination of the reference list indicates that the number of papers discussing F in granites has nearly doubled every five years since 1950. Soviet publications account for about half the list.

DISTRIBUTION OF F IN GRANITIC MATERIALS

Absolute contents

According to Correns (1956) granites exhibit a range of 20—3,600 ppm F, averaging about 600—900 ppm F. Similarly, Vinogradov (1962) suggests an average value of 800 ppm F for granites, and Turekian and Wedepohl (1961) propose 850 ppm F for low-Ca granites and 520 ppm for high-Ca granites.

The usefulness of these average values is limited as it is clear that different granite types, regardless of uncertain classifications and geneses, do exist and show greatly differing F contents (Fig. 1).

Thus Tauson (1974) finds that fractionated granites from tholeiitic, calc-alkaline, alkaline and K-rich alkaline series contain successively higher average F contents: 150, 700, 800 and 900 ppm, respectively.

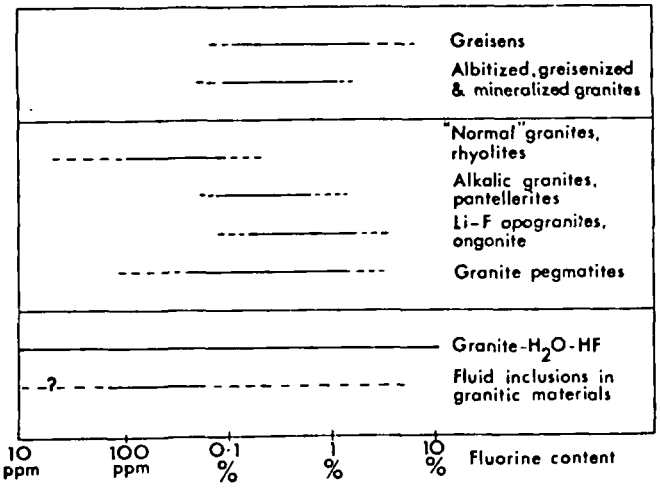

Fig. 1. Normal and extreme ranges of F contents in various granitic materials. Sources of data in the text.

The compilations of Allmann and Koritnig (1972) and Bowden (1974) suggest that F contents in pantellerites, and in alkali granites of varying alkalinity, most often range from about 1,000—3,000 ppm. F contents in some alkaline series (Table I) rise steadily (trend *A*), while others show a gentle decrease or fairly monotonous averages (trend *B*). The Nigerian granites (trend *C*) show a sharp F increase in the albitized riebeckite apogranites. Differences within provinces, e.g. the Gardar province, SW Greenland, represented by columns *1*, *2*, *3* and *6* of Table I, and between provinces seem apparent. Bowden and Whitley (1974) find that F contents increase from 1,300—2,800 ppm to 5,300 ppm as the peralkalinity index [(Na + K)/Al] increases from 0.88 to 1.10 in the roof zone of the outer granite ring dyke, Amo complex, Nigeria. Trace elements in fifteen obsidians of a pantelleritic trachyte —pantellerite series from Eburru Volcano, Kenya Rift Valley, fall into a F group (F—Zr—Rb) and a Cl group (Cl—Nb—Y) which show non-linear inter-group relations (Bailey and Macdonald, 1975). The variations in both trace and major elements are such that a vapour (fluid) phase, probably rich in halogens, is required to account for any magmatic evolution. There are no publications presenting F contributions from various minerals to the whole-rock contents of alkali granites. Alkali amphiboles (riebeckite, arfvedsonite) often contain 2—3% F, and are probably the chief contributor when present. Significantly fluorite was not recorded from the peralkaline granite (ekerite)

TABLE I

Selected examples of the three F trends (*A*, *B* and *C*) in alkaline plutonic series (F in wt.%)

	A			*B*			*C*
	1	*2*	*3*	*4*	*5*	*6*	*7*
Syenite	0.09*[1]	0.15	0.14	0.11	0.08	0.27	
Quartz syenite	0.11		0.21	0.09	0.09	0.32	0.18
Alkali granite	0.22	0.22	0.27	0.05	0.05	0.28	0.28*[2]
Alkali apogranite							0.66

1 = Kŭngnăt complex (Upton, 1960; Upton et al., 1971; Macdonald et al., 1973); *2* = Tugtutŏq dykes (Macdonald and Edge, 1970); *3* = Ilímaussaq intrusion (Gerasimovskii, 1969); *4* = Fukushinzan complex (Saito, 1950); *5* = Oslo province (Barth and Bruun, 1945); *6* = Central Tugtutŏq complex (Upton et al., 1971); *7* = Younger Granites, Nigeria (Jacobson et al., 1958; Bowden, 1966).

*[1] F decreases sharply within the layered syenites due to fluorapatite extraction (Upton, 1960).

*[2] Average alkali rhyolite has 0.12% F (Jacobson et al., 1958).

of the Oslo province, except in degassed varieties where it is located in miarolitic cavities (Dietrich et al., 1965).

Very low F contents (140 ppm average) are found in ultrametamorphic catazonal granites associated with gneissic terrains (Tauson, 1974). Biotite plagiogneisses from the Pamirs show mobilization and increasing losses of F during progressive granitization (migmatization or feldspathization) (Gavrilin et al., 1972). Quartzofeldspathic migmatite lenses and layers average about 200 ppm F compared with about 800 ppm in the surrounding gneisses. Biotite-rich borders to the lenses and layers contain 1,000—2,000 ppm F but are so rare that F has clearly been lost during migmatization.

F exhibits three trends in the more siliceous members of calc-alkaline plutonic series (Table II):

(*A*) A gentle increase.

(*B*) A decrease which generally follows an increase from granodiorite to biotite granite.

(*C*) A sharp increase into apogranites (F-rich roof-zone magmatic and metasomatized granites) which may succeed either trend *A* or *B*.

In all these trends, late-stage aplites show a marked decrease in F contents while any barren and rare-metal pegmatites successively show more elevated values.

Tauson (1967, 1974) considers that these three trends are respectively examples of closed-system fractionation, increased F degassing and re-absorption of the degassed F. The first trend occurs in abyssal batholiths or shallower bodies low in volatiles. The second — the most widely recorded trend — is typical of mesabyssal batholiths and of hypabyssal massifs with elevated

ic series (F in wt.%)

C
7
0.18
0.28*₂
0.66

al., 1973); 2 = (Gerasimovskii, h and Bruun, 1945); es, Nigeria

traction (Upton,

ocated in miarolitic

netamorphic 974). Biotite ng losses of F ation) (Gavrilin verage about gneisses. Biotite- n F but are so

lc-alkaline

nodiorite to

matic and meta-

in F contents nore elevated

spectively and re-absorption or shallower l trend — is ı elevated

TABLE II

Selected examples of the three fluorine trends (*A*, *B* and *C*) in calc-alkaline plutonic series (F in wt.%)

	A		*B*				*C*			10
	1	*2*	*3*	*4*	*5*	*6*	*7*	*8*	*9*	
Hob-Bi granodiorite		0.08	0.09	0.045						0.08
Bi granite	0.100	0.08	0.16	0.068	0.074	0.05	0.07	0.07		0.12
Mus ± Bi granite					0.046		0.12		0.16	0.11
Leucogranite	0.125	0.09	0.14	0.058		0.03		0.06		0.09
Apogranite							0.20	0.42	1.2	0.4
Aplite	0.025		0.07		0.02	0.02		0.04		0.07

1 = Susamyr batholith (Tauson, 1967); *2* = Shakhtaminsk massif (Tauson, 1967); *3* = average for 18 Soviet complexes (Kosals et al., 1973); *4* = Verkhne-Undinsk batholith (Tauson, 1967); *5* = average for Hercynian granitoids, Caucasus (Odikadze, 1971); *6* = S. Snake Range (Lee and Van Loenen, 1971); *7* = massif in E Transbaikalia (Tauson, 1974); *8* = Karlovy Vary massif (Klomínský and Absolonová, 1974); *9* = St. Austell granite (Exley, 1958); *10* = average contents from 31 series, references *1*—*8* (above), and Syritso and Chernik (1976), Dodge et al. (1968), Kosals and Mazurov (1968), Kostetskaya and Mordvinova (1968), Ivanov (1971), Groves (1972), Rozanov and Mineev (1973), Sheremet et al. (1973), Kozlov (1974), Tischendorf et al. (1974) and Zalashkova and Gerasimovskii (1974).
Bi = biotite; Hob = hornblende; Mus = muscovite.

volatile contents. Apogranites are usually hypabyssal bodies, either stocks or apical facies, of larger massifs.

Contaminated or hybridized granite series generally exhibit trend *B* (Lee and Van Loenen, 1970, 1971; Lutkov and Mogarovskiy, 1973). Lee and Van Loenen (1970) argue that the contaminating xenoliths and xenocrysts, which represent earlier contact metasomatized materials, are enriched in volatiles.

No attempt seems to have been made to explain these various trends by fractional crystallization or progressive melting models.

F shows no clear relation to SiO_2 in a limited sampling of Japanese acid igneous volcanics and plutonics (Kokubu, 1956). Column *10* of Table II averages the F trend of 31 calc-alkaline plutonic series; the gentle rise and fall of F may merely reflect the present bias towards meso- and hypabyssal massifs. Comparable averaging for gneissic and extrusive calc-alkaline series is impossible at present.

Palingenic alkalic granitoids average about 500 ppm F while further differentiation may yield granites with about 900 ppm (Tauson, 1974).

Yusupov (1970) found that granite massifs only developed chamber pegmatites with abundant rock crystal when F contents in the host granite reached 0.082—0.150%. However, massifs containing 0.156—0.540% F developed quartz and quartz—fluorite greisens in association with apical and domal parts of the massifs.

Both Shcherba (1970) and Glyuk et al. (1973) found heightened average F contents (0.18—0.30%) in ore-bearing granitoids. Glyuk et al. (1973) found that dry distillation of these granites at 1,200°C for 10 days could remove about 70% of the F leaving only about 0.07% F. However, Flinter et al. (1972) recorded that high F contents are neither indicators of nor associated with the occurrence of Sn, W, Mo or Cu mineralization in the New England complex, Australia.

F contents in glassy rhyolites and rhyodacites from W USA range from 20—4,900 ppm, with a mean close to 500 ppm (Powers, 1961; Coats et al., 1963; Griffitts and Powers, 1963). Inter-provincial differences exist with, for example, the Cascades and Shoshone areas averaging 0.04 and 0.097% F, respectively, and the Big Bend subprovince averaging 0.22%.

Noble et al. (1967) find that F contents increase from 0.07—0.08% in calc-alkaline glassy rhyolites to 0.17—0.18% in alkalic rhyolite glasses to 1.1—1.4% in pantellerites of W USA. On crystallization, these glasses lose about half of their F probably to groundwater over long periods. The percentage loss of F varies widely, being least in peralkaline groundmasses where arfvedsonite often crystallises. Some hydrated glasses also suffer F loss.

In the Gold Flat member of the Thirsty Canyon pantelleritic ignimbrite, Nevada, nonhydrated densely welded glass contains 1.1—1.4% F, hydrated welded glass has 0.88—1.14% F while welded rocks with a devitrified groundmass have only 0.44—0.62% F (Noble et al., 1967).

Shepherd (1940) showed that increasing vesicularity in obsidians from Little Glass Mountain, California, was correlated with a decrease in F values from 640 to 340 ppm.

These F losses readily explain the difference in F averages for granitic (810 ppm) and rhyolitic (480 ppm) rocks noted by Allmann and Koritnig (1972).

Regional and secular variations in granite F contents

A map showing F-rich and F-poor rhyolite provinces in W USA has been published by Coats et al. (1963). These provinces correlate fairly well with the distribution of American fluorite deposits and F levels in water supplies. Peters (1958) suggested that they may stem from geochemical anomalies which have persisted through magmatic-sedimentary recycling since the Precambrian.

However, judged on the results of Noble et al. (1967) these provincial variations in rhyolites are largely explained by variations in alkalinity. Most regional variations seem related to magma alkalinity, to lateral or vertical positioning in orogenic belts (Kovalenko, 1974) or to highly faulted provinces (Tolstoy et al., 1973), and have only been demonstrated for short geological periods.

For the Caucasus region, however, Odikadze (1971) shows that granites of four different ages and emplacement levels are all F-poor (Table III). Granitic micas and greisens of this area are also depressed in their F contents. This regional impoverishment is attributed to derivation from extremely F-poor source rocks — basement schists.

Consistent secular variations in granitic F contents, e.g. from areas of repeated granite formation, do not appear to have been pointed out. Average F levels were rather monotonous (0.08—0.12%) in Japanese granitoids of various ages (Kokubu, 1956). However, Valach (1968) considers that the F contents of magmas and volcanic gases in general, and also fluorite reserves, have all increased markedly since the end of the Precambrian.

Association of F with Sn and Li in granites

Granites with high F, Sn and Li contents are often associated with Sn—W—

TABLE III

Fluorine contents in granites and their micas from the Greater Caucasus (Odikadze, 1971)

Age	All granite types		Biotite		Muscovites	
	F(%)	number	F(%)	number	F(%)	number
Alpine	0.07	32	0.23	17	—	—
Kimmerian	0.03	7	0.21	11	—	—
Hercynian	0.08	179	0.26	30	0.26	18
Caledonian	0.028	27	0.10	16	0.12	15
Total	0.050	245	0.20	74	0.20	33

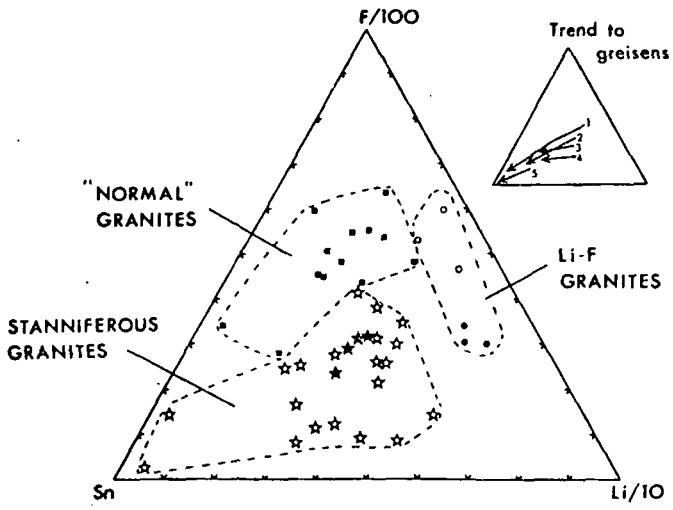

Fig. 2. Proportions of F, Li and Sn in normal, stanniferous and Li—F granites.
Full symbols: magmatic, open symbols: autometasomatized.
Data sources: (a) for normal granites: Vinogradov (1962), Tauson (1974), Bailey (unpublished compilations, 1975; (b) for stanniferous granites: Hall (1971), Burnol (1974), Gundsambuu (1974), Hesp (1974), Klomínský and Absolonová (1974), Kozlov (1974), Tauson (1974); (c) for Li—F granites: Kovalenko et al. (1973b), Gundsambuu (1974), Jarchovský (1974), Zalashkova and Gerasimovskii (1974).
Small triangle links granites to derivative greisens: *1* = Mongolia (Gundsambuu, 1974), *2* = Cornwall (Hall, 1971), *3* = Central Transbaikalia (Kozlov, 1974), *4* = E Transbaikalia (Tauson, 1974), *5* = SE Australia (Hesp, 1974).

Mo mineralization. The inter-relations of F, Sn and Li are illustrated in Fig. 2, where three main groups of granites are distinguished:

(1) Normal granites which cover the spectrum from tholeiitic, calc-alkaline to peralkaline granites, and from catazonal to epizonal environments (Tauson, 1974).

(2) Stanniferous granites where the F/(Sn + Li) ratio is lower than normal.

(3) Li—F granites, including ongonite (see below), which are relatively poor in Sn, but contain notable amounts of Ta, Rb, Cs and sometimes Be (Kovalenko, 1973, 1974).

The world-wide stanniferous granites include both magmatic and autometasomatic representatives. Typically an older, more widespread, group of intrusions with 400—800 ppm F are intruded by smaller stocks and cupolas of metasomatized leucogranite with 0.1—1.0% F. In the latter, F, Sn and Li contents show much higher dispersion, marked positive correlations with each other and with Rb, Ga and ore elements, and an increase towards the younger, more intensely altered facies (Tauson, 1974; Rub and Pavlov, 1974; Tischendorf et al., 1974; Klomínský and Absolonová, 1974). Mineralogically the younger granites are characterized by F—Li—Sn-rich micas, topaz and

cassiterite (Pälchen and Tischendorf, 1974).

Ryabchikov et al. (1974) found that partitioning of Sn into aqueous saline fluids from co-existing granitic melts was increased by an order of magnitude when F was introduced to the system and HF fugacity was buffered against topaz. Under pneumatolytic and hydrothermal conditions, Sn can be transported in the form of volatile halides and halide complexes, respectively (Hesp, 1973).

F-zoned granite intrusions

Intrusions may show F-zoning or -layering as follows:

(1) Passive concentration of F by fractional crystallization into residual roof-zone melts (Greenland and Lovering, 1966; Gundsambuu, 1974).

(2) F-rich residual granite bodies containing 0.2—0.3% F may exhibit degassed margins carrying only 0.04—0.06% F and with lowered contents of Sn, Li, Rb and Be (Kozlov, 1974).

(3) Intrusions where degassed F and associated mobile elements (Li, Sn, Be, Cs) become reconcentrated close to the roof zone and margins. The roof-zone metasomatic granites may contain up to 1.5% F (Groves, 1974; Jarchovský, 1974; Zalashkova and Gerasimovskii, 1974). The most complete expression of this metasomatic zoning is perhaps greisen, underlain by greisenized granites, microclinized and muscovitized granites, albitized granites, slightly altered two-mica granites and then unaltered biotitic granites (Ontoev, 1974).

Odikadze (1973) demonstrated slight migration of F and Cs into the contact zone of a rhyolite neck, Caucasus. Seraphim (1951) found that F contents rose sharply a few centimetres from two granite—sediment contacts.

Relation of F to level of granite emplacement

Rising granite plutons distribute their F and rare metals in mineral deposits according to a rough depth scheme. In the deeper intrusions associated with pegmatites (2—7 km) F is located notably in various micas. At higher levels (1—5 km) granite stocks are often associated with greisens carrying topaz, mica and fluorite, and with albitization occasionally cryolite. Shallow volcano-plutonic formations are associated with straightforward hydrothermal veins carrying fluorite (Beskin and Marin, 1974; Ginzburg et al., 1974; Varlamoff, 1974).

Macdonald et al. (1973) recorded F- and K-bearing aqueous solutions separating from peralkaline granite sheets in the Kûngnât Fjeld stock, SW Greenland.

For rare-metal granites, Kozlov (1974) gives the following F levels:

(1) palingenic granites associated with pegmatites	0.06—0.08%
(2) main facies of hypabyssal granites	0.08—0.12%
(3) subsurface granites, particularly apogranites	about 0.3%

TABLE IV

F-rich minerals associated with granitic materials

Name	Formula	F (wt. %)	Location
Fluorite	CaF_2	47.81—48.80	G, P, A, Gre
Cryolite*1	Na_3AlF_6	53.48—54.37	G, P, A, Gre
Fluocerite	CeF_3	19.49—28.71	P, Gre
Yttrofluorite	$(Ca,Y)(F,O)_2$	41.64—45.54	P, A, Gre
Gagarinite	$NaCaYF_6$	33.0—36.0	A
Bastnäsite	$Ce(CO_3)F$	6.23—9.94	G, P, A, Gre
Synchisite	$CeCa(CO_3)_2F$	5.04—5.82	P, A
Parisite	$Ce_2Ca(CO_3)_3F_2$	5.74—7.47	G, P
Pyrochlore	$NaCaNb_2O_6F$	2.63—4.31	G, P, A, Gre
Microlite	$(Ca,Na)_2Ta_2O_6(O,OH,F)$	0.58—8.08	P, A, Gre
Amblygonite	$LiAl(PO_4)F$	0.57—11.71	G, P, A, Gre
Apatite	$Ca_5(PO_4)_3(F,Cl,OH)$	1.35—3.77	G, P, Gre
Herderite	$Ca(BePO_4)(F, OH)$	0.87—11.32	P
Muscovite	$KAl_2(AlSi_3O_{10})(OH,F)_2$	0.02—2.95	G, P, Gre
Biotite	$K(Mg,Fe)_3(AlSi_3O_{10})(OH)_2$	0.08—3.5	G, P, A
Lepidolite	$KLi(Fe,Mg)Al(AlSi_4O_{10})(F,OH)_2$	0.62—9.19	G, P, A, Gre
Zinnwaldite*2	$KLiFe^{2+}Al(AlSi_3O_{10})(F,OH)_2$	1.28—9.15	G, P, A, Gre
Polylithionite	$KLi_2Al(Si_4O_{10})(F,OH)_2$	3.00—7.73	A
Tainiolite	$KLiMg_2(Si_4O_{10})F_2$	5.36—8.56	A
Holmquistite	$Li_2(Mg,Fe^{2+})_3(Al,Fe^{3+})_2(Si_8O_{22})(OH,F)_2$	0.14—2.55	P
Hornblende	$NaCa_2(Mg,Fe,Al)_5(Si,Al)_8O_{22}(OH,F)_2$	0.01—2.9	G
Riebeckite	$Na_2Fe_3^{2+}Fe_2^{3+}(Si_4O_{11})_2(OH,F)_2$	0.30—3.31	G, P, A
Arfvedsonite	$Na_3Fe_4^{2+}Fe^{3+}(Si_4O_{11})_2(OH,F)_2$	2.05—2.95	G
Ferrohastingsite	$NaCa_2Fe_4^{2+}(Al,Fe^{3+})(Si_6Al_2O_{22})(OH,F)_2$	0.02—1.20	G
Spodumene	$LiAl(SiO_3)_2$	0.02—0.55	G, P
Astrophyllite	$(K,Na)_3(Fe^{2+},Mn)_4TiSi_4O_{14}(OH)_2$	0.70—0.86	G, P, A
Wöhlerite	$NaCa_2(Zr,Nb)O(Si_2O_7)F$	2.80—2.98	G
Tourmaline	$Na(Mg,Fe)_3Al_6(BO_3)_3(Si_6O_{18})(OH)_4$	0.07—1.27	G, P, Gre
Sphene	$CaTiSiO_5$	0.28—1.36	G, P, A
Topaz	$Al_2SiO_4(OH,F)_2$	13.01—20.43	G, P, A, Gre
Yttrobrithiolite	$(Ce,Y)_3Ca_2(SiO_4)_3OH$	0.50—1.48	P

Information compiled mainly from Correns (1956), Kokubu (1956), Palache et al. (1957), Vlasov (1966), Deer et al. (1967) and Allmann and Koritnig (1972).

G = Granite; P = Granite pegmatite; A = Albitized riebeckite granite; Gre = Greisen.

*1 Associated with cryolite are the rare aluminofluorides: cryolithionite, ralstonite, prosopite, pachnolite, chiolite, thomsenolite, elpasolite, weberite, jarlite and gearksutite.

*2 Zinnwaldite includes the F-poor and F-rich varieties: protolithionite and cryophyllite.

Location
G, P, A, Gre
G, P, A, Gre
P, Gre
P, A, Gre
A
G, P, A, Gre
P, A
G, P
G, P, A, Gre
P, A, Gre
G, P, A, Gre
G, P, Gre
P
G, P, Gre
G, P, A
G, P, A, Gre
G, P, A, Gre
A
A
P
G
G, P, A
G
G
G, P
G, P, A
G
G, P, Gre
G, P, A
G, P, A, Gre
P

7), Vlasov (1966),

opite, pachnolite,

In general the rather incomplete evidence suggests that F contents increase in the shallower granites, and that F-bearing solutions are significantly separated and removed from their parent granite at these higher levels.

LOCATION OF F IN GRANITES

Following Correns (1956), F (1.36 Å) is located in:

(1) F-rich minerals — fluorite, apatite, etc.

(2) Replacing OH^- (1.4 Å) and O^{2-} (1.4 Å) ions in muscovite (mean 0.1—0.3% F), biotite (mean about 0.7%), hornblende (mean about 0.2%), and sphene (range 0.1—1.0%).

(3) Solid and fluid inclusions — micas in feldspars, fluid inclusions in quartz.

(4) Rock glasses — obsidians and pitchstones.

A list of F-bearing minerals, with formulae, F contents, and distribution in various granitic materials is given in Table IV.

Rock-forming minerals. In most calc-alkaline granites F is dominantly located in biotite, and to a lesser extent in hornblende and muscovite if present. Thus, biotite contributes about 50—90% of the F in granites of the central Sierra Nevada batholith, and hornblende 10—30% (Dodge et al., 1968, 1969). F ranges from 0.21—0.91% in biotite, and from 0.06—0.31% in hornblende.

Successive granite phases in the Bitu-Dzhida batholith, SW Baykalia, contain 4—12, 2—5 and 0—3% biotite. Whole-rock F contents fall from 5,800 to 1,300, to 620 ppm F, while biotite successively contains 65.5, 81.0 and 91.8% of each phase's F. The remainder occurs in sericite, apatite, sphene and tourmaline (Kosals and Mazurov, 1968).

In the homogeneous El'dzhurta biotite granite massif, Caucasus, biotite forms 7—8% of the massif, and averages 5,100 ppm F — about 38% of the massif's F. Fluorite is also present (Odikadze, 1968). A similar distribution occurs in a biotite granite from Schierke im Harz, where Koritnig (1951) calculated that 34% of the F occurred in biotite, 61% in fluorite and 5% in apatite.

In the two-mica granite (0.04—0.05% F) of the Marukh-Teberdin massif, Caucasus, biotite (0.40% F) carries 56% of the total F and muscovite (0.34% F) carries 41% (Odikadze, 1971).

The granites of the Dzhida complex, W Transbaykalia, average about 600 ppm F located in biotite (0.4—3.05% F), fluorite, sphene (0.36—0.82% F) and amphibole (0.75% F). Biotite contains 34—73% (average 59%) of all the F in five samples of the granite (Kostetskaya and Mordvinova, 1968).

It has been proposed that the F/OH ratio of micas reflects the fugacity ratio (f_{HF}/f_{H_2O}) in the co-existing fluid phase; it is also dependent on the interaction temperature and cationic ratios (Fe/Mg, Fe/Al) in the mica. Experimental results suggest that phlogopite is most effective in taking up F while the Fe-biotites are much less effective (Munoz and Eugster, 1969; Munoz and Ludington, 1974). With temperature decrease, f_{HF}/f_{H_2O} in the fluid phase and thus

F/OH in the co-existing mica also decrease. Under oxidising conditions when O may substitute for F in the biotite structure these relations may be less clear. From these experiments it is to be expected that under lower grade metamorphism or during crystallization, the F contents of biotites will fall. This is observed when biotites from granulite facies (average 0.65% F) and amphibolite facies (0.24—0.38% F) are compared (Filippov et al., 1974).

However, the same authors find that biotites in the cooler, more siliceous granites of a granite series, and with higher Fe/Mg ratios, have higher F contents (1.5% F) than early biotites (0.5%). This is a general feature. Fig. 3 indicates that biotites in:

(1) Calc-alkaline plutonic and volcanic series show a steady increase in F and F/OH.

(2) Alkali granites have distinctly higher F and generally lower OH contents.

(3) Three series, two of them clearly sub-alkaline, show a sharp decrease in F and F/OH from alkalic to calc-alkaline levels.

The biotites of the third (Kukulbei) series are unusual in that they are siderophyllites with significant Li contents and the biotites in the biotite granites are richer in F and Fe/Mg than those in the two-mica granites (Koval et al., 1972).

It may be that the experimental relation between F/OH in biotite and temperature breaks down at low T and P in the presence of significant F, H_2O and Li contents (cf. Rieder, 1971). Closed-system models may not be applicable to granites which exhibit degassing or subsequent interaction with meteoric water. Dehydration of biotites, formation under oxidising conditions, and deficiencies in the (OH, F, O) group (Foster, 1964; Rimšaite, 1967) require attention.

Marakushev and Tararin (1967) also find that the average F contents within 120 granitic biotites increase from 0.7 to 1.4%, as the Al_2O_3 values increase from 9% in phlogopite—annite biotites to 20% in biotites virtually corresponding to the eastonite—siderophyllite series.

Biotites in Central Asian granodiorites developed at the late geosynclinal stage have lower F contents (average 0.24%) than biotites in normal and leucocratic granites developed at the orogenic stage (average 1.00%), presumably under drier conditions (Filippov et al., 1974).

Stormer and Carmichael (1971) have indicated the applicability and discrepancies in using F^-—OH^- exchange in biotite and apatite as a geothermometer.

Pegmatitic biotites contain more F than co-existing muscovite, while co-existing biotites and amphiboles in Swedish granitic rocks have F contents of the same magnitude (Gillberg, 1964). Godfrey (1962), however, found that F contents in granitic biotites nearly always exceeded those in co-existing hornblende.

Haynes and Clark (1972) find that granitic biotites of N Chile contain 164—4,450 ppm F with higher levels (6,000—9,800 ppm) in biotites from porphyry Cu centres. Groves (1972) also finds high F contents in biotites of Sn mineralized granites, NE Tasmania.

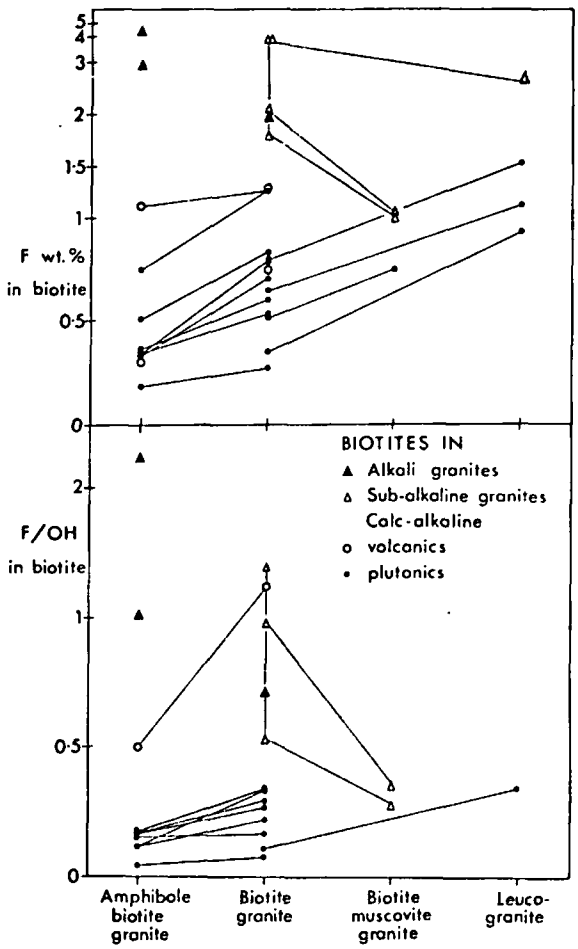

Fig. 3. Variation of F and F/OH in biotites from various granite series.
Data from: Larsen et al. (1937), Nockolds (1947), Godfrey (1962), Gillberg (1964), Deer et al. (1967), Rimšaite (1967), Tauson,(1967), Dupuy (1968), Kosals and Mazurov (1968), Dodge et al. (1969), Kostetskaya et al. (1969), Lee and Van Loenen (1970), Ivanov (1971), Stormer and Carmichael (1971), Koval et al. (1972), Sheremet et al. (1973) and Bowden and Turner (1974).

F is released during chloritization of granitic biotites; chlorites only contain 0.04—0.31% F (Godfrey, 1962).

Muscovite has average F contents which increase in the sequence: mica schist, 0.09%; granites, 0.16%; pegmatites, 0.55%; and greisen (no value given). F values in pegmatitic muscovites range from 0.14 to 1.41%, show regional variations, and generally correlate with Li values (Němec, 1969). Average F contents in different generations of muscovites in E Sayan pegmatites were: quartz—muscovite replacement stage (0.13—0.15%), quartz replacement stage (0.30%) and late alkali stage (0.08%) (Glebov et al., 1968).

The Li-micas are virtually restricted to granite pegmatites and metasomatized

granites. Experimentally it has been found that with increasing F contents and thus f_{HF} the stability of annite is lowered and that of Li–Fe micas favoured. Siderophyllite and polylithionite have an extensive stability field below 550°C at 2 kbar (Rieder, 1971). The experiments of Munoz (1971) at 2 kbar on two lepidolite end-members — polylithionite and trilithionite — suggest that, in the absence of quartz, lepidolite may appear as a liquidus phase if f_{HF} is high enough. Its usual restriction to replacement zones in pegmatites possibly reflects the presence of quartz, the low f_{HF} and the effect of other components.

Compilations of F contents in micas are presented by Foster (1960, 1964), Deer et al. (1967), Rimšaite (1967) and Allmann and Koritnig (1972).

Quartz is rarely analysed for F; the few available results from quartz in biotite granite, granite pegmatite and greisen all lie in the range 60—300 ppm (Stavrov and Bykova, 1961; Odikadze, 1971). The IR spectra of quartz crystals grown in fluoride solutions indicate that F enters as HF in complexes (Balitskiy et al., 1974).

Accessory minerals. In calc-alkaline plutonic series contents of apatite and sphene typically increase in the more calcic members (Lee and Dodge, 1964) but probably contribute less than 20% to the total F. Monazite and fluorite contents increase in the opposite direction and contents vary greatly in different regions.

In the Azov massif, SE Ukrainian shield, there is a contrast between older geosynclinal granites rich in sphene and apatite, and younger granites of the platform stage poor in these phases (Table V). The final columbite-bearing granites are rare-metal apogranites and have high contents of fluorite and topaz (Rozanov and Mineev, 1973).

Accessory minerals make a large contribution to the total F of the granites of SW England (Table VI). These granites show many magmatic characteristics but also exhibit considerable autometasomatism and recrystallization (Exley, 1958; Exley and Stone, 1964).

As F contents increase from 0.09% in an E Transbaykalia biotite granite to 0.71% in the associated metasomatic apogranite, the assemblage of F-rich accessories changes from apatite—fluorite to topaz—fluorite—apatite—microlite (Syritso and Chernik, 1967).

Granites carrying amblygonite and spodumene are typically altered leucogranites (Lyakhovich, 1965). Amblygonite granites are usually greisenized, potassic and rich in Rb, while spodumene granites are albitized and sodic. Vlasov (1966) outlines the contents of fluorite, tourmaline, bastnäsite, spodumene and amblygonite in various granite types from different regions of the Soviet Union.

Layered granites from Tigssaluk fjord, SW Greenland, probably stemming from a magma rich in F and other volatiles, contain sphene, apatite, allanite and rare zircon as early accessory phases and fluorite as a ubiquitous late mineral (Emeleus, 1963).

TABLE V

Contents of F-rich accessory minerals in granitoids of the Azov Sea region (Rozanov and Mineev, 1973)

Complex	Archaean anatectic, geosynclinal stage		Proterozoic intrusives, platform stage			
	I	II	IV	V	VIa	VIb
Mineral (ppm):						
Sphene	3,741	4,834	0.2	693	5.6	1.1
Apatite	3,662	1,332	382	507	317	61.1
Fluorite	24.3	1.0	2.8	4.1	5,091	7,696
Topaz	1.1	9.7	3.2	—	10.9	1,198
Tourmaline	11.0	—	1.4	—	34.3	6.2
Pyrochlore	—	—	0.1	2.4	1.0	1.5
Bastnäsite	0.1	170	—	9.1	861	145
Total (wt.%):	0.74	0.62	0.04	0.12	0.56	0.90
SiO_2 (wt.%)	66.3	69.0	71.9	67.5	73.8	73.8
F (wt.%)	0.03	0.08	0.06	0.06	0.26	0.58
F contribution from accessories (%)*	65	10	4	5	95	70

I = Granodiorites, plagiogranites; II = Biotite granites; IV = Amphibole—biotite granites; V = Granosyenite, VIa = Biotite leucogranites; VIb = Metasomatically altered (columbite-bearing apogranite) from VIa.
*Estimated by author.

F contents of apatites increase in the more siliceous igneous rocks (Taborszky, 1962) though this relation is less clear within the granite clan. Lee et al. (1973) find that the apatite of felsic granitoids is more than 90 mole% fluorapatite, but slightly less in the most mafic. Apatite (3.35% F) contributed about 10% of one sample's F. H_2O-free fluorapatites from the early quartz—muscovite replacement zones of E Siberian pegmatites have slightly higher F contents (2.80—3.36% F) than those from the subsequent quartz replacement zone (2.37—3.02% F) (Shmakin and Shiryayeva, 1968). Biggar (1967) studied the stability of different apatite types. The bonding of F and OH in various apatites has been investigated by IR spectrometry (Engel and Klee, 1972).

Multi-element analyses for accessory fluorite from granite do not seem to be available. Lyakhovich and Balanova (1971) found an average of 0.44% RE_2O_3 in accessory fluorite in intrusive granitoids. Yakubovich and Portnov (1967) found that post-magmatic fluorite related to alkalic rocks contains 0.*n*—*n*.0% SrO, whereas fluorite related to granitic rocks contains 0.00*n*—0.0*n*% SrO.

Magmatic tourmalines from the granites of Devon and Cornwall are richer in F (0.6—1.25%), Mn and Fe but poorer in Mg, Ca, Sr and Sn than hydrothermal tourmalines (0.33—0.6% F) (Power, 1968). On this basis the remarkable

TABLE VI

F-bearing minerals (vol.%) and F contents in SW England granites [after Exley (1958) and Exley and Stone (1964)]

Mineral	F (wt.%)	Biotite–muscovite granite	Early lithionite granite	Late lithionite granite	Fluorite granite	Amblygonite-bearing granite
Biotite	1.29*1	6.2	—	—	—	—
Muscovite	1.94*2	2.2	—	—	5.3	—
Lithionite*3	—	—	3.7	8.9	—	9.4
Secondary mica	—	—	9.2	9.2	10.8	—
Fluorite	—	0.2	0.3	1.1	1.6	—
Topaz	—	0.2	0.4	2.1	0.4	2.5
Apatite	—	tr.	0.1	0.8	0.4	tr.
Tourmaline	1.0*4	1.3	3.8	0.1	0.1	0.2
Amblygonite	—	—	—	—	—	1.7
SiO_2 (wt.%)		71.50	73.4	72.5	72.2	71.3
F (wt.%)		0.16	0.38	1.5	1.36	1.41
F contribution from accessories (%)*5		50	55	70	80	70

tr. = trace; — = not reported.
*1 Average of five biotite analyses (Exley and Stone, 1964).
*2 Average of five muscovite analyses (Hall, 1971).
*3 Structurally a zinnwaldite.
*4 Average magmatic tourmaline (Power, 1968).
*5 Estimated by author.

quartz—tourmaline dyke of Roche Rock, Cornwall, is the product of extreme fractionation rather than a completely tourmalinized granite.

Li—F granites and ongonites

Li—F-rich granites (about 0.6% F) and dyke rocks (ongonites, with up to 3.5% F) have recently been described from the South Gobi igneous belt of S Mongoliä (Kovalenko et al., 1970, 1972, 1973a, b; Kovalenko, 1973). Approaching the walls and roof of the Li—F-rich granite pluton, continued Li and F accumulation has produced the sequence of residual granites in Table VII. The plagioclase becomes more albitic, micas change to high Li—F varieties, and topaz becomes stable. There is a later development in the pluton of albitites and quartz—lepidolite greisen.

Ongonite — a topaz-bearing quartz keratophyre (sodic rhyolite) dyke rock — is the sub-volcanic analogue of the albite—lepidolite granites. It has the highest F contents (up to 3.5%) among natural granitic melts. An ongonite dyke, 1—2 m wide and over 300 m long, contained higher F contents (2.0—3.3%) in

TABLE VII

Mineralogical composition of a sequence of residual Li—F granites [after Kovalenko et al. (1970)]

Granite type	Mineral paragenesis					Plagioclase
Biotite granite	Q + K-feld	+ Plag	+ Bi	+ Mt		An_{22-25}
Albite—microcline granite	Q + K-feld	+ Plag	+ Zin	± Topaz	+ Mt	An_{5-10}
Albite—amazonite granite	Q + Amaz	+ Plag	+ Zin	+ Topaz	± Mt	Ab
Albite—lepidolite granite	Q + K-feld	+ Plag	+ Lepid	+ Topaz	± Mt	Ab

Ab = albite; Amaz = amazonite; An = anorthite; Bi = biotite; K-feld = K-feldspar; Lepid = lepidolite; Mt = magnetite; Plag = plagioclase; Q = quartz; Zin = zinnwaldite.

slightly higher pressure zones (pinches) than in the lower-pressure swells (0.8—2.0%). Those parts of the dyke saturated with F separated HF during crystallization and if trapped in closed pockets this HF reacted with the albitic components of the melt expanding the field of quartz at the expense of albite. Quartz/albite ratios for phenocrysts increase sharply from 0.1 at 30% crystallization to about 0.5 at 45% crystallization. With this degree of crystallization whole-rock F contents decreased to about 1.5% though the glassy groundmass retained its original saturation level (2.0—3.3%). Lower-pressure swells in the dyke which are undersaturated in F increase their F contents during crystallization until values in the glassy groundmasses level off at about 2.0—2.5% F. Thus, crystallization tends to homogenize the F contents of all the residual interstitial melts. Areas of the aphyric quenched margins of the dyke which possessed higher F contents, contained lower SiO_2 and Na_2O values, and unchanged K_2O and Al_2O_3 values, leading to an increase in the normative topaz, Li-mica, quartz and Na-silicate but a decrease in normative albite and orthoclase. The average of 86 dyke analyses shows: K, 2.9%; and Na, 4.1%; and in ppm: Li, 1,750; Rb, 1,950; Sr, 21; Ba, 24; Zr, 55; Hf, 10; Nb, 65; Ta, 68; Sn, 40; and Be, 26; yielding the ratios: K/Rb, 15; Zr/Hf, 5.5; and Nb/Ta, 1.0. The initial development of the ongonite melt is believed to be due to F accumulation in the apical zones of a pluton of alaskitic granite magma (originally containing 0.3—0.4% F).

Also in the Li—F granite family can be placed the lithionite—amazonite—albite apogranites (Beus et al., 1962; Syritso and Chernik, 1967; Zalashkova and Gerasimovskii, 1974). They are confined to stable areas that are reactivated by deep faults. The amazonite granites form the marginal and roof facies of biotite and leucogranite bodies, 1—10 km^2 in area. These parental granites contain 0.2—0.3% F, and through albitization (F—Na) and greisenization (F—Al) eventually yield the amazonite apogranites with 0.5—0.8% F and 0.04—0.16% Li.

Kovalenko et al. (1972) propose that the topaz-bearing, partly kaolinized, rhyolites of the Thomas Range, Utah, which contain 1.34—1.90% F and 0.08—0.43% Li (Shawe et al., 1964) should also be placed in the Li—F group.

TABLE VIII

Geochemical associations and F contents of granite pegmatites

Locality	Association	F (ppm)	Reference
F-poor:			
Spruce-Pine, North Carolina	simple pegmatite	100	Burnham (1967)
Keystone, South Dakota	simple pegmatite	1,000	Norton (1970)
S Norway	Ti—Nb—Ta—W—Be—Zr—REE	100—1,000*1	Bjørlykke (1937)
F-rich:			
Quartz Creek, Colorado	F—Ta—Nb—Li—Cs—Rb—Cl	100—6,000*1	Staatz and Trites (1955)
S Pohjanmaa, Finland	F—Li—Na—P—Be	2,000*1	Haarpala (1966)
Bernic Lake, Manitoba	F—Li—Cs—Rb—Na—P	5,000*1	Mulligan (1965)
Ivigtut, Greenland	F—Na—CO_3—S—Zr—Nb—Sn	5,000—30,000*1	Bøggild (1953)
Mt. Rosa, Colorado	F—Fe—Ti—Ce—Zr—Nb—Th	500—5,000*1	Gross and Heinrich (1966)
Miask, Urals	F—Na—Li—Be	—	Stepanov and Moleva (1962)
Volhynia, Ukraine	F—Be—B—Zr—Th—Li—S	5,400*2	Kalyuzhny (1962)
Mongolia	F—Li—Na—Ta	7,700*3	Gundsambuu (1974)
Mora Co., New Mexico	F—Li—Be—Ta—Nb—P—Bi	9,000	Jahns (1953)
Harding, New Mexico	F—Li—Be—Ta—Nb	5,500	Jahns (1953)
Harding, New Mexico	F—Li—Be—Ta—Nb	6,400	Cameron et al. (1949), Burnham and Jahns (1962)

*1 Estimated by author from mineralogical descriptions.
*2 Graphic pegmatite zone (Stavrov and Bykova, 1961).
*3 Average of eleven amazonite—albite pegmatites.

Granite pegmatites

The F contents of granite pegmatites are rarely determined because their coarse-grained and heterogeneous nature presents severe sampling problems. A brief survey of the literature suggests that variations in F contents, rather than averages, deserve more emphasis. Thus in the Quartz Creek pegmatite district, Colorado, rare Li—F-rich minerals only occur in less than 2% of the pegmatites of the district (Staatz and Trites, 1955). From mineralogical descriptions of this district, F contents have been estimated to range from 100—5,000 ppm (Table VIII). Maximum F contents probably occur in those few alkali granite pegmatites (Ivigtut, Mt. Rosa, Miask) rich in aluminofluorides such as cryolite (Na_3AlF_6) (Gross and Heinrich, 1966).

While it seems likely that complex pegmatites with rare minerals tend to have higher F contents, this is not always true. Thus the granite pegmatites of S Norway (Bjørlykke, 1937) with notable contents of Ti, Nb, Ta, W, Be, Zr and REE lack significant signs of F, Li and Sn. F is limited to minor biotite and accessory apatite, muscovites and topaz. Geochemical associations rich and lean in F in selected granite pegmatites are given in Table VIII.

On the basis of 220 major-element analyses of Soviet rare-metal granite pegmatites, Kalita et al. (1972) divided them into five groups (Table IX). Group-*I* pegmatites are typically lepidolite—albite pegmatites with exploitable contents of Li and Rb, sometimes Cs. They have the highest values and greatest variation of the (Na+K+Li)/(Ca+Mg+Fe+Ti+Mn) ratio (about 9—12). They are thus alkalic, ultra-aluminous and, according to Table IX, probably F-rich.

Heinrich (1948) has distinguished a group of N American granite pegmatites characterised by the association of fluorite with REE minerals, e.g. euxenite, monazite, allanite and gadolinite. Fluorite itself is often rich in REE.

Mineralogically, in the simple granite pegmatites F is located in biotite and accessory muscovite, apatite, fluorite or tourmaline. Complex granite pegmatites, however, can contain a number of more exotic F-rich phases (Table IV). Of the Li—F phases, both spodumene and amblygonite can occur at the magmatic and replacement stages, while lepidolite and zinnwaldite are confined to the late stages often replacing earlier micas. Holmquistite develops in marginal zones probably by interaction with basic country rocks. REE phases include bastnäsite occasionally found in alkali granite pegmatites and fluocerite generally associated with orthite and gadolinite. Microlite is a fairly abundant mineral of granitic pegmatites crystallising in miarolitic cavities or in replacement zones. Herderite is a widespread replacement product of beryl. Geochemically then F is associated with Na, Li, OH^-, CO_3^{2-}, REE, less commonly Ta, Be and PO_4^{3-}, in the phases of complex granite pegmatites.

During the crystallization of complex pegmatite magmas F concentrates in the residual melts and fluids. Only minor amounts of F are removed by early biotite, apatite and tourmaline into the outer granitic zones. Some F is precipitated in intermediate and core zones as spodumene, amblygonite,

TABLE IX

Petrochemical subdivision of Soviet rare-metal granite pegmatites with F contents [after Kalita et al. (1972)]

Group	Si/Al	F (%)			Typical mineralization
		range	average	number	
I	2.5—3.5	0.16—1.70	0.87	5	Ta—Li
II	3.5—4	0.02—0.50	0.23	4	Li—Rb—Cs—Ta—Nb—Be
III	4—5	0.02—1.35	0.15*	7	Be—Ta
IV	5—6	—	no data	—	Be—Y—Nb
V	6—7	—	no data	—	REE—Th—Y—Nb

Si/Al grouping based on 220 analyses; F results are only available for sixteen samples.
* Excluding the highest value.

muscovite or microlite but the highest contents are probably fixed in replacement pockets where later generations of these minerals may be associated with Li-micas or coloured tourmalines, topaz, cryolite, etc.

A different crystallization model if presented for the Li—F-rich Brown Derby No.1 granite pegmatite, Colorado, by Rosenberg (1972a). Following resurgent boiling, topaz crystals developed in the roof-zone aqueous fluid phase, were partly resorbed while sinking through the underlying melt, and then collected on the floor of the chamber. Alkalis and F selectively diffused into the aqueous phase which crystallised as replacement pods with lepidolite and cleavelandite. Rosenberg (1972b) synthesized topaz from the system AlF_3—Al_2O_3—SiO_2—H_2O at 350—900°C and 2 kbar pressure. In F-deficient assemblages, topaz has F/OH ratios reflecting f_{HF}/f_{H_2O} and thus temperature. Application of this tentative thermometer to the assumedly closed Colorado pegmatite yielded the reasonable temperature of 750°C.

F in fluid inclusions of granites

F contents in granitic fluid inclusions are nearly always outweighed by water, CO_2 and Cl. Even in inclusions from Sn deposits often thought to have involved F transport contents of F are only about 0.1%. Typically percentages of salts in solution are below 10 wt. % and daughter (trapped) crystals are fairly rare (Roedder, 1972).

However, dense F-rich brines occur in fluid inclusions of the Volhynia granite pegmatites, NW Ukraine, and are now described in some detail. This Precambrian pegmatite field is associated with contacts between the Korosten'skiy granites and older gabbro-norites. The pure-line pegmatites occur as dykes, veins, lenses and nests. Imperfect graphic, feldspathic and quartzose zones may surround a vugh. In some pegmatites an additional zone of leaching and recrystallization occurs (Lazarenko et al., 1968).

The grain size of host granites and the level of F both increase gradually into the pegmatites suggesting closed-system crystallization (Stavrov and Bykova, 1961). The central vughs may contain morion, smoky and clear quartz, topaz, tourmaline, fluorite, zinnwaldite, etc. (Kalyuzhny, 1962). The leaching zone may contain siderite, calcite, rutile, opal, columbite, fluorite, bertrandite and tourmaline (Lazarenko et al., 1968).

Different fluid inclusions can occur both within single crystals, within the same mineral of different zones of a pegmatite and within different pegmatites. Four groups of inclusions are here distinguished:

Group 1. Gigashvili (1969) describes primary solid—gas inclusions in quartz from a zone of silicification underlying cavities in a pegmatite. The hydromica, albite, topaz, (?) alunite and lepidolite solid phases co-exist with a gas phase (15—25 vol.%). A very high temperature of 960° C is required to melt most of the phases but phase transformation begins at 700° C. It is assumed that the host quartz crystallized from a boiling aqueous solution containing many accidental crystallites to which bubbles of steam adhered.

Group 2 multi-phase inclusions correspond to a high-temperature stage of dense brines, consisting chiefly of chlorides and fluorides of Na, K and Fe^{2+}. Of lesser importance are carbonates and hydrous carbonates of Mg and (?) Ca. These inclusions may contain up to 70—90% of crystals, but contents range down to 10% and (presumably) merge into group-3 varieties. Associated with the crystals is a vapour bubble, generally 10—20% by volume of the inclusion, and a solution.

Some of the solid phases are probably accidental crystals formed (at least partly) at pre-inclusion temperatures, but these are subordinate to genuine daughter minerals (Kalyuzhny, 1962). Among the daughter minerals with their vol. % are: halite (8—12), sylvite (0.5—3), a chloride of Al and Zn (1—2), elpasolite (K_2NaAlF_6, 2—8) and caracolite ($PbOHCl{\cdot}Na_2SO_4$, rare). Cryolite occurs as solid inclusions in topaz, as cubic crystals in some large gaseous inclusions, or rarely in liquid inclusions within topaz. 25 other crystals were distinguished but not identified or assigned an origin.

Lyakhov (1967) studied multi-phase inclusions from the earliest, central morion zone of quartz crystals. These inclusions did not completely homogenize but exploded at atmospheric pressure and temperatures of 450—500° C. The main phases are: halite (20—25%), $FeCl_2{\cdot}2H_2O$ (20—25%), mineral 4 (unnamed, 10—15%), mineral 5 (< 15%), elpasolite (< 15%), cryolite (< 10%), sylvite (< 2%) and others less than 1%. Fourteen minerals were separated but not all are found in any one inclusion. Cryolite was observed in only two inclusions and was less than 10%. It is considerably more abundant as solid inclusions in the base of the intermediate, smoky-quartz zone.

Lemmlein et al. (1962) found cryolite, quartz, muscovite and fluorite with an unknown phase in inclusions in topaz. During heating to 740° C (700° C?) under external pressure to prevent decrepitation, large amounts of the daughter

minerals (about 70 vol.%) and part of the topaz host slowly dissolved to form a hydrous glass, though much of the quartz still had not dissolved. Other inclusions were completely homogenized at 700° C forming a hydrous silicate melt.

Motorina (1967) considers the brines to be located in pseudosecondary inclusions and to contain as much as 70% dissolved salts and to homogenize at 465—550° C. Additional photographs of multi-phase Volhynia inclusions are given by Roedder (1972, plates 7, 8 and 12).

Group 3 inclusions contain more gas than those of group 2, a lower volume of crystals and fewer crystalline phases (1—4) of which halite is dominant. Appreciable Mg and Fe^{3+} are also found. Lyakhov (1967) has described such inclusions from the morion and intermediate, smoky zone of quartz. They had a pH of about 5.2 compared with 6.6 ± 0.1 in the denser brines.

Group 4 liquid—vapour inclusions contain quite dilute solutions in which Na^+, Ca^{2+}, SO_4^{2-} and HCO_3^- are detected. The pH varies from 6.4 to 8.0 and no daughter minerals occur (Kalyuzhny et al., 1967). One such inclusion contained 5.7% NaCl, 0.22% KCl, 0.06% $CaCl_2$ and 0.03% $Ca(HCO_3)_2$ (Maslova, 1961). F^- could not be detected even qualitatively. Fifteen vapour-phase analyses showed that H_2S (up to 94 vol.%) and CO_2 (up to 73 vol. %) are the dominant gases.

The minerals of the final zone of leaching and recrystallization contain fluid inclusions which show they originated over a temperature range of 100—450° C at variable pressure and solution concentration (Lazarenko et al., 1968).

It is here suggested that the sequence of inclusion types and chemistries described from groups *1—4* is the most complete expression of the evolution of the inclusions in the Volhynian pegmatites. The complete sequence is certainly not developed at every locality; more simple inclusions can be found in all zones of some pegmatites (Kalyuzhny et al., 1967).

Based on published data and photographs an attempt has been made to estimate the proportions of silicates, salts plus CO_2, and water in the various Volhynia inclusions as well as their approximate F contents (Table X, Fig. 4). Some of the values are highly speculative but the general evolution seems fairly clear. Salts and CO_2 are plotted together though their properties greatly differ in hydrous granite systems.

The main trends shown by Volhynia fluid inclusions are:

(A) The successive predominance as the temperature falls of: (i) silicate phases plus topaz and cryolite (700—960° C); (ii) very saline brines (perhaps 450—750° C); and (iii) dilute hydrothermal solutions (100—450° C).

(B) Increases in H_2O, CO_2 and carbonates, H_2S and sulphates, H_2O/Cl, Cl/F, Ca^{2+}, and Fe^{3+}/Fe^{2+}.

The evolution of fluid inclusions in the aegirine—dalyite granite (0.15% F) of Ascension Island shows similarities to the above scheme, but F contents are not available (Roedder and Coombs, 1967).

TABLE X

Estimated proportions of silicates, salts plus CO_2, and water as well as F values in Volhynia fluid inclusions

Group		Silicates	Salts + CO_2	Water	F (wt.%)
1	average	73	18	9	5
	range	60—80	15—30	1—15	—
2	average	25	42	33	2.5
	range	3—65	20—85	5—60	—
3	average	6	47	47	0.5
	range	2—10	30—55	35—70	—
4	average	1	34	65	0.1
	range	0—2	5—35	60—95	—

See text for sources of data.

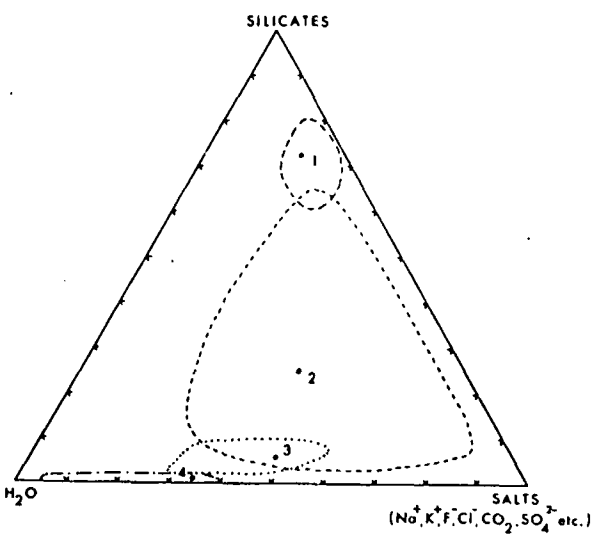

Fig. 4. Evolution of silicate—salts + CO_2—H_2O in fluid inclusions of Volhynia pegmatites. NW Ukraine.
Pressure equals about 0.3—0.4 kbar. Numbered points are estimated average compositions for inclusions in Groups *1—4*. See text for sources of data.

Rôle of F during post-magmatic alteration of granites

Under post-magmatic supercritical conditions (Shcherba, 1970) F probably combines with a variety of elements forming highly soluble complexes, e.g. $[AlF_2(H_2O)_4]^+$, $(SiF_6)^{2-}$, $NaAlF_4$, $KBeF_3$, $[Sn(OH,F)_6]^{2-}$. These F-bearing complexes may possess alkaline properties and are related to the early alkaline stage of post-magmatic alteration (600—450°C). As the temperature and/or pressure fall the early complexes decompose and F and other volatiles are

released, in some cases as a true gas phase. This marks the onset of greisenization (500—300° C). Subsequently F combines with Al and Ca in the topaz and fluorite of hydrothermal quartz veins (400—200° C).

Some alkali granite stocks and sheets have suffered post-magmatic metasomatism and conversion to F-rich albitized riebeckite granites (Nigeria, Kazakhstan, E Siberia). Albite, microcline, quartz and riebeckite are the principal minerals but common accessories are aegirine, astrophyllite, Li-micas, fluorite, cryolite, thomsenolite, amblygonite, zircon, thorite, pyrochlore and gagarinite. These granites nearly always show high contents of F — up to 1.5% — mainly due to fluorite and cryolite. Geochemically they are characterized by high F, Li, Rb, Be, Ga, REE, Zr and Nb and low K/Rb ratios (Vlasov, 1966; Archangelskaya, 1968; Bowden and Turner, 1974).

Post-magmatic greisenization nearly always takes place under the influence of SiO_2—F—Cl-rich aqueous solutions derived from granitoids [review by Shcherba (1970)]. F-bearing minerals such as sericite, muscovite, Li-micas, tourmaline, topaz and fluorite are common in greisens, while F contents typically range from 0.4—6 wt.%. The associated granitoids generally contain higher F levels (0.05—0.19%) than normal (0.08%). Where F-metasomatism is dominant during greisenization, as opposed to Cl-metasomatism, then deposition of W, Sn, Be and Li rather than Mo is more effective. The variable mobilities and stabilities of F and Cl complexes of rare metals partly explains the depositional zonation of greisen deposits.

Kalenov (1964) has described greisenization from E Mongolia where the participation of F was inconspicuous.

In the Hercynian greisens of the Greater Caucasus, quartz—muscovite greisens (0.16—0.17% F) contain less F than quartz—tourmaline greisens (0.22—0.25% F). These low F contents, and the absence of quartz—topaz and quartz—fluorite greisens are part of a regional F impoverishment (see Table III). In the Dzirul' quartz—muscovite greisen, muscovite (0.79% F) contains 97% of the total F; the remainder is in quartz (0.01% F) and accessories (Odikadze, 1971).

Compared with the ratio of F : Li : Sn in associated granites (Fig. 2), greisens show a marked increase in the proportion of Sn, even though absolute contents of F and Li are greater than in the parent granite.

Zakharchenko (1974) finds that gas—liquid inclusions from rich ore greisens contain abundant daughter minerals (up to 10—20 minerals, up to 40—70% by volume). Many daughter minerals contain F, Li, K and other rare-metal mobilizers.

Behaviour of F in volcanic gases

The HF contents of volcanic gases and fumarole condensates are generally only 0.001—0.03 vol.%, though slightly higher amounts of F can be added to altered rocks near fumaroles. In contrast the very small F_2-gas contents released by crushing granites and pitchstones may amount to several volume per cent

of the total released gases suggesting preferred retention in rocks (magmas) rather than in gases (White and Waring, 1963). SiF_4 is an insignificant gaseous species of volcanoes, and F-rich gases cannot be responsible for the removal of any significant amount of silica from magmas (Rosenberg, 1973). HCl/HF ratios in volcanic gases are nearly always greater than 10 but occasionally as low as 2. In contrast the molar Cl/F ratios for igneous rocks are usually about 0.5.

Zies (1929) estimated 320 ppm HF in fumarole gases and an annual production of $0.2 \cdot 10^6$ tons of HF and $1.25 \cdot 10^6$ tons of HCl over 77 km^2 of the Valley of Ten Thousand Smokes, Alaska, where rhyolitic ash flows were erupted. Lovering (1957) showed that rhyolitic wall rocks (0.05% F) to Fumarole No. 1 in the Valley of Ten Thousand Smokes gained F (0.08—0.21%, average 0.11%).

F contents in gases from the dacitic Showashinzan Volcano, Japan, vary widely in different fumaroles from 13 ppm at 187° C to about 300 ppm at 750° C (Sugiura et al., 1963). F/Cl ratios in the gases decrease from 0.3 to 0.05 at lower temperatures suggesting preferential removal of F compounds at these temperatures. F and F/Cl values are even lower in hot springs (0.15—12.5 mg/l, 10^{-3}—10^{-1}) and seawater (1.2 mg/l, about 10^{-4}) (Kokubu, 1956; Sugiura et al., 1963).

Relation of economic fluorides to granite

Fluorite is a relatively common minor gangue mineral in many types of ore deposits, but is of economic importance mainly in shallow-seated deposits. This agrees with increasing contents of fluorite in the hypabyssal and sub-volcanic granites (e.g. Varlamoff, 1974) and reflects the increased degassing of F and lower solubility of CaF_2 under low *P—T* conditions. Fluorite deposits commonly form in breccia pipes within vein systems indicating active corrosion and collapse during mineralization (Peters, 1958). In western U.S.A. fluorite deposits are concentrated in the eastern portion of the Cordillera (notably Colorado, New Mexico) and are spatially related to volatile-rich alkali granites and other alkalic igneous rocks.

Cryolite is associated with alkali granites showing rare-metal mineralization and develops during alkali fluoride metasomatism of deep gneissic-schist sequences or hypabyssal stocks in re-activated, consolidated terrains (Kudrin and Ginzburg, 1970). Cryolite also develops at the replacement stage of a few alkali granite pegmatites (Gross and Heinrich, 1966). The only cryolite deposit, at Ivigtut in S Greenland, amounts to about $12 \cdot 10^6$ tons and consists of units rich in siderite—cryolite, cryolite—fluorite, fluorite—topaz, siderite and quartz. It is located in the roof zone of a small, greisenized alkali granite stock (Pauly, 1974).

Bastnäsite and monazite are the main REE-bearing phases in hydrothermal carbonatite — $5 \cdot 10^6$ tons with nearly 5% REE — occurring at Mountain Pass, California. This carbonatite developed after emplacement of a highly potassic alkali granite and monzonitic rocks (Olson et al., 1954).

EXPERIMENTAL BEHAVIOUR OF F IN GRANITIC MELTS

Structural position of F in granitic melts

It has generally been accepted for granitic melts that the F^- ion (1.33 Å), because of its similarity in size to the O^{2-} ion (1.32 Å), will mainly break up some of the Si—O chains forming Si—F bonds instead, i.e. depolymerize the melt (Buerger, 1948). However with decreasing SiO_2/alkali ratios, it is known that more and more of the F becomes linked with Na, Ca and other melt modifiers rather than with Si (Kogarko et al., 1968). The proportion of F linked in Si—F and Na—F bonds in granite melts is not clear. Insecure evidence comes from experiments on the anhydrous system SiO_2—Na_2O—NaF. When the Na_2O/SiO_2 ratio of the melt is about 1 : 15 as in granites then the molar ratio of NaF/SiF_4 in the co-existing gas phase is 0.3—0.35.

When Si—F bonds in the form of Na_2SiF_6 are added to a Na_2O—SiO_2 melt, the F is released from the melt mainly as NaF. The addition of Al to this system produces aluminosilicate groups and these are known to be stable even in the presence of very high F contents (Kogarko, 1967). On crystallization, much of the F retained in femic-poor granite melts is precipitated as fluorite and F does not significantly enter quartz and feldspar. When F-rich micas and amphiboles are significantly present in granites, the F enters the structure as an additional anion, like OH^-, forming bonds with Al, Na, Ca, Mg, etc., but not with Si. The Na—F bondings found in the anhydrous vapour phase and the Na—F and Ca—F bonds precipitated in silicates are probably derived from similar bonds of the parent melt.

Kogarko and Krigman (1973) calculated from melting experiments in fluoride—silicate systems that the presence of high F contents does not lead to the depolymerization of Si—O complexes. They also calculate that in a system such as CaO—CaF_2—SiO_2 where SiF_4 is a potential product, the activity coefficient of SiO_2 increases as F (and F/O) values rise.

Release of F from granitic melts

The partition coefficient for F between vapour phase and granite magma is low, namely 0.33 or less (Burnham, 1967; Munoz and Eugster, 1969). When the pH_2O of the magmatic gas phase equals 1,000 atm., the partial pressure of HF in equilibrium with the granitic melt was found to be 2.76 atm. (Evtiukhina et al., 1967). However, during differentiation towards more siliceous granitic melts there are increasing losses of F to the vapour phase. The small but increasing degassing is known from:

(1) Anhydrous experiments where the SiO_2/Na_2O ratio was increased, and there was a simultaneous increase in the molar SiF_4/NaF ratio of the released vapours (Kogarko et al., 1968).

(2) Thermodynamic calculations for equations such as:

$$MeF + \tfrac{1}{2}\,H_2O + \tfrac{1}{2}\,SiO_2 \quad \rightleftharpoons \quad \tfrac{1}{2}\,MeSiO_3 + HF$$

where H_2O and HF are the principal gas phases and Me may be K, Na, Ca, Mg, etc. An increase in the SiO_2 content or a decrease in the contents of the less electronegative cations [K(0.8) < Na (0.9) < Ca (1.0) < Mg (1.2)] causes a considerable increase in the separation of F into the gas phase as HF (Kogarko et al., 1968). During the fractionation of peralkaline acid magmas the $(K_2O + Na_2O)/(CaO + MgO)$ ratio increases and this favours retention of F despite the increasing SiO_2 contents. However, during cooling and crystallization of this pantelleritic magma, much Na appears to be lost and the above ratio decreases. Loss of Na and peralkalinity of the melt is probably inter-connected with the loss of volatiles including F, since these elements promote each other's solubility in igneous melts.

(3) The geological observation that greisens (HF and SiO_2 metasomatised granites) are typically associated with the most siliceous granites—alaskites (Kogarko et al., 1968).

It seems likely that volatiles will migrate as bubbles rather than by diffusion through a granite melt (Burnham, 1967), though diffusion might become more important as alkali and volatile contents increase (Kogarko et al., 1974).

Influence of F on water solubility in granitic melts

Normal granite melts contain less than 0.3% F; their maximum water solubility at 1 kbar pressure is found to be of the order of 4 wt. % (Burnham and Jahns, 1958). These authors noted that water solubility was not discernibly greater for the Harding, New Mexico, granite pegmatite (Table VIII) containing appreciable F and Li. Water saturation levels increase with pressure but are still only 15—20 wt.% at 10 kbar pressure. The coexisting aqueous phase is capable of dissolving only about 10 wt.% of solutes giving a solubility gap of about 70% at these deeper crustal pressures.

The solubility of H_2O in granite melts when F and other mineralizers are greater than 1—2 wt.% is not known quantitatively, but indirect evidence comes from albitic melts and qualitative results from granite melts and co-existing vapours.

In the absence of F, an albite melt can only contain up to about 4.2 wt.% H_2O at 1 kbar and 910—923° C (Tuttle and Bowen, 1958; Burnham and Jahns, 1962). However, addition of only 0.5 wt.% NaF to the melt raises the saturation level for H_2O to 7 wt.%, while addition of more than 1 wt.% NaF increases the level in the univariant melt $[Ab_{86}(NaF)_{14}]$ to about 30 wt.% H_2O (Koster van Groos and Wyllie, 1968). The co-existing hydrous vapour contains about 10% solids, giving an immiscibility gap of about 60%. Re-connaissance experiments in the same system indicate that the immiscibility gap is sharply reduced to only 15% at 4 kbar pressure, and a continuous gradation from volatile-rich silicate melts to silicate-rich vapours should occur slightly above this pressure.

As the F content of granite—H_2O systems is increased, the co-existing vapour phase dissolves higher contents of solutes. On quenching experimental capsules,

a white crust is deposited on the capsule walls. It contains quartz and probably different Na—Al fluorides which may be hydrated (Wyllie and Tuttle, 1961). Glyuk and Anfilogov (1973a) also noted precipitates within a solution of gel-like sediment on quenching their capsules. Crystals of Na_2SiF_6, K_2SiF_6 and a powdery mixture probably of different fluorides, alumino- and silico-fluorides were identified. Slow cooling of these vapours should yield dense saline hydrothermal solutions rich in F, Si, Al and alkalis. Similar crusts and precipitates were not significant in F-free granite—H_2O runs.

Burnham (1967) found that the aqueous phase in equilibrium with a simple granite pegmatite (F, 0.01%; Li_2O, 0.01%) contained 2—3 wt.% solutes at 4 kbar pressure but only 0.5—1.0 wt.% at 2 kbar. Such dilute solutions can be matched with the fluid inclusions typically associated with granites.

According to Tuttle and Bowen (1958), granite magmas with abundant volatiles and alkali silicates may exhibit a continuum from silicate melt to hydrothermal solution. Luth and Tuttle (1969) attained complete miscibility at 5 kbar and 650° C by adding the equivalent of 11% normative Na-meta-silicate to the granite—H_2O system. While Li, HF and NaF and to some extent P promote water solubility and lower the solidus temperature, CO_2, NH_3 and HCl have the opposite effect (Wyllie and Tuttle, 1964). Thus, for a granite—H_2O system at 2.75 kbar with 5 wt.% HF the solidus is located at 603° C and for 5 wt.% Li_2O at 575° C compared with 665° C for water only.

Retention of water and other volatiles in a cooling granite melt is favoured by high pressure and a low water/salt ratio (roughly 0.96 ± 0.05). Thus a residual melt with a ratio of 2.0 is boiling from about 520—290° C during which the ratio diminishes to 1.2, when the silicate melt (41% H_2O, 35% salts, 24% silicates) ceases to exist. A melt with a ratio of 1.0 changes continuously into a solution containing 46% H_2O, 46% salts and only 8% silicates (Smith, 1963, fig. 12-31).

While water solubility is probably at a maximum (10—30 wt.% ?) in some Li—F granite melts, especially if highly peralkaline, the contents of F, H_2O and alkali silicate necessary for graduation to a hydrothermal solution must be rarely attained in the upper crust.

Despite their lower than normal temperatures, F-rich residual granite melts should be less viscous. Thus Wyllie and Tuttle (1961) noted that well formed, large albite crystals developed when HF was added to the albite—H_2O system. Convection currents should also be easily set up and maintained, and effective crystal fractionation may promote mineralogical banding (Kogarko, 1974).

Phase relations in F-rich granite systems

It is predicted that increasing the acid properties of granite melts by increased contents of F and H_2O, will raise the activity coefficient of SiO_2 (thereby expanding the quartz field) and will also raise the concentration of Fe^{2+} relative to Fe^{3+} (Kogarko, 1974).

In fact quite complex reactions are known to occur in hydrous albite and

granite melts that contain large amounts of HF (Von Platen and Winkler, 1961; Von Platen, 1965; Wyllie and Tuttle, 1961; Glyuk and Anfilogov, 1973a).

Von Platen and Winkler (1961) and von Platen (1965) show that, for normal granite, the minimum melt composition co-existing with 0.5 *M* HF solution at 2 kbar vapour pressure is richer in orthoclase and albitic plagioclase components (Q 31, Or 34, Ab 32, An 3, Ab/An 10.7) than melts only co-existing with H_2O at 2 kbar pressure (Q 39, Or 20, Ab 36, An 5, Ab/An 7.2). Melts exist to about 35° C lower in the HF-bearing system.

On cooling at 2 kbar vapour pressure, hydrous granitic melts crystallise magnetite (710° C), biotite (700° C), K-feldspar (697° C), quartz (683° C) and plagioclase (676° C) in that order over a temperature interval of 35° C. Granite melts co-existing with HF, however, crystallise quartz first at 663° C, followed by plagioclase (655° C), biotite (653° C) and K-feldspar (640° C), giving a crystallization interval of about 23° C. The changes in crystallization order are mainly of a reactive nature as the mafics and feldspars are less stable and tend to dissolve in fluoridic granite melts.

The HF-free system shows a greater degree of crystallization at a given temperature above the solidus. Crystallization begins at 710° C and the melt is 15% crystallised at 10° C above the solidus. However, crystallization in the HF-bearing system is delayed until a lower temperature (663° C) and even 10° C above the solidus only 9% of the melt has crystallized. This attests to the greater solubility of components in the fluoridic granite melt.

With increasing contents of F in the granite system the following reactions occur (Glyuk and Anfilogov, 1973a) (Fig. 5):

(*1*)	F-biotite + HF	→	topaz + quartz + KF + MgF_2 + $FeSiF_6$ + H_2O
(*2*)	orthoclase + HF	→	topaz + KF + H_2O
(*3*)	albite + HF	→	topaz + quartz + NaF + H_2O
(*4*)	topaz + HF	→	(a) quartz + Al_2F_6 + H_2O
			(b) F-bearing quartz + Al_2F_6 + H_2O
(*5a*)	quartz + HF	→	SiF_4 + H_2O
(*5b*)	F-bearing quartz + HF	→	SiF_4 + H_2O

F-rich biotite, orthoclase and albite react with HF to form topaz, quartz, and add alkali and metal fluorides to the coexisting vapour and melt. As the temperature is raised and the percentage of co-existing melt increases, these reactions can take place at lower F contents. Eventually topaz gives way to quartz containing about 0.1—0.2% F, and this quartz and normal quartz are the final minerals to dissolve. Not all the Al of the feldspars is used to make topaz; much is transferred into the co-existing vapour which quenches to give aluminofluorides and silico-aluminofluorides. Topaz is never more than 10 vol.% of all the crystalline phases. These detailed experiments confirm the earlier work at 2.75 kbar of Wyllie and Tuttle (1961), and of von Platen (1965) at 2 kbar, who both found that with increasing HF contents the quartz field expands at the expense of feldspars.

Above the liquidus at about 810° C, 1 kbar pressure, and with 1—11% F in

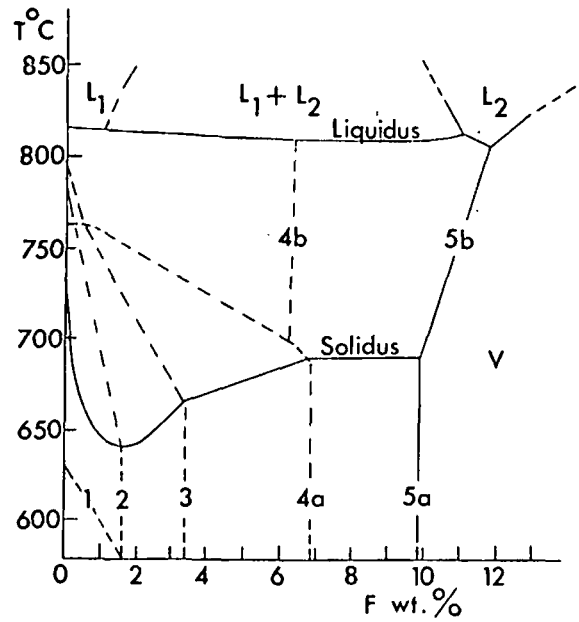

Fig. 5. T—X diagram of phase relations in the system granite—H_2O—HF at 1,000 kg/cm² (redrawn after Glyuk and Anfilogov, 1973a).
A supercritical hydrous solution co-exists with all the fields except V which is a supercritical hydrous fluoride melt. L_1 silicate melt, L_2 fluoride melt. See text for reactions *1—5b*.

the system, a silicate melt co-exists with immiscible droplets of a fluoride melt (Glyuk and Anfilogov, 1973a). The two melts coalesce when F is about 11 wt.%, or at F values from 1—11 wt.% when temperatures are considerably higher than 820° C. Similarly in the system granite—H_2O—NaF at pH_2O of 1,000 kg/cm² separate silicate and fluoride melts exist from 4.4—99 wt.% NaF in the charge (Anfilogov et al., 1973). In this system the solidus is lowered from 760° C (F-free) to 580° C (NaF = 4.4 wt.%), and only K-feldspar reacts out of the melting system. In the system granite—H_2O—KF at 1,000 kg/cm² (Glyuk and Anfilogov, 1973b), two immiscible melts exist from 1 to about 10 wt.% F and the solidus is lowered by 460° C at 1 wt.% F. In this system melts at all F contents have K-feldspar on the liquidus; quartz and an unknown phase appear on cooling but albite is always a subsolidus phase.

Exposure of granite samples to the vapour of a fluosilicate melt at 1,100—900° C and 1 atm. pressure melts the samples completely and they gradually recrystallise. Primary plagioclase is replaced by K-feldspar and fluorite. At 900—600° C granites are "baked" and feldspars acquire rims of sanidine. No alteration is observed at 600—500° C (Khetchikov et al., in Khitarov, 1967).

Cryolite stability in granite systems

Kogarko (1966) and Stormer and Carmichael (1970) have discussed the

stability of cryolite, fluorite and villiaumite (NaF) in various igneous environments.

Kogarko (1966) calculates cryolite stability in a variety of chemical reactions not necessarily close to granitic conditions, e.g.:

$$(1) \quad Na_3AlF_6 + \tfrac{3}{2}\,Me_2O \rightarrow 3\,NaF + 3\,MeF + \tfrac{1}{2}\,Al_2O_3$$

Cryolite dissociates in the presence of strong bases (K_2O, Na_2O, CaO) at 600° C, but is stable with the oxides of weaker bases (Al_2O_3, SiO_2).

$$(2) \quad Na_3AlF_6 + 2\,Na_2SiO_3 \rightarrow \tfrac{1}{2}\,NaAlSiO_4 + \tfrac{1}{2}\,NaAlSi_3O_8 + 6\,NaF$$

With higher SiO_2 concentration in the Na-silicate (e.g., $Na_2Si_2O_5$ as opposed to Na_4SiO_4) cryolite becomes stable.

(3) Na_3AlF_6 reacting with Al_2O_3-variable phases ($NaAlO_2$, nepheline, albite). Calculations indicated slight instability with $NaAlO_2$ which was confirmed by experiment, but stability with nepheline and especially with albite.

In an environment with high Ca contents the complex anion AlF_6^{3-} dissociates, Na—F and Ca—F bonds are developed, while Al forms acid complexes.

Stormer and Carmichael (1970) find for the reaction:

$$\text{acmite} + Na_3AlF_6 \rightarrow NaF + \text{magnetite} + \text{albite} + \text{quartz} + O_2$$

that reducing the activity of anorthite, acmite and silica will favour stability for cryolite rather than fluorite. However, the silica activity must not be too low or villiaumite will form instead of cryolite.

The possible role of CO_2 in the Ivigtut cryolite deposit is considered using the following reaction:

$$\text{albite} + \text{acmite} + F_2 + CO_2 \rightarrow Na_3AlF_6 + \text{siderite} + \text{quartz} + O_2$$

Fixing the activity of the other components, greater CO_2 fugacities will encourage cryolite formation. Other volatiles especially sulphur species have the same effect.

These thermodynamic equations indicate that cryolite is stable in SiO_2-volatile-rich, Ca-poor environments, in agreement with its known occurrences.

When cryolite is mixed and melted with nepheline, albite or silica, immiscibility fields are developed, generally towards higher F and Na contents (Kogarko et al., 1974). One of the liquids is essentially ionic and is rich in salt components such as Na^+, F^- and AlF_6^{3-} while the other is a polymerized silicate melt. In the laboratory the separation and concentration of the two melts can be improved by higher F contents, introduction of coalescence centres, varying the charge size and by centrifugation over long periods. The influence of H_2O on the immiscibility fields in the Na, Al, Si, O, F system is not known, but immiscibility is still likely as shown by the results for the granite—H_2O—NaF system (Glyuk and Anfilogov, 1973b).

DISCUSSION

It remains to assess the present measure of agreement between the experimental and natural behaviour of F in granitic materials, and to indicate some of the many gaps in information and understanding.

An intrinsic and important property of F in the granitic environment is its gentle degassing at late and post-magmatic stages and its relocation in nearby melts, notably roof zones and margins, or in already crystallized plutons (Fig. 6). This phenomenon partly explains the enormous range of F contents in granites. F loss is indicated by decreasing trends in some alkaline and calc-alkaline series, by its loss during crystallization of rhyolitic magmas, by reduced values in aplites and some marginal zones of plutons, and by the common occurrence of fluorite and topaz as gangue minerals in hydrothermal veins associated with granite intrusions. The gentleness of the loss is indicated by low HF and F/Cl values in volcanic gases and fluid inclusions, by vapour: magma partition coefficients, the low partial pressure of HF compared with H_2O, HCl and CO_2, and by thermodynamic calculations.

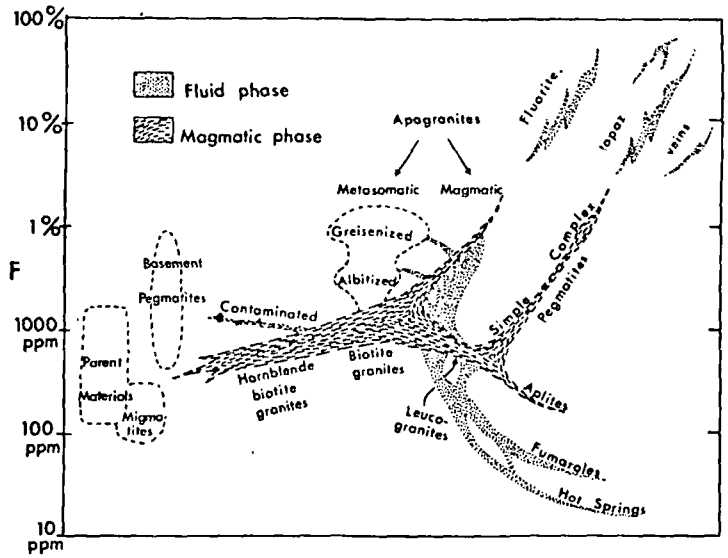

Fig. 6. Schematic flow diagram of F variation in the granite system (typically calc-alkaline plutonic).
Degrees of degassing and re-absorption are highly variable in nature while absolute F contents depend on alkalinity, level of emplacement and may vary regionally. The magmatic phase may evolve to either the more mafic or less mafic end members under progressive melting, hybridism or crystallization.

The resorption of F in granite melts seems related to a particular magma-tectonic regime and evolution. Parental melts tend to be alkalic (sometimes peralkaline), with $Na/K > 1$, and with relatively high F levels (0.1—0.3%), but these features are far from universal. After emplacement of this magma

in small epizonal plutons, differential degassing of CO_2, HCl and later H_2O concentrates the more soluble F. However slight degassing of F, probably in gas bubbles with about 0.1 vol.% HF, will steadily transfer F to the higher levels of the magma body where most of it will be resorbed. When the parent magma is alkalic a small percentage loss of F is significant in absolute terms, while the high alkali contents will promote resorption of the F. During crystallization, especially if the growing F contents induce quartz and feldspars to crystallize early rather than biotite, F will be concentrated in residual and interstitial melts. With a high degree of crystallization F may become saturated in the interstitial melt so that considerable volumes of F are released by further crystallization. During late- and post-magmatic activity Na is lost from peralkaline melts and Na and F will promote each other's resorption in any nearby residual melts. Small plutons are likely to show marked variations in temperature and degree of crystallization, so that the post-magmatic stage (involving Na and F redistribution) in one part of the pluton may be coeval with a late-magmatic stage elsewhere (involving Na and F uptake). Variable degrees of crystallization are compatible with chilled margins and roofs which can seal in the magma column. In addition the increasing F (and probably Li) contents increasingly delay the completion of crystallization in the residual magmas to lower temperatures (36—110°C according to different authors), so that these residual magmas still exist when F-poorer parts of the intrusion have entered the post-magmatic stage. Depth of magma emplacement is critical since at higher pressures degassing of F is minimal while at shallower levels F escapes very readily from plutons which themselves become rapidly solidified.

The saturation limit for F introduced as HF in true granite melts is about 9—11 wt.% at 1,000 kg/cm^2, but glassy ongonite dykes show saturation close to 2.5% F while their fully crystallised plutonic analogues contain only 0.6% F. Addition of alkali fluorides to hydrous granite melts at 1,000 kg/cm^2 indicates that high F (about 10 wt.%), and Na or K values, can be retained in a granite melt if liquation is ineffective. Such alkali fluoridic melts have not been found in nature. Enhanced Na and F contents should appear as cryolite and in this environment the instability of K-feldspar may generate and release K—F-rich solutions. In fact cryolite develops at post-magmatic stages during albitization or pegmatite replacement. This agrees with the formation of aluminofluorides during crystallization of solute-rich vapours which co-exist with F-rich granite melts.

Kovalenko et al. (1970) pointed out that the petrology of ongonite and Li—F granites is compatible with experimental features of F-rich granite systems. Thus the granitic assemblage of Na-rich and K-rich feldspars, Li-micas, topaz and quartz is known to be stable to lower than normal temperatures. The quartz and topaz phenocrysts of ongonite, and its high quartz/albite phenocryst ratios, agree with experimental phase relations. The lowest temperature melt in the granite—H_2O—HF system at 1,000 kg/cm^2 contains about 2.5 wt.% F as does ongonite. Typical of highly fractionated alkali acid magmas, normative Na silicate increases along with F and there are high levels of Li, Sn and Be but very low Sr and Ba.

Contents of F and other salt components in experimental fluids co-existing with "normal" granite are very low and match those of fluid inclusions in most granite materials. Experiments on F-rich granite, however, reveal high F contents in co-existing fluids; natural analogues may occur in fluid inclusions from Volhynian pegmatites and rich ore greisens. These inclusions may exhibit the continuum between granite melt and hydrothermal solution long predicted by experimentalists.

The close geochemical correlation between Sn, Li and F in most granites, autometasomatic derivatives (Fig. 2), and granitic micas, agrees with the significant levels of F and Li in fluid inclusions of rich ore greisens which often carry cassiterite and the known ability of F-rich solutions to partition and transport Sn. F and Li are highly soluble in experimental melts, are combined in the spodumene, amblygonite and Li-micas of Li-rich pegmatites, and show parallel losses from degassed plutons or pluton margins.

Future research should be aimed at better estimates of F losses during the magmatic, crystallization and post-crystallization stages of granites. Are the impressive F gains by roof-zone greisens in fact only a small percentage of the original F tonnage of the complete parent pluton? Knowing the chemistry and mineralogy of a granite or partly crystallised rhyolite can we reconstruct pre-crystallization F contents? Are other elements (Sn, Li, Rb, Cs, Be, Ga, W) always degassed along with F? Are F losses during catazonal granitization dispersed regionally or rapidly attracted to incipient melt areas? F contouring of plutons of different sizes and emplacement levels may tell about their degassing history.

There is virtually no data for F from tholeiitic acid igneous series, charnockites, trondhjemites and from many gneisses and migmatites. F balances are absent for these rocks, and for alkali granites and pegmatites. Analyses of quartz and feldspar, before and after leaching experiments, are minimal. Modal analyses of sparse, but probably widespread, F-rich accessories, and controls on their formation are hardly available. Partition coefficients for F and H_2O between micas, amphiboles and co-existing melts during fractional crystallization and melting should be sought in nature and by experiment.

F levels exhaled by rhyolitic volcanoes of varying silica content and alkalinity and in ash flows, pumice and lava erupted on land or under water remain unchecked.

Experiments on granite—F systems point to immiscibility phenomena, melts with abnormally high F, Na or K contents, and the presence of F-rich quartz — all features not yet found in nature.

The granite family, of course, derives from and disintegrates to other rock types and forms only a small, albeit significant, part of the F cycle.

ACKNOWLEDGEMENTS

Professor H. Pauly introduced the author to the problems of fluorine geochemistry and his continued encouragement is much appreciated. Excellent

comments were kindly made on an earlier draft of this paper by Drs. L.N. Kogarko, I.D. Ryabchikov and R.G. Platt. My main debt is acknowledged by the reference list.

REFERENCES

Allmann, R. and Koritnig, S., 1972. Fluorine. In: K.H. Wedepohl (Editor), Handbook of Geochemistry, Vol. II/1, Springer, Berlin, Ch. 9.

Anfilogov, V.N., Glyuk, D.S. and Trufanova, L.G., 1973. Phase relations in interaction between granite and sodium fluoride at water vapour pressure of 1000 kg/cm². Geochem. Int., 10: 30—33.

Archangelskaya, V.V., 1968. Tantal—niobium ores in ancient metasomatic rocks of E. Siberia. Geol. Rudn. Mestorozhd., 5: 29—40 (in Russian).

Bailey, D.K. and MacDonald, R., 1975. Fluorine and chlorine in peralkaline liquids and the need for magma generation in an open system. Mineral. Soc. Bull., 27: 3—4.

Balitskiy, V.S., Makhina, I.B. and Tsinober, L.I., 1974. Fluorine in synthetic quartz crystals. Geochem. Int., 11:-465.

Barth, T.F.W. and Bruun, B., 1945. Fluorine in the Oslo petrographic province. Skr. Nor. Vidensk.-Akad. Oslo, I, Mat.-Naturvidensk. Kl., 8: 1—12.

Beskin, S.M. and Marin, Yu.B., 1974. Types of rare-metal deposits of granite formations. In: M. Štemprok (Editor), Metallization Associated with Acid Magmatism, Vol. 1, Geological Survey, Prague, pp. 367—371.

Beus, A.A., Severov, E.A., Sitnin, A.A. and Subbotin, K.D., 1962. Albitized and greisenized granites (apogranites). Nauka, Moscow (in Russian).

Biggar, G.M., 1967. Apatite compositions and liquidus phase relationships on the join $Ca(OH)_2$—CaF_2—$Ca_3(PO_4)_2$—H_2O from 250 to 4000 bars. Mineral. Mag., 36: 539—564.

Bjørlykke, H., 1937. The granite pegmatites of southern Norway. Am. Mineral., 22: 241—267.

Bøggild, O.B., 1953. The mineralogy of Greenland. Medd. Grønl., 149(3): 1—442.

Bowden, P., 1966. Lithium in Younger Granites of Northern Nigeria. Geochim. Cosmochim. Acta, 30: 555—564.

Bowden, P., 1974. Oversaturated alkaline rocks: granites, pantellerites and comendites. In: H. Sørensen (Editor), The Alkaline Rocks, Wiley, London, pp. 109—123.

Bowden, P. and Turner, D.C., 1974. Peralkaline and associated ring-complexes in the Nigeria-Niger province, West Africa. In: H. Sørensen (Editor), The Alkaline Rocks, Wiley, London, pp. 330—351.

Bowden, P. and Whitley, J.E., 1974. Rare-earth patterns in peralkaline and associated granites. Lithos, 7: 15—21.

Buerger, M.J., 1948. The structural nature of the mineraliser action of fluorine and hydroxyl. Am. Mineral., 33: 744—747.

Burnham, C.W., 1967. Hydrothermal fluids at the magmatic stage. In: H.L. Barnes (Editor), Geochemistry of Hydrothermal Ore Deposits, Holt, Rinehart and Winston, New York, N.Y., pp. 34—76.

Burnham, C.W. and Jahns, R.H., 1958. Experimental studies of pegmatite genesis: the solubility of water in silicate melts. Bull. Geol. Soc. Am., 69: 1544—1545 (abstract).

Burnham, C.W. and Jahns, R.H., 1962. A method for determining the solubility of water in silicate melts. Am. J. Sci., 260: 721—745.

Burnol, L., 1974. Association des caractéristiques et l'évolution pétrographiques et géochimiques des leucogranites de la partie nord-ouest du Massif central français avec les différents types de concentration en tungstène, béryllium, lithium, étain et niobium-tantale. In: M. Štemprok (Editor), Metallization Associated with Acid Magmatism, Vol. 1, Geological Survey, Prague, pp. 237—248.

Cameron, E.N., Jahns, R.H., McNair, A.H. and Page, L.R., 1949. Internal structure of granitic pegmatites. Econ. Geol. 2: 1—115 (monography).

Coats, R.R., Goss, W.D. and Rader, L.F., 1963. Distribution of fluorine in unaltered silicic volcanic rocks of the western conterminous United States. Econ. Geol., 58: 941—951.
Correns, C.W., 1956. Geochemistry of the halogens. Phys. Chem. Earth, 1: 181—233.
Deer, W.A., Howie, R.A. and Zussman, J., 1967. Rock-Forming Minerals, Vols. I—V. Longmans, London.
Dietrich, R.V., Heier, K.S. and Taylor, S.R., 1965. Studies on the igneous rock complex of the Oslo region, XX, Petrology and geochemistry of ekerite. Skr. Nor. Videnskak.-Akad. Oslo, I, Mat.-Naturvidensk., Kl., Ny Ser., 19, 31 pp.
Dodge, F.C.W., Papike, J.J. and Mays, R.E., 1968. Hornblendes from granitic rocks of the central Sierra Nevada batholith, California, J. Petrol., 9: 378—410.
Dodge, F.C.W., Smith, V.C. and Mays, R.E., 1969. Biotites from granitic rocks of the central Sierra Nevada batholith, California, J. Petrol., 10: 250—271.
Dupuy, C., 1968. Composition chimique des biotites de la granodiorite du Monte Capanne (Ile d'Elbe) et des ignimbrites de Toscane (Italie). Sci. Terre, 13: 209—231.
Emeleus, C.H., 1963. Structural and petrographic observations on layered granites from southern Greenland. Mineral. Soc. Am., Spec. Pap., 1: 22—29.
Engel, G. and Klee, W.E., 1972. Infrared spectra of the hydroxyl ions in various apatites. J. Solid State Chem., 5: 28—34.
Evtiukhina, I.A., Kogarko, L.N., Kunin, L.L., Malkin, V.I. and Rudchenko, L.N., 1967. Acid—base properties of some alumino-silicate melts, simplified analogues of natural rocks. Dokl. Akad. Nauk, S.S.S.R., 175: 1369—1371 (in Russian).
Exley, C.S., 1958. Magmatic differentiation and alteration in the St. Austell granite. Q.J. Geol.Soc., 114: 197—230.
Exley, C.S. and Stone, M., 1964. The granitic rocks of south-west England. In: K.F.G. Hosking and G.J. Shrimpton (Editors), Present Views of Some Aspects of the Geology of Cornwall and Devon, R. Geol. Soc. Cornwall, Penzance, pp. 131—184.
Filippov, L.V., Savimova, Ye.N., Kapitonova, T.A. and Andreyeva, T.P., 1974. Fluorine in Mg—Fe micas from granitoids of various magmatic formations in the folded belt of Central Asia. Geochem. Int., 11: 185—194.
Fleischer, M. and Robinson, W.O., 1963. Some problems of the geochemistry of fluorine. In: D.M. Shaw (Editor), Studies in Analytical Geochemistry, University of Toronto Press, Toronto, Ont., pp. 58—75.
Flinter, B.H., Hesp, W.R. and Rigby, D., 1972. Selected geochemical, mineralogical and petrological features of granitoids of the New England complex, Australia, and their relation to Sn, W, Mo and Cu mineralization. Econ. Geol., 67: 445—457.
Foster, M.D., 1960. Interpretation of the composition of lithium micas. U.S. Geol. Surv. Prof. Pap., 354-E: 115—147.
Foster, M.D., 1964. Water content of micas and chlorites. U.S. Geol. Surv., Prof. Pap., 474-F: F1—F15.
Gavrilin, R.D., Agafonnikova, L.S. and Savinova, E.N., 1972. Behaviour of fluorine in the initial stages of granitization. Geochem. Int., 9: 180—185.
Gerasimovskii, V.I., 1969. Geochemistry of the Ilimaussaq Alkaline Massif. Nauka, Moscow (in Russian).
Gigashvili, G.M., 1969. Primary solid—gas inclusions in quartz from Volhynian pegmatites. L'vov Gos. Univ. Mineral. Sb., 24(3): 343—347 (in Russian).
Gillberg, M., 1964. Halogens and hydroxyl contents of micas and amphiboles in Swedish granitic rocks. Geochim. Cosmochim. Acta, 28: 495—516.
Ginzburg, A.I., Kupriyanova, I.I. and Fel'dman, L.G., 1974. A model for the geological-geochemical system "granite intrusive—rare-metal mineralization". In: M. Štemprok (Editor), Metallization Associated with Acid Magmatism, Vol. 1, Geological Survey, Prague, pp. 95—98.
Glebov, M.P., Legeydo, V.A., Rybakova, M.M. and Shiryayeva, V.A., 1968. Composition of muscovite from pegmatites of East Sayan formed under conditions of varying alkalinity. Geochem. Int., 5: 1016—1022.
Glyuk, D.S. and Anfilogov, V.N., 1973a. Phase equilibria in the system granite—H_2O—HF at a pressure of 1000 kg/cm². Geokhimiya, 1973(3): 434—438 (in Russian).

Glyuk, D.S. and Anfilogov, V.N., 1973b. Phase equilibria in the system granite—H_2O—KF at water vapour pressures of 1000 kg/cm². Akad. Nauk S.S.S.R., Dokl., 210: 938—940 (in Russian).

Glyuk, D.S., Kozlov, V.D., Svadkovskaya, L.N. and Legeydo, V.A., 1973. Determination of the forms of occurrence of fluorine in granitic rocks of the Ingodinsk stock, southern Transbaikalia, by distilling off from the melt. Geokhimiya, 1973(2): 309—310 (in Russian).

Godfrey, J.D., 1962. The deuterium content of hydrous minerals from the East-Central Sierra Nevada and Yosemite National Park. Geochim. Cosmochim. Acta, 26: 1215—1245.

Greenland, L. and Lovering, J.F., 1966. Fractionation of fluorine, chlorine and other trace elements during differentiation of a tholeiitic magma. Geochim. Cosmochim. Acta, 30: 963—982.

Griffitts, W.R. and Powers, H.A., 1963. Beryllium and fluorine content of some silicic volcanic glasses from western United States. U.S. Geol. Surv., Prof. Pap., 475-B: B18—B19.

Gross, E.B. and Heinrich, E.W., 1966. Petrology and mineralogy of the Mount Rosa area, El Paso and Teller counties, Colorado, II. Pegmatites. Am. Mineral., 51: 299—323.

Groves, D.I., 1972. The geochemical evolution of tin-bearing granites in the Blue Tier batholith, Tasmania. Econ. Geol., 67: 445—457.

Groves, D.I., 1974. Geochemical variation within tin-bearing granites, Blue Tier Batholith, NE Tasmania. In: M. Štemprok (Editor), Metallization Associated with Acid Magmatism, Vol. 1, Geological Survey, Prague, pp. 154—158.

Gundsambuu, Ts., 1974. Genetic relationship between the tin—tungsten deposits and granitic magmatism of Mongolia. In: M. Štemprok (Editor), Metallization Associated with Acid Magmatism, Vol. 1, Geological Survey, Prague, pp. 99—103.

Haarpala, I., 1966. On the granitic pegmatites in the Peräseinäjoki—Alavus area, south Pohjanmaa, Finland. Bull. Comm. Géol. Finl., 224: 1—98.

Hall, A., 1971. Greisenisation in the granite of Cligga Head, Cornwall. Proc. Geol. Assoc., 82: 209—230.

Haynes, S.J. and Clark, A.H., 1972. Distribution of chlorine and fluorine in granitoid rocks and associated ore deposits, northern Chile, Geol. Soc. Am., Abstr. (1972 Annu. Meet.), 4(7): 531.

Heinrich, E.W., 1948. Fluorite — rare earth mineral pegmatites of Chaffee and Fremont counties, Colorado. Am. Mineral., 33: 64—75.

Hesp, W.R., 1973. Transport of tin in acid igneous rocks. Věstn. Ústřed. Ústavu Geol., 48: 197—205

Hesp, W.R., 1974. Geochemical features of Sn—Ta—Nb mineralization associated with granitic rocks in south-eastern Australia. In: M. Štemprok (Editor), Metallization Associated with Acid Magmatism, Vol. 1, Geological Survey, Prague, pp. 170—180.

Ivanov, V.S., 1971. Composition of biotite in granitoids, as influenced by temperature and chemical activity of potassium. Int. Geol. Rev., 13: 649—657.

Jacobson, R.R.E., Macleod, W.N. and Black, R., 1958. Ring-complexes in the Younger Granite Province of northern Nigeria. Mem. Geol. Soc. London, 1: 1—72.

Jahns, R.H., 1953. The genesis of pegmatites, II. Quantitative analysis of lithium-bearing pegmatite, Mora County, New Mexico. Am. Mineral., 38: 1078—1112.

Jarchovský, T., 1974. Geochemical characteristic of lithium granite from Krásno (Slavkovský les Mts.). In: M. Štemprok (Editor), Metallization Associated with Acid Magmatism, Vol. 1, Geological Survey, Prague, pp. 181—188.

Kalenov, A.D., 1964. Greisens of eastern Mongolia and some features of their origin. Int. Geol. Rev., 6: 119—128.

Kalita, A.P., Ayderdzis, D.Ya., Melent'yev, G.B., Filippova, Yu.I. and Bol'shakova, T.N., 1972. Comparative petrochemical analysis of rare metal granite pegmatites. Geochem. Int., 9: 558—566.

Kalyuzhny, V.A., 1962. The study of the composition of captive minerals in polyphase inclusions: L'vov. Int. Geol. Rev., 4: 127—138.
Kalyuzhny, V.A., Lyakhov, Yu.V., Gryn'kiv, Z.I., Kovalishin, Z.I. and Voznyak, D.K., 1967. Age relationship and the composition of gas—liquid inclusions in quartz from the Volynian pegmatites. Geochem. Int., 4: 626—633.
Khitarov, N.I., 1967. Report on new experimental work in the field of deep-seated processes. Geochem. Int., 4: 907—920.
Klominský, J. and Absolonová, E., 1974. Geochemistry of the Karlovy Vary granite massif (Czechoslovakia). In: M. Štemprok (Editor), Metallization Associated with Acid Magmatism, Vol. 1, Geological Survey, Prague, pp. 189—196.
Kogarko, L.N., 1966. Physico-chemical analysis of cryolite paragenesis. Geokhimiya, 1966(11): 1300—1310 (in Russian).
Kogarko, L.N., 1967. Immiscibility region in the melts containing Si, Al, Na, O and F. Dokl. Akad. Nauk S.S.S.R., 176(4): 918—920.
Kogarko, L.N., 1974. Role of volatiles. In: H. Sørensen (Editor), The Alkaline Rocks, Wiley, London, pp. 474—487.
Kogarko, L.N. and Krigman, L.D., 1973. Structural position of fluorine in silicate melts, based on melting diagram data. Geokhimiya, 1973(1): 49—56.
Kogarko, L.N., Krigman, L.D. and Sharudilo, N.S., 1968. Experimental investigations of the effect of alkalinity of silicate melts on the separation of fluorine into the gas phase. Geochem. Int., 5: 782—790.
Kogarko, L.N., Ryabchikov, I.D. and Sørensen, H., 1974. Liquid fractionation. In: H. Sørensen (Editor), The Alkaline Rocks, Wiley, London, pp. 474—487.
Kokubu, N., 1956. Fluorine in rocks. Mem. Fac. Sci., Kyushu Univ., Ser. C2, 3: 1—95.
Koritnig, S., 1951. Ein Beitrag zur Geochemie des Fluor. Geochim. Cosmochim. Acta, 1: 89—116.
Kosals, Ya.K. and Mazurov, M.P., 1968. Behaviour of the rare alkalis, boron, fluorine, and beryllium during the emplacement of the Bitu-Dzhida granitic batholith, southwest Baykalia. Geochem. Int., 5: 1024—1034.
Kosals, Ya.A., Nedashkovskiy, P.G., Petrov, L.L. and Serykh, V.I., 1973. Beryllium distribution in granitoid plagioclase. Geochem. Int., 10: 753—767.
Koster van Groos, A.F. and Wyllie, P.J., 1968. Melting relationships in the system $NaAlSi_3O_8 - NaF - H_2O$ to 4 kilobars pressure. J. Geol., 76: 50—70.
Kostetskaya, Ye.V. and Mordvinova, V.I., 1968. Distribution of fluorine in the minerals of granitoids of the Dzhida complex, west Transbaykalia. Geochem. Int., 5: 519—524.
Kostetskaya, E.V., Petrov, L.L., Petrova, Z.I. and Mordvinova, V.I., 1969. Distribution of beryllium and fluorine and correlation between their contents in the minerals and rocks of the Dzhida Paleozoic granitoid complex. Geochem. Int., 6: 72—79.
Koval, P.V., Kuz'min, M.I., Antipin, V.S., Zakhanov, M.N., Znamenskiy, Ye.B., Gormasheva, G.S. and Yuchenko, S.A., 1972. Composition of biotite from granitoids in east Transbaykalia. Geochem. Int., 9: 656—668.
Kovalenko, V.I., 1973. Distribution of fluorine in a topaz-bearing quartz keratophyre (ongonite) and solubility of fluorine in granitic melts. Geochem. Int., 10: 41—49.
Kovalenko, V.I., 1974. On the genesis of rare-metal granites and their mineralization. In: M. Štemprok (Editor), Metallization Associated with Acid Magmatism, Vol. 1, Geological Survey, Prague, pp. 197—200.
Kovalenko, V.I., Kuz'min, M.I. and Letnikov, F.A., 1970. Magmatic origin of lithium- and fluorine-bearing rare-metal granite. Dokl. Acad. Sci., U.S.S.R., Earth Sci. Sect., 190: 189—191.
Kovalenko, V.I., Fin'ko, V.I., Letnikov, F.A. and Kuzmin, M.I., 1972. Certain effusive and subvolcanoc rocks with relatively high concentrations of rare elements. Int. Geol. Rev., 14: 599—608.

Kovalenko, V.I., Kuzmin, M.I., Pavlenko, A.C. and Perfiliev, R.S., 1973a. The South Gobi belt of rare-metal alkalic rocks of the Mongolian Peoples Republic and its structural setting. Dokl. Akad. Nauk S.S.S.R., 210 (4): 911—914.

Kovalenko, V.I., Kuzmin, M.I., Antipin, V.S., Petrov, L.L., Legeydo, V.A., Abramova, V.D., Tsikhanskiy, V.D., Koval, L.P. and Nikolaev, D.Kh., 1973b. Behaviour of rare elements in the process of crystallization of Li—F—quartz keratophyres (ongonites). Geokhimiya, 1973(8): 1242—1245.

Kozlov, V.D., 1974. The sequence of phases and facies in the massifs of rare-metal granites in Transbaikalia and the problem of their ore-bearing capacity. In: M. Štemprok (Editor), Metallization Associated with Acid Magmatism, Vol. 1, Geological Survey, Prague, pp. 201—205.

Kudrin, V.S. and Ginzburg, A.I., 1970. Cryolite deposits in metasomatic granitoids. Bull. Mosc. Nat. Soc. New Ser., Vol. 75, Geol. Sect., 45(3): 144.

Larsen, E.S., Irving, J., Gonyer, F.A. and Larsen, 3rd, E.S., 1937. Petrologic results of a study of the minerals from the Tertiary volcanic rocks of the San Juan region, Colorado, Am. Mineral., 22: 889—905.

Lazarenko, Ye.K., Matkovskiy, O.I., Pavlishin, V.I. and Sorokin, Yu.G., 1968. New data on the mineralogy of the Volynia pegmatites. Dokl. Acad. Sci., U.S.S.R., Earth Sci. Sect., 176: 37—39.

Lee, D.E. and Dodge, F.C.W., 1964. Accessory minerals in some granitoid rocks in California and Nevada as a function of calcium content. Am. Mineral., 49: 1660—1669.

Lee, D.E. and Van Loenen, R.E., 1970. Biotites from hybrid granitoid rocks of the southern Snake Range, Nevada. U.S. Geol. Surv., Prof. Pap., 700-D: D196—D206.

Lee, D.E. and Van Loenen, R.E,, 1971. Hybrid granitoid rocks of the southern Snake Range, Nevada. U.S. Geol. Surv., Prof. Pap., 668, 48 pp.

Lee, D.E., Van Loenen, R.E. and Mays, R.E., 1973. Accessory apatite from hybrid granitoid rocks of the southern Snake Range, Nevada. U.S. Geol. Surv., J. Res., 1: 89—98.

Lemmlein, G.G., Kliya, M.O. and Ostrovskii, I.A., 1962. The conditions for the formation of minerals in pegmatites according to data on primary inclusions in topaz. Dokl. Akad. Nauk S.S.S.R., 7(1): 4—6.

Lovering, T.S., 1957. Halogen-acid alteration of ash at Fumarole No. 1, Valley of Ten Thousand Smokes, Alaska. Bull. Geol. Soc. Am., 68: 1585—1604.

Luth, W.C. and Tuttle, O.F., 1969. The hydrous vapor phase in equilibrium with granite and granite magmas. Geol. Soc. Am., Mem., 115: 513—548.

Lutkov, V.S. and Mogarovskiy, V.V., 1973. Geochemistry of hybridism in granitoids (illustrated by the Pamirs). Geochem. Int., 10: 1199—1208.

Lyakhov, Yu.V., 1967. Mineral composition of multiphase inclusions in morions from Volynian pegmatites. Geochem. Int., 4: 618—625.

Lyakhovich, V.V., 1965. Petrographic and mineralogical features of amblygonite- and spodumene-carrying granites. Int. Geol. Rev., 7: 157—169.

Lyakhovich, V.V. and Balanova, T.T., 1971. Mean contents and compositions of rare earths in the accessory minerals of granitoids. Geokhimiya, 1971(2): 131—143.

Macdonald, R. and Edge, R.A., 1970. Trace element distribution in alkaline dykes from the Tugtutǒq region, south Greenland. Bull. Geol. Soc. Den., 20: 38—58.

Macdonald, R., Upton, B.G.J. and Thomas, J.E., 1973. Potassium- and fluorine-rich hydrous phase coexisting with peralkaline granite in south Greenland. Earth Planet. Sci. Lett., 18: 217—222.

Marakushev, A.A. and Tararin, I.A., 1967. Mineralogical criteria of alkalinity of granitoids. Int. Geol. Rev., 9: 78—91.

Maslova, I.N., 1961. Ultramicrochemical investigation of compositions of the liquid and vapour phases in two-phase inclusions in quartz from Volynia. Geochemistry, 2: 190—195.

Motorina, I.N., 1967. Multiphase inclusions in topazes from the pegmatites of Volyn'. Dokl. Acad. Sci., U.S.S.R., Earth Sci. Sect., 175: 135—137.

Mulligan, R., 1965. Geology of Canadium lithium deposits. Geol. Surv. Can., Econ. Geol. Rep., 21, 131 pp.
Munoz, J.L., 1971. Hydrothermal stability relations of synthetic lepidolite. Am. Mineral., 56: 2069—2087.
Munoz, J.L. and Eugster, H.P., 1969. Experimental control of fluorine reactions in hydrothermal systems. Am. Mineral., 54: 943—959.
Munoz, J.L. and Ludington, S.D., 1974. Fluoride—hydroxyl exchange in biotite. Am. J. Sci., 274: 396—413.
Němec, D., 1969. Fluorine in pegmatitic muscovites. Geochem. Int., 6: 58—68.
Noble, D.C., Smith, V.C. and Peck, L.C., 1967. Loss of halogens from crystallised and glassy silicic volcanic rocks. Geochim. Cosmochim. Acta, 31: 215—223.
Nockolds, S.R., 1947. The relation between chemical composition and paragenesis in the biotite micas of igneous rocks. Am. J. Sci., 245: 401—420.
Norton, J.J., 1970. Composition of a pegmatite, Keystone, South Dakota. Am. Mineral., 55: 981—1002.
Odikadze, G.L., 1968. Distribution of the rarer and ore elements in the El'dzhurta intrusive massif, Kabarda-Balkar, A.S.S.R. Geochem. Int., 5: 519—524.
Odikadze, G.L., 1971. Distribution of fluorine in the granitoids of the Greater Caucasus and Dzirul' massif. Geochem. Int., 8: 314—323.
Odikadze, G.L., 1973. Contents of K, Rb, Cs and F in some Caucasus volcanic formations. Geochem. Int., 10: 163—173.
Olson, J.C., Shawe, D.R., Pray, L.C. and Sharp, W.N., 1954. Rare-earth mineral deposits of the Mountain Pass district, San Bernardino County, California. U.S. Geol. Surv., Prof. Pap., 261, 1—75.
Ontoev, D.O., 1974. Relationship between the multistage tungsten, molybdenum and tin deposits and the structural history of granitoid intrusive complexes. In: M. Štemprok (Editor), Metallization Associated with Acid Magmatism, Vol. 1, Geological Survey, Prague, pp. 104—108.
Palache, C., Berman, H. and Frondel, C., 1957. The System of Mineralogy, Vols. I and II. Wiley, New York, N.Y., 7th ed.
Pälchen, W. and Tischendorf, G., 1974. Some special problems of petrology and geochemistry in the Erzgebirge, G.D.R. In: M. Štemprok (Editor), Metallization Associated with Acid Magmatism, Vol. 1, Geological Survey, Prague, pp. 206—209.
Pauly, H., 1974. Ivigtut cryolite deposit, SW-Greenland. In: M. Štemprok(Editor), Metallization Associated with Acid Magmatism, Vol. 1, Geological Survey, Prague, pp. 393—399.
Peters, W.C., 1958. Geologic characteristics of fluorspar deposits in the western United States. Econ. Geol., 53: 663—688.
Power, G.M., 1968. Chemical variation in tourmalines from south-west England. Mineral. Mag., 36: 1078—1089.
Powers, H.A., 1961. Chlorine and fluorine in silicic volcanic glass. U.S. Geol. Surv., Prof. Pap., 424-B: B261—B263.
Rieder, M., 1971. Stability and physical properties of synthetic lithium—iron micas. Am. Mineral., 56: 256—280.
Rimšaite, J.H.Y., 1967. Studies of rock-forming micas. Geol. Surv. Can. Bull., 149, 82 pp.
Roedder, E., 1972. Composition of fluid inclusions. In: Data of geochemistry, 6th Edition, U.S. Geol. Surv., Prof. Pap., 440-JJ, Ch. JJ, 164 pp.
Roedder, E. and Coombs, D.S., 1967. Immiscibility in granitic melts, indicated by fluid inclusions in ejected granitic blocks from Ascension Island. J. Petrol., 8: 417—451.
Rosenberg, P.E., 1972a. Paragenesis of the topaz-bearing portion of the Brown Derby No. 1 pegmatite, Gunnison County, Colorado. Am. Mineral., 57: 571—583.
Rosenberg, P.E., 1972b. Compositional variations in synthetic topaz. Am. Mineral., 57: 169—187.
Rosenberg, P.E., 1973. HF/SiF_4 ratios in volcanic and magmatic gases. Geochim. Cosmochim. Acta, 37: 109—112.

Rozanov, K.I. and Mineev, D.A., 1973. Geochemical characterization of Precambrian granitoids of the Azov Sea region. Geochem. Int., 10: 163—173.
Rub, M.G. and Pavlov, V.A., 1974. Geochemical and petrographical features of granitoids accompanied by stanniferous, rare-earth and tungsten mineralization. In: M. Štemprok (Editor), Metallization Associated with Acid Magmatism, Vol. 1, Geological Survey, Prague, pp. 210—214.
Ryabchikov, I.D., Durasova, N.A. and Barsukov, V.L., 1974. The role of volatiles in the mobilization of tin from granitic magmas. In: M. Štemprok (Editor), Metallization Associated with Acid Magmatism, Vol. 1, Geological Survey, Prague, pp. 287—288.
Saito, N., 1950. Geochemistry of the Fukushinzan alkaline igneous complex, I. On the distribution of chemical elements in alkaline rocks. Sci. Rep. Fac. Sci. Kyushi Univ., 1: 121 (in Japanese).
Seraphim, R.H., 1951. Some aspects of the geochemistry of fluorine. Thesis. M.I.T., Cambridge, Mass.
Shawe, D.R. Mountjoy, W. and Duke, W., 1964. Lithium associated with beryllium in rhyolite tuff at Spor Mountain, Western Juab County, Utah. U.S. Geol. Surv., Prof. Pap., 501-C: C86—C87.
Shcherba, G.N., 1970. Greisens. Int. Geol. Rev., 12(2): 114—150 and 12(3): 239—255.
Shepherd, E.S., 1940. Note on the fluorine content of rocks and ocean bottom samples. Am. J. Sci., 238: 117—128.
Sheremet, Ye.M., Gormasheva, G.S. and Legeydo, V.A., 1973. Geochemical criteria for the productivity of potential ore-bearing granitoids in the Gudzhir intrusive complex in west Transbaykalia. Geochem. Int., 10: 1125—1135.
Shmakin, B.M. and Shiryayeva, V.A., 1968. Distribution of rare earth and some other elements in apatites of muscovite pegmatites, eastern Siberia. Geochem. Int., 5: 796—803.
Smith, F.G., 1963. Physical Geochemistry, Addison-Wesley, Reading, Mass., 624 pp.
Staatz, M.H. and Trites, A.F., 1955. Geology of the Quartz Creek pegmatite district, Gunnison County, Colorado. U.S. Geol. Surv., Prof. Pap., 265, 111 pp.
Stavrov, O.D. and Bykova, T.A., 1961. Distribution of some rare and volatile elements in the rocks and pegmatites of the Korosten'skii pluton. Geochemistry, pp. 370—374.
Stepanov, V.I. and Moleva, V.A., 1962. On the ralstonite from Ilmen Mountain, central Kazakhstan and Kamchatka. Zap. Vses. Mineral. Ova., 91 (Ed. 5): 556—572 (in Russian).
Stormer, J.C. and Carmichael, I.S.E., 1970. Villiaumite and the occurrence of fluoride minerals in igneous rocks. Am. Mineral., 55: 126—134.
Stormer, J.C. and Carmichael, I.S.E., 1971. Fluorine—hydroxyl exchange in apatite and biotite: a potential igneous geothermometer. Contrib. Mineral. Petrol., 31: 121—131.
Sugiura, T., Mizutani, Y. and Oana, S., 1963. Fluorine, chlorine, bromine and iodine in volcanic gases. J. Earth Sci. Nagoya Univ., 11: 272—278.
Syritso, L.F. and Chernik, L.N., 1967. Evolution in accessory mineral paragenesis, during metasomatic alteration of granites in eastern Transbaykalia massifs. Int. Geol. Rev., 9: 814—827.
Taborszky, F.K., 1962. Geochemie des Apatites in Tiefengestein am Beispiel des Odenwaldes. Beitr. Mineral. Petrol., 8: 354—392.
Tauson, L.V., 1967. Geochemical behaviour of rare elements during crystallization and differentiation of granitic magmas. Geochem. Int., 4: 1067—1075.
Tauson, L.V., 1974. The geochemical types of granitoids and their potential ore capacity. In: M. Štemprok (Editor), Metallization Associated with Acid Magmatism, Vol. 1, Geological Survey, Prague, pp. 221—227.
Tischendorf, G., Lange, H. and Schust, F., 1974. On the relation between granites and tin deposits in the Erzgebirge, G.D.R. In: M. Štemprok (Editor), Metallization Associated with Acid Magmatism, Vol. 1, Geological Survey, Prague, pp. 132—136.

Tolstoy, M.I., Ostafiychuk, I.M. and Molyavko, V.G., 1973. Geochemical characteristics of granitoids of the Korosten'sk intrusive complex, Ukrainian shield. Geochem. Int., 10: 1215—1232.

Turekian, K.K. and Wedepohl, K.H., 1961. Distribution of the elements in some major units of the Earth's crust. Bull. Geol. Soc. Am., 72: 172—191.

Tuttle, O.F. and Bowen, N.L., 1958. Origin of granite in the light of experimental studies in the system $NaAlSi_3O_8$—$KAlSi_3O_8$—SiO_2—H_2O. Geol. Soc. Am., Mem., 74, 153 pp.

Upton, B.G.J., 1960. The alkaline igneous complex of the Kŭngnăt Fjeld, south Greenland. Medd. Grønl., 123(4): 1—145.

Upton, B.G.J., Thomas, J.E. and Macdonald, R., 1971. Chemical variation within three alkaline complexes in south Greenland. Lithos, 4: 163—184.

Valach, R., 1968. Distribution of fluorine and water in the igneous rocks of the earth's crust. Geochem. Int., 5: 559—572.

Varlamoff, N., 1974. Classification and spatio-temporal distribution of tin and associated mineral deposits. In: M. Štemprok (Editor), Metallization Associated with Acid Magmatism, Vol. 1, Geological Survey, Prague, pp. 137—144.

Vinogradov, A.P., 1962. Mean element contents in the main types of crustal igneous rocks. Geochemistry, 5: 641—664.

Vlasov, K.A., 1966. Geochemistry and mineralogy of rare elements and genetic types of their deposits. Vols. II and III. Acad. Sci., U.S.S.R., Moscow. (Translated 1968, Israel Program for Scientific Translations, Jerusalem.)

Von Platen, H., 1965. Kristallisation granitischer Schmelzen, Beitr. Mineral. Petrogr., 11: 334—381.

Von Platen, H. and Winkler, H.G.F., 1961. Kristallisation eines Obsidians bei Anwesenheit von H_2O, NH_3, HCl and HF unter 2000 Atm. Druck. Fortschr. Mineral., 39: 355.

White, D.E. and Waring, G.A., 1963. Volcanic emanations. In: Data of Geochemistry, 6th Edition. U.S. Geol. Surv., Prof. Pap., 440-K, Ch.K., pp. K1—K29.

Wyllie, P.J. and Tuttle, O.F., 1961. Experimental investigation of silicate systems containing two volatile components, II. The effects of NH_3 and HF, in addition to H_2O, on the melting temperatures of albite and granite. Am. J. Sci., 259: 128—143.

Wyllie, P.J. and Tuttle, O.F., 1964. Experimental investigations of silicate systems containing two volatile constituents, III. The effect of SO_3, P_2O_5, HCl and Li_2O, in addition to H_2O, on the melting temperatures of albite and granite. Am. J. Sci., 262: 930—939.

Yakubovich, K.I. and Portnov, A.M., 1967. Strontium as a geochemical indicator of genetic connection between mineralization and alkalic rocks. Dokl. Acad. Sci., U.S.S.R., Earth Sci. Sect., 175: 185—186.

Yusupov, S.Sh., 1970. Rock crystal in pegmatites and fluorine concentration in the enclosing granites. Int. Geol. Rev., 12(8): 959—961.

Zakharchenko, A.I., 1974. Genesis of rare-metal deposits in the formation of parent granites and post-magmatic bodies (on the data of inclusions of melts and fluids in minerals). In: M. Štemprok (Editor), Metallization Associated with Acid Magmatism, Vol. 1, Geological Survey, Prague, pp. 289—293.

Zalashkova, N.E. and Gerasimovskii, V.V., 1974. Petrographic and geochemical features of rare-metal amazonite granites. In: M. Štemprok (Editor), Metallization Associated with Acid Magmatism, Vol. 1, Geological Survey, Prague, pp. 232—236.

Zies, E.G., 1929. The Valley of Ten Thousand Smokes, I. The acid gases contributed to the sea during volcanic activity. Natl. Geogr. Soc., Contrib. Tech. Pap., I. Katmai Ser., 4: 1—79.

Marine Geology, 20 (1976) 205—228
Elsevier Scientific Publishing Company, Amsterdam — Printed in The Netherlands

THE GEOCHEMISTRY OF BASAL SEDIMENTS FROM THE NORTH ATLANTIC OCEAN

ARTHUR HOROWITZ* and DAVID S. CRONAN
Applied Geochemistry Research Group, Imperial College, London (Great Britain)

(Received July 7, 1975)

ABSTRACT

Horowitz, A. and Cronan, D. S., 1976. The geochemistry of basal sediments from the North Atlantic Ocean. Mar. Geol., 20: 205—228.

Chemical analyses of North Atlantic D.S.D.P. (Deep Sea Drilling Project) sediments indicate that basal sediments generally contain higher concentrations of Fe, Mn, Mg, Pb, and Ni, and similar or lower concentrations of Ti, Al, Cr, Cu, Zn, and Li than the material overlying them. Partition studies on selected samples indicate that the enriched metals in the basal sediments are usually held in a fashion similar to that in basal sediments from the Pacific, other D.S.D.P. sediments, and modern North Atlantic ridge and non-ridge material.

Although, on average, chemical differences between basal sediments of varying ages are apparent, normalization of the data indicates that the processes leading to metal enrichment on the crest of the Mid-Atlantic Ridge appear to have been approximately constant in intensity since Cretaceous times. In addition, the bulk composition of detrital sediments also appears to have been relatively constant over the same time period. Paleocene sediments from site 118 are, however, an exception to this rule, there apparently having been an increased detrital influx during this period.

The bulk geochemistry, partitioning patterns, and mineralogy of sediments from D.S.D.P. 9A indicates that post-depositional migration of such elements as Mn, Ni, Cu, Zn, and Pb may have occurred. The basement encountered at the base of site 138 is thought to be a basaltic sill, but the overlying basal sediments are geochemically similar to other metalliferous basal sediments from the North Atlantic. These results, as well as those from site 114 where true oceanic basement was encountered, but where there was an estimated 7 m.y. hiatus between basaltic extrusion and basal sediment deposition, indicate that ridge-crest sediments are not necessarily deposited during active volcanism but can be formed after the volcanism has ceased. The predominant processes for metal enrichment in these deposits and those formed in association with other submarine volcanic features is a combination of shallow hydrothermal activity, submarine weathering of basalt, and the formation of ferromanganese oxides which can scavenge metals from seawater. In addition, it seems as though the formation of submarine metalliferous sediments is not restricted to active-ridge areas.

*Present address: Dept. of Earth and Environmental Sciences, Queens College, C.U.N.Y., Flushing, New York 11367, U.S.A.

INTRODUCTION

Until fairly recently, almost all the geochemical studies concerned with active-ridge and other metalliferous sediments associated with submarine volcanic features dealt with surface or near-surface deposits (Bostrom and Peterson, 1966, 1969; Bostrom et al., 1969; Horowitz, 1970; Bender et al., 1971; Cronan, 1972; Piper, 1973; Sayles and Bischoff, 1973; Bertine, 1974). However, with the advent of the Deep Sea Drilling Project (D.S.D.P.), geochemists have been able to examine material covering much of the sedimentary column of the oceans. Since 1970, a number of occurrences of metalliferous sediments, usually in contact with, or directly overlying the basement, and which are thought to be the ancient analogues of ridge-crest sediments which have moved to their present positions as a result of sea-floor spreading, have been reported in the literature. This type of sediment has been described from the Pacific by Von der Borch and Rex (1970), Von der Borch et al. (1971), Cook (1971), Heath and Moberly (1971), Cronan et al. (1972), Dymond et al. (1973) and Cronan (1974), from the Atlantic by Peterson et al. (1970) and Bostrom et al. (1972) and from the Indian Ocean by Cronan et al. (1974).

Of considerable importance in understanding the geochemistry of basal metalliferous sediments is the way in which different elements are partitioned between their various constituent phases. Cronan and Garrett (1973) reported that most of the Fe and Mn is located in separate phases (Mn in the acid-reducible phase, Fe in the HCl-soluble phase) whilst the other enriched metals, such as Cu, Zn, Ni, and Pb are concentrated, to varying degrees, throughout all phases. These results are similar to those reported by Dymond et al. (1973) for other Pacific metalliferous sediments and are quite similar to the results reported for surface sediments from the northern Mid-Atlantic Ridge (Chester and Messiha-Hanna, 1970) from the Reykjanes Ridge (Horowitz, 1974a), from near the East Pacific Rise (Sayles and Bischoff, 1973) and from normal Pacific and Atlantic sediments (Chester and Hughes, 1966, 1969; Chester and Messiha-Hanna, 1970). The major difference between Atlantic and Pacific partitioning patterns lies in the quantities of lattice-held metals which are significantly higher in the Atlantic than in the Pacific, probably the result of the much greater detrital input in the former region (Ku et al., 1968). In general, it appears as if geochemical partitioning is similar in both ancient and modern metalliferous sediments, as well as in normal pelagic sediments.

In order to further investigate the geochemistry of basal metalliferous sediments, particularly from an ocean of high detrital input, a series of D.S.D.P. samples from three North Atlantic traverses (Legs II, XII, and XIV) have been obtained and analyzed. The locations of the sample sites are given in Fig. 1. Detailed information on both the relevant sample sites, and the cores obtained from them, can be found in the pertinent volumes of the *Initial Reports* (Leg II: Peterson et al., 1970; Leg XII: Laughton et al., 1972: Leg XIV: Hayes et al., 1972).

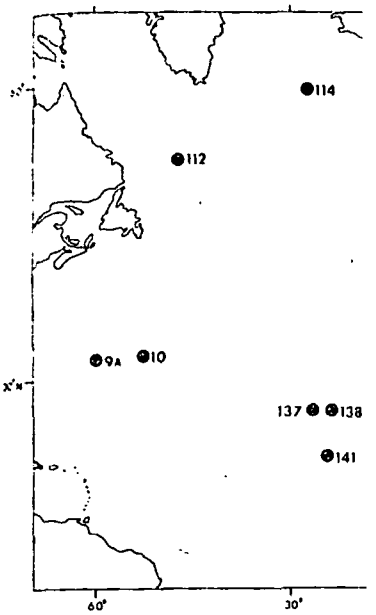

Fig.1. The location of the D.S.D.P.

METHODS

The sediment samples were
analysis, the samples were gro
mortar. In the case of the mor
a tungsten-carbide pestle and
Chemical analyses were carr
a combined HF—$HClO_4$—HN
$HClO_4$. All determinations we
accuracy of the analyses were
(U.S.G.S. standards BCR-1, G-
consisting of previously analyz
of the analyses have been repo

BULK GEOCHEMICAL DATA

The bulk chemical analyses
an untreated basis in Table I,
either Al + Fe + Mn, 4 Al + F
by various other workers (Bos
1972; Piper, 1973) does not m
Sediment samples were obt
sites which bottomed in basalt
relation to the underlying base

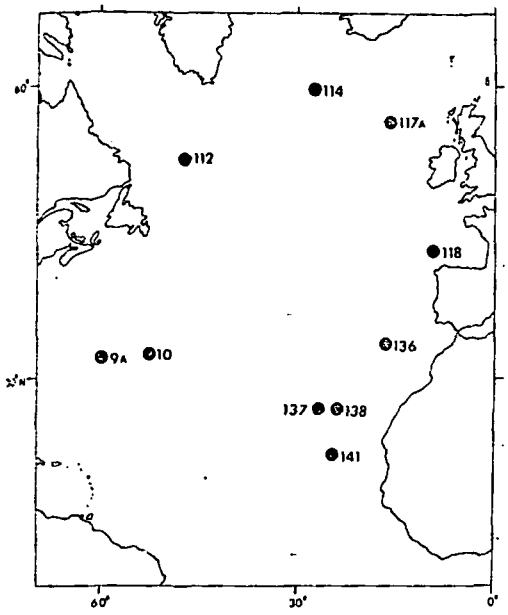

Fig.1. The location of the D.S.D.P. North Atlantic sediment sample sites.

METHODS

The sediment samples were oven dried at $< 40°$ C. Prior to chemical analysis, the samples were ground to $< 31\ \mu m$ with an agate pestle and mortar. In the case of the more indurated sediments, a pre-grinding with a tungsten-carbide pestle and mortar was necessary.

Chemical analyses were carried out on a Perkin-Elmer 403 A.A.S. after a combined $HF-HClO_4-HNO_3$ digestion involving a double fuming with $HClO_4$. All determinations were done in duplicate and the precision and accuracy of the analyses were checked by using seven internal standards (U.S.G.S. standards BCR-1, G-2, and W-1, and four in-house standards consisting of previously analyzed sediment). The precision and accuracy of the analyses have been reported elsewhere (Horowitz, 1974a b).

BULK GEOCHEMICAL DATA

The bulk chemical analyses of all the D.S.D.P. samples are presented on an untreated basis in Table I, as a carbonate correction or normalizing to either Al + Fe + Mn, 4 Al + Fe + Mn + Ti, or Al_2O_3, as has been suggested by various other workers (Bostrom and Peterson, 1969; Bostrom et al., 1972; Piper, 1973) does not markedly alter the element distribution patterns.

Sediment samples were obtained from various North Atlantic D.S.D.P. sites which bottomed in basalt in order to try to detect element trends in relation to the underlying basement. As can be seen in Table I, no

TABLE I

Chemical analyses of the D.S.D.P. sediment samples

Sample	Fe (%)	Mn (%)	Al_2O_3 (%)	TiO_2 (%)	Mg (%)	Ca (%)	Cu (p.p.m.)	Zn (p.p.m.)	Pb (p.p.m.)	Cr (p.p.m.)	Ni (p.p.m.)	Li (p.p.m.)
Hole 9A												
5-2-120-122*	6.67	0.13	9.55	0.42	0.76	0.30	24	70	35	50	28	21
5-2- 77- 79*	4.05	0.09	6.90	0.27	0.47	0.30	17	40	35	50	20	26
5-2- 40- 42*	3.95	0.07	7.70	0.32	0.50	0.40	19	34	55	55	18	23
5-2- 10- 12*	5.55	0.10	6.55	0.27	0.48	0.35	23	41	25	55	10	24
5-1- 90- 92*	7.35	0.26	10.5	0.52	1.15	0.40	42	90	70	50	28	18
5-1- 60- 62*	8.45	0.39	10.6	0.47	1.12	0.58	45	94	67	70	40	17
4-1-130-132	4.88	0.05	11.5	0.55	1.13	0.38	87	114	85	75	53	16
4-1- 80- 82	4.33	0.04	10.2	0.49	0.97	0.55	73	103	77	67	37	14
3-4-125-127	5.40	0.57	10.0	0.49	1.06	0.55	113	162	55	37	67	20
3-4- 25- 27	5.50	0.57	10.4	0.50	0.24	0.45	121	147	85	55	102	22
3-3- 75- 77	5.23	0.30	14.0	0.69	1.62	0.50	123	138	70	90	103	50
3-2-125-127	4.20	0.33	8.10	0.47	0.97	0.45	94	105	75	70	58	18
3-1-105-107	7.63	0.86	12.4	0.69	1.47	0.55	174	167	100	75	138	25
1-6- 50- 52	4.40	0.80	15.6	0.59	1.58	0.55	189	152	65	105	172	73
1-4-100-102	2.95	0.55	10.3	0.36	1.32	0.62	143	196	40	83	92	45
1-1- 25- 27	5.00	0.74	16.6	0.52	1.63	1.60	238	152	85	60	160	80
C.F.B. basal	6.00	0.17	7.75	0.32	0.75		28	62	48	55	24	22
C.F.B. non-basal	4.95	0.48	11.9	0.54	1.19		136	144	74	72	98	36
Hole 10												
18-5-135-137*	0.28	0.06	0.35	0.10	0.45	38.5	16	38	77	20	68	5
18-5- 85- 87*	0.36	0.08	0.62	0.10	0.36	39.2	19	41	80	35	63	5
18-5- 55- 57*	0.36	0.06	0.98	0.15	0.77	35.4	17	40	70	23	50	5
18-5- 5- 7*	0.38	0.07	0.62	0.12	0.47	38.7	20	43	73	20	43	5
18-4- 77- 79	0.45	0.07	1.18	0.13	2.36	33.2	22	36	95	15	20	10
18-3- 75- 77	0.35	0.05	0.68	0.13	0.57	36.7	21	35	97	13	50	7
C.F.B. basal	2.30	0.46	4.16	0.77	3.38		119	267	495	162	370	33
C.F.B. non-basal	1.60	0.25	3.73	0.54	5.66		88	147	396	58	150	36
Hole 112												
16-1-108-110*	3.40	0.23	4.65	0.22	1.22	5.35	53	46	45	50	28	51
16-1- 50- 52*	8.45	0.05	12.3	0.54	2.11	0.60	19	149	75	75	73	48
16-1- 10- 12*	8.50	0.05	12.2	0.65	2.35	0.65	36	153	63	95	62	56
15-6-110-112	4.40	0.08	11.3	0.52	1.24	9.60	77	92	105	95	125	24
15-1- 30- 32	3.88	0.09	11.3	0.53	1.14	11.0	72	100	95	80	53	24
C.F.B. basal	6.95	0.12	9.95	0.48	1.95		39	118	63	76	56	54
C.F.B. non-basal	5.48	0.10	15.0	0.70	1.55		98	108	133	116	118	32

C.F.B. basal	6.00	0.17	7.75	0.32	0.75		28	62	48	55	24	22
C.F.B. non-basal	4.95	0.48	11.9	0.54	1.19		136	144	74	72	98	36
Hole 10												
18-5-135-137*	0.28	0.06	0.35	0.10	0.45	38.5	16	38	77	20	68	5
18-5- 85- 87*	0.36	0.08	0.62	0.10	0.36	39.2	19	41	80	35	63	5
18-5- 55- 57*	0.36	0.06	0.98	0.15	0.77	35.4	17	40	70	23	50	5
18-5- 5- 7*	0.38	0.07	0.62	0.12	0.47	38.7	20	43	73	20	43	5
18-4- 77- 79	0.45	0.07	1.18	0.13	2.36	33.2	22	36	95	15	20	10
18-3- 75- 77	0.35	0.05	0.68	0.13	0.57	36.7	21	35	97	13	50	7
C.F.B. basal	2.30	0.46	4.16	0.77	3.38		119	267	495	162	370	33
C.F.B. non-basal	1.60	0.25	3.73	0.54	5.66		88	147	396	58	150	36
Hole 112												
16-1-108-110*	3.40	0.23	4.65	0.22	1.22	5.35	53	46	45	50	28	51
16-1- 50- 52*	8.45	0.05	12.3	0.54	2.11	0.60	19	149	75	75	73	48
16-1- 10- 12*	8.50	0.05	12.2	0.65	2.35	0.65	36	153	63	95	62	56
15-6-110-112	4.40	0.08	11.3	0.52	1.24	9.60	77	92	105	95	125	24
15-1- 30- 32	3.88	0.09	11.3	0.53	1.14	11.0	72	100	95	80	53	24
C.F.B. basal	6.95	0.12	9.95	0.48	1.95		39	118	63	76	56	54
C.F.B. non-basal	5.48	0.10	15.0	0.70	1.55		98	108	133	116	118	32
Hole 114												
6-6-140-142*	6.90	0.10	9.90	2.32	1.83	11.1	71	116	60	75	48	15
6-6-100-102*	7.60	0.07	10.6	2.12	1.63	8.50	87	106	57	70	27	17
6-6- 55- 57*	5.10	0.06	8.05	1.38	1.34	16.3	73	86	60	55	30	20
6-6- 5- 7*	6.20	0.07	8.65	1.58	1.66	13.3	71	109	56	65	28	14
6-5-145-147*	6.40	0.08	9.35	1.83	1.74	12.9	71	104	57	65	33	16
6-5- 80- 82*	6.95	0.07	9.25	1.69	1.66	11.9	72	101	60	95	40	15
6-5- 10- 12*	8.10	0.08	11.7	2.17	1.86	8.10	90	113	57	50	37	18
6-4-131-133*	8.20	0.08	12.7	2.64	2.02	7.25	100	133	47	60	63	17
6-4-105-107*	7.27	0.05	6.60	1.82	1.37	14.8	47	102	67	60	23	17
6-1- 49- 51*	8.15	0.07	9.30	2.45	1.84	11.4	65	130	60	63	33	17
6-1- 18- 20*	4.90	0.06	6.05	1.64	1.15	17.5	41	98	70	65	48	16
5-6-135-137	7.00	0.09	9.80	2.10	2.00	12.4	93	106	70	65	33	16
5-6- 75- 77	6.80	0.06	7.00	2.15	1.55	16.4	68	110	73	53	30	16
5-5- 75- 77	6.35	0.05	6.25	2.22	1.31	18.1	51	102	83	40	30	16
5-4- 78- 80	6.80	0.06	9.80	2.52	1.47	12.7	93	112	63	57	20	24
4-3- 85- 87	8.75	0.12	12.6	2.47	2.42	7.10	105	119	60	80	30	19
3-5-100-102	7.30	0.10	10.8	2.31	2.36	10.0	85	115	55	75	43	16
3-5- 25- 27	7.35	0.10	10.6	1.75	1.92	8.60	87	122	60	63	27	14
3-3- 5- 7	7.90	0.10	10.3	1.80	1.71	8.30	74	137	43	70	20	16
2-6- 75- 77	7.60	0.12	11.5	2.02	2.50	8.83	94	130	57	105	57	24
2-5-100-102	8.00	0.10	13.0	1.92	2.30	6.75	86	174	87	87	37	34
2-4- 75- 77	7.90	0.13	11.8	2.14	2.48	8.00	86	235	60	90	40	24

TABLE I (*continued*)

Sample	Fe (%)	Mn (%)	Al_2O_3 (%)	TiO_2 (%)	Mg (%)	Ca (%)	Cu (p.p.m.)	Zn (p.p.m.)	Pb (p.p.m.)	Cr (p.p.m.)	Ni (p.p.m.)	Li (p.p.m.)
2-3- 75- 77	7.60	0.13	12.0	2.00	2.31	8.60	94	149	70	75	25	25
2-2- 75- 77	8.00	0.13	11.8	2.04	2.55	8.25	96	159	47	93	23	27
2-1- 90- 92	8.35	0.13	11.9	2.15	2.60	7.40	87	143	53	87	27	23
2-1- 5- 7	8.00	0.13	11.6	2.08	2.31	8.95	95	180	60	77	43	22
1-5- 75- 77	6.70	0.09	11.5	1.50	2.12	8.25	76	123	40	85	20	34
1-3- 75- 77	7.20	0.09	12.9	1.77	2.38	5.60	80	142	70	90	35	40
1-1-124-126	7.17	0.07	13.8	1.83	2.30	3.40	76	149	160	107	55	55
C.F.B. basal	9.37	0.12	12.6	2.84	2.34		99	150	84	92	53	21
C.F.B. non-basal	8.12	0.10	12.2	2.34	2.36		92	156	86	95	37	29
Hole 117A												
10-1-135-137*	9.65	0.08	14.4	1.95	5.40	2.37	64	132	47	280	153	76
10-1-115-117*	10.4	0.07	13.3	1.84	6.34	2.35	64	113	50	305	170	90
9-1- 50- 52*	8.15	0.10	11.2	1.45	4.23	9.00	38	112	55	265	107	53
9-1- 38- 40*	8.88	0.09	11.7	1.65	4.20	8.05	46	116	60	245	120	55
8-2-145-147	8.30	0.04	12.1	1.91	3.33	5.37	66	151	67	227	88	25
8-2- 75- 77	4.20	0.11	9.80	1.95	1.56	14.0	38	68	60	85	38	24
8-2- 5- 7	6.95	0.06	11.1	1.67	2.45	8.20	73	121	47	185	83	24
8-1-140-142	8.90	0.05	12.2	2.47	2.63	4.03	52	187	50	175	88	27
8-1- 75- 77	11.2	0.04	11.2	2.24	3.60	2.84	47	156	58	108	97	29
8-1- 10- 12	7.25	0.06	13.1	1.82	2.37	5.60	98	147	63	215	117	35
C.F.B. basal	10.5	0.08	14.6	2.00	5.57		60	134	66	308	155	77
C.F.B. non-basal	8.78	0.06	13.3	2.33	3.00		71	156	60	188	96	31
Hole 118												
19-1- 25- 27*	5.10	0.34	16.7	0.72	1.18	0.57	53	118	70	80	75	66
19-1- 5- 7*	5.40	0.66	16.7	0.81	1.20	0.60	67	136	77	63	95	65
18-2- 90- 92*	4.03	0.26	15.6	0.62	1.28	2.52	66	125	55	80	68	89
18-2- 75- 77*	4.90	0.12	14.7	0.61	1.35	2.00	50	127	70	70	47	99
18-2- 50- 52*	4.91	0.66	16.1	0.69	1.19	0.97	67	131	123	80	58	65
18-1-146-148	4.07	0.24	16.6	0.63	1.05	5.95	64	129	50	82	70	63
18-1- 75- 77	5.05	0.19	16.2	0.72	1.12	2.50	67	118	57	83	53	61
18-1- 70- 72	4.73	0.28	15.8	0.70	1.12	0.45	59	126	65	100	53	68
17-1-145-147	4.80	0.08	15.0	0.79	1.16	0.60	50	120	75	100	103	68
17-1-110-112	4.70	0.08	15.7	0.75	1.18	0.55	60	126	55	110	60	67
C.F.B. basal	4.70	0.41	16.1	0.80	1.30		62	103	81	76	70	78
C.F.B. non-basal	4.50	0.18	16.9	0.85	1.12		62	130	60	96	66	69
Hole 136												
8-1-148-150*	7.40	0.04	13.4	1.18	2.18	0.67	101	191	73	170	55	67
8-1-100-102*	2.40	0.06	3.75	1.15	1.01	28.0	33	54	67	60	53	15

8-1- 75- 77	11.2	0.04	11.2	2.24	3.60	2.84	47	156	58	108	97	29
8-1- 10- 12	7.26	0.06	13.1	1.82	2.37	5.60	98	147	63	215	117	35
C.F.B. basal	10.5	0.08	14.6	2.00	5.57		60	134	66	308	155	77
C.F.B. non-basal	8.78	0.06	13.3	2.33	3.00		71	156	60	188	96	31
Hole 118												
19-1- 25- 27*	5.10	0.34	16.7	0.72	1.18	0.57	53	118	70	80	75	66
19-1- 5- 7*	5.40	0.66	16.7	0.81	1.20	0.60	67	136	77	63	95	65
18-2- 90- 92*	4.03	0.26	15.6	0.62	1.28	2.52	66	125	55	80	68	59
18-2- 75- 77*	4.00	0.12	14.7	0.61	1.35	2.00	59	127	70	70	62	55
18-2- 50- 52*	4.91	0.66	16.1	0.69	1.19	0.97	67	131	123	80	58	65
18-1-146-148	4.07	0.24	16.6	0.63	1.05	5.95	64	129	50	82	70	63
18-1- 75- 77	5.05	0.19	16.2	0.72	1.12	2.50	67	118	57	83	53	61
18-1- 70- 72	4.73	0.28	15.8	0.70	1.12	0.45	59	126	65	100	53	68
17-1-145-147	4.80	0.08	15.0	0.79	1.16	0.60	50	120	75	100	103	68
17-1-110-112	4.70	0.08	15.7	0.75	1.18	0.55	60	126	55	110	60	67
C.F.B. basal	4.70	0.41	16.1	0.80	1.30		62	103	81	76	70	78
C.F.B. non-basal	4.50	0.18	16.9	0.85	1.12		62	130	60	96	66	69
Hole 136												
8-1-148-150*	7.40	0.04	13.4	1.18	2.18	0.67	101	191	73	170	55	67
8-1-100-102*	2.40	0.06	3.75	1.15	1.01	28.0	33	54	67	60	53	15
8-1- 50- 52*	7.20	0.21	12.5	3.50	2.14	6.90	70	114	60	110	97	47
8-1- 5- 7*	7.17	0.12	12.3	3.25	2.28	5.57	72	162	43	143	90	50
6-2-137-139	11.6	0.20	13.5	5.58	1.99	3.35	139	154	53	183	97	40
6-2- 70- 72	9.50	0.16	14.6	5.09	2.15	0.92	107	160	47	140	85	41
6-2- 15- 17	7.10	0.11	14.3	3.67	2.03	3.15	49	131	55	70	78	49
6-1-145-147	9.00	0.30	15.6	4.10	2.09	1.70	113	177	67	93	110	53
6-1-100-102	6.35	0.25	14.9	2.32	2.27	2.40	91	178	70	105	58	51
6-1- 60- 62	6.35	0.25	15.3	2.05	2.45	1.73	85	201	80	137	75	53
6-1- 25- 27	5.70	0.13	11.7	1.67	1.86	11.5	94	126	73	93	77	41
C.F.B. basal	7.30	0.14	12.5	3.00	2.35		83	160	82	146	95	50
C.B.F. non-basal	8.10	0.20	14.8	3.62	2.10		101	170	63	118	82	53
Hole 137												
16-4-140-142*	2.56	0.30	4.77	0.25	1.41	24.3	39	87	90	50	63	15
16-4- 90- 92*	1.33	0.40	2.88	0.23	0.59	30.2	63	83	95	45	88	12
16-4- 60- 62*	2.43	0.24	4.20	0.25	0.93	18.3	147	232	93	31	67	16
16-4- 5- 7*	4.10	0.11	6.90	0.22	1.42	10.7	65	85	60	45	20	20
16-3-148-150	2.33	0.24	6.20	0.26	1.19	21.0	750	99	85	50	78	20
16-3-115-117	4.40	0.09	8.60	0.30	1.48	7.80	38	91	70	95	28	22
16-3- 90- 92	2.53	0.22	4.50	0.23	0.83	18.3	30	66	57	43	30	14
16-3- 20- 22	3.23	0.18	5.95	0.24	1.14	16.9	37	88	67	50	30	14
16-2-146-148	3.50	0.12	6.75	0.30	1.24	11.8	59	113	60	45	30	17

TABLE I (*continued*)

Sample	Fe (%)	Mn (%)	Al_2O_3 (%)	TiO_2 (%)	Mg (%)	Ca (%)	Cu (p.p.m.)	Zn (p.p.m.)	Pb (p.p.m.)	Cr (p.p.m.)	Ni (p.p.m.)	Li (p.p.m.)
16-2-100-102	3.50	0.12	7.65	0.40	1.61	12.0	40	88	70	85	63	21
16-2- 45- 47	3.95	0.12	8.60	0.39	1.48	10.5	108	182	65	105	118	23
16-2- 25- 27	4.75	0.04	11.5	0.52	2.15	3.75	117	95	85	110	33	31
C.F.B. basal	5.20	0.61	8.80	0.47	2.26		167	258	200	100	153	30
C.F.B. non-basal	4.65	0.21	10.4	0.59	1.91		250	147	101	91	75	35
Hole 138												
6-3-145-147*	3.78	0.84	5.80	0.29	6.05	12.1	69	127	85	80	123	16
6-3- 70- 72*	3.80	0.63	7.55	0.35	4.53	10.6	70	109	40	40	20	22
6-3- 20- 22*	3.90	0.48	8.65	0.34	3.92	7.80	164	158	65	75	50	24
6-2-145-147	6.30	0.05	12.0	1.67	2.12	1.50	78	136	57	130	118	27
6-2-100-102	2.68	0.04	13.1	1.74	1.30	0.90	87	96	45	90	153	14
6-2- 20- 22	3.60	0.04	9.90	0.42	1.78	1.25	55	131	40	110	20	24
C.F.B. basal	3.98	0.67	7.55	0.34	4.98		104	135	65	69	69	20
C.F.B. non-basal	4.20	0.04	11.7	1.30	1.75		73	121	45	107	96	24
Hole 141												
S.W.1*	2.45	0.03	12.0	0.63	1.26	0.77	25	227	40	67	20	20
9-5-148-150	5.40	0.07	15.8	0.78	1.05	0.40	48	122	45	130	73	74
9-5- 75- 77	4.83	0.07	15.3	0.80	1.03	0.40	51	122	60	145	58	73
9-5- 10- 12	4.55	0.05	15.9	0.79	1.04	0.40	51	113	65	140	58	69
9-4-148-150	4.70	0.06	15.0	0.71	1.12	0.45	48	95	55	85	55	58
9-4- 75- 77	3.90	0.03	14.7	0.63	1.31	0.50	83	113	50	155	73	73
9-4- 10- 12	4.55	0.04	16.4	0.79	1.47	0.40	37	105	50	130	48	52
C.F.B. basal	2.45	0.03	12.0	0.63	1.26		25	227	40	67	20	20
C.F.B. non-basal	4.34	0.05	15.0	0.73	1.18		49	128	52	122	55	60
All core avg.	5.61	0.16	5.62	0.76	1.81	8.28	78	121	64	90	62	34
C.F.B. all core avg.	6.65	0.18	6.53	0.96	2.30	—	85	148	95	118	83	38

The bottom-most sample analyzed from each hole is listed first, the next closest is listed second, etc. The samples marked with an asterisk (*) are considered to be basal sediments on the basis of their location with respect to their distance from the basement, or their mineralogy. Actual distances, and the pertinent mineralogies can be found in the appropriate volumes of the *Initial Reports*. The basal and non-basal averages listed after the individual analyses for each hole, are presented on a carbonate free basis (C.F.B.) to facilitate comparisons with sediments from other areas.

9-5-148-150	5.40	0.07	15.8	0.78	1.05	0.40	48	122	45	150	78	73
9-5- 75- 77	4.83	0.07	15.3	0.80	1.03	0.40	51	122	60	145	58	73
9-5- 10- 12	4.55	0.05	15.9	0.79	1.04	0.40	51	113	65	140	58	69
9-4-148-150	4.70	0.06	15.0	0.71	1.12	0.45	48	95	55	85	55	58
9-4- 75- 77	3.90	0.03	14.7	0.63	1.31	0.50	83	113	50	155	73	73
9-4- 10- 12	4.55	0.04	16.4	0.79	1.47	0.40	37	105	50	130	48	52
C.F.B. basal	2.45	0.03	12.0	0.63	1.26		25	227	40	67	20	20
C.F.B. non-basal	4.34	0.05	15.0	0.73	1.18		49	128	52	122	55	60
All core avg.	5.61	0.16	5.62	0.76	1.81	8.28	78	121	64	90	62	34
C.F.B. all core avg.	6.65	0.18	6.53	0.96	2.30	—	85	148	95	118	83	38

The bottom-most sample analyzed from each hole is listed first, the next closest is listed second, etc. The samples marked with an asterisk (*) are considered to be basal sediments on the basis of their location with respect to their distance from the basement, or their mineralogy. Actual distances, and the pertinent mineralogies can be found in the appropriate volumes of the *Initial Reports*. The basal and non-basal averages listed after the individual analyses for each hole, are presented on a carbonate free basis (C.F.B.) to facilitate comparisons with sediments from other areas.

continuous trends were found. However, in order to investigate if any general differences exist between the basal sediments and those overlying them, the average chemical composition of the basal samples was compared with the average chemical values for the material recovered further above at each of the sample sites. Sites 138 and 141 have been excluded from these computations as they are not thought to have bottomed in true oceanic basement. Of those elements that are normally enriched in active-ridge and basal sediments (Fe, Mn, Cu, Zn, Cr, Pb, and Ni), all except Cu and Zn have higher average values in the basal sediments whilst Al and Ti, normally depleted in active-ridge and basal sediments, generally have lower concentrations in the basal sediments than in the overlying material. These conclusions are not true for every hole individually, but are valid for the majority of them (Table I).

The elevated Pb values in the basal samples generally correspond to high values of calcium carbonate, supporting the view that carbonate can act as a host for this metal (Horowitz, 1974a). It is also of interest to note that Mg generally has a higher concentration in the basal sediments than in the overlying material. Some of the elevated Mg levels could be due to the presence of dolomite which has been detected in some of the basal sediments (Peterson et al., 1970; Laughton et al., 1972; Hayes et al., 1972). However, elevated Mg levels also occur in basal material where no dolomite has been detected. Here the Mg could come from the underlying basaltic basement; its presence probably being caused by either basaltic debris and/or through the alteration of the basalt. Elevated Mg levels have also been found in the sediments overlying the Reykjanes Ridge and the Mid-Atlantic Ridge at 45° N (Horowitz, 1974a, b).

The lack of elevated Cu and Zn concentrations in the basal sediments is somewhat surprising as both metals are normally enriched in both active-ridge and basal sediments (Bostrom and Peterson, 1966, 1969; Horowitz, 1970; Bruty et al., 1972; Dymond et al., 1973; Sayles and Bischoff, 1973; Piper, 1973; Cronan, 1974). This lack may be due to the fact that the detrital phases of the North Atlantic sediments contain relatively high concentrations of both metals, or that the quantity of ridge-derived Cu and Zn is not high enough to appear elevated in comparison with the detrital contributions. This feature has already been noted for Zn in some surface sediments from the Mid-Atlantic Ridge by Horowitz (1970).

It should be pointed out, that although the basal sediments described here do contain higher concentrations of such metals as Fe, Mn and Ni than in those above, there are no strikingly high metal concentrations such as those that have been reported for basal sediments from the Pacific (Cronan et al., 1972; Dymond et al., 1973). Nevertheless, the basal sediments in comparison with the overlying material do contain significantly higher concentrations of some metals, and on this basis, could be termed metalliferous. However, it must also be noted that some of the most metal-rich samples in the D.S.D.P. North Atlantic suite occur well away from the basement (Table I). Due to the position of these samples in the various

holes, the elevated metal concentrations are unlikely to be attributable to active-ridge processes as these normally only influence the lowermost few meters of sediment (Von der Borch and Rex, 1970; Cronan et al., 1972). Other processes, such as those involving scavenging of metals from seawater, adsorption onto clays, authigenic mineral formation, or detrital input would have to be invoked to explain these high metal levels. The fact that the metal concentrations are so high in some non-basal sediments would indicate, at least in the North Atlantic, that these other processes are at least as effective as active-ridge processes in concentrating and depositing metals.

GEOCHEMICAL PARTITIONING DATA

Partition studies were carried out on 16 samples selected on the basis of the bulk chemical analyses. Six of these were basal sediments, 8 were metal-rich samples from core sections unassociated with basement, and 2 were metal-rich samples from the bottom-most section of hole 138. The methods employed in this study have been described elsewhere (Horowitz, 1974a). The results of the various chemical attacks are presented in Table II. In general, the Fe and Mn are in separate phases; most of the Mn (57%) is in the acid-reducible phase whilst most of the Fe (91%) is in the HCl-soluble and insoluble phases. The other trace metals, normally enriched in both surface and basal metalliferous sediments, are distributed in varying amounts, between all phases. These results are similar to those reported for surface sediments from the crest of the Reykjanes Ridge (Horowitz, 1974a) and generally, also similar to other results reported for surface sediments from the northern Mid-Atlantic Ridge by Chester and Messiha-Hanna (1970). In addition, they are similar to those reported for basal sediments from the East Pacific Rise area, although the hydroxylamine leach did not remove as great a percentage of material from the North Atlantic Samples as from the Pacific samples. This difference is probably due to the much greater detrital input in the North Atlantic than in the Pacific, resulting in a greater percentage of resistant detrital minerals relative to the more soluble authigenic minerals in Atlantic sediments. The partition patterns for the metal-rich, non-basal sediments, fall within the reported ranges for metal-rich basal sediments, metal-rich surface sediments and non-metalliferous sediments from the North Atlantic. This similarity in partitioning would indicate that the metals in marine sediments are all incorporated in a similar fashion regardless of their time of formation or mode of origin and that the metal distributions in the older sediments have apparently not been significantly affected by diagenesis.

The major elements Al, Ti, and Mg, and the minor element Li, which are usually associated with detrital phases, were only slightly affected by the acetic-acid and the hydroxylamine—HCl leaches. However, they were noticeably affected by the hot 50% HCl leach (Table II). Nevertheless, most

TABLE II

Chemical results from the partition studies of selected D.S.D.P. sediments

Sample	Fe		Mn		Al_2O_3		TiO_2		Mg		Ca		Cu		Zn		Pb		Cr		Ni		Li		% of original
	a (%)	b (%)	a (%)	b (%)	a (%)	b (%)	a (%)	b (%)	a (%)	b (%)	a (%)	b (%)	a (p.p.m.)	b (%)	a (p.p.m.)	b (%)	a (p.p.m.)	b (%)	a (p.p.m.)	b (%)	a (p.p.m.)	b (%)	a (p.p.m.)	b (%)	
2-9A-5-1-90-92	7.35		0.26		10.5		0.52		1.15		0.40		42		90		70		50		28		18		
HAc	7.15	3	0.15	42	10.3	2	0.49	6	1.03	10	0.39	2	39	7	89	1	54	23	49	2	15	46	18	0	98.2
Hydrox	7.06	1	0.03	47	10.2	1	0.44	9	0.91	11	0.20	50	29	24	78	12	47	11	46	6	10	18	17	6	97.6
HCl	0.81	84	0.01	7	5.7	43	0.36	15	0.27	56	0.13	18	7	52	31	53	27	18	35	22	7	11	13	22	88.6
2-9A-3-4-125-127	5.40		0.57		10.0		0.49		1.06		0.55		113		162		55		37		67		20		
HAc	5.18	4	0.25	56	9.5	5	0.45	8	0.98	8	0.43	15	109	4	156	4	36	35	34	8	43	36	18	10	96.2
Hydrox	5.08	2	0.22	5	9.1	4	0.43	4	0.91	6	0.32	20	101	7	124	20	29	12	31	8	39	6	18	0	95.6
HCl	4.00	20	0.02	37	5.2	39	0.29	29	0.23	64	0.18	25	8	82	29	58	16	24	20	30	4	52	8	50	79.8
2-9A-3-1-105-107	7.63		0.86		12.4		0.69		1.47		0.55		174		167		100		75		138		25		
HAc	7.38	3	0.84	2	12.1	2	0.65	6	1.40	5	0.44	20	165	5	161	4	96	4	70	7	116	16	25	0	96.6
Hydrox	6.94	6	0.33	60	11.8	3	0.59	9	1.28	8	0.29	27	147	11	146	9	76	20	57	17	62	40	25	0	95.2
HCl	0.53	84	0.01	37	6.3	44	0.48	14	0.24	71	0.16	24	12	77	34	63	28	48	29	37	8	38	10	40	79.9
2-9A-1-6-50-52	4.40		0.80		15.6		0.59		0.58		0.55		189		152		65		105		172		73		
HAc	4.37	1	0.76	5	14.9	4	0.60	0	1.46	8	0.51	7	181	4	147	3	62	5	98	7	164	5	71	3	98.1
Hydrox	4.12	5	0.38	48	14.5	3	0.56	5	1.33	8	0.29	40	156	9	127	13	49	20	88	9	85	46	69	3	97.5
HCl	0.81	76	0.02	45	11.1	22	0.45	19	0.37	61	0.23	11	45	63	50	51	32	26	41	45	14	41	38	42	90.3
2-9A-1-1-25-27	5.00		0.74		16.6		0.52		1.63		1.60		238		152		85		60		160		80		
HAc	5.00	0	0.72	3	16.2	2	0.49	6	1.52	7	1.32	18	226	5	142	7	78	8	57	5	147	8	78	3	97.9
Hydrox	4.90	2	0.21	66	15.3	6	0.46	6	1.43	5	1.27	3	196	13	118	15	52	31	54	5	83	40	76	3	98.8
HCl	1.11	76	0.02	28	10.1	31	0.37	17	0.37	65	1.02	16	88	45	60	39	25	32	43	18	34	31	48	34	85.1
12-112-16--1-108-110	3.40		0.23		4.7		0.22		1.22		5.35		53		46		45		50		28		51		
HAc	3.31	3	0.22	4	4.6	1	0.22	0	1.17	4	0.32	94	52	2	46	0	35	22	48	4	26	7	51	0	86.1
Hydrox	3.05	7	0.02	87	4.5	2	0.20	9	1.13	3	0.22	2	44	15	42	9	26	20	42	12	16	36	51	0	87.0
HCl	0.47	76	0.01	5	2.9	35	0.12	37	0.25	73	0.17	1	10	64	21	45	12	31	15	54	4	43	22	57	83.0
12-114-6-6-140-142	6.90		0.10		9.9		2.32		1.83		11.1		71		116		60		75		48		15		
Hac	6.84	1	0.10	0	9.9	0	2.25	3	1.70	7	1.54	87	67	6	109	6	53	11	72	4	45	6	14	7	75.1
Hydrox	6.66	4	0.06	40	9.6	3	2.22	1	1.62	5	1.48	1	60	10	96	11	48	9	66	8	21	50	14	0	74.3
HCl	2.60	57	0.04	20	5.7	40	1.10	43	0.91	38	1.04	4	23	52	46	44	32	27	39	36	7	30	5	60	64.7
12-114-2-4-75-77	7.90		0.13		11.8		2.14		2.48		8.00		86		235		64		90		40		24		
HAc	7.72	2	0.12	8	11.6	2	2.08	3	2.20	11	0.86	89	79	8	228	3	54	10	87	3	36	10	22	8	81.6
Hydrox	7.28	6	0.10	15	10.8	6	1.88	9	2.10	4	0.80	1	73	7	214	6	48	10	75	14	30	15	20	9	80.4
HCl	2.27	63	0.02	62	5.4	46	0.94	44	0.86	50	0.63	2	23	59	65	63	20	47	29	51	7	58	6	58	72.3
12-118-19-1-50-52	5.40		0.66		16.7		0.81		1.20		0.60		67		136		77		63		95		65		
HAc	5.29	2	0.64	3	16.2	3	0.76	6	1.14	5	0.49	18	63	6	128	6	75	3	59	6	92	3	63	3	98.2
Hydrox	5.25	1	0.14	76	15.4	5	0.66	13	1.12	2	0.15	57	54	13	112	12	54	27	54	8	34	61	63	0	97.6
HCl	1.02	78	0.02	18	11.9	21	0.43	28	0.30	68	0.10	8	13	62	43	50	25	38	34	32	9	27	44	29	84.6

													0.24	71	0.16	24	12																
2-9A-1-6-50-52	4.40		0.80		15.6		0.59		0.58		0.55		189		152		65		105		172		73									
HAc	4.37	1	0.76	5	14.9	4	0.60	0	1.46	8	0.51	7	181	4	147	3	62	5	98	7	164	5	71	3	98.1							
Hydrox	4.12	5	0.38	48	14.5	3	0.56	5	1.33	8	0.29	40	156	9	127	13	49	20	88	9	85	46	69	3	97.5							
HCl	0.81	76	0.02	45	11.1	22	0.45	19	0.37	61	0.23	11	45	63	50	51	32	26	41	45	14	41	38	42	90.3							
2-9A-1-1-25-27	5.00		0.74		16.6		0.52		1.63		1.60		238		152		85		60		160		80									
HAc	5.00	0	0.72	3	16.2	2	0.49	6	1.52	7	1.32	18	226	5	142	7	78	8	57	5	147	8	78	3	97.9							
Hydrox	4.90	2	0.21	66	15.3	6	0.46	6	1.43	5	1.27	3	196	13	118	15	52	31	54	5	83	40	76	3	98.8							
HCl	1.11	76	0.02	28	10.1	31	0.37	17	0.37	65	1.02	16	88	45	60	39	25	32	43	18	34	31	48	34	85.1							
12-112-16--1-108-110	3.40		0.23		4.7		0.22		1.22		5.35		53		46		45		50		28		51									
HAc	3.31	3	0.22	4	4.6	1	0.22	0	1.17	4	0.32	94	52	2	46	0	35	22	48	4	26	7	51	0	86.1							
Hydrox	3.05	7	0.02	87	4.5	2	0.20	9	1.13	3	0.22	2	44	15	42	9	26	20	42	12	16	36	51	0	87.0							
HCl	0.47	76	0.01	5	2.9	35	0.12	37	0.25	73	0.17	1	10	64	21	45	12	31	15	54	4	43	22	37	81.5							
12-114-6-6-140-142	6.90		0.10		9.9		2.32		1.83		11.1		71		116		66		75		28											
Hac	6.84	1	0.10	0	9.9	0	2.25	3	1.70	7	1.54	87	67	6	109	6	53	11	72	4	45	0	14	3	75.1							
Hydrox	6.66	4	0.06	40	9.6	3	2.22	1	1.62	5	1.48	1	60	10	96	11	48	9	66	8	21	50	14	0	74.3							
HCl	2.60	57	0.04	20	5.7	40	1.10	43	0.91	38	1.04	4	23	52	46	44	32	27	39	36	7	30.	5	60	64.7							
12-114-2-4-75-77	7.90		0.13		11.8		2.14		2.48		8.00		86		235		64		90		40		24									
HAc	7.72	2	0.12	8	11.6	2	2.08	3	2.20	11	0.86	89	79	8	228	3	54	10	87	3	36	10	22	8	81.6							
Hydrox	7.28	6	0.10	15	10.8	6	1.88	9	2.10	4	0.80	1	73	7	214	6	48	10	75	14	30	15	20	9	80.4							
HCl	2.27	63	0.02	62	5.4	46	0.94	44	0.86	50	0.63	2	23	59	65	63	20	47	29	51	7	58	6	58	72.3							
12-118-19-1-50-52	5.40		0.66		16.7		0.81		1.20		0.60		67		136		77		63		95		65									
HAc	5.29	2	0.64	3	16.2	3	0.76	6	1.14	5	0.49	18	63	6	128	6	75	3	59	6	92	3	63	3	98.2							
Hydrox	5.25	1	0.14	76	15.4	5	0.66	13	1.12	2	0.15	57	54	13	112	12	54	27	54	8	34	61	63	0	97.6							
HCl	1.02	78	0.02	18	11.9	21	0.43	28	0.30	68	0.10	8	13	62	43	50	25	38	34	32	9	27	44	29	84.6							
12-118-18-2-50-52	4.91		0.66		16.1		0.69		1.19		0.97		67		131		123		80		58		65									
HAc	4.75	3	0.60	9	15.7	2	0.70	0	1.07	10	0.42	57	65	3	127	3	115	7	76	5	53	9	64	1	96.5							
Hydrox	4.28	10	0.10	76	14.7	7	0.64	7	0.95	10	0.21	22	50	22	108	15	79	27	70	8	24	50	63	2	95.2							
HCl	0.68	73	0.01	13	10.5	26	0.52	18	0.25	58	0.14	7	8	63	33	57	17	52	42	35	12	20	35	43	83.3							
14-136-8-1-50-52	7.20		0.21		12.5		3.50		2.14		6.90		70		114		60		110		97		47									
HAc	7.20	0	0.19	10	12.5	0	3.46	1	2.08	3	0.96	73	68	3	110	4	54	10	109	1	92	5	47	0	86.5							
Hydrox	7.10	1	0.05	71	12.1	3	3.29	5	2.05	1	0.78	8	53	21	84	22	38	28	96	12	47	47	46	2	84.9							
HCl	0.55	93	0.01	14	2.9	74	1.96	38	1.16	42	0.13	4	6	67	14	62	11	44	45	45	8	40	3	92	55.8							
14-136-6-1-100-102	6.35		0.25		14.9		2.32		2.27		2.40		91		178		70		105		58		51									
HAc	6.20	2	0.25	0	14.9	0	2.28	2	2.06	2	1.16	52	89	2	172	3	65	7	102	3	54	7	50	2	96.6							
Hydrox	5.86	6	0.06	80	14.3	4	2.16	5	1.80	12	0.24	38	75	16	115	32	48	24	93	8	24	52	49	2	96.0							
HCl	1.26	72	0.01	16	8.2	41	1.53	25	0.44	60	0.15	4	11	70	33	47	22	38	60	32	7	29	20	57	74.2							
14-137-16-4-90-92	1.33		0.40		2.9		0.23		0.59		30.2		63		83		95		45		88		12									
HAc	1.34	0	0.38	5	2.8	1	0.22	4	0.45	24	1.22	96	60	5	80	4	75	21	43	4	83	6	12	0	34.4							
Hydrox	1.20	10	0.03	87	2.8	2	0.19	13	0.37	13	0.68	2	38	35	32	57	14	43	37	14	34	55	10	17	31.7							
HCl	0.25	71	0.01	5	0.9	63	0.08	31	0.11	44	0.37	1	12	39	9	27	7	24	20	38	10	28	3	58	23.9							
14-137-16-3-90-92	2.53		0.22		4.5		0.23		0.83		18.3		30		66		57		43		30		14									
HAc	2.31	9	0.19	14	4.1	8	0.20	13	0.77	7	1.26	93	26	13	57	14	44	23	37	14	26	13	12	14	54.5							
Hydrox	2.08	9	0.03	72	3.8	7	0.18	9	0.71	7	1.09	1	16	34	41	9	26	31	31	14	10	54	11	7	51.5							
HCl	0.69	55	0.01	10	2.2	35	0.14	17	0.24	57	0.27	4	7	30	19	48	10	29	19	28	5	16	7	29	47.9							

TABLE II (*continued*)

Sample	Fe		Mn		Al_2O_3		TiO_2		Mg		Ca		Cu		Zn		Pb		Cr		Ni		Li		% of original
	a (%)	b (%)	a (%)	b (%)	a (%)	b (%)	a (%)	b (%)	a (%)	b (%)	a (%)	b (%)	a (p.p.m.)	b (%)	a (p.p.m.)	b (%)	a (p.p.m.)	b (%)	a (p.p.m.)	b (%)	a (p.p.m.)	b (%)	a (p.p.m.)	b (%)	
14-138-6-3-145-147	3.78		0.84		5.8		0.29		6.05		12.1		69		127		85		80		123		16		
HAc	3.54	1	0.66	21	5.7	1	0.28	3	5.45	10	10.1	17	63	9	120	6	77	9	77	4	110	11	16	0	96.1
Hydrox	3.05	2	0.21	54	4.9	15	0.23	14	3.61	30	5.55	46	42	30	76	34	50	32	66	14	55	44	14	12	84.0
HCl	1.86	48	0.03	21	3.3	28	0.14	35	0.49	52	0.28	44	18	35	29	37	21	34	40	32	18	30	10	25	69.5
14-138-6-3-20-22	3.90		0.48		8.7		0.34		3.92		7.80		164		158		65		75		50		24		
HAc	3.62	7	0.27	44	8.6	1	0.32	6	3.47	12	5.46	30	152	7	141	11	55	15	71	5	38	24	24	0	94.8
Hydrox	2.74	23	0.12	31	6.5	24	0.23	26	2.21	6	3.51	35	115	23	79	39	19	71	30	55	19	38	18	25	74.5
HCl	1.37	35	0.01	23	4.2	27	0.18	17	0.39	72	0.20	42	65	30	26	34	16	4	26	5	9	44	10	33	65.3
Summary of the partition studies																									
Attack:																									
HAc		3		14		2		4		9		48		6		5		13		5		13		3	
Hydrox		6		57		6		9		8		21		18		20		26		13		41		5	
HCl		66		23		38		27		58		13		56		49		32		34		34		46	
Residue*		25		6		52		60		25		18		20		26		29		48		12		46	

*The values listed along the row marked "Residue" have been determined by subtraction.
The rows labelled with the sample number list the bulk chemical concentrations in the samples. The rows labelled HAc (acetic acid attack), Hydrox (combined acid-reducing agent attack), and HCl (hot 50% HCl attack) refer to the type of partial attack. Column *a* presents the chemical concentrations recalculated to the original sample weight and column *b* presents the percentage of metal removed by each attack.

of the Mg was removed by tl
Mg is associated with clay m
alumino-silicates. Roughly e
by the HCl as remained undi

Some of the basal and nor
9-9A-3-4-125-127, 14-36-16-
90-22) displayed rather unus
percentage of the Mn in thes
attack. This type of Mn beha
by Goldberg and Arrhenius (
Copeland (1970). Copeland
acid is used to attack carbon
broken down and the Mn wi
and Arrhenius (1958) and Cl
ability of dilute acetic acid t
effect being solution of both
(1967) have found that aceti
from mineral surfaces and fr
the D.S.D.P. samples are rela
14-137-16-4-90-92, 14-138-6
of acetic acid on Mn-coated
therefore, the majority of th
from a combination of the o

VARIATIONS IN METAL ENRI
TIME

Examination of the data p
Mn, Al and Ti concentrations
true oceanic basement was th
difference in the concentratio
Mn principally reflect the abu
Al and Ti reflect the abundar
enrichments occurred in the
enrichments occurred in the
composition, as can be seen
markedly but appears to hav
(site 136), the Paleocene (sit
Pliocene (site 114).

In order to directly compa
necessary to remove the dilu
organic matter, dried sea salt
data was normalized followi
(1972). However, P has not
with biogenic activity and/o
calculated Al/4 Al + Fe + M

of the Mg was removed by the HCl, probably indicating that most of the Mg is associated with clay minerals and other less resistant silicates and alumino-silicates. Roughly equivalent concentrations of Li were removed by the HCl as remained undissolved in the residue.

Some of the basal and non-basal sediments (samples 2-9A-5-1-90-92, 2-9A-3-4-125-127, 14-36-16-3-90-92, 14-138-6-3-145-147, and 14-138-6-3-20-22) displayed rather unusual Mn partition patterns. A relatively high percentage of the Mn in these samples was removed by the acetic-acid attack. This type of Mn behavior has been previously noted in sediments by Goldberg and Arrhenius (1958), Chester and Hughes (1967) and Copeland (1970). Copeland (1970) has shown that if an excess of acetic acid is used to attack carbonate-rich sediments, then Mn coatings can be broken down and the Mn will go into solution. Furthermore, both Goldberg and Arrhenius (1958) and Chester and Hughes (1967) have noted the ability of dilute acetic acid to attack on unidentified metal hydrate; the effect being solution of both Mn and Fe. In addition, Chester and Hughes (1967) have found that acetic acid has the ability to remove adsorbed Mn from mineral surfaces and from exchange sites in clays. Because most of the D.S.D.P. samples are relatively low in carbonate, (except samples 14-137-16-4-90-92, 14-138-6-3-145-147 and 14-138-6-3-20-22) the effect of acetic acid on Mn-coated carbonate is not likely to be too important; therefore, the majority of the Mn removed by the acid probably derives from a combination of the other sources listed above.

VARIATIONS IN METAL ENRICHMENT IN THE NORTH ATLANTIC THROUGH TIME

Examination of the data presented in Table III (listing the average Fe, Mn, Al and Ti concentrations for the basal sediments from each site where true oceanic basement was thought to be encountered) indicates a marked difference in the concentrations of these elements through time. Fe and Mn principally reflect the abundance of authigenic constituents whilst Al and Ti reflect the abundance of detrital constituents. The largest Mn enrichments occurred in the Late Albian (site 137) and the largest Fe enrichments occurred in the Late Paleocene (site 117A). Detrital input or composition, as can be seen from the Al and Ti variations, also varied markedly but appears to have been greatest during the Aptian—Cenomanian (site 136), the Paleocene (sites 118 and 117A) and during the Miocene—Pliocene (site 114).

In order to directly compare basal sediments of different ages, it is necessary to remove the diluting effects of biogenic carbonate and silicate, organic matter, dried sea salt and zeolitic water. To accomplish this, the data was normalized following the procedures outlined by Bostrom et al. (1972). However, P has not been included because of its known association with biogenic activity and/or organic matter (Bostrom et al., 1972). The calculated Al/4 Al + Fe + Mn + Ti ratios should provide a strong indication

TABLE III

Average concentrations and Al/4 Al + Fe + Mn + Ti ratios for basal D.S.D.P. sediments of varying ages

Hole	Age name	Age (m.y.B.P.)	Fe(%)	Mn(%)	Al(%)	Ti(%)	R*
136	Aptian—Cenomanian	~106	7.3	0.14	6.60	1.80	0.19
137	Late Albian	~103	5.2	0.61	4.70	0.30	0.19
9A	Santonian	~ 82	6.0	0.17	4.60	0.23	0.19
10	Campanian	~ 76	2.3	0.46	2.20	0.46	0.18
118	Paleocene	~ 61	4.7	0.41	8.50	0.48	0.22
117A	Upper Paleocene	~ 56	10.5	0.08	7.70	1.20	0.18
112	Paleocene—Eocene	~ 54	7.0	0.12	5.30	0.29	0.18
114	Miocene—Pliocene	~ 11	9.6	0.12	6.70	1.70	0.18

*R = Al/4 Al + Fe + Mn + Ti ratio.

According to Bostrom et al. (1972), normalization to 4 Al + Fe + Mn + Ti should remove the diluting effects of biogenic carbonate and silicate, dried sea-salts, organic matter, and zeolitic water. As the concentration of the detrital phases (as indicated by Si = 3 Al, Al, and Ti) increases, the ratio will also increase whilst as the authigenic constituents increase (as indicated by Fe and Mn), the ratio will decrease. The average values for Fe, Mn, Al, and Ti were determined from the basal sediments, in the appropriate holes, and are marked with an asterisk (*) in Table I. The various ages listed in the table are based on the microfossil assemblages reported in the pertinent volumes of the *Initial Reports*.

of the amount of metals tied up in authigenic phases (represented by the Fe and Mn) as well as the amount present in detrital constituents (represented by Si = 3Al, Al, and Ti), and should, because of the removal of most of the dilutents normally present in marine sediments, permit the direct comparison of the authigenic constituents of sediments from different locations and of different ages. As the detrital phases increase, the ratio will increase whilst as the authigenic constituents increase, the ratio will decrease.

As can also be seen from Table III the ratio for the Paleocene (site 118) differs from all the others in that it is significantly higher (0.22 as compared to either 0.18 or 0.19). This could indicate either a decrease in authigenic mineral deposition or an increase and/or alteration in the chemistry of detrital input during this period in comparison with the sediments of other ages. The latter alternative is favored in view of both the high Al content of the Paleocene sediments (Table III) and their mineralogy (Laughton et al., 1972). This change may be related to the major reshuffling of spreading centers which occurred in the North Atlantic around this time (Le Pichon et al., 1971; Laughton et al., 1972).

With the exception of the Paleocene sediments, basal North Atlantic material appears to be fairly uniform geochemically on the basis of the Al/4 Al + Fe + Mn + Ti ratios. This would indicate that both authigenic mineral deposition and detrital input have been, on average, relatively constant in this area except for the Paleocene, since Aptian—Cenomanian times (about 106 m.y.B.P.).

THE GEOCHEMISTRY OF SE

Sediments recovered at I
D.S.D.P. 9A, have been exa
the very bottom of hole 9A
sediments are depleted in F
hole 9. This result is unusu
basement are usually enrich
1972; Bostrom et al., 1972
due to the post-depositiona
migration of Mn and some

The description of the b
that they contain both side
1970). As both minerals ar
(Krumbein and Garrels, 19
material. It seems much m
sediments were deposited,
more reducing. Under such
(1973) have shown that th
is variable but the general
elements. This type of bel
sediments of 9A in such n
those above (Tables I and

The partition patterns
(Table II), are somewhat
and Ni were soluble in th
below, and then diffused
reaching sufficiently oxic
possible that at least part
number of the mineral gr
at the same time, these fi
Ni, and Pb. As has been
be attacked by acetic aci
the view that post-depos
not contradict it.

It should be noted th
appearing to have occur
spread process in North
based on data from the
the amounts of siderite
large, and both minerals

THE GEOCHEMISTRY OI

In order to investiga
the possibility of basal

basal D.S.D.P. sediments

Al(%)	Ti(%)	R*
6.60	1.80	0.19
4.70	0.30	0.19
4.60	0.23	0.19
2.20	0.46	0.1[illegible]
8.50	0.48	0.2[illegible]
7.70	1.20	0.1[illegible]
5.30	0.29	0.1[illegible]
6.70	1.70	0.1[illegible]

[illegible] + Mn + Ti should remove
salts, organic matter, and
dicated by Si = 3 Al. Al,
genic constituents increase
e values for Fe, Mn, Al,
priate holes, and are
the table are based on
f the *Initial Reports*.

represented by the
onstituents (represent
moval of most of the
t the direct comparison
rent locations and of
will increase whilst
decrease.
Paleocene (site 118)
her (0.22 as compared
crease in authigenic
the chemistry of
ne sediments of other
he high Al content
ralogy (Laughton et al.,
ffling of spreading
this time (Le Pichon

al North Atlantic
n the basis of the
at both authigenic
erage, relatively
ptian—Cenomanian

THE GEOCHEMISTRY OF SEDIMENTS FROM D.S.D.P. 9A

Sediments recovered at D.S.D.P. 9, above those investigated here from D.S.D.P. 9A, have been examined geochemically by Bruty et al. (1973). At the very bottom of hole 9A (samples from core 5, sections 1 and 2), the sediments are depleted in Fe, Mn, Cu; Zn, Pb, and Ni relative to those from hole 9. This result is unusual as the basal sediments nearest to the basaltic basement are usually enriched in many of these metals, (Cronan et al., 1972; Bostrom et al., 1972; Dymond et al., 1973; this study), and may be due to the post-depositional breakdown of Mn oxides and the upward migration of Mn and some of its associated metals.

The description of the basal sediments from hole 9A includes a report that they contain both siderite ($FeCO_3$) and rhodocrocite ($MnCo_3$) (Rex, 1970). As both minerals are relatively unstable under oxidizing conditions (Krumbein and Garrels, 1952) it is unlikely that they represent detrital material. It seems much more likely that they formed after the basal sediments were deposited, when the depositional environment became more reducing. Under such mildly reducing conditions, Duchart et al. (1973) have shown that the behavior of Fe and Cu as well as Zn, Ni, and Pb is variable but the general trend is for the upward mobility of all these elements. This type of behavior might explain the depletion of the basal sediments of 9A in such metals as Fe, Mn, Ni, Cu, Zn and Pb relative to those above (Tables I and IV).

The partition patterns for samples from both sections of the hole (Table II), are somewhat unusual in that a large proportion of the Mn, Pb, and Ni were soluble in the acetic acid. If these metals were mobilized from below, and then diffused upward, they could have been redeposited upon reaching sufficiently oxidizing sediments. Under these conditions, it is possible that at least part of the Mn was deposited as thin oxide films on a number of the mineral grains or may have been adsorbed onto clay minerals; at the same time, these films would also scavenge the remobilized Cu, Zn, Ni, and Pb. As has been mentioned previously, this type of Mn deposit can be attacked by acetic acid. Therefore, the partitioning patterns could support the view that post-depositional migration has occurred, and certainly do not contradict it.

It should be noted that post-depositional migration of elements, although appearing to have occurred in hole 9A, does not seem to be a very widespread process in North Atlantic D.S.D.P. sediments. This conclusion is based on data from the *Initial Reports* (II, XII, and XIV) which indicate that the amounts of siderite and rhodocrocite reported in these cores is not very large, and both minerals have been found at only three other North Atlantic sites.

THE GEOCHEMISTRY OF SEDIMENTS FROM D.S.D.P. 114

In order to investigate both long-term geochemical variations, as well as the possibility of basal metalliferous sediments occurring near the Reykjanes

TABLE IV

Comparison of the chemical composition of sediments from holes 9 and 9A

Samples	Fe (%)	Mn (%)	Al (%)	Ti (%)	Mg (%)	Cu (p.p.m.)	Zn (p.p.m.)	Pb (p.p.m.)	Cr (p.p.m.)	Ni (p.p.m.)	Li (p.p.m.)
9A basal	6.00	0.17	8.63	0.38	0.75	29	62	48	55	24	22
9A non-basal	4.95	0.48	11.9	0.54	1.30	135	144	74	72	98	37
9A all samples	5.35	0.37	10.6	0.47	1.09	95	113	64	62	70	31
9*	7.01	0.30	—	—	—	92	151	68	111	112	—

*Results from Bruty et al. (1973).

Ridge, a series of samples fr
Ridge, were analyzed (Table
core 2, and some of the I
or the D.S.D.P. 114 sample
and near-surface samples ob
1974a, b). This would tend
sediments in this region has
times.

There are no apparent tre
The basal sediments in the c
metalliferous sediments fro
elevated concentrations of I
ridge sediments from the sa
sediments obtained further
contain higher concentratio
this situation, a sample of b
from core 2 (12-114-2-4-75
chemical attacks (Table II).
partition patterns are simila
Reykjanes Ridge crest (Hor
the North Atlantic in that t
the other enriched metals ar
all phases. By contrast, the s
pattern similar to that displ
inactive Iceland—Faroes Ric

The presence at this site c
found on the crest of the Re
because the sediments direc
younger (according to the m
basalt (estimated by paleom
metalliferous active-ridge an
the extrusion of new basalt
their formation are based o
involved. Recently, Bertine
can form from the submarir
with the formation of ferro
metal from seawater. Consi
at site 114 at the time the b
be a more likely explanatio
than direct association with

THE GEOCHEMISTRY OF SE

The igneous rock encoun
on both petrographic and s
not true oceanic basement

Ridge, a series of samples from site 114, drilled on the eastern flank of the Ridge, were analyzed (Table I). With the exception of some of the Zn values in core 2, and some of the Li values in core 1, all the metal concentrations for the D.S.D.P. 114 samples fall within the ranges found for the surface and near-surface samples obtained in this area (Sarginson, 1970; Horowitz, 1974a, b). This would tend to indicate that the geochemistry of the sediments in this region has been fairly constant since Miocene—Pliocene times.

There are no apparent trends which extend through the entire sequence. The basal sediments in the core appear to be analogous to the surface metalliferous sediments from the Reykjanes Ridge crest which contain elevated concentrations of Fe, Mn, Cu, Cr, Zn, Ni, Al, and Ti relative to non-ridge sediments from the same latitude (Horowitz, 1974a). However, sediments obtained further above the basement, notably those from core 2, contain higher concentrations of Mn, Zn, and Cr. In order to try and clarify this situation, a sample of basal sediment (12-114-6-6-140-142) and a sample from core 2 (12-114-2-4-75-77) were subjected to a series of partial chemical attacks (Table II). The results indicate that the basal sediment partition patterns are similar to those in present-day sediments from the Reykjanes Ridge crest (Horowitz, 1974a) as well as other sediments from the North Atlantic in that the Fe and Mn are largely in separate phases and the other enriched metals are distributed, in varying amounts, throughout all phases. By contrast, the sample from core 2 displays a detrital-type pattern similar to that displayed by sediments found on the surface of the inactive Iceland—Faroes Ridge (Horowitz, 1974a).

The presence at this site of basal sediments similar in composition to those found on the crest of the Reykjanes Ridge today is somewhat unusual because the sediments directly overlying the basalt appear to be 7 m.y. younger (according to the microfossil assemblages) than the age of the basalt (estimated by paleomagnetic means, Laughton et al., 1972). Normally, metalliferous active-ridge and basal sediments are directly associated with the extrusion of new basalt and most of the theories proposed to explain their formation are based on the fact that elevated temperatures are involved. Recently, Bertine (1974) has suggested that metalliferous sediments can form from the submarine weathering of cold tholeiitic basalt combined with the formation of ferromanganese oxides which scavenge additional metal from seawater. Considering the conditions that probably prevailed at site 114 at the time the basal sediments were deposited, this appears to be a more likely explanation for the formation of these sediments rather than direct association with active-ridge volcanism.

THE GEOCHEMISTRY OF SEDIMENTS FROM D.S.D.P. 138

The igneous rock encountered at the bottom of site 138 was considered on both petrographic and stratigraphic grounds to be a basaltic sill and not true oceanic basement (Hayes et al., 1972). In spite of these observa-

tions, the analytical results for the sediments obtained from the lowermost core section at this site (6-3, Table I), bear a strong resemblance to sediments that have been found in contact with normal oceanic basement in the North Atlantic (Table I), and to present-day surface Atlantic active-ridge metalliferous sediments. The sediments from section 6-3, when compared with the overlying material from section 6-2, contain higher concentrations of Mn, Mg, and Pb and lower concentrations of Al, Ti, and Cr (Table I), the Mn levels are amongst the highest in the D.S.D.P. North Atlantic suite. In addition, if sample 14-138-6-2-145-147 which contains detrital pyrite (Hayes et al., 1972) is excluded, then the sediments from section 6-3 also contain more Fe than the overlying deposits.

The partitioning patterns for two samples from the basal section (14-138-6-3-145-147 and 14-138-6-3-20-22) were similar to the partitioning patterns of other North Atlantic basal sediments (Table II). However, the acetic-acid leach removed significant quantities of the Mn as it did in samples from 9A. The basal sediments from this site contain large amounts of both ankerite and dolomite and the latter shows signs of secondary growth (Hayes et al., 1972). Some of the Mn in these sediments was probably incorporated as oxide coatings on these minerals and this factor, in addition to the others mentioned previously, would probably explain the acetic-acid-soluble Mn. Thus, on the grounds of both bulk geochemical data, as well as partitioning patterns, the basal sediments from site 138 appear to be similar to basal sediments from other parts of the North Atlantic which were deposited in contact with true oceanic basement.

These findings suggest that metalliferous sediments can occur simply in the presence of basalt, and the actual presence of an active ridge may not be necessary for their formation. This would tend to support the views of Corliss (1971) and Bertine (1974), that the metalliferous sediments found in association with active oceanic ridges are due to the presence of basalt which has been leached by seawater rather than to some type of deep-seated volcanic emanation associated with sea-floor spreading as proposed by Bostrom and his co-workers (1966, 1969, 1972 etc.).

If this conclusion is correct, it is necessary to explain why metalliferous sediments have not been reported to date on inactive, but basaltic oceanic ridges. The results from site 138, as well as from basal North Atlantic and Pacific D.S.D.P. cores indicate that the effects of the basalt occur over only very short distances (Von der Borch and Rex, 1970; Cronan et al, 1972; Cronan, 1974). Therefore, the effects of the underlying basalt would not be expected to appear in the surface sediments on inactive ridges which are covered by substantial sediment deposits. Nevertheless, material cored near the basaltic surface of an inactive ridge would, on the basis of the findings at D.S.D.P. 138, be expected to have elevated metal concentrations. Bostrom et al. (1972) have investigated such near-basement material (site 21, Leg III, D.S.D.P.) recovered on the inactive Rio Grande Rise and report that they have relatively high Mn concentrations (2.2 to 5.0% on a carbonate free

basis). In addition, the Al/
Rise are similar to those fo
factors would tend to indi
Rio Grande Rise are simila
sea-floor spreading. This v
enrichments in basal and a
a volcanic process peculia
anywhere in the ocean in
Additional support for thi
observation that basal sed
East Ridge in the Indian C
as well as enriched Cu, Zn
(Fleet, personal communi

It is evident from these
produce metal-rich sedim
basalt in contact with sol
sources for most of the e
a combination of hydroth
(1971), submarine weath
scavenged for seawater b
of metalliferous sedimen
active-ridge areas.

CONCLUSIONS

(1) Basal sediments fr
ing material, are enriche
Ti, Cu, Zn, and Li. The
not as high as those repo
in the North Atlantic bu
overlying material, they

(2) The partitioning
are similar to those repo
pelagic sediments. The
metals are distributed,
partitioning patterns in
tion in basal North Atl
is consistent with the h
Atlantic and is in agree
sediments from both o

(3) On the basis of
in the composition of
ever, recalculation of t
and zeolitic water free
authigenic mineral dep
Cenomanian (106 m.y

basis). In addition, the Al/4 Al + Fe + Mn + Ti ratios for the Rio Grande Rise are similar to those found for basal North Atlantic sediments. These factors would tend to indicate that the basal sediments from the inactive Rio Grande Rise are similar to those overlying past and present sites of sea-floor spreading. This would further support the view that the metal enrichments in basal and active-ridge sediments are not necessarily due to a volcanic process peculiar to active mid-ocean ridges, but can occur anywhere in the ocean in conjunction with submarine volcanic processes. Additional support for this contention is forthcoming from the recent observation that basal sediments overlying basalt on the inactive Ninety–East Ridge in the Indian Ocean also display elevated Mn concentrations as well as enriched Cu, Zn and Ni levels relative to the overlying sediment (Fleet, personal communication, 1974).

It is evident from these observations that heat may not be necessary to produce metal-rich sediments and that all that is required is the presence of basalt in contact with solutions able to leach it. It appears likely that the sources for most of the enriched metals in sediments on active ridges are a combination of hydrothermal activity of the type described by Corliss (1971), submarine weathering as described by Bertine (1974), and metals scavenged for seawater by ferromanganese oxides. Therefore, the formation of metalliferous sediments in the oceans may not be restricted solely to active-ridge areas.

CONCLUSIONS

(1) Basal sediments from the North Atlantic, when compared with overlying material, are enriched in Fe, Mn, Mg, Ni, Cr, and Pb and depleted in Al, Ti, Cu, Zn, and Li. The absolute values of the enriched metals are generally not as high as those reported for present-day active-ridge surface sediments in the North Atlantic but, as they contain higher concentrations than the overlying material, they have been termed metalliferous.

(2) The partitioning patterns of both the basal and non-basal sediments are similar to those reported for other basal sediments and for normal pelagic sediments. The Fe and Mn is largely in separate phases and the other metals are distributed, in varying amounts, throughout all phases. The partitioning patterns indicate that there is a much larger detrital contribution in basal North Atlantic sediments than in basal Pacific sediments. This is consistent with the high detrital sedimentation rates reported for the Atlantic and is in agreement with data from present-day active-ridge surface sediments from both oceans.

(3) On the basis of bulk analyses, there have been significant variations in the composition of basal North Atlantic sediments through time. However, recalculation of the data on a carbonate, silica, sea-salt, organic matter, and zeolitic water free basis indicates that the nature of detrital input and authigenic mineral deposition, has been relatively constant since Aptian–Cenomanian (106 m.y. B.P.) times. One exception appears to be the

Paleocene (site 118) when a significant increase in detrital sedimentation occurred.

(4) The bulk geochemistry, partitioning patterns, and mineralogy of sediments from site 9A indicates that post-depositional migration of such elements as Mn, Ni, Cu, Zn, and Pb may have occurred. In order to evaluate the extent of this phenomenon throughout the North Atlantic, additional geochemical and mineralogical studies on other D.S.D.P. North Atlantic samples are required.

(5) Detailed geochemical studies on sediments recovered on the eastern flank of the Reykjanes Ridge (site 114) indicate that the basal sediments are slightly enriched in Fe, Mn, Al, Ti, Zn, Cr, and Ni which would make them analogous to those found on the surface of the Reykjanes Ridge today.

(6) Although basalt was encountered at the bottom of site 138, it was judged to be a basaltic sill rather than true oceanic basement. The overlying sediments, however, are geochemically similar to "normal" basal and active ridge metalliferous material. The results from this site and site 114, as well as those that have already been published on basal material recovered overlying basalt on the inactive Rio Grande Rise, would indicate that the predominant processes, for metal enrichment in sediments overlying both mid-ocean ridges and other submarine volcanic features, is a combination of shallow hydrothermal activity, submarine weathering of basalt, and the precipitation of ferromanganese oxides. Furthermore, the formation of these sediments can continue after active volcanism has ceased.

ACKNOWLEDGEMENTS

The work described in this paper was conducted in the A.G.R.G. Imperial College under a grant from the U.K. Natural Environment Research Council. Deep Sea Drilling Project samples were supplied through the assistance of the U.S. National Science Foundation. This paper formed part of the Ph.D. dissertation of one of the authors (A.H.) which was submitted to the University of London.

REFERENCES

Bender, M., Broecker, W., Gornitz, V., Middel, U., Kay, R., Sun, S. and Biscaye, P., 1971. Geochemistry of three cores from the East Pacific Rise. Earth Planet. Sci. Lett., 12: 425—433.

Bertine, K., 1974. Origin of Lau Basin sediments. Geochim. Cosmochim. Acta, 38: 629—640.

Bonatti, E., Fisher, D., Joensuu, O. and Rydell, H., 1971. Postdepositional mobility of some transition elements, phosphorus, uranium, and thorium in deep-sea sediments. Geochim. Cosmochim. Acta, 35: 189—201.

Bostrom, K. and Peterson, M., 1966. Precipitates from hydrothermal exhalations on the East Pacific Rise. Econ. Geol., 61: 1258—1265.

Bostrom, K. and Peterson, M., 1969. Origin of aluminum-poor sediments in areas of high heat flow on the East Pacific Rise. Mar. Geol., 7: 427—447.

Bostrom, K., Peterson, M., Joensuu, O
ferromanganese sediments on active
Bostrom, K., Joensuu, O., Valdes, S. a
Atlantic Ocean sediments since Lat
Bruty, D., Chester, R., Royle, L. and
North Atlantic deep-sea sediments.
Bruty, D., Chester, R. and Aston, S., 1
sea sediments. Nature Phys. Sci., 24
Chester, R. and Hughes, M., 1966. The
a North Pacific deep-sea clay core.
Chester, R. and Hughes, M., 1967. A c
ganese minerals, carbonate minerals
sediments. Chem. Geol., 2: 249—26
Chester, R. and Hughes, M., 1969. Tra
clay core. Deep-Sea Res., 16: 639—
Chester, R. and Messiha-Hanna, R., 19
Atlantic deep-sea sediments. Geoch
Cook, H., 1971. Iron and manganese r
equatorial Pacific, Leg IX, D.S.D.P.
530—531.
Copeland, R., 1970. Trace Element Di
Thesis, Massachusetts Institute of T
Corliss, J., 1971. The origin of metal-l
J. Geophys. Res., 76: 8128—8138.
Cronan, D., 1972. The Mid-Atlantic R
ferruginous sediments from the Me
Cronan, D., 1974. Authigenic mineral
In: E. Goldberg (Editor), The Sea.
Cronan, D. and Garrett, D., 1973. Th
sediments collected during the D.S
Cronan, D., Van Andel, Tj., Heath, G
Charleston, S., Knapps, A., Rodol
sediments from the eastern equato
61—63.
Cronan, D., Damiani, V., Kinsman, D
Aden and western Indian Ocean.
of the D.S.D.P. U.S. Government
Duchart, P., Calvert, S. and Price, N.
waters of shallow marine sedimen
Dymond, J., Corliss, J., Heath, G., F
metalliferous sediments from the
Goldberg, E. and Arrhenius, G., 195
Cosmochim. Acta, 13: 153—212.
Hayes, D., et al., 1972. Initial Repo
Printing Office, Washington, D.C
Heath, G. and Moberly, R., 1971. N
Pacific, Leg VII, D.S.D.P. In: E.
Sea Drilling Project. U.S. Goverr
987—990.
Horowitz, A., 1970. The distributic
oceanic ridges. Mar. Geol., 9: 24
Horowitz, A., 1974a. The Geochen
Ridge and the Iceland—Faroes F
Horowitz, A., 1974b. Geochemical
Mid-Atlantic Ridge. Thesis, Uni

Bostrom, K., Peterson, M., Joensuu, O. and Fisher, D., 1969. Aluminum-poor ferromanganese sediments on active oceanic ridges. J. Geophys. Res., 74: 3261—3270.
Bostrom, K., Joensuu, O., Valdes, S. and Riera, M., 1972. Geochemical history of South Atlantic Ocean sediments since Late Cretaceous. Mar. Geol., 12: 85—121.
Bruty, D., Chester, R., Royle, L. and Elderfield, H., 1972. Distribution of zinc in North Atlantic deep-sea sediments. Nature Phys. Sci., 237: 86—87.
Bruty, D., Chester, R. and Aston, S., 1973. Trace elements in ancient Atlantic deep-sea sediments. Nature Phys. Sci., 245: 73—74.
Chester, R. and Hughes, M., 1966. The distribution of manganese, iron, and nickel in a North Pacific deep-sea clay core. Deep-Sea Res., 13: 627—634.
Chester, R. and Hughes, M., 1967. A chemical technique for the separation of ferromanganese minerals, carbonate minerals, and adsorbed trace elements from pelagic sediments. Chem. Geol., 2: 249—262.
Chester, R. and Hughes, M., 1969. Trace element geochemistry of a North Pacific pelagic clay core. Deep-Sea Res., 16: 639—654.
Chester, R. and Messiha-Hanna, R., 1970. Trace element partition patterns in North Atlantic deep-sea sediments. Geochim. Cosmochim. Acta, 34: 1121—1128.
Cook, H., 1971. Iron and manganese rich sediments overlying oceanic basalt basement, equatorial Pacific, Leg IX, D.S.D.P. Geol. Soc. Am. (abstract with programs), 3(7): 530—531.
Copeland, R., 1970. Trace Element Distribution in Sediments of the Mid-Atlantic Ridge. Thesis, Massachusetts Institute of Technology, Cambridge, Mass.
Corliss, J., 1971. The origin of metal-bearing submarine hydrothermal solutions. J. Geophys. Res., 76: 8128—8138.
Cronan, D., 1972. The Mid-Atlantic Ridge Near 45° N. XVII, Al, As, Hg, and Mn in ferruginous sediments from the Median Valley. Can. J. Earth Sci., 9: 319—323.
Cronan, D., 1974. Authigenic minerals in deep-sea sediments. In: E. Goldberg (Editor), The Sea. Wiley, New York, N.Y., 5: 491—525.
Cronan, D. and Garrett, D., 1973. The distribution of elements in metalliferous Pacific sediments collected during the D.S.D.P. Nature Phys. Sci., 242: 88—89.
Cronan, D., Van Andel, Tj., Heath, G., Dinkleman, M., Bennett, R., Bukry, D., Charleston, S., Knapps, A., Rodolfo, K. and Yeats, R., 1972. Iron-rich basal sediments from the eastern equatorial Pacific: Leg XVI, D.S.D.P. Science, 175: 61—63.
Cronan, D., Damiani, V., Kinsman, D. and Thiede, J., 1974. Sediments from the Gulf of Aden and western Indian Ocean. In: R. L. Fischer et al. (Editors), Initial Reports of the D.S.D.P. U.S. Government Printing Office, Washington, D.C., XXIV: 1047—1110.
Duchart, P., Calvert, S. and Price, N., 1973. Distribution of trace metals in the pore waters of shallow marine sediments. Limnol. Oceanogr., 18: 605—610.
Dymond, J., Corliss, J., Heath, G., Field, C., Dasch, J. and Veeh, H., 1973. Origin of metalliferous sediments from the Pacific Ocean. Geol. Soc. Am. Bull., 84: 3355—3372.
Goldberg, E. and Arrhenius, G., 1958. Chemistry of Pacific pelagic sediments. Geochim. Cosmochim. Acta, 13: 153—212.
Hayes, D., et al., 1972. Initial Reports of the Deep Sea Drilling Project. U.S. Government Printing Office, Washington, D.C. VII: 156 pp.
Heath, G. and Moberly, R., 1971. Noncalcareous pelagic sediments from the western Pacific, Leg VII, D.S.D.P. In: E. Winterer et al. (Editors), Initial Reports of the Deep Sea Drilling Project. U.S. Government Printing Office, Washington, D.C., VII: 987—990.
Horowitz, A., 1970. The distribution of Pb, Ag, Sn, Tl, and Zn in sediments on active oceanic ridges. Mar. Geol., 9: 241—259.
Horowitz, A., 1974a. The Geochemistry of sediments from the northern Reykjanes Ridge and the Iceland—Faroes Ridge. Mar. Geol., 17: 103—122.
Horowitz, A., 1974b. Geochemical Investigations of Sediments Associated with the Mid-Atlantic Ridge. Thesis, University of London, 247 pp.

Krumbein, W. and Garrels, R., 1952. Origin and classification of chemical sediments in terms of pH and oxidation—reduction potentials. J. Geol., 60: 1—33.

Ku, T., Broeker, W. and Opdyke, N., 1968. Comparison of sedimentation rates measured by paleomagnetic and the ionium methods of age determination. Earth Planet. Sci. Lett., 4: 1—16.

Laughton, A., 1972. The southern Labrador Sea — A key to the Mesozoic and Early Tertiary evolution of the North Atlantic. In: A. Loughton et al. (Editors), Initial Reports of the Deep Sea Drilling Project. U.S. Government Printing Office, Washington, D.C., XII: 1155—1179.

Laughton, A., et al., 1972. Initial Reports of the Deep Sea Drilling Project. U.S. Government Printing Office, Washington, D.C., XII: 1243 pp.

LePichon, X., Hyndman, R. and Pautot, G., 1971. Geophysical study of the opening of the Labrador Sea. J. Geophys. Res., 76: 4724—4733.

Peterson, M. et al., 1970. Initial Reports of the Deep Sea Drilling Project. U.S. Government Printing Office, Washington, D.C., II: 501 pp.

Piper, D., 1973. Origin of metalliferous sediments from the East Pacific Rise. Earth Planet. Sci. Lett., 19: 75—82.

Rex, R., 1970. X-ray mineralogy studies — Leg II. In: M. Peterson et al. (Editors), Initial Reports of the Deep Sea Drilling Project. U.S. Government Printing Office, Washington, D.C., II: 329—346.

Sayles, F. and Bischoff, J., 1973. Ferromanganoan sediments in the equatorial east Pacific. Earth Planet. Sci. Lett., 19: 330—336.

Sarginson, M., 1970. Geochemical Studies of Sediments from the Gulf of Paria, Venezuela: and the Atlantic Ocean North of the Faroe Islands. Thesis, University of Durham.

Von der Borch, C. and Rex, R., 1970. Amorphous iron oxide precipitates in sediments cored during Leg V, D.S.D.P. In: D. McManus et al. (Editors). Initial Reports of the Deep Sea Drilling Project. U.S. Government Printing Office, Washington, D.C., V: 541—544.

Von Der Borch, C., Nesteroff, W. and Galehouse, J., 1971. Iron-rich sediments cored during Leg VIII of the D.S.D.P. In: J. Tracey Jr. et al. (Editors), Initial Reports of The Deep Sea Drilling Project. U.S. Government Printing Office, Washington, D.C., VIII: 829—836.

Marine Geology, 20 (1976
© Elsevier Scientific Publi

PETROGRAPHIC AN
DEEP-SEA CORE FR

TOSHIO FURUTA

Ocean Research Institute,

(Received September 9, 1

ABSTRACT

Furuta, T., 1976. Petrogr
the northwest Pacific.

All the tephra layers s
and clinopyroxenes as ess
of them biotite, zircon, a
range between 1.49 and
artificial glass beads as w
sources are possibly acidi
graphic features of the fe
tephra originated not fro

INTRODUCTION

In the case of Japa
distributed east of th
westerly wind. Tephr
found over a distanc
Volcano in central Ja
amount of volcanic e
difficult to trace the
tary strata under the
tephra in the deep-se
most fascinating and
from experiments th
diameter rapidly sinl
they fall, while large
current before they
fine particles of tepl
similar to those on l

An example of a
Pleistocene eruption

Journal of Geochemical Exploration, 10 (1978) 117—138

GEOCHEMICAL DISPERSION OF HEAVY METALS VIA ORGANIC COMPLEXING: A LABORATORY STUDY OF COPPER, LEAD, ZINC, AND NICKEL BEHAVIOUR AT A SIMULATED SEDIMENT-WATER BOUNDARY

K.S. JACKSON* and G.B. SKIPPEN

Geology Department, Carleton University, Ottawa, Ont. (Canada)

(Received September 13, 1977; revised and accepted July 10, 1978)

ABSTRACT

Jackson, K.S. and Skippen, G.B., 1978. Geochemical dispersion of heavy metals via organic complexing: a laboratory study of copper, lead, zinc, and nickel behaviour at a simulated sediment-water boundary. J. Geochem. Explor., 10: 117—138.

Data are presented in this study from laboratory model experiments describing the behaviour of Cu, Pb, Zn and Ni at a simulated sediment-water boundary. The interactions involved are sorption by kaolin and by bentonite, organic complexing in solution by fulvic acid and by humic acid, carbonate reactions, hydrolysis, and desorption of the cations from a clay-bound phase and from their metal hydroxides by the organic acids. The organic acids increase the solubility of Cu, Zn and Ni in the presence of clay. The Pb solubility is variable and can even decrease, particularly at acidic pH, with organic complexing likely due to colloidal coagulation. Both Zn and Ni are influenced by hydrolysis at basic pH. When carbonate was added to the metal-organic acid-clay mixtures, a further decrease in solubility was observed for Ni and, to a lesser extent, for Zn. The organic acids prove capable of re-mobilizing Cu, Pb, Zn and Ni from the solid phases examined. However, there is a general kinetic hindrance to the desorption particularly at basic pH. Copper desorption appears to be the most kinetically hindered. Conclusions pertinent to the geochemical dispersion of these metals are drawn.

INTRODUCTION

The ability of organic acids in solution to solubilize minerals has been studied by many authors (e.g., Bondarenko, 1968; Baker, 1973; Kodama and Schitzer, 1973; Rashid and Leonard, 1973; Boyle et al., 1974) including the very early work of Harrar (1929) and Fetzer (1946). The dispersion of elements as affected by this mechanism has considerable geochemical significance. Thus soluble humic matter has the potential to act as a strong weathering agent on many mineral species and may cause the release of elements from sediment. Mineral stability and metal-organic affinity are the probable controlling factors.

*Present address: Bureau of Mineral Resources, Canberra, A.C.T., 2601, Australia.

The fate of trace elements, once liberated from weathering mineral phases, is further influenced by soluble organic compounds. The stabilization of various metallic cations in solution by organic acids has been experimentally investigated by many authors (e.g. Ong et al., 1970; Rashid, 1971; Bondarenko, 1972; Theiss and Singer, 1973). These workers have considered the effects of pH (hydrolysis), sulphide ion and carbonate ion on the metal-organic reaction in solution. Duursma (1970) has also considered the effects of sorption by a solid sedimentary phase of metal-inorganic and metal-organic complex species.

Thermodynamic and conditional stability constants for various soluble metal fulvates and humates have been determined by several authors (e.g., Schnitzer and Hansen, 1970; Cheam, 1973; Gamble and Schnitzer, 1973; Stevenson et al., 1973; Cheam and Gamble, 1974). The pH and ionic strength of the solution have an important effect on the stability of such complexes (Van Dijk, 1971; Schnitzer and Khan, 1972). From consideration of the literature, it is concluded that the Irving and Williams (1948) order of complex stability for bivalent metal ions is only partially applicable to fulvic and humic acid reactions and, furthermore, that humic acid will form stronger complexes than will fulvic acid.

Duursma (1970) studied the effect of soluble amino acids on the sorption of metals by marine and river sediments at pH 8. The data showed that the sorption of Co and Zn is reduced by the addition of 10^{-2} to 10^{-3} *M* leucine with the reduction almost equalling that calculated from known stability constants for metal-leucine complexes. In extrapolating to the lower concentrations of a natural system, it was concluded that such an organic influence on the metal distribution between sediment and water could only be a result of humic matter interactions. This is based on the higher natural concentration of humic compounds and their greater chelation capacity.

In the present work, the interactions of dissolved metallic cation(s) with a solid phase and dissolved humic and fulvic acids were investigated experimentally. Inherent in this geochemical process is the liberation of sediment-bound cations into the stream water via organic complexing. So, in effect, an equilibration point was approached from two directions. Firstly, Cu, Pb, Zn and Ni divalent cations were in solution with humic or fulvic acid; a solid, inorganic (clay) phase was introduced and the system allowed to equilibrate. Secondly, with the same bulk chemistry, the equilibration point was approached with the cations now initially in a solid phase either as clay adsorbed species or hydroxide precipitates. The influence of carbonate/bicarbonate anions on the equilibration points was also studied. The experiments then approach the complexity of a natural system and provide a basic model for studying the geochemical dispersion of elements in natural waters where organic chelation is involved.

EXPERIMENTAL

In designing experiments to model this natural process the following points were taken into consideration:

(1) Humic and fulvic acids are the most abundant organic complexing agents found in natural waters and sediments.

(2) A sediment's cation-exchange capacity will be determined by its organic matter and clay content; for this study, clay minerals were chosen because of experimental ease of handling and relationship to a field study conducted as part of a more major project (Jackson, 1975).

(3) Next to cation hydrolysis, inorganic reactions involving carbonate species were considered of most importance, particularly in relation to the natural stream waters of southeastern Ontario sampled as part of the field study.

Humic and fulvic acid extraction

Shoreline humic sediments were collected from Lake Fortune in the Gatineau Hills, Quebec. The crushed and dried mud was extracted with three 500-ml aliquots of 0.1 *M* $Na_4P_2O_7$. The combined extract (1500 ml) was acidified to pH 2 and the acid-insoluble humic acid fraction was separated by centrifuge. The remaining extract solution was allowed to air-dry leaving the fulvic acid residue. Both fractions were washed with distilled water, taken into aqueous solution and passed through cation-exchange resin (Rexyn 101H). The humic and fulvic acid eluates were allowed to air dry in a fume hood and then stored as a dried, crushed solid in screw-capped, glass vials. Both acids were characterized by organic carbon analyses, IR spectra and acid-base titrations. The black humic acid contained 49.5% C and 3.4 mequiv. COOH/g. The light yellow fulvic acid contained 40.5% C and 6.7 mequiv. COOH/g.

Cation solutions

All cation solutions were prepared by the dilution of atomic absorption standard reference solutions supplied by Fisher Scientific Co. The reference solutions used were all initially 1000 ppm divalent cation prepared as nitrate solution. Copper, Pb, Zn and Ni solutions were employed.

Clay

Two clays were employed in the study: flint clay and bentonite. The bentonite was supplied by Fisher Scientific Co. and characterized as a montmorillonite clay with a cation-exchange capacity of 78.20 ± 1.60 mequiv./100 g. The flint clay was supplied by the National Bureau of Standards (No. 97), Washington, and characterized as kaolinite, both ordered and disordered, with a cation-exchange capacity of 7.84 ± 0.24 mequiv./100 g.

Design of experiments

Sorption. The basic requirement of the experimental system was to enable cation solutions, in the presence and absence of organic acids, to interact

effectively with a solid phase. To achieve this, both time and a form of mechanical shaking were considered important.

The study was carried out as four reaction sequences, each being conducted at five pH values within the range of 4—9. The reaction sequences were:

(a) Cation solution only: hydrolysis (initially 25 ppm each of Cu, Ni, Zn and Pb).

(b) Reaction of cations and soluble organic acid: hydrolysis and organic complexing (initially 25 ppm each of Cu, Ni, Zn and Pb in a 0.5% w/v fulvic acid solution or a 0.2% w/v humic acid solution).

(c) Reaction of cations, organic acid and sediment: hydrolysis, organic complexing and sorption, initially as in (b) but now in the pesence of 100-mg and 250-mg quantities of bentonite or of kaolinite (flint clay).

(d) Reaction of cations and sediment: hydrolysis and sorption, initially as in (a) but now with the 100-mg and 250-mg quantities of clay present.

All reactions were carried out in 4-dram plastic vials with snap caps. The four reaction sequences as outlined may be abbreviated in future discussions as follows: (a) M, (b) M + F or M + H, (c) M + F + K, M + F + B, M + H + K or M + H + B, and (d) M + K or M + B where M stands for metallic cations, F for fulvic acid, H for humic acid, K for kaolinite (flint clay) and B for bentonite.

The mixtures were allowed to equilibrate with gentle shaking at room temperature over a period of 30 days. pH was then measured and the total cation content of the clear, supernatant solution determined by atomic absorption using a Jarrell-Ash unit. Centrifuging was usually required to clear the supernatant solution particularly for the bentonite reactions. Blanks were recorded on water + clay and water + organic acid and found to contribute no detectable Cu, Pb, Zn or Ni to the system. An error of ± 1 ppm was estimated for the Cu, Pb, Zn and Ni analyses.

The ionic strengths of these solutions, determined partly by the sodium and chloride ions added during the pH adjustment step, are low and are estimated to be between 0.002 and 0.005. Low ionic strength solutions were desired because of the correlation with the low ionic strengths encountered in natural waters (Garrels and Christ, 1965, p. 57).

In selecting metal and organic acid concentrations, field analytical data for Cu, Pb, Zn, Ni and C were taken into consideration. A reasonable estimate for an average trace metal content in stream waters was taken as 10 ppb. This is propably somewhat low for Zn and high for Pb, Cu, and Ni. A similar estimate for total dissolved organic carbon was taken as 10 ppm. A problem with relating field organic carbon analyses to an experimental system arises from the unknown relationship between total organic carbon measurements and the actual number of functional group or active organic acid sites that are present in the organic carbon. Metal contents were set initially at 25 ppm owing to analytical restrictions; organic-acid concentrations were set between 2000 and 5000 ppm.

Desorption. The ability of humic and fulvic acids to desorb both clay-adsorbed metals and hydroxide precipitates was studied using the following procedure:

(1) Set up cation plus clay suspensions at two initial pH values, termed pH_i, of 5.5 and 8.5. Allow these suspensions to equilibrate over 14 days (this was experimentally shown to be an adequate period of time).

(2) To evaluate the effect of pH on desorption, take five cation-clay suspensions of each pH_i and adjust pH (using NaOH and HCl solutions) to five values within the pH 4—9 range.

(3) To evaluate the effect of humic and fulvic acids on the desorption, take five cation-clay suspensions of each pH_i, add appropriate aliquots of the organic acid and adjust pH to five values within the 4—9 range.

At the end of a further 30 days, metal contents in the supernatant solutions were determined again using atomic absorption as previously discussed. The desorption reactions are analogous in bulk chemistry to the above described "sorption" reactions where the clay is the last reactant added.

Carbonate reactions. A carbonate/bicarbonate solution of pH 9 was obtained by preparing a solution of 0.30*M* $NaHCO_3$ (25.20 g/l) and 0.014*M* Na_2CO_3 (1.484 g/l).

The effect of bicarbonate/carbonate anions on the metal-organic acid-clay system was investigated by setting up reactions analogous to those discussed but now including the bicarbonate/carbonate retaining the same initial metal and organic acid concentrations as used above. To do this, it was necessary to first adjust the pH of the cation alone (M) and cation plus organic (M + O) reaction aliquots to about 9 prior to addition of the carbonate/bicarbonate solution. The $NaHCO_3$ concentration in the reaction mixture was 0.1*M*. The initial pH's of the reactions were set at about 7.60, 8.10 and 8.50 by dropwise addition of HCl or NaOH. This will cause some loss of carbonate due to its acid reaction. After the setting up of these reactions, the procedures regarding time of interaction and subsequent analyses are as previously outlined.

The ionic strength of these reaction solutions will be determined by the bicarbonate/carbonate system, in particular, the bicarbonate anion, and is therefore approximately 0.1, bearing in mind that the carbonate ion will be considerably less than 0.014*M* under conditions now established.

Desorption studies on the carbonate/bicarbonate systems were also conducted using a similar procedure to that previously discussed. However, it was now necessary to add the organic acid to the equilibrated cation—clay suspensions and adjust pH to about 8.5—9. The appropriate carbonate/bicarbonate solution aliquot was then added to three reaction suspensions and the pH adjusted to three values in the 7.5—8.5 range.

RESULTS AND DISCUSSION

Sorption

Metal hydrolysis reaction curves are shown in Fig. 1. The order of metal hydroxide precipitation observed in these reactions with increasing pH is Cu and

Pb occurring at almost identical pH followed by Zn and then Ni. Solubility products for the hydroxides of Cu, Pb, Zn and Ni are recorded in Sillen and Martell (1964, 1971). However, the values of the solubility products presented vary considerably with the technique and conditions of the determination. This is prohibitive to a theoretical calculation of the pH for which the metal hydroxides will precipitate under the experimental conditions used here. It is observed that the solubility products given for a particular set of conditions increase in the order Cu, Zn and Ni. The position of Pb is variable but it usually corresponds fairly well with Cu. The hydrolysis reaction curves obtained are consistent with the solubility product data for at least the order of hydrolysis.

The metal plus fulvic acid (M + F) and metal plus humic acid (M + H) reaction curves are shown in Figs. 1 and 2, respectively. The M + H reaction curves show that, with the four metals in competition for the humic acid active sites, only Cu is strongly retained in solution. The Ni and Zn solubilities exhibit a dependence on pH (hydrolysis). The Pb solubility at pH < 6.3 falls below the Pb hydrolysis curve. The large ionic size of Pb does imply that it is likely to cause humate or fulvate colloid coagulation in preference to Cu, Zn or Ni (Ong et al., 1970). It is concluded that Pb humate precipitation is occurring in this reaction. However, at basic pH, the humic acid reaction holds Pb in solution. In the presence of fulvic acid, Zn and Cu are almost totally retained in solution throughout the pH range. Nickel solubility again is strongly influenced by hydrolysis at basic pH. Lead solubility at pH < 6.3 is interpreted as evidence for Pb fulvate precipitation.

The reactions now to be discussed contain the solid phase. The sorption and desorption curves for a particular reaction are presented in the one figure. The desorption curves will be referred to later in the text.

The metal plus kaolin (M + K) reaction curves are shown in Fig. 3. The effect of hydrolysis on these curves is evident with increasing pH. Increasing the weight

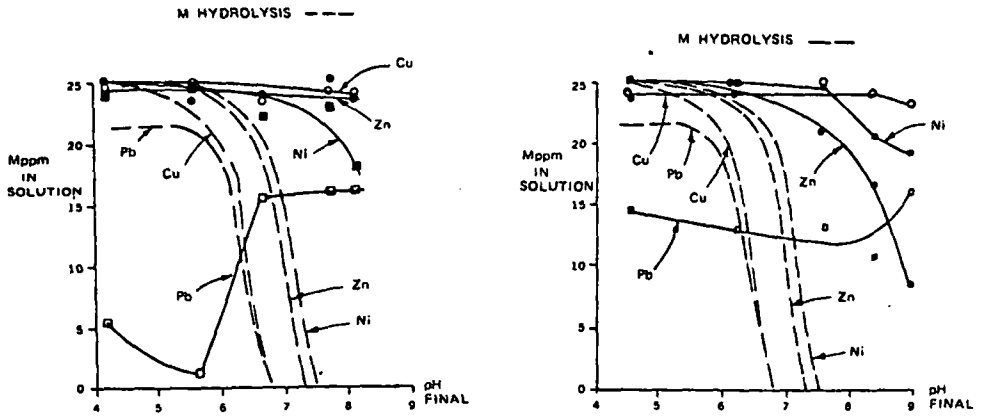

Fig. 1. Metal—fulvic acid reaction curves (also shown are the metal hydrolysis curves). Legend for all figures: ○ = Cu; ■ = Ni; □ = Pb; ● = Zn.

Fig. 2. Metal—humic acid reaction curves (also shown are the metal hydrolysis curves).

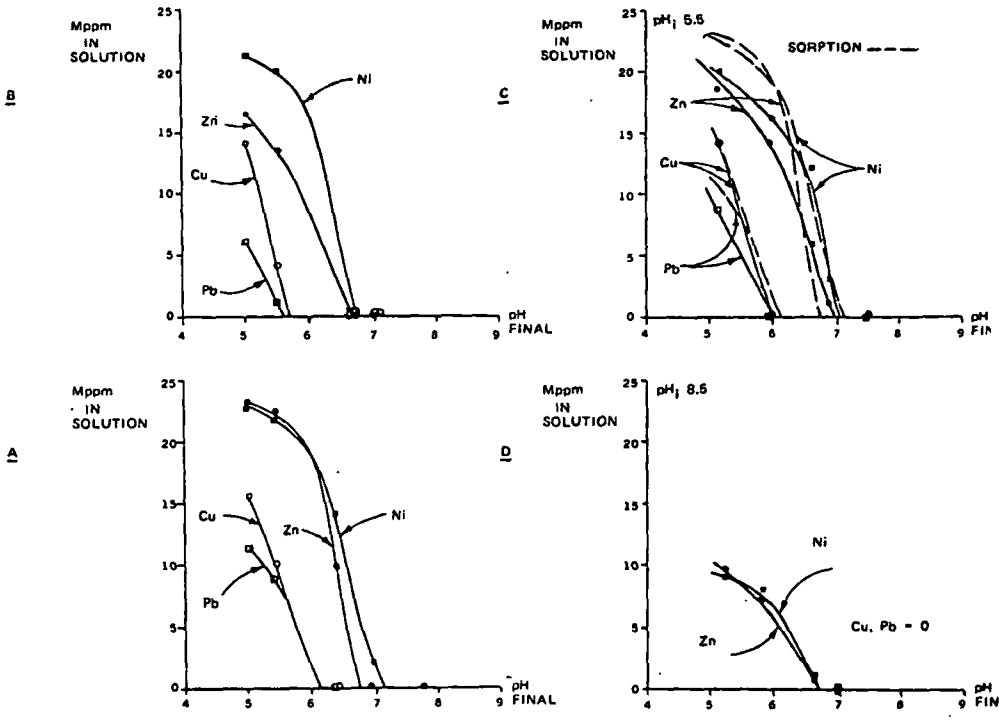

Fig. 3. Metal—kaolin reaction curves for both sorption and desorption. A. Sorption curves for 100 mg kaolin. B. Sorption curves for 250 mg kaolin. C. Desorption curves for clay-bound metal (100 mg kaolin and pH$_i$ 5.5) with sorption curves from A also shown. D. Desorption curves for metal hydroxides (100 mg kaolin and pH$_i$ 8.5).

of kaolin to 250 mg leads to increased sorption of all four elements but the increase is most pronounced for Pb and Zn. The metal plus bentonite (M + B) reaction curves (Fig. 4), in comparison with the M + K reaction, clearly reflect the larger cation-exchange capacity of bentonite. Hydrolysis is again evident at basic pH. With increased weight of bentonite, the metal sorption is increased but it is difficult to discern preferential ion exchange (sorption) among the four elements.

In the presence of kaolin plus humic acid (M + H + K reaction curves shown in Fig. 5), all four metals are retained in solution. Cu is strongly retained in solution showing little reactivity in sorption and in hydrolysis. Increasing the kaolin weight has little effect on sorption of the Cu species in solution except around pH 5. The Ni solubility is influenced by hydrolysis and sorption, the latter point being demonstrated by the slightly decreased Ni solubility with increased kaolin weight and also by comparison with M + H reaction. Zinc solubility is also influenced by hydrolysis and sorption but sorption effects are now more pronounced. Lead solubility is influenced by sorption (compare M + H with M + H + K). The order of metal retention in solution by humic acid in competition with hydrolysis and sorption is Cu > Ni > Zn ⩾ Pb; the position

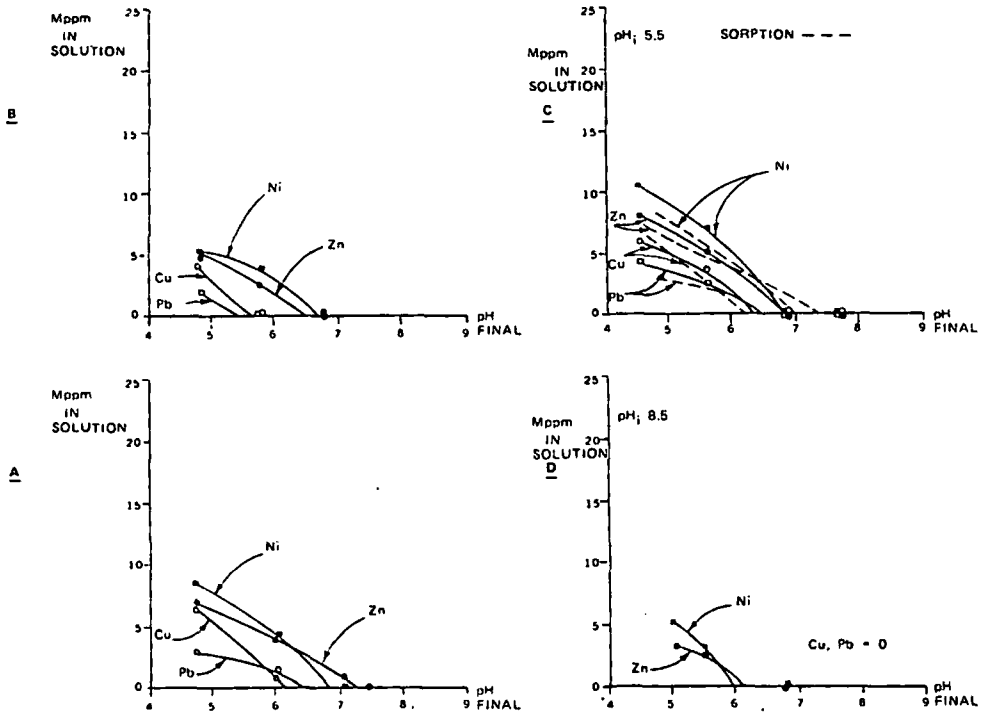

Fig. 4. Metal—bentonite reaction curves for both sorption and desorption. A. Sorption curves for 100 mg bentonite. B. Sorption curves for 250 mg bentonite. C. Desorption curves for clay-bound metal (100 mg bentonite and pH$_i$ 5.5) with sorption curves from A also shown. D. Desorption curves for metal hydroxides (100 mg bentonite and pH$_i$ 8.5).

of Zn and Pb is pH-dependent with Zn and Pb solubilities equalizing at higher pH values. At lower pH values, Cu solubility does fall below that of Ni.

The M + H + B reaction curves (Fig. 6) show metal behaviour similar to the above discussed M + H + K reaction. In the presence of bentonite, all four metals show decreased solubilities compared to the kaolin reaction; this is consistent with the higher cation-exchange capacity of bentonite. The increased weight of bentonite has little effect on the metal solubilities; Zn and also Ni are most strongly influenced by the increased sorption, particularly at pH < 6. The metal solubility order is Cu > Ni > Zn ≥ Pb with the same variation with pH as was observed for the M + H + K reaction.

In the fulvic acid, M + F + K, reactions (Fig. 7), Cu is quite strongly retained in solution throughout the pH range whereas Ni is affected by hydrolysis. The influence of sorption on Cu is most pronounced around pH 5. Zinc and Pb exhibit minima in their solubilities around pH 5.8. In the M + F reaction (Fig. 1), Pb showed similar behaviour. As a further point, the Pb and Zn curves show decreased solubility at low pH when compared to the M + K reaction (Fig. 3). The precipitation of Pb and possibly Zn fulvates is offered as an explanation for this behaviour. The fact that the Zn curve in M + F + K does not follow

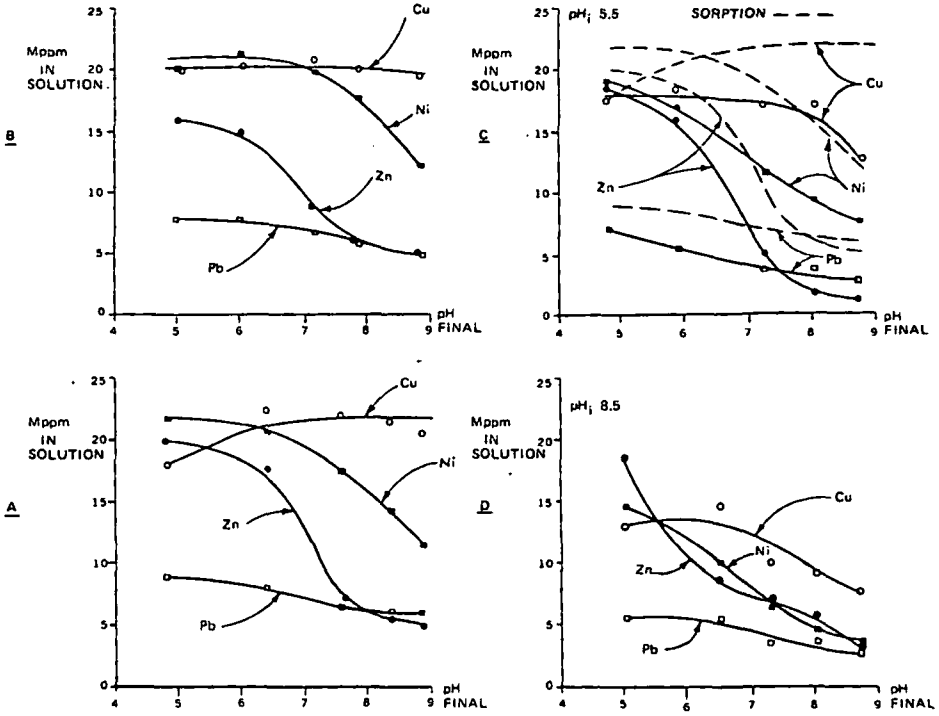

Fig. 5. Metal—humic acid—kaolin reaction curves for both sorption and desorption. A. Sorption curves for 100 mg kaolin. B. Sorption curves for 250 mg kaolin. C. Desorption curves for clay-bound metal (100 mg kaolin and pH$_i$ 5.5) with sorption curves from A also shown. D. Desorption curves for metal hydroxides (100 mg kaolin and pH$_i$ 8.5).

from the M + F result indicates that sorption reactions are also likely playing a significant role in determining the Zn solubility. Of the four elements, Zn is most strongly affected by the increase in kaolin weight further emphasizing the significance of sorption reactions in determining Zn solubility.

Copper, Pb, Zn,and Ni are retained in solution for the bentonite plus fulvic acid reactions (M + F + B) shown in Fig. 8. Compared to M + F + K, metal solubility is reduced for the four metals in the bentonite reaction. The increase in bentonite weight leads to a pronounced decrease in the Cu solubility, particularly at acidic pH, and a somewhat less decrease in Ni and Zn solubilities. In the presence of 100 mg bentonite, Ni solubility is again influenced by hydrolysis at basic pH values. At pH > 6, the decrease in metal solubilities observed when comparing M + F + K and M + F + B is most pronounced for Zn. This can be taken as further evidence of the dependence the Zn solubility has on sorption reactions. The Pb solubility for the bentonite reaction is low and is attributed to the combination of sorption, hydrolysis and Pb fulvate coagulation. For bentonite and kaolinite, the fulvic acid reactions show a similar order of soluble metal retention, Cu > Zn—Ni > Pb; Zn and Ni exhibit crossover points in both reactions.

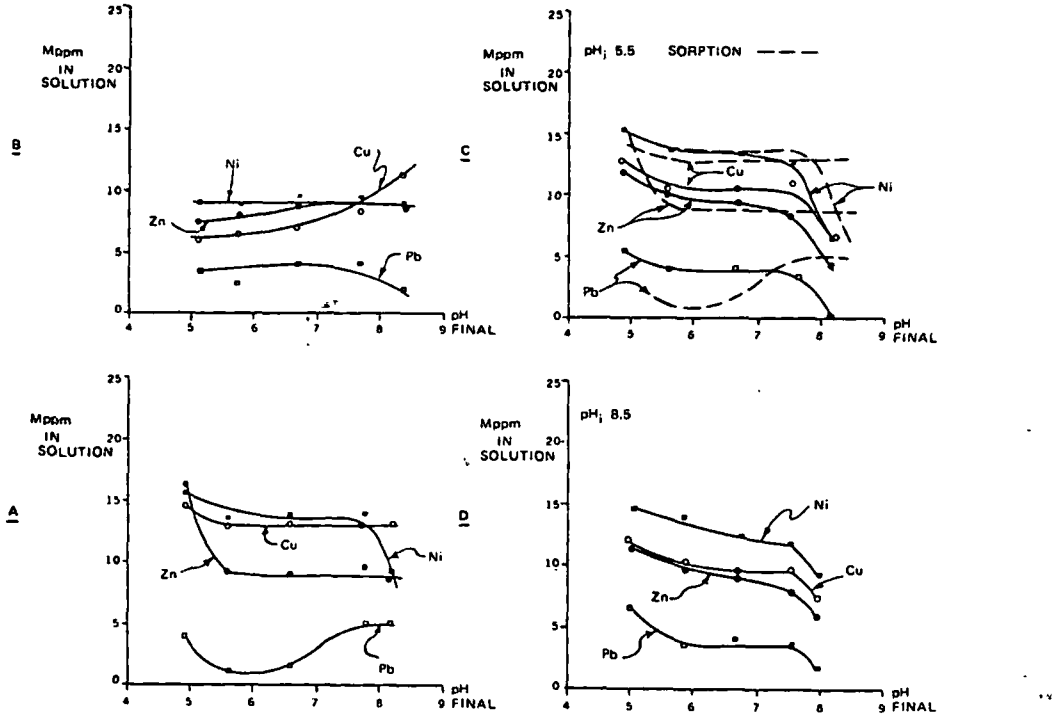

Fig. 8. Metal—fulvic acid—bentonite reaction curves for both sorption and desorption. A. Sorption curves for 100 mg bentonite. B. Sorption curves for 250 mg bentonite. C. Desorption curves for clay-bound metal (100 mg bentonite and pH_i 5.5) with sorption curves from A also shown. D. Desorption curves for metal hydroxides (100 mg bentonite and pH_i 8.5).

acid active sites were in excess. In the estimation of organic acid bidentate active site milliequivalence, two assumptions were necessary. Based on the humic matter characterizations reported by Schnitzer and Khan (1972) and Gamble and Schnitzer (1973), a number average molecular weight of 950 was assumed for the Lake Fortune humic and fulvic acids with each acid containing three bidentate active sites. The estimated milliequivalence ratios for the four metals and fulvic acid then are approximately 3:3:3:1:130 for Cu: Ni: Zn: Pb: fulvic acid sites. For the humic acid, the ratios are about 3:3:3:1:50 for Cu: Ni: Zn: Pb: humic acid sites.

However, in the following discussion, it has been assumed that the organic species exhibit negligible involvement in sorption reactions under the experimental conditions employed.

The metal-organic acid chelation reaction can be simply represented as:

$$M + L = ML$$

where M is the free metal cation, L is the organic ligand (humic or fulvic acid) and ML is the metal-organic complex.

Firstly, it should be noted that the equilibrium constant of this general reaction (i.e., the stability constant for ML) will be dependent on solution ionic strength. The solution ionic strength for the study varied from 0.002 to 0.005. This variation will cause a negligible shift in the stability constant (Schnitzer and Khan, 1972). Sorption of M by the clay will decrease the activity of M thus displacing the reaction to the left with a resultant decrease in ML activity and hence metal solubility. The magnitude of this effect will be dependent on the equilibrium constant for this reaction with the effect being minimized for more stable complexes. Loss of M due to hydroxide formation (hydrolysis) would also follow the same logic. A lack of stability data applicable to the experimental conditions prohibits a further quantitative evaluation of this effect. Nevertheless, the solubilities of the four metals within the organic reaction mixtures discussed are considered to be a direct reflection of the metal humate and fulvate stabilities.

The following conclusions regarding the behaviour of Cu, Ni, Pb and Zn can be made:

(1) Humic and fulvic acid, when in excess of the cations, have the potential to retain Cu, Pb, Zn and Ni in solution in competition with hydrolysis and sorption onto clay.

(2) Copper shows the highest affinity of the four elements for organic reaction throughout the pH range with a possible exception at pH 5.

(3) Copper and Ni humates are more stable then their corresponding fulvates.

(4) Zinc fulvate is more stable than the humate complex at basic pH.

(5) All four elements are susceptible to clay sorption, even in the presence of organic acids, but Zn is most strongly affected.

(6) Nickel solubility is most strongly influenced by pH (hydrolysis) as it decreases considerably at basic pH.

(7) Lead humate and fulvate appear susceptible to colloidal coagulation.

Desorption

The sorption and desorption experiments have identical bulk chemistries but the effect of an increased solid weight (250 mg) was excluded from the desorption study. The objective of this study was to investigate the reversibility of the following reaction:

$$M + MO + C = (M—C) + (MO—C)$$

where M represents metallic cation, MO the metal-organic complex, C the inorganic absorber including clay and hydroxide precipitate, (M—C) the clay-bound metal species, and (MO—C) the clay-bound metal organic species.

Such a study tests the extent to which equilibrium has been approached in the experiments and also represents an alternative model for geochemical processes. For the sorption study, the starting point was M + MO in solution over a range of pH values with subsequent addition of clay to determine how much metal was taken out of solution by sorption onto the clay. At basic pH,

the added influence of hydroxide precipitation on metal solubility was also determined. The sorption experiments can be considered then to model the ability of an inorganic phase to inhibit the dispersion of Cu, Pb, Zn and Ni cations in organic-rich waters.

For the desorption study, the reaction is set up in one case (pH_i 5.5) with (M—C) initially present and little metal hydroxide (as seen from Fig. 1). In the second case (pH_i 8.5), the reaction is set up with predominantly metal hydroxide precipitate and also likely some (M—C). In both cases, after the initial equilibration, the humic- or fulvic-acid solutions are introduced and pH adjusted in the 4—9 range. The desorption experiments then model the ability of an organic acid to remobilize metals from a sediment-bound phase, either as clay-sorbed species or as hydroxide precipitates. Given sufficient time to attain equilibrium, the sorption and desorption reactions should reach the same equilibrium points. However, kinetic factors can prevent the achievement of equilibrium for either sorption or desorption in geochemical processes and a comparison of these reactions is likely to identify metals that might be susceptible to this problem.

After the initial sorption steps and prior to the addition of the organic acid, the starting soluble metal contents of the desorption solutions used in the kaolin and bentonite reactions were obtained from the M + K and M + B reaction curves (Figs. 4 and 5, respectively). These initial metal contents for the desorption stock solutions are given in Table I.

TABLE I

Initial metal concentrations (in ppm) for reaction solutions used in desorption studies

		Cu	Ni	Pb	Zn
M + K	pH_i 5.5*	3.0	20.0	3.0	20.0
	pH_i 8.5*	0	0	0	0
M + B	pH_i 5.5*	1.5	4.5	1.5	4.0
	pH_i 8.5*	0	0	0	0

*Note. An allowance was made for the change in pH during the sorption step when obtaining the metal concentrations from the reaction curves. pH 5.9 was used for the acidic sorption (pH_i 5.5) and pH 7.8 for the basic sorption (pH_i 8.5).

The effect of pH variation alone has been tested in the desorption studies with the results shown in Figs. 3 and 4. For both M + K and M + B, desorption of a clay-bound metal (pH_i 5.5) agrees within experimental limits with the equivalent sorption reaction indicating that no kinetic barriers exist to this desorption process. For the hydroxide precipitate case (pH_i 8.5), sorption and desorption reactions do not agree. For M + K and M + B, Cu and Pb show no detectable desorption; Ni and Zn are desorbed to 50% or less of the values obtained for the sorption reactions. The failure to attain equilibrium for initially basic pH values is attributed to unfavourable kinetics for the dissolution of the hydroxide precipitates.

For the fulvic acid reactions in the presence of kaolin, the order of metal solubility and the shape of the reaction curves are quite similar for sorption and desorption (Fig. 7). The desorption of clay-sorbed metal (pH_i 5.5) does suffer from unfavourable kinetics at pH > 6 with the discrepancies being greatest for Cu and Zn suggesting that these elements are most susceptible to kinetic effects. Fulvic acid does dissolve the metal hydroxides (pH_i 8.5) to a significant extent with unfavourable kinetics strongly affecting the solubilities of all four metals, particularly at pH > 6.

For M + F + B, desorption of both clay-sorbed metal and metal hydroxides leads to a similar metal solubility (Fig. 8) and is in agreement, within experimental limits, with the sorption data up to about pH 8. At higher pH, the metal solubility is less for the desorption reaction. Hence, kinetic effects seem important only at higher pH for the bentonite desorption reactions.

Kinetic effects are also apparent for the M + H + K desorption reactions (Fig. 5). For the initially clay-sorbed metals, all four show significant solubility but kinetic effects become apparent at pH > 6 with the discrepancies between sorption and desorption being similar for the four metals. Humic acid has a considerable dissolution effect on the metal hydroxides. In comparison with the sorption curves, metal solubilities are decreased implying a kinetic barrier to the hydroxide desorption with Cu apparently the most affected.

Desorption from the clay-sorbed phase and from the hydroxides leads to a similar end result in the M + H + B reaction (Fig. 6). Comparison of the sorption and desorption curves shows agreement within experimental limits for Pb, Zn and Ni. The decreased Cu solubility observed in the desorption experiments at pH > 6 implies that Cu desorption from both the bentonite-sorbed phase and the hydroxide precipitate is kinetically disfavoured.

In summary, the experimental evidence indicates the following:

(1) Humic and fulvic acids are capable of remobilizing Cu, Pb, Zn and Ni from a clay-sorbed phase and their metal hydroxide precipitates. Similar results have been obtained by other workers (e.g., Banat et al., 1974).

(2) Metal desorption is generally kinetically inhibited particularly at basic pH; desorption from a metal hydroxide phase is the more unfavourable process.

(3) Of the four metals, Cu desorption appears to be the most kinetically inhibited.

(4) The order of metal solubility for sorption and desorption for each reaction is essentially the same.

Carbonate reactions

Bicarbonate/carbonate anions represent potentially significant inorganic ligands in stream waters of interest to the authors. As reported by Livingstone (1963), bicarbonate contents for several streams in Ontario and Quebec ranged between 6 and 230 ppm. Based on 10 ppm total dissolved organic carbon in

stream water, these bicarbonate contents represent an approximate 10—100-fold excess over the organic. In the experimental system, there is an approximate 10 times excess of bicarbonate over organic acid sites. To increase the bicarbonate excess would necessitate a further increase in the solution ionic strength with consequent major variation in the metal-humate and -fulvate stabilities (Schnitzer and Khan, 1972). The metal- to organic acid active site milliequivalence ratios are the same as those estimated for the above sorption-desorption reactions, i.e. organic acid sites are in excess.

Variations in metal behaviour are observed for these reactions but ionic strength considerations are now important. The change in ionic strength from 0.005 (carbonate-free) to 0.1 (excess bicarbonate) leads to approximately a 10-fold decrease in the stability constants for Cu, Pb, Zn and Ni fulvates at pH 3 (Schnitzer and Khan, 1972).

The data for the metal-organic acid reactions (Fig. 9) indicate a decreased metal solubility compared to the carbonate-free reactions (Figs. 1 and 2). For

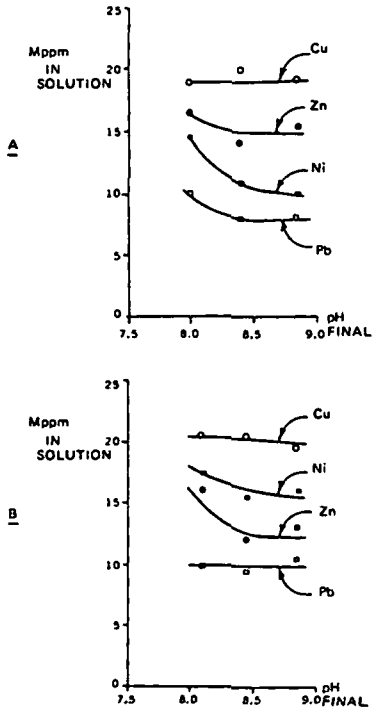

Fig. 9. Metal—organic acid reaction curves in the presence of bicarbonate/carbonate. A. Fulvic acid. B. Humic acid.

the fulvic acid reactions, Pb solubilities are almost identical. Nickel shows the greatest decrease (6—10 ppm) with Zn and Cu being affected to a lesser extent (3—5 ppm). For the humic acid reactions, all four cations exhibit a significant decrease in solubility (4—8 ppm) with Zn being the most strongly affected. The solubility order for M + F is Cu > Zn > Ni > Pb and, for M + H, Cu > Ni > Zn > Pb.

The preferential destabilization of Ni in the fulvic acid reactions can be related to the data of Rashid and Leonard (1973). These workers found that at pH 8.5, the order of carbonate precipitation in the presence of humic acid was Ni followed by Cu, Mn, and Fe. The humic acid reactions may more strongly reflect the decreased humate stability due to the increased ionic strength (salinity) causing preferential flocculation of the higher-molecular-weight humic fractions. This has led to almost equivalent, but significant decreases in solubility for all four elements. The fulvic acid reactions are almost certainly influenced by the decreased fulvate stabilities but, for Ni, there does appear to be a preferential destabilization due to the presence of bicarbonate/carbonate.

Consideration of the data for the metal-fulvic acid-clay reactions (Fig. 10)

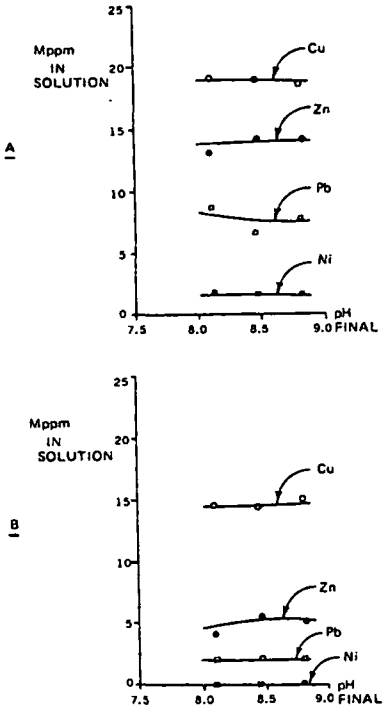

Fig. 10. Metal—fulvic acid—clay reaction curves in the presence of bicarbonate/carbonate. A. Kaolin. B. Bentonite.

leads to the same conclusion. All four metals show a decreased solubility compared to the carbonate-free reactions (Figs. 7 and 8) with the effect being most pronounced for Ni. In the M + F + B reaction, Ni now has a non-detectable solubility. The Cu and Pb solubility decreases are within experimental limits compared to the carbonate-free system. Zinc does show a significant solubility decrease of about 5 ppm in both M + F + K and M + F + B.

For the metal-humic acid-clay reactions (Fig. 11), a decreased solubility of all four metals is again evident (compare with Figs. 5 and 6). The variations in Pb solubility are within experimental limits; Cu solubility decreases by 2—3 ppm for both bentonite and kaolin. Zn solubility decreases by about 2 ppm for the kaolin but by 6—7 ppm in the bentonite reaction. Nickel solubility decreases by about 3 ppm in the kaolin reaction and by about 5—6 ppm in the bentonite reaction. This represents further evidence of a preferential destabilization of Ni and possibly Zn fulvates and humates in the presence of bicarbonate.

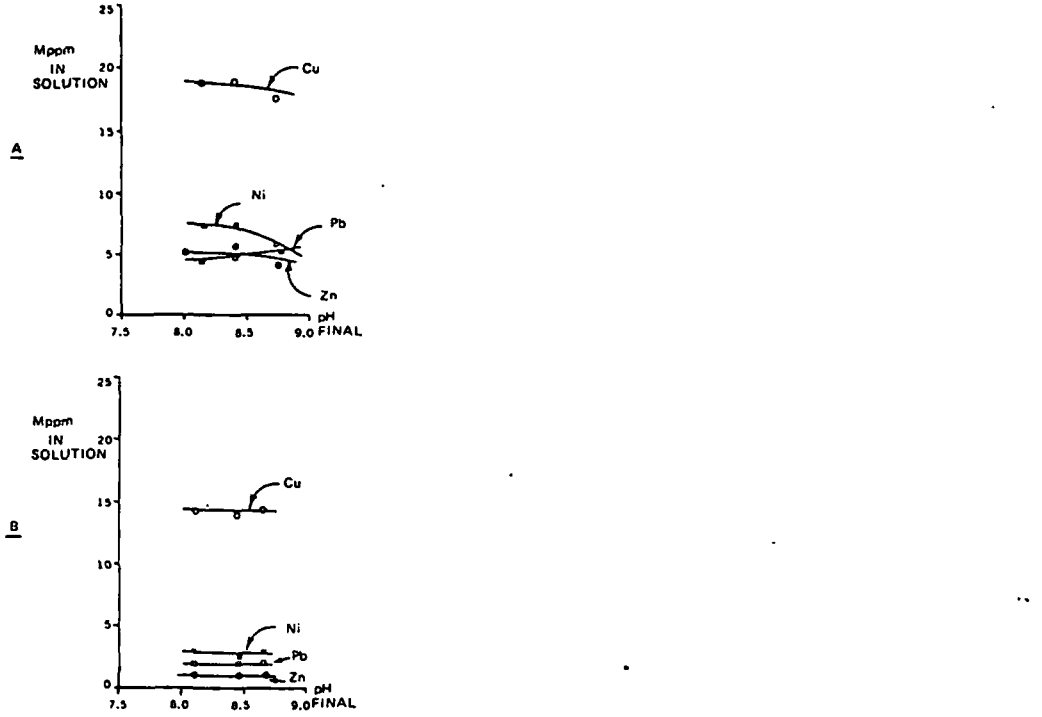

Fig. 11. Metal—humic-acid—clay reaction curves in the presence of bicarbonate/carbonate. A. Kaolin. B. Bentonite.

In summary, with a significant bicarbonate excess, Cu, Pb, Zn and Ni show decreased solubilities. The decrease is minimal and often within experimental limits for Cu and Pb. Nickel appears the most affected, but Zn is also strongly influenced by the bicarbonate/carbonate reactions. It is difficult to assess to what extent the solubility decreases can be attributed to the change in humate and fulvate stabilities due to the increased solution ionic strength. Ionic strength effects are perhaps greatest for Zn considering that Zn exhibits the lowest affinity for organic complexing of the four elements at pH 3 (Schnitzer and Khan, 1972). A major problem is the lack of applicable stability constant data at basic pH values. It is concluded that bicarbonate/carbonate has a significant effect on Ni solubility, and possibly on Zn solubility, in the presence of soluble

organic acids and clay. Lead and Cu solubilities decrease slightly in response to decreased humate and fulvate stabilities.

Carbonate and bicarbonate are weak ligands but their possible involvement in mixed ligand complexes should be considered. Manning and Ramamoorthy (1973) showed that the inorganic ligands can be involved in such complex formation with a second, organic ligand. The data presented do not permit an assessment of possible mixed ligand formation.

Desorption experiments conducted for the bicarbonate/carbonate reaction mixtures lead to the same conclusions as discussed for the carbonate-free reactions. Again, comparison of the sorption and desorption reaction curves shows the kinetic hindrance to desorption (particularly as the carbonate reactions are carried out at basic pH values). Details of these data are not presented here in view of the volume of information involved (see Jackson, 1975), but the conclusions drawn are relevant to this discussion:

(1) Decreased solubilities for the desorption of clay-adsorbed cations (pH_i 5.5) are less than those observed for the desorption from metal hydroxides (pH_i 8.5).

(2) Decreased metal solubilities for the various desorption reactions are consistently greatest for Cu.

GEOCHEMICAL SIGNIFICANCE

The experimental data presented do have certain implications regarding the geochemical dispersion of Cu, Pb, Zn and Ni in natural waters. In the sorption experiments, all four cations were stabilized in solution by humic and fulvic acid complexing; the effect generally decreases in the order Cu, Ni, Zn, and Pb. Hence, an influx of soluble organic matter into stream water will favour the prolonged dispersion of these elements in solution. The solubilities of Zn and particularly Ni are most affected by hydrolysis leading to a destabilizing of the soluble humate and fulvate complexes. Sorption onto a clay surface also destabilizes the Zn and Ni organic complexes. These two factors will shorten the dispersion of both Zn and Ni. Lead-organic complexes appear susceptible to colloidal coagulation phenomena producing a decreased Pb dispersion. However, this effect would decrease with the lowering in molecular weight likely encountered in natural stream water organic complexing agents.

The geochemical significance of the desorption study is clear. Fulvic and humic acid prove capable of not only stabilizing Cu, Pb, Zn, and Ni in solution, but also of remobilizing these elements from a sediment phase including both metal hydroxides and metal adsorbed to clay. The geochemical dispersion of an element is vitally dependent upon its aqueous solubility. However, it is first necessary for an element to be taken up into solution from a solid phase before organic complexing can influence its dispersion. The desorption of all four metals appears to be kinetically hindered particularly where metal hydroxides are involved. Copper is most affected by unfavourable kinetics. This might lead

to a situation where Cu, in comparison to Ni, Zn and Pb, is released from a sediment phase at a considerably lower rate and is less available for organic complexing in solution and hence its dispersion is restricted.

The bicarbonate/carbonate mixtures have indicated that Ni, and possibly Zn, solubilities decrease due to the interference of carbonate reactions. Streams draining through carbonate terrains are therefore likely to be low in soluble Ni content irrespective of the soluble organic carbon content. Such a consideration is important when studying the geochemical dispersion of elements within natural waters draining through varied bedrock geology featuring carbonate units.

FUTURE WORK

The general application of these conclusions is still uncertain. As with any laboratory model, comparison with the natural system is essential. The authors have done this to some extent (Jackson, 1975) and did find reasonable agreement between the model and the field data which will be published as a separate paper. The major limitations to the present laboratory model which could be overcome in future work are: (1) the use of an inorganic adsorbent only — nature employs both organic and inorganic adsorbents; (2) working with ppm cation levels whereas natural contents are usually in the ppb range; and (3) the absolute excess of organic acid sites over the total cation content.

In natural, organic-rich streams, a similar situation would exist with organic sites in excess of the ppb levels of Cu, Pb, Zn, Ni, Mn and Fe. However, Ca, Mg, Na and K are likely in the ppm range and might well reduce the number of organic active sites available for further reaction; the extent of organic complexing by these elements in natural waters is uncertain (Duursma, 1970; Beck et al., 1974). Obviously, a whole new batch of experiments should also be set up based on the inorganic interferences due to sulphide and Fe and Mn oxides. Metal accumulation by micro-organisms present in stream water could also be taken into account. Nevertheless, with the present model, the authors believe meaningful results have been obtained.

ACKNOWLEDGEMENTS

The authors acknowledge the significant contribution of ideas made by Dr. C.R. Langford during the progress of this work. The manuscript benefited from a critical review by Dr. I.R. Jonasson. The project was funded by NRC grant number A4253. Financial support (to K.S.J.) of a Shell Scholarship and Carleton Scholarships is acknowledged.

REFERENCES

Baker, W.E., 1973. The role of humic acids from Tasmanian podzolic soils in mineral degradation and metal mobilization. Geochim. Cosmochim. Acta, 37: 269—281.

Banat, K., Forstner, U. and Muller, G., 1974. Experimental mobilization of metals from aquatic sediments by nitrilotriacetic acid. Chem. Geol., 14: 199—207.

Beck, K.C., Reuter, J.H. and Perdue, E.M., 1974. Organic and inorganic geochemistry of some Coastal Plain rivers of the southeastern United States. Geochim. Cosmochim. Acta, 38: 341—364.

Bondarenko, G.P., 1968. An experimental study on the solubility of galena in the presence of fulvic acids. Translated from Geokhimiya, 5: 631—636.

Bondarenko, G.P., 1972. Stability of soluble co-ordination compounds of copper with humic and fulvic acids. Translated from Geokhimiya, 8: 1012—1023.

Boyle, J.R., Voigt, G.K. and Sawhney, B.H., 1974. Chemical weathering of biotite by organic acids. Soil Sci., 117: 42—45.

Cheam, V., 1973. Chelation study of copper (11): fulvic acid system. Can. J. Soil Sci., 53: 377—382.

Cheam, V. and Gamble, D.S., 1974. Metal—fulvic acid equilibrium in aqueous $NaNO_3$ solution. Hg(11), Cd(11) and Cu(11) fulvate complexes. Can. J. Soil Sci., 54: 413—418.

Duursma, E.K., 1970. Organic chelation of ^{60}Co and ^{65}Zn by leucine in relation to sorption by sediments. In: D.H. Wood (Editor), Proceedings of the Symposion on Organic Matter in Natural Waters. Inst. Mar. Sci. Occas. Publ., 1: 387—397.

Fetzer, W.G., 1946. Humic acids and true organic acids as solvents of minerals. Econ. Geol., 41: 47—56.

Gamble, D.S. and Schnitzer, M., 1973. The chemistry of fulvic acid and its reactions with metal ions. In: P.C. Singer (Editor), Trace Metals and Metal-Organic Interactions in Natural Waters, Ann Arbor Sci. Publ., Ann Arbor, Mich., pp. 265—302.

Garrels, R.M. and Christ, C.L., 1965. Solutions, Minerals and Equilibria, Harper and Row, New York, N.Y.

Greenland, D.J., 1971. Interaction between humic and fulvic acids and clays. Soil Sci., 111: 34—41.

Harrar, N.J., 1929. Solvent effects of certain organic acids upon oxides of iron. Econ. Geol., 24: 50—61.

Irving, H. and Williams, R.J.P., 1948. Order of stability of metal complexes. Nature, 162: 746—747.

Jackson, K.S., 1975. Geochemical Dispersion of Elements via Organic Complexing. Ph.D. Thesis, Carleton University, Ottawa, 344 pp. (unpublished).

Kodama, H. and Schnitzer, M., 1968. Effects of interlayer cations on the adsorption of a soil humic compound by montmorillonite. Soil Sci., 106: 73—74.

Kodama, H. and Schnitzer, M., 1973. Dissolution of chlorite minerals by fulvic acid. Can. J. Soil Sci., 53: 240—243.

Livingstone, D.A., 1963. Data of Geochemistry. Chapter G. Chemical composition of rivers and lakes. U.S. Geol. Surv. Prof. Pap., 440-G: G1—G64 (6th ed.).

Manning, P.G. and Ramamoorthy, S., 1973. Equilibrium studies of metal-ion complexes of interest to natural waters, 7. Mixed ligand complexes of Cu(11) involving fulvic acid as primary ligand. J. Inorg. Nucl. Chem., 35: 1577—1581.

Ong, H.L., Swanson, V.E. and Bisque, R.E., 1970. Natural organic acids as agents of chemica weathering. U.S. Geol. Surv. Prof. Pap., 700-C: C130—C137.

Rashid, M.A., 1971. Role of humic acids of marine origin and their different molecular-weight fractions in complexing di- and tri-valent metals. Soil Sci., 111: 298—306.

Rashid, M.A. and Leonard, J.D., 1973. Modifications in the solubility and precipitation behaviour of various metals as a result of their interactions with sedimentary humic acid. Chem. Geol., 11: 89—97.

Rashid, M.A., Buckley, D.E. and Robertson, K.R., 1972. Interactions of a marine humic acid with clay minerals and a natural sediment. Geoderma, 8: 11—27.

Schnitzer, M. and Hansen, E.H., 1970. Organo-metallic interactions in soils, 8. An evaluation of methods for the determination of stability constants of metal—fulvic acid complexes. Soil Sci., 109: 333—340.

Geothermal Energy

Program Summary Document

FY 1981

Assistant Secretary for Resource Applications
U.S. Department of Energy

January 1980

TABLE OF CONTENTS

		Page
I.	PROGRAM OVERVIEW	1
	A. Hydrothermal Resources	3
	B. Hydrothermal Commercialization	4
	C. Geopressured Resources	4
	D. Geothermal Technology Development	5
II.	HYDROTHERMAL RESOURCES	9
	A. Resource Definition	11
	B. Non-Electric Applications	16
	C. Environmental Control	18
	D. Facilities	21
	1. Demonstration Plants	22
	2. Raft River Pilot Plant	24
	3. Hawaii Geothermal Wellhead Generator	25
	4. Geothermal Loop Experimental Facility (GLEF)	25
	5. Geothermal Component Test Facility (GCTF)	26
III.	HYDROTHERMAL COMMERCIALIZATION	29
	A. Planning and Analysis	30
	1. Planning	30
	2. National Progress Monitoring	31
	3. Interagency Coordination and Federal Policy Development	32
	4. Economic Evaluation and Barrier Analysis	32
	B. Private Sector Development	34
	1. Market Assessment	34
	2. Hydrothermal Applications	35
	3. Outreach Activities	36
	4. Geothermal Loan Guaranty Program	37
IV.	GEOPRESSURED RESOURCES	39
	A. Program Coordination	41
	B. Resource Definition	42
	C. Engineering Applications	45
	D. Environmental Control	47

TABLE OF CONTENTS (concluded)

		Page
V.	GEOTHERMAL TECHNOLOGY DEVELOPMENT	49
	A. Component Technology Development	50
	1. Drilling and Completion Technology	50
	2. Energy Conversion Technology	53
	3. Reservoir Stimulation	57
	4. Geochemical Engineering and Materials	58
	5. Geoscience Technology Development	62
	B. Hot Dry Rock	64
VI.	INTERNATIONAL GEOTHERMAL ENERGY ACTIVITIES	69
VII.	PROGRAM MANAGEMENT	71
	A. Headquarters Organization	71
	B. Field Organization	72

LIST OF TABLES

Table Number		Page
I-1	Funding Levels for Geothermal Energy Programs, FY 1979 through FY 1981	8
II-1	Funding Levels for Hydrothermal Resources Subprograms, FY 1979 through FY 1981	10
III-1	Funding Levels for Hydrothermal Commercialization Subprograms, FY 1979 through FY 1981	29
IV-1	Funding Levels for Geopressured Resources Subprograms, FY 1979 Through FY 1981	41
V-1	Funding Levels for Geothermal Technology Development Subprograms, FY 1979 through FY 1981	49

I. PROGRAM OVERVIEW

Geothermal energy is the internal heat of the earth. Much of it is recoverable with current or near-current technology. Geothermal energy can be used for electric power production, residential and commercial space heating and cooling, industrial process heat, and agricultural applications.

Three principal types of geothermal resources are exploitable through the year 2000. In order of technology readiness, these resources are:

- Hydrothermal,
- Geopressured (including dissolved natural gas), and
- Hot dry rock.

In hydrothermal systems, natural water circulation moves heat from deep sources toward the earth's surface. Geothermal fluids (water and steam) tapped by drilling can be used to generate electricity or provide direct heat.

Geopressured resources, located primarily in sedimentary basins along the Gulf Coast of Texas and Louisiana, consist of water and dissolved methane at high pressure and moderately high temperature. In addition to recoverable methane, geopressured resources offer thermal energy and mechanical energy derived from high fluid pressures. The methane, however, has the greatest immediate value.

Hot dry rock (HDR) resources are geologic formations at accessible depths with abnormally high heat content but little or no water. Usable energy is extracted by circulating a heat transfer fluid, such as water, through deep wells that are connected by manmade fractures in the rock. Like hydrothermal energy, HDR can be used for electric power production or direct heat applications.

Of the three types, hydrothermal resources are most ready for commercialization, since much of this resource can be used economically now. Rapid commercial development of the Nation's hydrothermal resources is a major

objective of the federal geothermal program. The program approach for development of hydrothermal resources for electric and direct heat applications is to: (1) complete, with the cooperation of state and local government entities and the private sector, site-specific commercialization plans for each known hydrothermal area; (2) identify technical, economic, and institutional barriers to development at each prospect and plan actions to overcome or alleviate impediments to development; (3) conduct cost-shared demonstrations and operate experimental facilities where necessary to stimulate commercial development; (4) encourage greater participation in the Geothermal Loan Guaranty program; (5) continue resource assessment and reservoir confirmation activities to provide for the expansion of the resource base and reserves necessary to support the future growth of the geothermal industry; and (6) maintain a vigorous supporting research and development program to provide new and improved technology for finding the required resources, reducing energy conversion costs, and controlling potential environmental impacts. In this approach, the Hydrothermal Commercialization program is supported by the Hydrothermal Resources program and the Geothermal Technology Development program.

Commercial development of geopressured energy may begin in the mid 1980's. Economic feasibility will depend on the amount of methane that a given well can produce, a highly uncertain factor at present. The Geopressured Resources program is supported by many of activities in the Geothermal Technology Development program.

Hot dry rock is currently seen as a longer-term possibility. Significant improvements in drilling and fracturing technology are necessary to bring about commercial use of this potentially large resource. Commercialization may occur by the mid 1990's. The hot dry rock activities are a major component of the Geothermal Technology Development program.

The following sections describe each of the four geothermal program areas: (A) Hydrothermal Resources, (B) Hydrothermal Commercialization, (C) Geopressured Resources, and (D) Geothermal Technology Development. The Division of Geothermal Resource Management (DGRM) has responsibility for the Hydrothermal Commercialization Program, while the Division of Geothermal Energy (DGE)

carries the responsibility for the Hydrothermal Resources, Geopressured Resources, and Geothermal Technology Development programs.

A. Hydrothermal Resources

Objectives of the Hydrothermal Resource program are to define and confirm high-temperature reservoirs suitable for electric power generation; to demonstrate such power generation; to identify low-and moderate-temperature prospects with potential for direct heat applications; to assess environmental, health, and safety factors affecting geothermal development; and to develop appropriate control technology.

The Resource Definition subprogram includes the assessment of U.S. hydrothermal reservoirs and the confirmation of hydrothermal prospects through selective drilling and testing projects. DGE participates in regional and national assessments of hydrothermal resources in cooperation with the U.S. Geological Survey (USGS). Low- to moderate-temperature reservoirs are identified through a cooperative program with state agencies. These low-temperature resources are confirmed through user-coupled drilling programs. In addition, DGE conducts exploratory drilling programs in cooperation with industry to confirm high-temperature reservoirs with near-term commercial potential.

The objectives of some 22 demonstration projects administered under the Non-Electric Applications subprogram are to provide evidence of the viability of geothermal non-electric applications in a number of geographical regions and to obtain technical and economic data under field operating conditions.

Assessing environmental, health, and safety concerns affecting geothermal development and developing ways of monitoring and ameliorating them are the primary objectives of the Environmental Control subprogram. The release of hydrogen sulfide to the atmosphere, land surface subsidence caused by the withdrawal of fluids from geothermal reservoirs, and seismicity induced by geothermal fluid extraction and injection are examples of geothermal environmental concerns.

The Facilities subprogram supports field facilities for testing and demonstrating new techniques, equipment, and systems. This support includes the construction and operation of commercial-scale 50-megawatt geothermal electric power plants employing different energy conversion technologies. A major program objective is to demonstrate the economic feasibility and environmental acceptability of producing electric power from geothermal resources. These and other facilities provide a foundation for subsequent commercial development of hydrothermal resources.

B. Hydrothermal Commercialization

The Hydrothermal Commercialization program seeks to accelerate commercial utilization of hydrothermal resources for electric power and for direct heat applications, thereby displacing fossil fuels.

Activities of this program include formulation of geothermal commercial development plans, development of a national geothermal progress monitoring system, assessment of the market penetration potential for hydrothermal resources, and identification of direct heat markets suitable for early penetration. Further activities are development planning in cooperation with local and state officials and potential users, support for economic and engineering feasibility studies, continuing interagency coordination and policy development under the aegis of the Interagency Geothermal Coordinating Council (IGCC), and outreach programs to acquaint potential users with the availability and competitive cost of hydrothermal energy and with the availability of financial assistance through various federal development programs.

C. Geopressured Resources

The Geopressured program seeks to resolve key technical and economic uncertainties now impeding commercial development of geopressured resources. Major questions concern the size of the resource base, the amount of

economically recoverable methane contained in geopressured aquifers, the production capacities and lifetimes of individual reservoirs, the economic feasibility of using the thermal and hydraulic energy obtainable from these reservoirs, and possible environmental effects of energy production from geopressured reservoirs.

A major thrust of the program is the determination of reservoir characteristics of geopressured aquifers on the Texas and Louisiana Gulf Coast by means of production tests of new and existing wells. Several successful short-term tests of existing wells, originally drilled for oil and gas, have been conducted under the Wells-of-Opportunity subprogram. Long-term tests to define characteristics of large reservoirs and to monitor environmental effects require drilling of new wells. A new well was drilled successfully in Texas in FY 1979. Three new wells will be drilled in FY 1980 and three more in FY 1981.

Environmental assessment activities are conducted concurrently with well site selection and well drilling and testing activities. Monitoring efforts and experimental programs at well sites yield information on the environmental effects of sustained high-volume production of geopressured brines.

Engineering activities focus on conceptual design of surface facilities, production cost analysis, and well drilling and completion technology development. The Geopressured program is developing equipment and production techniques in response to the particular temperature, pressure, and salinity regimes characteristic of geopressured reservoirs.

Finally, DGE is working with agencies at various levels of government and with the private sector to analyze the legal, institutional, economic, and technological factors affecting geopressured resource development.

D. Geothermal Technology Development

The objective of the Geothermal Technology Development program is to reduce geothermal costs by improving technology, thus expanding the economically recoverable

resource base. The two major subprograms are Component Technology Development and Hot Dry Rock.

The Component Technology subprogram is carrying out R&D in the five areas summarized below.

The Drilling and Completion Technology subprogram emphasizes improvements in drill bits, downhole motors, and drilling fluids in order to achieve a 25 percent reduction in well costs by 1983 and a 50 percent reduction by 1986.

The Energy Conversion Technology subprogram seeks to reduce geothermal electric power generating costs. The subprogram is directed primarily toward performance improvements and cost reductions in energy conversion system components, particularly heat exchangers.

The Reservoir Stimulation subprogram is developing new explosive and hydraulic fracturing techniques to increase the fluid productivity of geothermal wells. By increasing well productivity, stimulation technology can reduce the number of wells required to exploit a reservoir.

The Geochemical Engineering and Materials subprogram pursues technical solutions to problems associated with the handling and disposal of geothermal fluids. This work focuses on development of economical materials durable enough to be used in hostile geothermal environments.

The Geosciences subprogram activities include exploration technology, reservoir engineering, logging instrumentation, and log interpretation. Exploration technology is designed to improve the accuracy of pre-drilling reservoir assessments. Reservoir engineering is concerned with accurate prediction of reservoir productivity and longevity. Other geosciences activities include the development of measuring devices that can survive geothermal environments and of geothermal well log interpretation to determine reservoir characteristics from borehole information.

The second major subprogram is Hot Dry Rock. The hot dry rock resource requires a major technology advance if its commercial exploitation is to start before the end of the century. Recent operation of a five-megawatt HDR thermal loop at Fenton Hill, New Mexico, has improved the prospects for eventual technical success. In addition to

the Fenton Hill work, DOE is continuing regional and national activities to assess the HDR resource.

Funding levels for each of the programs and subprograms described above are presented in Table I-1.

The following four sections, structured along the lines of the FY 1981 budget, present detailed program descriptions. Each program description contains a general discussion of relevant technical aspects, a summary of project status and plans, a milestone chart presenting major decision points through FY 1985, and funding levels for FY 1979 through FY 1981.

A section which describes the nature and extent of DOE's participation in international geothermal projects and activities follows the program descriptions. The final section describes DOE geothermal program management functions at headquarters and in the field.

TABLE I-1
Funding Levels for Geothermal Energy Programs
FY 1979 through FY 1981

	BUDGET AUTHORITY (DOLLARS IN THOUSANDS)			
	ACTUAL FY 1979	ESTIMATE FY 1980	ESTIMATE FY 1981	INCREASE (DECREASE)
GEOTHERMAL ENERGY				
HYDROTHERMAL RESOURCES				
Resource Definition	26,163	13,406	19,398	5,992
Non-Electric Applications	10,238	12,200	16,000	3,800
Environmental Control	1,859	1,300	2,600	1,300
Facilities	22,968	33,694	15,002	(18,692)
Capital Equipment	1,232	800	0	(800)
Total Hydrothermal Resources	62,460	61,400	53,000	(8,400)
HYDROTHERMAL COMMERCIALIZATION				
Planning and Analysis	5,239	5,000	5,040	40
Private Sector Development	4,410	4,860	4,960	100
Total Hydrothermal Commercialization	9,649	9,860	10,000	140
GEOPRESSURED RESOURCES				
Program Coordination	1,192	882	2,200	1,318
Resource Definition	24,455	32,329	31,000	(1329)
Engineering Applications	72	839	900	61
Environmental Control	551	1,650	1,700	50
Facilities	0	0	0	0
Capital Equipment	111	300	200	(100)
Total Geopressured Resources	26,381	36,000	36,000	0
GEOTHERMAL TECHNOLOGY DEVELOPMENT				
Component Technology Development				
Drilling and Completion	5,432	7,000	8,250	1,250
Energy Conversion	9,344	7,100	12,800	5,700
Reservoir Stimulation	4,442	3,000	4,500	1,500
Geochemical Engineering and Materials	7,071	3,600	5,005	1,405
Geosciences	8,477	4,200	7,835	3,635
Subtotal Component Development	34,766	24,900	38,390	13,490
Hot Dry Rock	15,077	14,000	13,500	(500)
Capital Equipment	1,479	2,100	1,110	(990)
Total Geothermal Technology Development	51,322	41,000	53,000	12,000
TOTAL GEOTHERMAL ENERGY	149,812	148,260	152,000	3,740

II. HYDROTHERMAL RESOURCES

Hydrothermal resources consist of hot water and steam trapped in porous or fractured rocks beneath overlying geologic formations. A specific hydrothermal system is classified as 'vapor' or 'liquid' according to the principal state of the subsurface fluid. Different energy conversion systems are used to recover the energy found in each of these types of hydrothermal resources. Electricity is generated from dry-steam deposits by passing the steam directly through turbines. Liquid-dominated deposits are exploited for power either by partially flashing the hot liquid into usable steam at the surface (flash-steam system) or by transferring its heat to a secondary working fluid, such as freon, which in turn is passed through the turbines (binary-cycle system).

Energy derived from hydrothermal resources also can be used for direct thermal applications. These nonelectric applications, primarily space and process heating, are feasible at temperatures suitable for electric power generation and at lower temperatures. Hot water is piped directly from the geothermal reservoir to the point of use.

Thirty-seven states contain hydrothermal resources; several western regions contain known major resources. Substantial electric power and direct use capacity is expected to be realized by 1984. Projections of approximately 2600 megawatts of electric power generating capacity and nearly 300 megawatts of thermal power by 1984 reflect the potential for this resource.

The Hydrothermal Resources program provides research, development and demonstration (RD&D) support to hydrothermal commercialization activities. This support includes:

- Assessment and confirmation of geothermal reservoirs in cooperation with the USGS, state agencies, and industry.

- Field experiments to demonstrate the engineering and economic aspects of direct heat uses of geothermal resources. The participants are selected by competitive solicitation of cost-shared projects.

- Experimental facilities constructed and operated to perfect new geothermal equipment and process techniques, particularly for electric power production. These techniques will reduce the costs of exploiting hydrothermal resources.

- Major demonstration plants to generate commercial quantities (50 MW_e) of electric power from moderate-and high-temperature geothermal fluids. These plants will provide operating experience needed to establish the technical and economic viability of the technology at full commercial scale. They will be built and operated by industry, which will share the cost.

The Hydrothermal Resources program is divided into four major subprograms: Resource Definition, Non-Electric Applications, Environmental Control, and Facilities. Funding levels for these subprograms are presented in Table II-1.

Table II-1
Funding Levels for Hydrothermal Resources
Subprograms
FY 1979 through FY 1981

HYDROTHERMAL RESOURCES	BUDGET AUTHORITY (DOLLARS IN THOUSANDS)			
Subprograms	ACTUAL FY 1979	ESTIMATE FY 1980	ESTIMATE FY 1981	INCREASE (DECREASE)
Resource Definition	26,163	13,406	19,398	5,992
Non-Electric Applications	10,238	12,200	16,000	3,800
Environmental Control	1,859	1,300	2,600	1,300
Facilities	22,968	33,694	15,002	(18,692)
Capital Equipment	1,232	800	0	(800)
Total	62,460	61,400	53,000	(8,400)

A. Resource Definition

This subprogram provides quantitative assessment of the hydrothermal resource potential and confirms hydrothermal prospects through selective drilling. Other major objectives are to:

- Evaluate the hydrothermal resource potential of the United States,
- Determine the geographical distribution of the hydrothermal resource,
- Confirm the existence and commercial potential of high-temperature reservoirs suitable for both electric power generation and direct heat uses, and
- Identify and confirm low- and moderate-temperature prospects with potential for direct heat application.

In pursuit of these objectives, DGE works with the U.S. Geological Survey in conducting regional and national assessments of hydrothermal resources. Additionally, DGE supports drilling to confirm high-temperature reservoirs with near-term commercial potential under programs cost-shared with private resource developers. Areas of high promise for low- to moderate-temperature reservoirs are the targets of geological and geophysical analyses in projects supported by joint federal and state funding. Further, an exploratory drilling program focuses on several regions with potential for direct heat applications, but without confirmed hydrothermal resources.

The map on the following page illustrates known and potential U.S. hydrothermal resources.

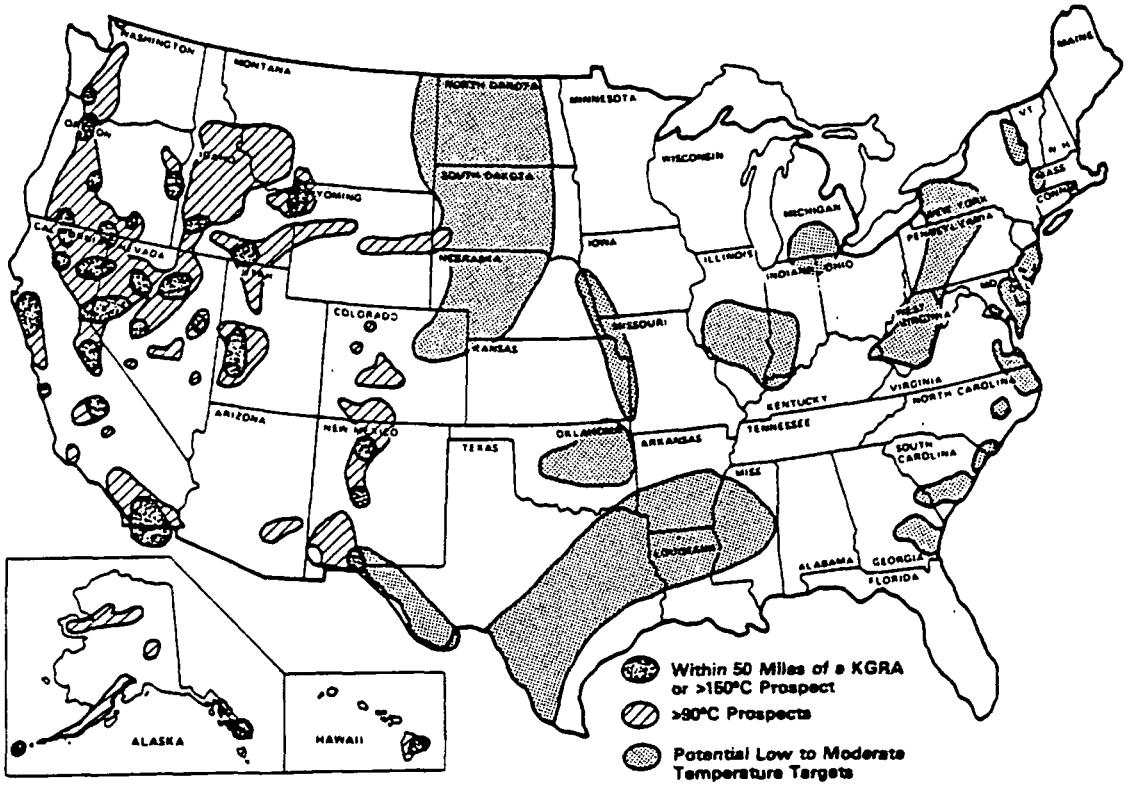

Known and Potential Hydrothermal Resources

Status

- National Geothermal Resource Assessment Update

With DOE support, the U.S. Geological Survey (USGS) has completed a major update of its assessment of U.S. geothermal resources. The results were published in January 1979 as USGS Circular 790. The update reaffirms the existence of large amounts of energy contained within the hydrothermal and geopressured resource bases.

This activity parallels active USGS and state participation in the DOE State-Coupled program. This program is directed at assessment of low- and moderate-temperature geothermal resources for direct heat applications. This relationship will continue to provide new information on low- and moderate-temperature resource areas.

- Industry-Coupled Reservoir Case Study

The objective of the Industry-Coupled Reservoir Case Study is to accelerate confirmation of geothermal reservoirs with apparent commercial potential for producing electricity. The Division of Geothermal Energy (DGE) shares exploratory drilling costs with industry in exchange for publication of reservoir data. In FY 1978, six companies participated in the program. Twenty shallow thermal gradient holes and four deep exploratory wells were drilled in the Roosevelt Hot Springs and the Cove Fort-Sulfurdale areas of south central Utah. In FY 1979, nine companies participated in the program. The program was extended to northern Nevada, where twelve sites are being investigated as candidates for exploratory drilling.

The National Energy Act (1978) provided incentives encouraging the development of geothermal resources, including investment tax credits, expensing of intangible drilling costs, and a percentage depletion allowance. These incentives will facilitate the financial involvement of industry in the exploration for and confirmation of high-temperature geothermal reservoirs, thereby minimizing further direct participation by DOE.

- State-Coupled Program

Low- and moderate-temperature resources for direct heat applications are being defined in a program that involves joint participation by DOE and 30 of the 37 states identified as having hydrothermal resource potential. In Phase I, analysis of existing geological and

geophysical data establishes the probability and distribution of these resources. As promising resources are identified, Phase II is initiated to provide a more detailed assessment of target areas with commercial potential. This phase may include the drilling of deep holes to confirm the existence and nature of the resources. One such project initiated in the Atlantic Coastal Plain region has delineated probable reservoir targets as part of the Phase I activity. Phase II activities are described in the next section.

Geothermal resource maps have been published for Oregon, Nevada and Arizona. Maps for Montana are being prepared. Maps for several other states participating in the State-Coupled program will be published during FY 1980.

- Exploratory Drilling for Low- and Moderate-Temperature Resource Confirmation

A limited exploratory drilling program has been completed in several regions where there is significant market potential for hydrothermal energy for non-electric purposes and where there are suspected but unconfirmed resources. Examples include the Snake River Plain, the Atlantic Coastal Plain, and the Mt. Hood region. An expanded User-Coupled Drilling program is under consideration. DOE would select a team comprised of a developer and a user to undertake a cost-shared project, consisting of surface exploration and exploratory drilling, to locate and confirm a reservoir suitable for commercial development near the user. Exploratory drilling activities conducted by DOE include the following:

- A 5500-foot deep test well drilled at Crisfield, Maryland recovered 133°F water at a potential flow rate of 325 gallons per minute. One additional exploratory well will be drilled in the Atlantic Coastal Plain during FY 1980.

- A well was drilled to a depth of 10,500 feet in the Snake River Plain to explore the possibility of locating moderate- to high-temperature fluids.

A planned use of the fluids, if located, was to provide a source of heat for a chemical processing plant at DOE Idaho National Engineering Laboratory. The well encountered temperatures of 300°F, but the volume of fluid found was insufficient to meet plant needs.

- Two deep wells will be drilled in the Mt. Hood, Oregon, area in FY 1980. Hydrothermal energy at this location might be useful for district heating in the city of Portland and for the space heating of facilities on or near Mt. Hood.

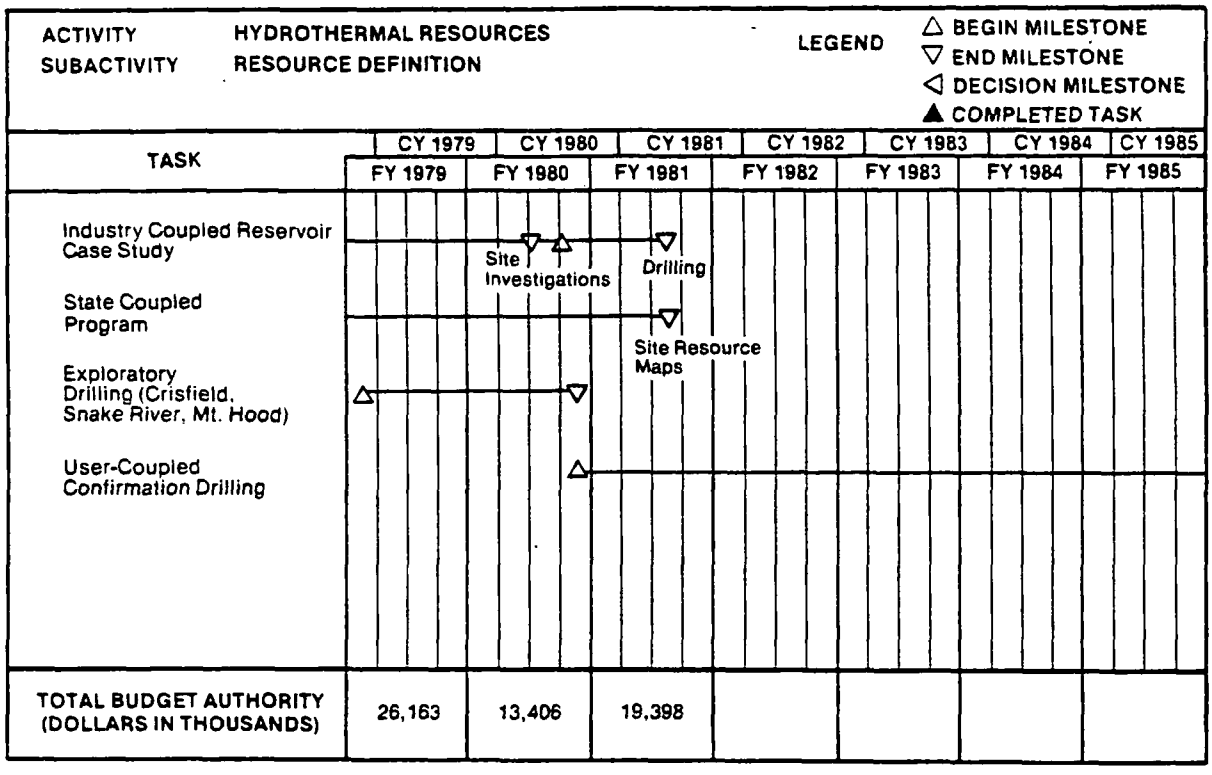

B. Non-Electric Applications

There is a large potential market for geothermal energy for industrial processing, agribusiness, and space and water heating in both commercial and residential buildings. The objectives of direct applications demonstration projects are to provide visible evidence of the viability of geothermal non-electric applications in a number of geographical regions and to obtain definitive technical and economic data under field operating conditions.

The following map indicates the locations of DOE direct heat applications field experiments.

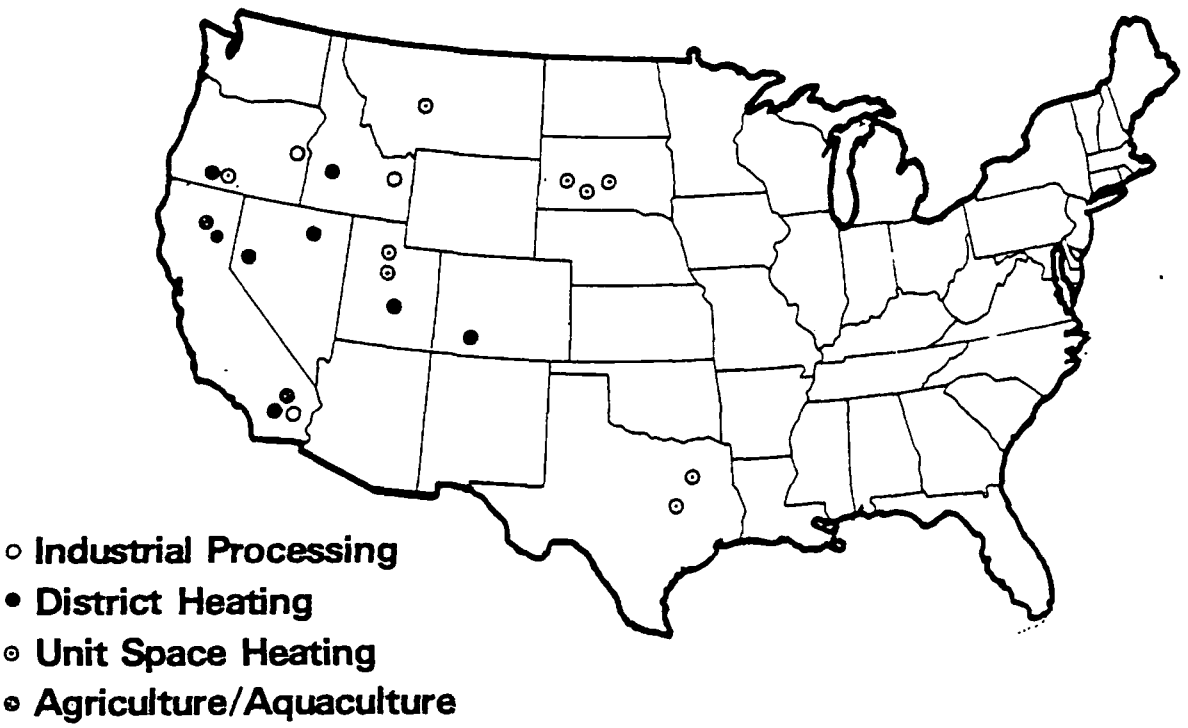

DOE Direct Heat Applications Field Experiments

Status

The first solicitation for geothermal direct-use field experiments was issued during the summer of 1977. Twenty-two proposals were received. Eight were selected for subsequent contracts, with the Government's share of the cost varying from 46 to 80 percent. A total of $2.1 million was obligated in FY 1978 for the initial phases of these projects, resulting in commitments of $2.9 million in FY 1979, and $650 thousand in FY 1980 to complete the work.

A second solicitation issued in April 1978 resulted in 40 proposals; 14 were selected for initial FY 1979 funding of approximately $4.9 million. Approximately $10.0 million will be required in FY 1980 and approximately $7.0 million in FY 1981 to complete this group of field experiments. Government cost-sharing amounts to approximately 60 percent of the total project cost.

Of the 22 current projects, the majority are for space heating, while a few are directed at agriculture and aquaculture, and 3 involve industrial processing. Although most of these projects are in the western states, greater emphasis will be placed on locating future demonstration sites in the East as suitable geothermal resources are defined there.

Milestones for Non-Electric Applications are shown on the next page.

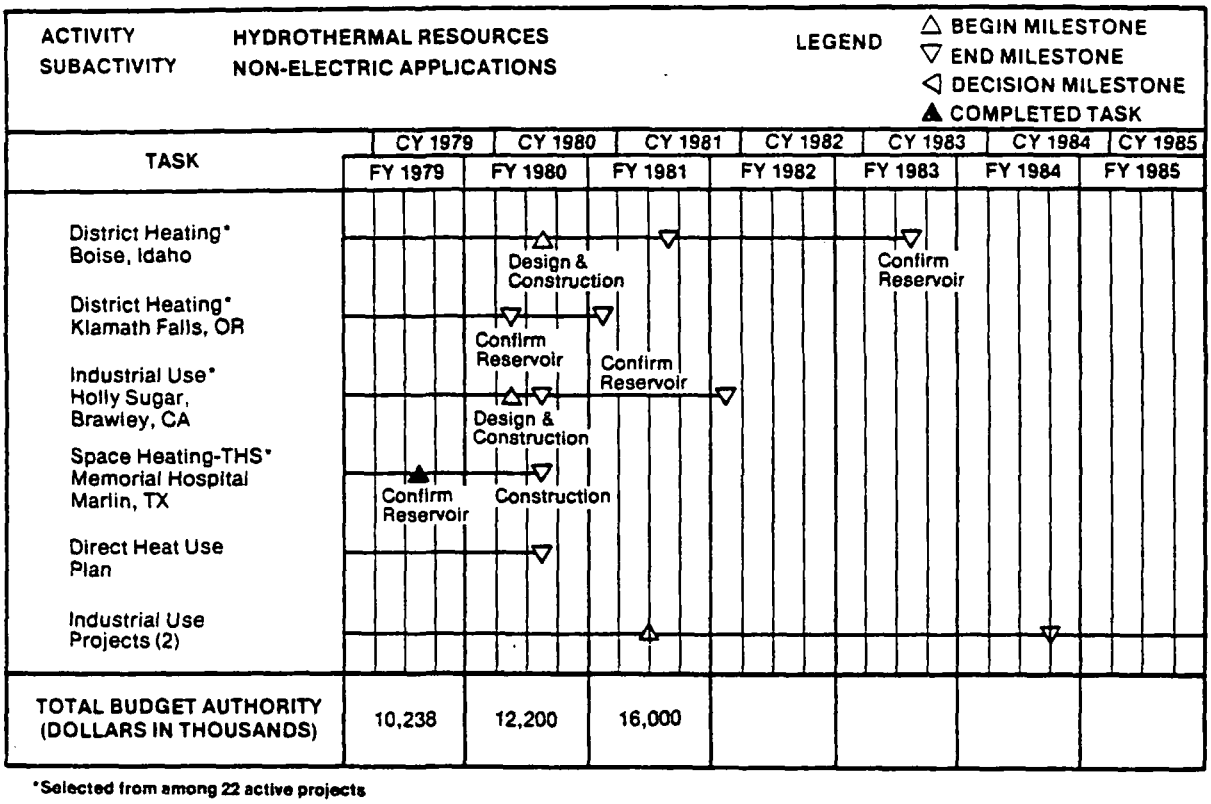

*Selected from among 22 active projects

C. Environmental Control

Environmental, health and safety factors affecting geothermal development were identified and discussed in the Environmental Development Plan (EDP) for Geothermal Energy Systems. Although the use of geothermal heat causes less environmental damage than does the use of many competitive energy sources, there are adverse impacts. Release of hydrogen sulfide (H_2S) is a major air quality concern and can cause corrosion of sensitive electrical components. The withdrawal of fluids from geothermal reservoirs may cause land surface subsidence. Additionally, seismic disturbances may result from geothermal fluid extraction and injection processes.

- Air

Some hydrothermal fluids contain dissolved noncondensible gases such as hydrogen sulfide, ammonia, boric acid, and radon. If these are released to the air in large quantities, they could produce toxic effects. Further, hydrogen sulfide has a disagreeable odor which, if emitted in large quantities, could be a nuisance.

- Water

Disposal of those hydrothermal and geopressured fluids which may contain toxic substances is a waste management problem. Care must be taken to assure that ground water quality will not be affected by accidental surface spills or leaks in underground pipes.

- Land

When large quantities of fluid have been extracted from the ground, land subsidence may occur. Earthquakes may be induced by the injection of water into underground fault structures.

- Health and Safety

Well blowouts have occurred during geothermal drilling activities. Excessive noise can result from the drilling of wells during the exploratory and development phases and from venting during the testing and operating phases. These events require appropriate control technology and procedures.

Status

The Division of Geothermal Energy (DGE) has examined each of these major environmental issues and has established environmental control research programs as needed. Experimental impact definition studies of liquid and solid waste disposal and well blowout are underway.

In addition to environmental control studies, DGE sponsors environmental monitoring for each of its major field projects in part to support program preparation of Environmental Assessments/Impact Statements (EA/EIS). To further assist with EA/EIS preparation, DGE has developed guidelines for environmental reports by contractors.

In FY 1980, two research activities in control technology will continue. The Subsidence subprogram will develop a system to monitor subsidence and compaction at depth. The Induced Seismicity subprogram will evaluate the potential for earthquake generation from geothermal activities and will provide seismic monitoring in the vicinity of geothermal fields under development.

A hydrogen sulfide removal system has been successfully tested at The Geysers Geothermal Field in California. Better than 98 percent removal efficiency was achieved. The system was developed by the EIC Corporation of Boston under a cost-sharing contract between DOE and the Pacific Gas and Electric Company (PG&E). The Environmental Protection Agency also participated in the tests.

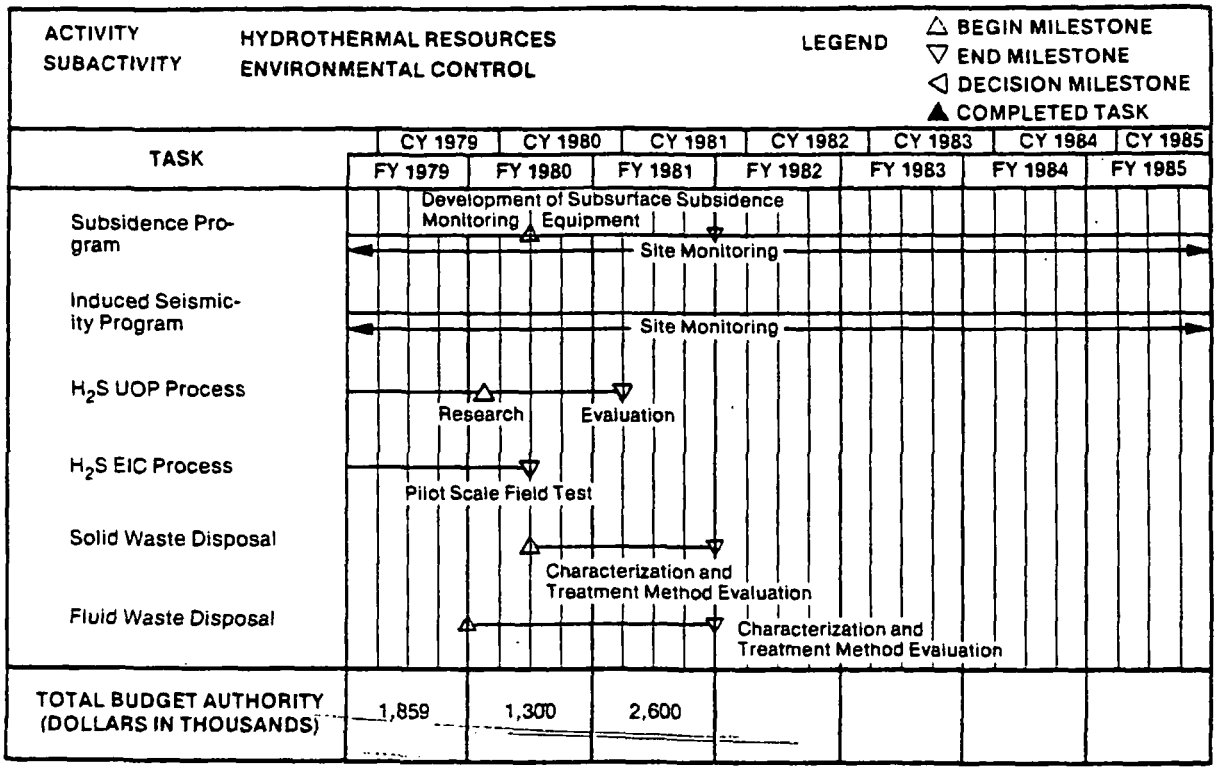

D. Facilities

Geothermal demonstration plants and other facilities provide technical and economic operating data, hands-on experience for industry, and demonstration of new techniques, equipment, and systems, all at pilot or commercial scale. These facilities foster wider acceptance and use of this alternative energy source. In many areas, industry will construct commercial plants subsequent to successful demonstrations. The following subsections describe DOE hydrothermal experimental facilities.

1. Demonstration Plants

The thrust of this activity is to design, construct, and operate commercial-size geothermal electric power plants based on proven technology. Successful demonstrations will stimulate nonfederal development of liquid-dominated hydrothermal resources for generating electric power.

The plants will demonstrate that production of electric power can be economical, environmentally sound, and socially acceptable. Project objectives are to:

- Demonstrate reservoir performance characteristics of specific liquid-dominated hydrothermal reservoirs,
- Demonstrate the validity of reservoir engineering estimates of reservoir productivity (capacity and longevity),
- Demonstrate commercial-scale energy conversion system technologies,
- Initiate commercial development at resource sites with great potential,
- Reduce unnecessary regulatory requirements and resolve other legal and institutional impediments to geothermal development, and
- Provide the financial community with a basis for estimating the risks and benefits associated with geothermal investments.

Each demonstration plant will generate statistically reliable engineering and cost data on reservoir performance and on plant construction, operation, and maintenance for up to five years. This in turn will demonstrate predictable technical, economic, and environmental performance with acceptable risk on a commercial scale.

For the information derived from the project to be useful, federal involvement must not distort the data from

normal business practices. Therefore DOE delegates management of the demonstration projects to industrial participants to ensure that the projects provide a realistic basis for the private sector to assess commercial feasibility.

Status

Under a cooperative agreement, both DOE and the competitively selected industrial participants will share the costs of design, construction, and operation of a 50-MW_e commercial-scale geothermal flash-steam demonstration plant at Valles Caldera, New Mexico. The arrangement involves paying back to the Government its portion of the investment from operating revenues.

In September 1977, ERDA issued the Geothermal Demonstration Powerplant Program Opportunity Notice (PON-EG-77-N-03-1717). In July 1978, the DOE Under Secretary determined, following presentation of the Source Evaluation Board findings, that negotiations for the construction and operation of the 50-MW_e commercial-scale geothermal demonstration plant should be initiated with Union Oil Company of California and the Public Service Company of New Mexico, under a cost-shared cooperative agreement. The proposed site is the Baca Ranch in Valles Caldera, New Mexico.

A letter cooperative agreement was executed between DOE, Union Oil, and the Public Service Company of New Mexico on September 29, 1978. The final cooperative agreement was completed on August 6, 1979. The final Environmental Impact Statement was scheduled for publication in early 1980. The plant should be operational by the second quarter of FY 1982.

An artist's conception of the first 50-MW_e demonstration plant is shown overleaf.

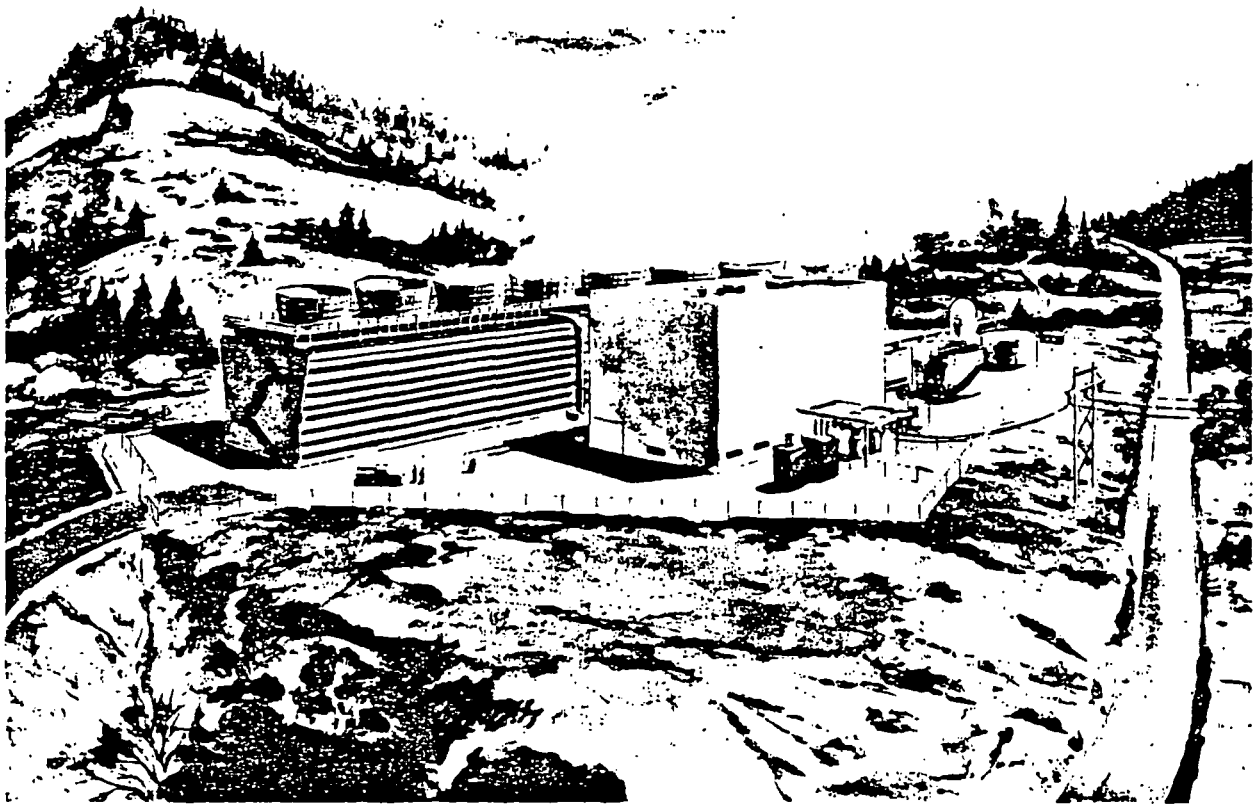

50-MW_e Hydrothermal Demonstration Plant

2. Raft River Pilot Plant

This project is a 5-MW_e binary cycle plant that uses a Rankine cycle to convert energy from a moderate-temperature hydrothermal resource (300°F) to electric power. Plant operating data will supply valuable information on the geothermal reservoir and plant equipment, operations, and economics for future commercialization of moderate-temperature resources.

Status

Plant construction is about 80 percent complete. The system is now being fitted with a turbine generator set, and additional well tests are being undertaken. This plant is expected to be operational by the end of FY 1980.

3. Hawaii Geothermal Wellhead Generator

The objective of this project is to evaluate the feasibility of using a wellhead generator to produce base-load electrical power. The 3-MW_e generator will use the geothermal fluid from a well already drilled into the rift zone of an active volcano. The design calls for mounting of the major power plant components, where economically feasible, so that they can be moved to other sites if threatened by lava flows. The project is expected to lead to commercial applications of wellhead generators in remote areas of the western U.S., Hawaii, and other parts of the world.

The construction phase started in the third quarter of FY 1979 and will be completed in the fourth quarter of FY 1980. The wellhead generator is being installed on a geothermal well in the Puna District, Hawaii.

Construction of this facility is on schedule and major equipment has been ordered. The geothermal well, which required recementing in FY 1979, is scheduled to begin production in the first quarter of FY 1981.

4. Geothermal Loop Experimental Facility (GLEF)

This facility, located near Niland, California, was established to evaluate the feasibility of flash-steam and flash-binary systems in the production of electric power from high-temperature/high-salinity resources. The project is cost-shared on an equal basis with the San Diego Gas and Electric Company.

The GLEF was constructed in 1975. The facility evaluated the flash-binary system initially and was later modified to evaluate a two-stage flash-steam plant with redundant flash trains. The latter plant design can increase production efficiency from well below 75 percent to over 85 percent and significantly reduce electricity production costs.

Studies have produced effective pre-injection fluid treatment procedures to eliminate injection clogging problems. Additionally, problems of scaling and corrosion have been solved. The facility completed its testing during FY 1979. The data derived from the facility have prompted Magma Power Company to build a 50-MW_e flash-steam plant on this site. This plant will be operational by late calendar year 1982 or early calendar year 1983.

5. Geothermal Component Test Facility (GCTF)

This facility provides moderate-temperature, low-salinity geothermal fluid and supporting services to experimenters for R&D testing of equipment and components to be used in geothermal systems.

The GCTF, located in East Mesa, California, is currently being used by several industrial firms and DOE contractors. It will be operational until demand diminishes.

ACTIVITY HYDROTHERMAL RESOURCES
SUBACTIVITY FACILITIES

LEGEND
△ BEGIN MILESTONE
▽ END MILESTONE
◁ DECISION MILESTONE
▲ COMPLETED TASK

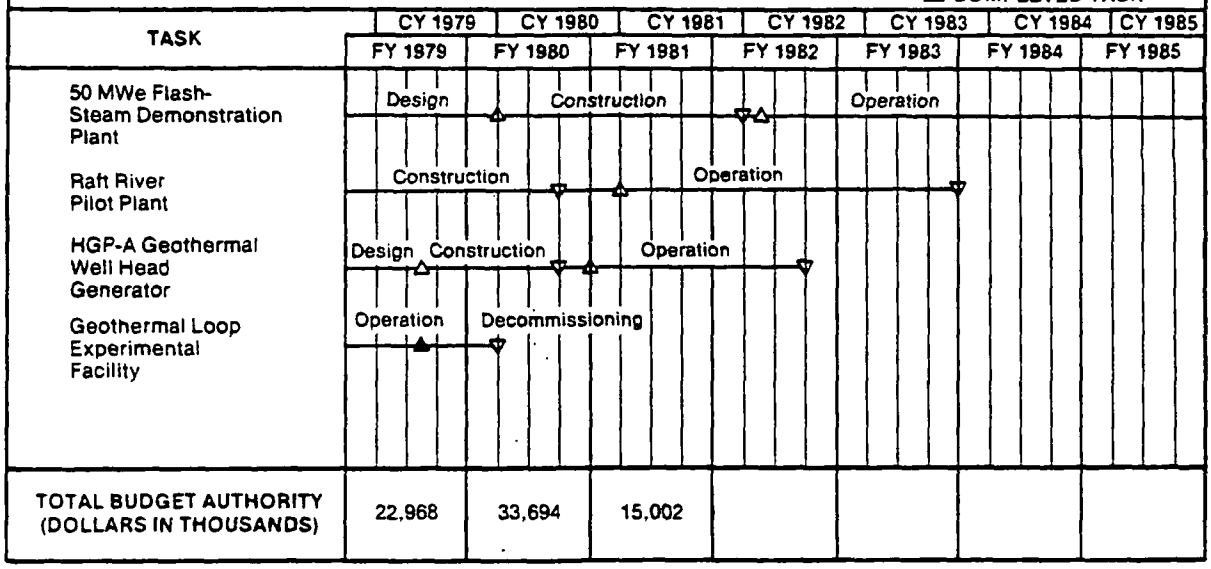

III. HYDROTHERMAL COMMERCIALIZATION

The Hydrothermal Commercialization program is designed to enable industry to maximize utilization of the Nation's geothermal resources in an environmentally and socially acceptable manner in the near term.

The major objective of the Hydrothermal Commercialization program is to accelerate the rate of commercial utilization of hydrothermal resources for electric power production and direct heat applications so that geothermal energy will make a significant contribution to domestic energy production. The development of hydrothermal resources will lead to the installation of new electric generating facilities needed to satisfy regional electric power demands, displacing fossil fuel required for this purpose. The Hydrothermal Commercialization program consists of two major subprograms: Planning and Analysis and Private Sector Development.

Funding levels of the Hydrothermal Commercialization program are presented in Table III-1.

Table III-1
Funding Levels for Hydrothermal
Commercialization Subprograms
FY 1979 through FY 1981

HYDROTHERMAL COMMERCIALIZATION	BUDGET AUTHORITY (DOLLARS IN THOUSANDS)			
Subprograms	ACTUAL FY 1979	ESTIMATE FY 1980	ESTIMATE FY 1981	INCREASE (DECREASE)
Planning and Analysis	5,239	5,000	5,040	40
Private Sector Development	4,410	4,860	4,960	100
Total	9,649	9,860	10,000	140

A. Planning and Analysis

This facet of the Hydrothermal Commercialization program comprises activities that establish program needs, priorities, and strategies through analyses of the economics of geothermal energy use, market penetration, institutional and legal barriers, and federal policies. To this end, the Division of Geothermal Resource Management (DGRM) prepares commercial development plans on site-specific, regional, and national levels and monitors progress made toward accomplishment of national objectives.

1. Planning

Geothermal commercial development plans at the local, state, and national levels are formulated to promote the rapid and efficient development of major geothermal prospects. State, local, and industrial entities participate in developing these plans.

Status

The statewide geothermal development planning projects and site-specific commercialization project planning in 15 Western and 3 Atlantic Coastal Plain states will continue through FY 1980. These cost-shared cooperative projects are targeted for three-year federal financial support followed by state-supported project continuation. Projects in additional states will begin in FY 1981.

2. National Progress Monitoring

The Division of Geothermal Resource Management has initiated the design and implementation of a national geothermal progress monitoring system as a foundation for assessing early indications of success or shortfall in commercialization. This will facilitate the adjustment of geothermal programs and plans. The system will provide periodic reports on status and progress and will maintain selected data bases to support progress evaluations.

The diagram below illustrates the geothermal progress monitoring network.

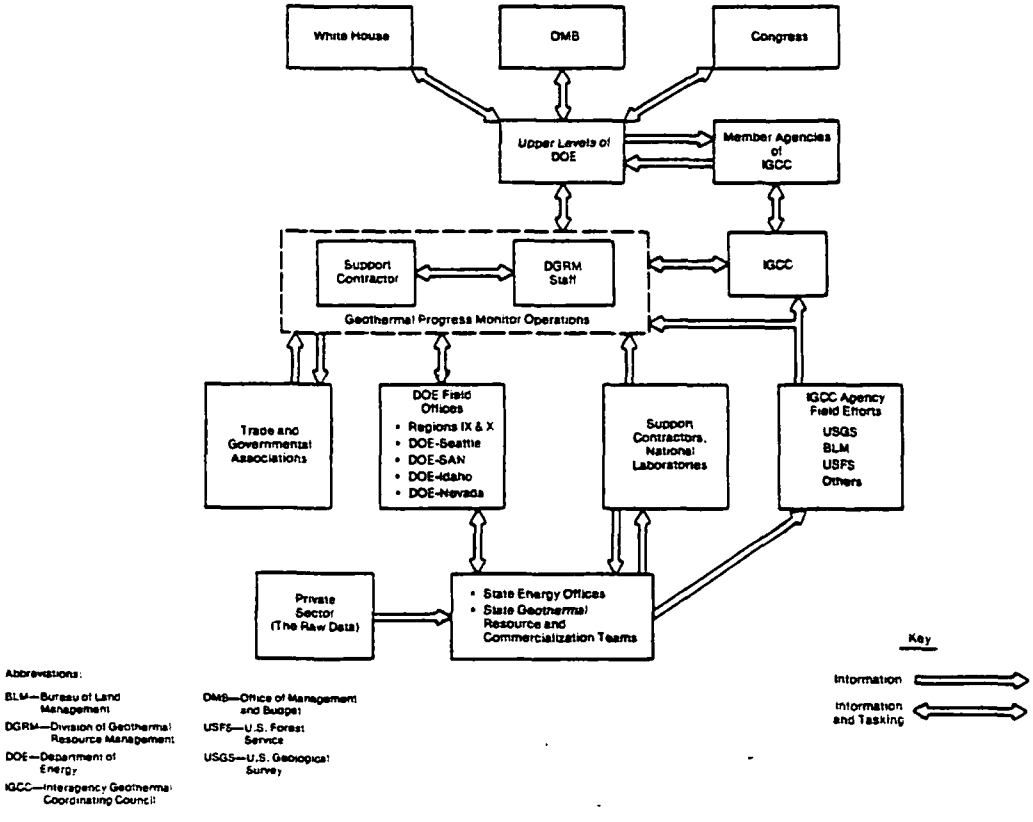

Geothermal Progress Monitoring Network

Status

The design of the system will be completed in FY 1980 and relevant information will be acquired, analyzed, and published. The system will report the pace of geothermal commercialization and thus measure the impact of the federal geothermal program.

3. Interagency Coordination and Federal Policy Development

The major purpose of this activity is to support the Interagency Geothermal Coordinating Council (IGCC) and to provide an interagency forum for the review of federal policies, regulations, and legislation related to geothermal matters. This activity also coordinates the IGCC annual report to Congress, as required by law.

Status

The panels and working groups of the IGCC continuously review new regulations, coordinate federal cooperative planning, and identify regulatory and legal changes and new policy measures that could affect the achievement of commercialization goals.

4. Economic Evaluation and Barrier Analysis

In this effort, DGRM conducts economic evaluations and barrier analyses to establish the market penetration potential for hydrothermal resources and to support the design of optimum marketing strategies. Further, impacts

of laws and regulations at the federal, state, and local levels on hydrothermal resource commercialization are evaluated and programs to overcome barriers are implemented.

Status

The market penetration likely in various geographic and industrial sector categories under alternative economic, policy, and technology assumptions will be estimated during FY 1980. Also, a cost-benefit analysis of the effectiveness of present and proposed federal program and policy measures will be conducted.

An analysis of existing federal, state, and local laws and regulations will form the basis for recommendations to enhance commercialization, particularly for direct heat applications. In FY 1980, basic economic data necessary to support DOE analysis and program prioritization will be generated.

Milestones for Planning and Analysis are shown on the following page.

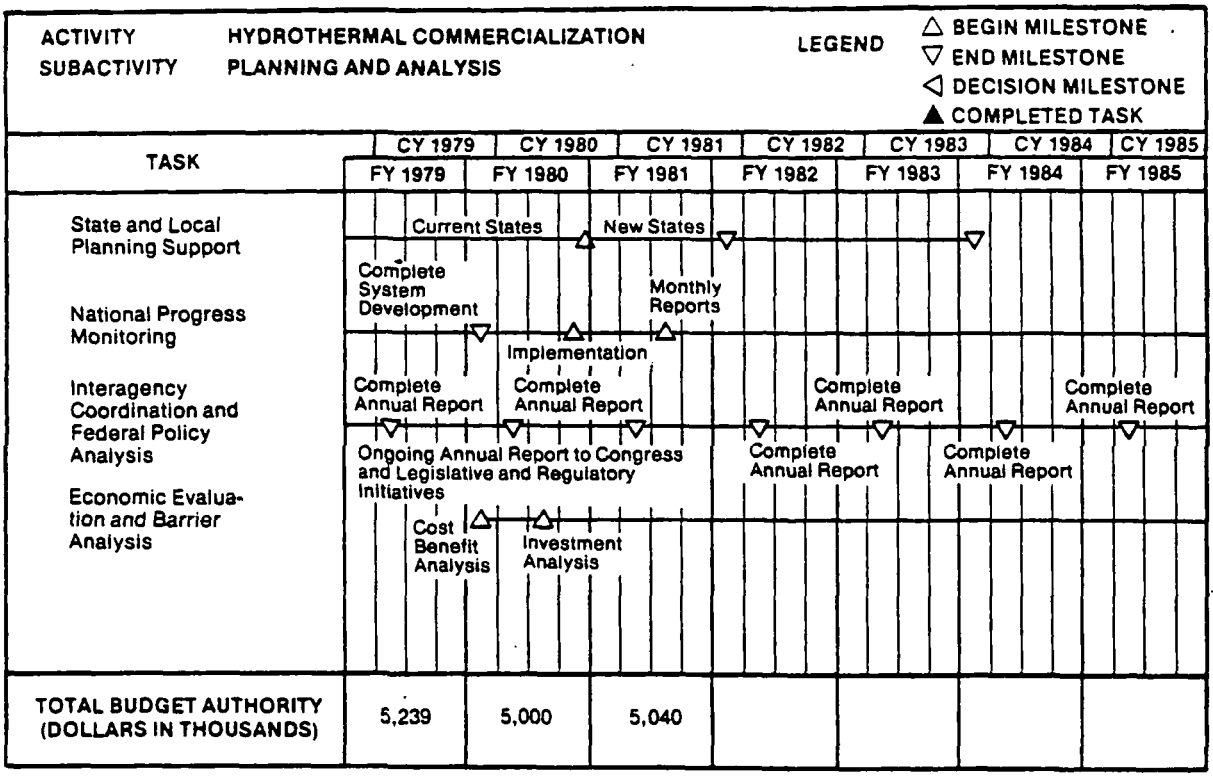

B. Private Sector Development

This aspect of the Hydrothermal Commercialization program seeks to stimulate private sector development through identification of and support for site-specific commercial opportunities for direct heat applications. Funds are provided for site- and application-specific engineering and economic studies of large-scale direct heat applications performed by the private sector. Support of regional community assistance centers is rendered along with technical consultation and information dissemination as part of an information outreach program.

1. Market Assessment

This effort seeks to identify market strategy and specific markets suitable for early penetration on a site-by-site, industry-by-industry, or project-by-project

basis. A further goal is to establish the economic competitiveness of geothermal energy with alternative fuels on a case-specific basis through removal of barriers and provision of incentives.

Status

During FY 1980, market analyses will be performed to define the market according to particular end-uses, size of market, location with respect to resource, density of users within a geographic area, and engineering feasibility. An analysis of energy supply and demand on a site-specific basis will be initiated to predict the degree of market potential and to identify actions and events which would increase market penetration. The potential for market penetration will be assessed through evaluation of the cost of competing energy sources, value of special attributes, and effects of alternative fuel availability.

Environmental, legal, and institutional barriers and financing problems related to specific projects will be addressed in FY 1980. A marketing strategy which considers these constraints at the state and local levels will be developed. Cooperative studies with various industries will be completed to determine the market potential of geothermal energy.

2. Hydrothermal Applications

The aim of this activity is to stimulate private sector interest in development of geothermal direct heat applications through direct developer/user participation and cost-sharing in feasibility analyses and direct heat utilization demonstration projects.

Status

The technical/economic studies concerning institutional uses, district heating, and industrial use of geothermal energy will be completed. Seven to nine additional assessments will be initiated to establish the feasibility of specific direct heat applications. A few selected industrial-scale site-specific pilot projects will be conducted under this program. A number of cost-shared field demonstrations will also be administered under the Program Opportunity Notice (PON) program. The experience gained from these projects will provide actual cost data for a variety of applications (see Section II.B, Non-Electric Applications).

3. Outreach Activities

This aspect of the private sector development effort strives to increase the general level of public and private understanding, interest, and enthusiasm for using geothermal energy as an alternative to imported or depletable domestic resources.

Status

Outreach activities undertaken in FY 1980 will include technical consultation with potential industry, community, and utility end users and public education programs that involve the dissemination of information on geothermal applications. When appropriate, DGRM will function as a broker between the developer and user to facilitate agreements and user commitments for commercial development.

4. Geothermal Loan Guaranty Program

In order to encourage and assist the private sector in accelerating the development and utilization of geothermal resources, DGRM supports a loan guaranty program to minimize a lender's financial risk so that credit can be made available for the construction and operation of geothermal projects, research and development projects, and field exploration. Further goals of the program are to encourage normal borrower-lender relationships and flow of credit to the geothermal industry in time without the need for loan guaranties, to enhance competition, to encourage new entrants into the geothermal market, and to commercialize a wide variety of geothermal resource areas and utilization projects.

Status

The Geothermal Loan Guaranty program (GLGP), continuing in FY 1980, provides guaranties to lenders on loans made for geothermal projects. Lenders perform traditional loan servicing functions so that experience is gained with each geothermal project. Guaranties are provided for both electric and direct heat projects.

The GLGP presently has guaranteed $43.4 million on four loans totalling $64.4 million. Applications are now pending for guaranties totaling $87.4 million on loans totaling $126.3 million. Three projects will provide an added 77 MW_e to current electricity production, and other projects will provide 117 billion Btu/yr for food processing.

ACTIVITY: HYDROTHERMAL COMMERCIALIZATION
SUBACTIVITY: PRIVATE SECTOR DEVELOPMENT

LEGEND
△ BEGIN MILESTONE
▽ END MILESTONE
◁ DECISION MILESTONE
▲ COMPLETED TASK

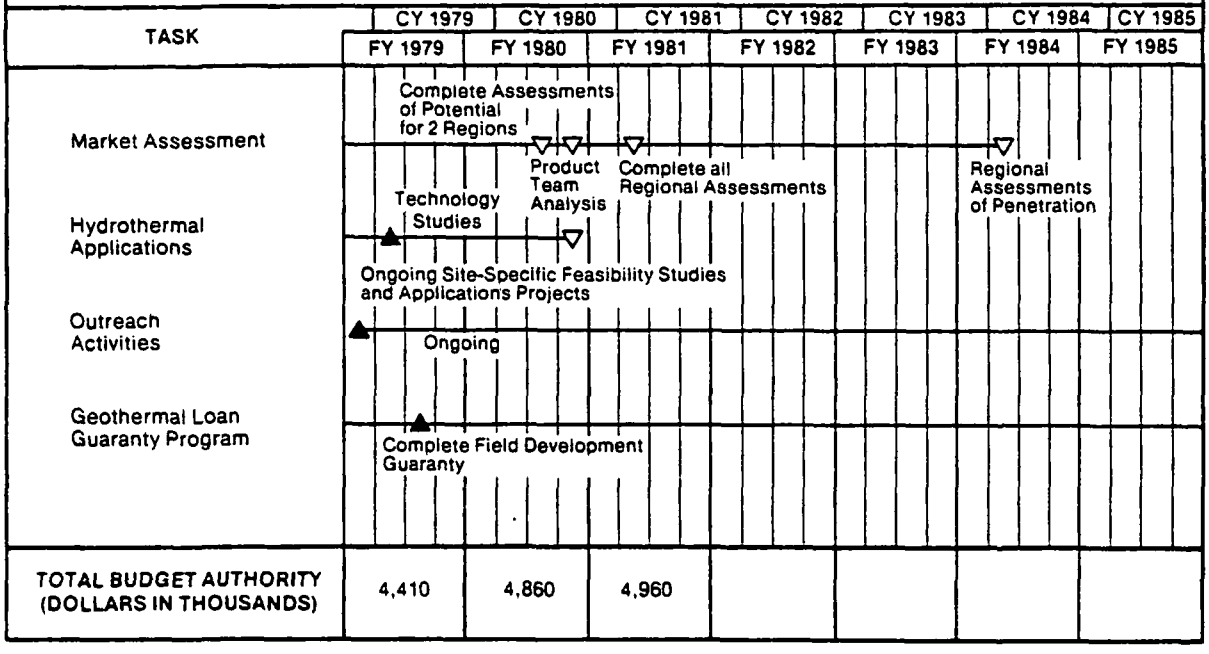

TOTAL BUDGET AUTHORITY (DOLLARS IN THOUSANDS)	4,410	4,860	4,960				

IV. GEOPRESSURED RESOURCES

Geopressured resources are high-pressure aquifers that contain dissolved methane gas. Methane is the major target of the energy recovery process, although thermal and mechanical hydraulic energy may also be obtained from the geopressured fluids. Recovery of the latter two forms, however, will be contingent on economical recovery of methane.

Geopressured aquifers, 12,000 to 20,000 feet deep, occur in the U.S. primarily in two broad zones parallel to the Texas/Louisiana coastline. Reservoir modeling and mapping of the Gulf States have identified numerous candidate sites for exploration. Extensive data from thousands of deep wells, drilled originally for oil and gas, prove the existence of these high-temperature, high-pressure zones and identify the geologic conditions under which they occur. The resource is estimated to contain between 3,000 and 50,000 quads of energy and thus constitutes a major U.S. energy target. Geopressured energy utilization goals are 2000 megawatts thermal (MW_t) and 3 quads per year methane production by the year 2000.

The objectives of the Geopressured program are to determine:

- The magnitude of the resource base,
- The amount of methane that is technically feasible to produce,
- The probable production lifetimes of the individual reservoirs,
- The economics of methane production,
- The economics of developing the associated thermal and mechanical energy, assuming that methane recovery is economical,

and to resolve environmental and institutional issues associated with developing the geopressured resource.

The existing Gulf Coast oil and gas production industry is expected to undertake rapid commercial development

of geopressured resources, provided that the resource base is shown to be sufficiently large and that its energy content can be tapped economically without adverse environmental effects.

The Division of Geothermal Energy supports resource definition and environmental assessment activities at the University of Texas, Austin and the Louisiana State University, Baton Rouge.

The program focuses on production tests of wells drilled into geopressured reservoirs. The results will reveal reservoir characteristics and the basic drive mechanisms that cause fluid and gas production, thereby allowing reservoir productivity and longevity to be estimated. Because the characteristics of geopressured aquifiers vary widely, and because reservoir performance under production conditions is a complex phenomenon, a substantial number of tests will be required before the potential of the total resource can be estimated reliably.

After the geopressured fluid has been brought to the surface, the associated methane can be recovered with existing technology. Although some improvements in well completion technology and in methods for managing reservoir production may be required, the conversion of thermal and mechanical energy to electric power (or the direct use of the thermal energy) apparently does not present significant technical barriers. Another issue to be considered is disposal of the brine, which would be produced in large volumes. The most practical method appears to be injection into subsurface formations, but the long-term effects of such operations have not yet been firmly established.

The Geopressured program is divided into four major subprograms: Program Coordination, Resource Definition, Engineering Applications, and Environmental Control.

Funding for each of these components is presented in Table IV-1.

Table IV-1
Funding Levels for Geopressured Resources Subprograms
FY 1979 through FY 1981

GEOPRESSURED RESOURCES	BUDGET AUTHORITY (DOLLARS IN THOUSANDS)			
ACTIVITIES	ACTUAL FY 79	ESTIMATE FY 80	ESTIMATE FY 81	INCREASE (DECREASE)
Program Coordination	1,192	882	2,200	1,318
Resource Definition	24,455	32,329	31,000	(1329)
Engineering Applications	72	839	900	61
Environmental Control	551	1,650	1,700	50
Facilities	0	0	0	0
Capital Equipment	111	300	200	(100)
Total	26,381	36,000	36,000	0

A. Program Coordination

The purpose of this activity is to determine the economic, environmental, institutional, and technological viability of developing the geopressured resource and to provide overall program planning. Policy options and technical programs are being assessed in coordination with federal, state, and local government agencies, industries, utilities, field operators, and public interest groups. This coordination of regional planning activities is organized through Louisiana State University and the University of Texas.

Status

Under these projects, resource characterization data are currently being gathered. These data will be used to identify impediments to geopressured resource development. This information, along with analyses of social and institutional factors that may affect geopressured energy use, will help identify impediments to commercial development of these resources.

In addition, studies focusing on the legal issues surrounding geopressured resource development have been carried out by Louisiana State University and the University of Texas.

DGE is also cooperating with the Gas Research Institute in the investigation of the potential for recovery of methane from geopressured resources.

B. Resource Definition

The purpose of the Geopressured Resource Definition subprogram is to determine location, size, temperature, pressure, methane content and production characteristics of geopressured sandstone aquifers along the Texas and Louisiana Gulf Coast. This complex analysis is based on geophysical log data from thousands of existing wells (originally drilled for oil and gas), on seismic surveys and core analyses, and on production testing of both new and existing wells.

The location of Gulf Coast geopressured sandstone aquifers is shown on the facing page.

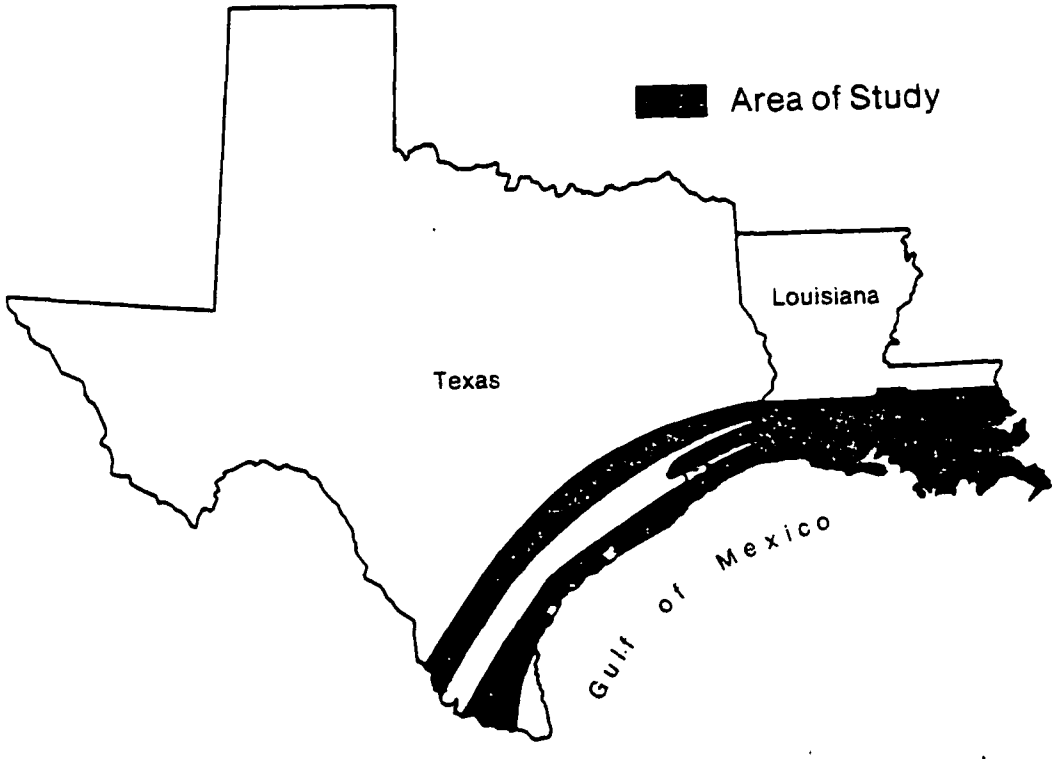

Gulf Coast Geopressured Zones

Status

Detailed examination of geopressured aquifers is continuing in FY 1980. The resulting data allow estimation of the resource base and aid in selecting sites for well drilling and teting projects.

Testing of existing wells, originally drilled to explore for oil and gas, is a means of obtaining geopressured aquifer data at moderate production rates in tests lasting only a few weeks. Tests of existing wells under the Wells-of-Opportunity subprogram will help define

requirements for development of the geopressured energy source. The first successful test of a geopressured aquifer, conducted in Vermillion Parish, Louisiana in 1977, produced methane-saturated brine. Additional tests in a well located in St. Mary's Parish were conducted in FY 1979. Existing well tests will continue in FY 1980 and FY 1981.

Though existing wells are suitable for short-term testing, these conventional oil and gas wells are not appropriate for long-term tests of fluid production at high flow rates. Long-term tests are needed to define properly the production capacities and longevities of large geopressured reservoirs, to determine the technical and economic aspects of brine disposal, and to define the probability of land surface subsidence and other environmental effects.

In 1979, DOE successfully drilled the Pleasant Bayou geopressured test well in Brazoria County, Texas, which is currently undergoing tests. Tests on this well will continue through FY 1981.

Approximately fifteen new geopressured wells will be drilled and tested through 1984 (about three per year) and about the same number of existing wells will be subjected to short-term tests.

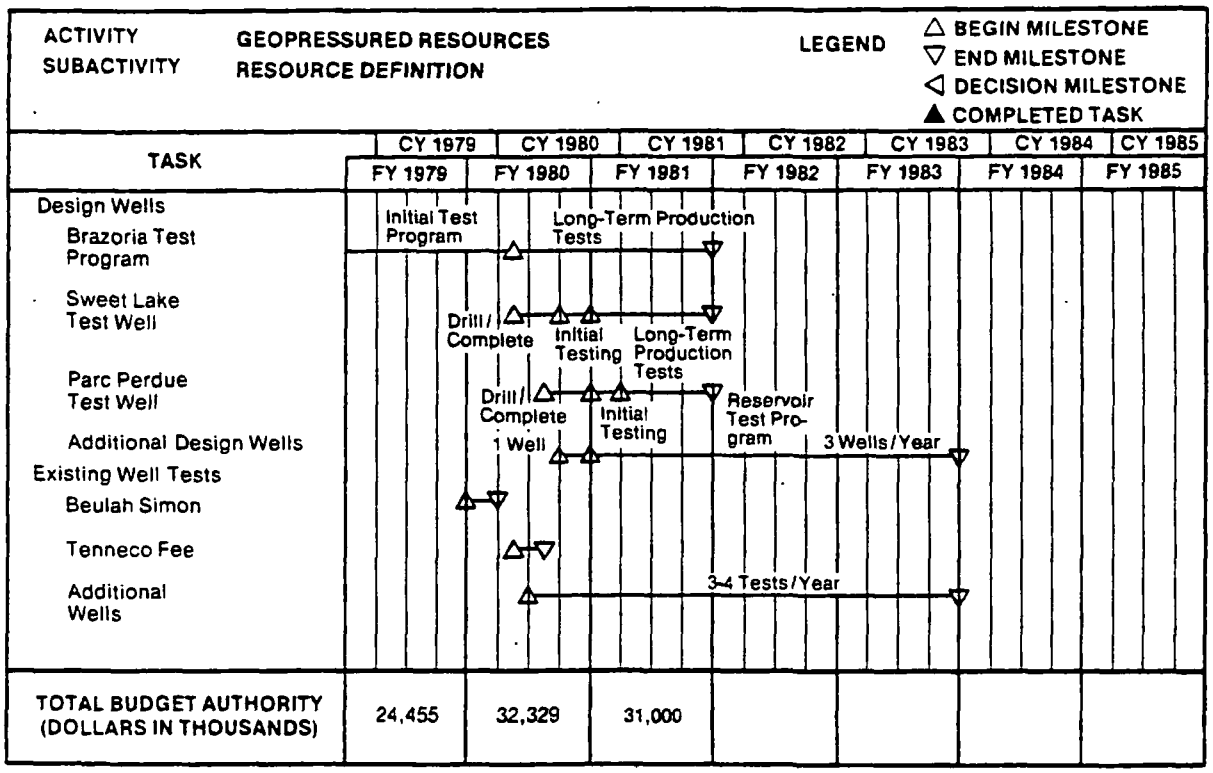

C. Engineering Applications

Efforts in this area are directed toward reducing the cost of developing and using geopressured resources. The program is carried out under the following basic categories: (1) surface technology and resource utilization and (2) well drilling and completion.

Status

Surface technology and resource utilization activities have been conducted in the areas of methane fuel

production, direct heat utilization, and electricity production. This work includes the conceptual design of facilities and preliminary economic analyses related to production costs. When the preliminary results of market analyses and well production tests become available in FY 1981, a decision will be made whether to support experimental facilities for electric power generation and direct heat applications from geopressured resources. Appropriate experiments would be undertaken in FY 1982 and FY 1983. Methane stripping studies will take place in FY 1980.

Well drilling and completion technology development will focus on problems related to the high temperature, pressure, and salinity associated with geothermal wells. A program to develop and demonstrate equipment and production methods suitable to geothermal geopressured resources will be carried out in the FY 1980-FY 1982 time period.

The diagram below conceptualizes a geopressured binary-cycle power plant installation.

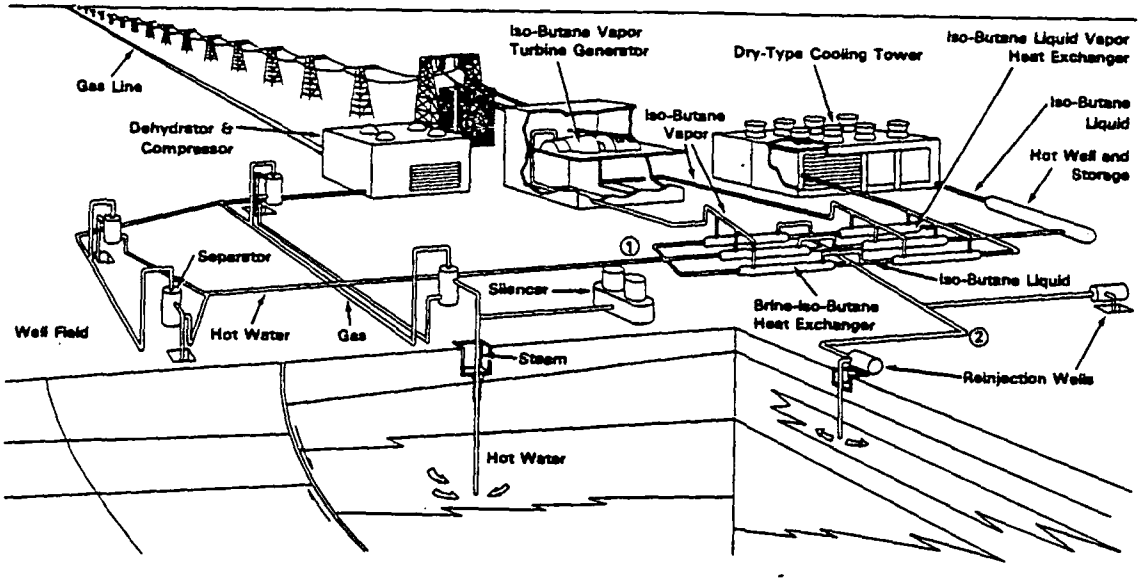

Geopressured Binary-Cycle Power Plant

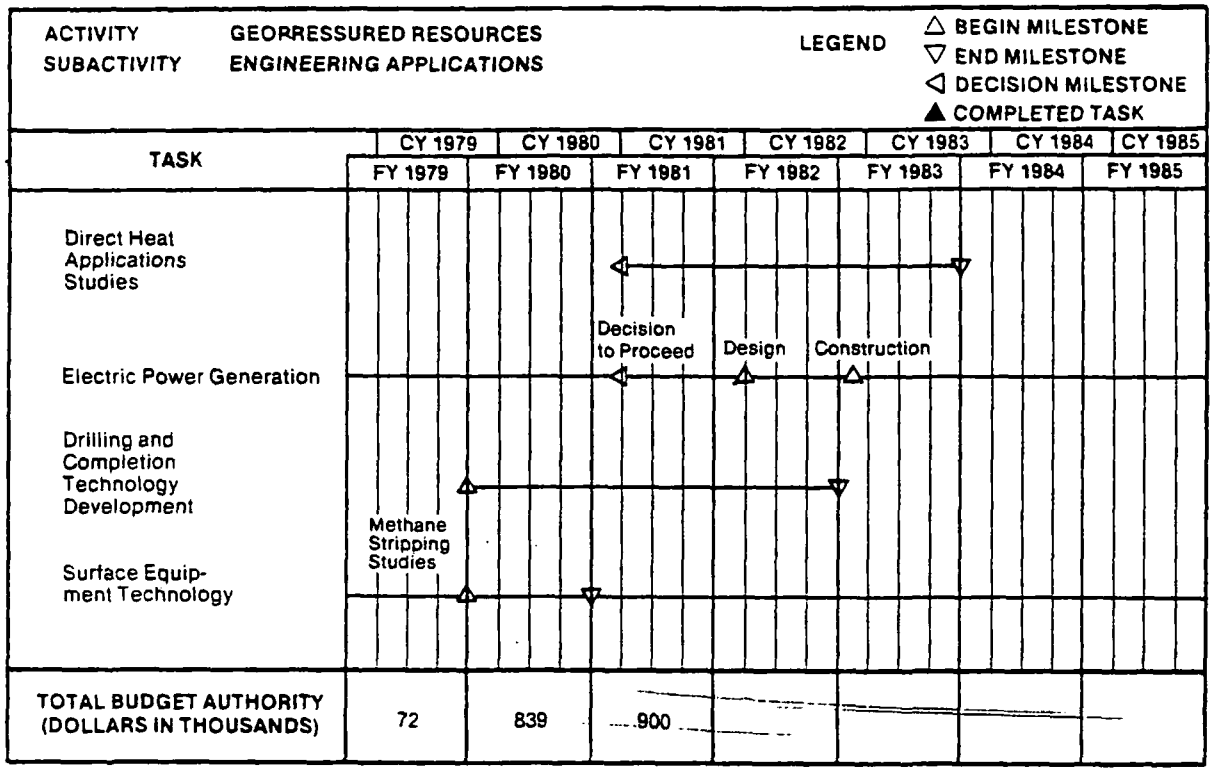

D. Environmental Control

The Geopressured program also includes support for continued research on possible environmental effects of sustained high volume production of geopressured brines. Land subsidence is the principal concern addressed by environmental research. The environmental implications of disposing of geopressured well fluids are also being observed through test well monitoring.

Status

The Pleasant Bayou Test Well in Brazoria County, Texas has been instrumented to measure all environmental parameters, including subsidence, micro-seismicity, and air and water quality. Data obtained from the monitoring of

the well tests will be used to assess the potential impact of geopressured aquifer development.

The disposal of large volumes of brine by reinjection is also under study. The predictive capability of mathematical reservoir models will be tested against well performance data to confirm their reliability.

Environmental assessment and monitoring of well sites in Texas and Louisiana will be accelerated to keep pace with the drilling. Appropriate environmental documentation (Environmental Assessments) will be prepared as necessary in connection with well testing activities conducted under the Resource Definition subprogram.

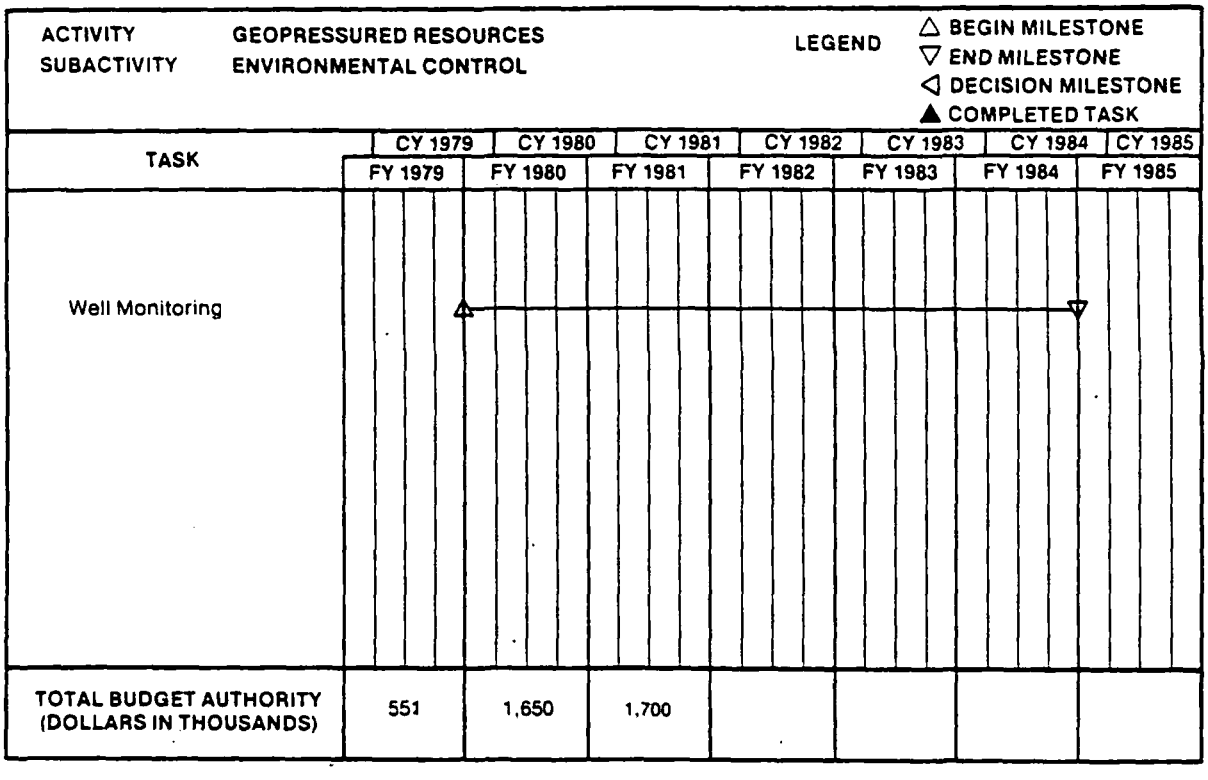

V. GEOTHERMAL TECHNOLOGY DEVELOPMENT

Geothermal energy can be exploited with technology similar to that used for oil and gas exploration and production. Oil field and water well equipment can be used safely and economically for some low-temperature geothermal applications, but conditions associated with moderate- and high-temperature geothermal resources often exceed the design capabilities of existing techniques, materials, and equipment.

The objective of the Geothermal Technology Development program is to provide improved technology in order to maximize early geothermal exploitation and to expand the economically recoverable resource base. Further, industry is encouraged to develop and market equipment and technology suitable for all geothermal environments. The program is divided into two major subprograms: Component Technology Development and Hot Dry Rock. Funding for Geothermal Technology Development is shown in Table V-1.

Table V-1
Funding Levels for Geothermal Technology Development Subprograms
FY 1979 through FY 1981

GEOTHERMAL TECHNOLOGY DEVELOPMENT	BUDGET AUTHORITY (DOLLARS IN THOUSANDS)			
ACTIVITIES	ACTUAL FY 79	ESTIMATE FY 80	ESTIMATE FY 81	INCREASE (DECREASE)
Component Technology Development				
Drilling & Completion	5,432	7,000	8,250	1,250
Energy Conversion	9,344	7,100	12,800	5,700
Reservoir Stimulation	4,442	3,000	4,500	1,500
Geochemical Engineering & Materials	7,071	3,600	5,005	1,405
Geosciences	8,477	4,200	7,835	3,635
Subtotal Component Development	34,766	24,900	38,390	13,490
Hot Dry Rock	15,077	14,000	13,500	(500)
Capital Equipment	1,479	2,100	1,110	(990)
Total	51,322	41,000	53,000	12,000

A. Component Technology Development

The Component Technology subprogram is organized to correspond to the activities associated with discovery and exploitation of a geothermal resource.

Drilling and well completion technology improvements could reduce the cost of geothermal wells 25 percent by 1983 and 50 percent by 1986. These technology improvements would affect the cost of the projected 10,000 wells that must be drilled in order to bring 25,000 MW_e of geothermal power on line.

The Conversion subprogram is developing pumps, heat exchangers, and systems for use with moderate-temperature geothermal fluid for economical production of electricity.

The Reservoir Stimulation subprogram is working on ways to increase production from individual wells, thereby reducing the number of wells required to exploit a reservoir.

The Geochemical Engineering and Materials subprogram addresses the special character of geothermal fluids and their interaction with other materials. Program efforts focus on developing materials and methods to combat problems of scaling, corrosion, injection well plugging, and materials failure.

The Geosciences subprogram concentrates on improving the technologies for exploration, reservoir engineering, logging instrumentation, and log interpretation.

1. Drilling and Completion Technology

This subprogram supports the development of advanced drill bits, downhole motors, drilling fluids, well completion methods, and advanced drilling systems that could reduce the cost of geothermal wells by as much as 25 percent by 1983 and 50 percent by 1986. The projected 10,000 wells that must be drilled in order to achieve the year 2000 target of 25,000 MW_e of geothermal electric power capacity would be affected by these economies.

In the initial stage, emphasis is placed on improvements in drill bits, downhole motors, and drilling fluids. Such improvements are necessary to demonstrate technology to meet the 25 percent cost reduction goal. The second stage includes the development of a new drilling system which would be required in order to achieve the 1986 cost reduction goal of 50 percent.

Status

An improved unsealed geothermal roller cone bit was developed and commercialized. This improved bit was designed specifically for drilling hot, hard fractured rock and was field tested at The Geysers Geothermal Field in California. The bits drilled 30 percent longer than conventional bits drilling the same formation at similar temperatures. Use of this new bit can save a minimum of four percent of the total well costs.

A successful field test of the downhole replaceable chain drill bit, developed by Sandia Laboratories, was conducted. This test confirmed the cost benefit of changing the cutting surface of the bit downhole. Commercialization efforts are presently underway. The figure on the next page shows the components of this "continuous chain" drill bit.

A new technique for removing scale from pipe was demonstrated. This new cavitating descaling system is a critical element in overall geothermal development, because it provides a nondestructive and efficient method for cleaning heat exchangers. The basic technology also will be applied to removing scale from geothermal production and injection wells.

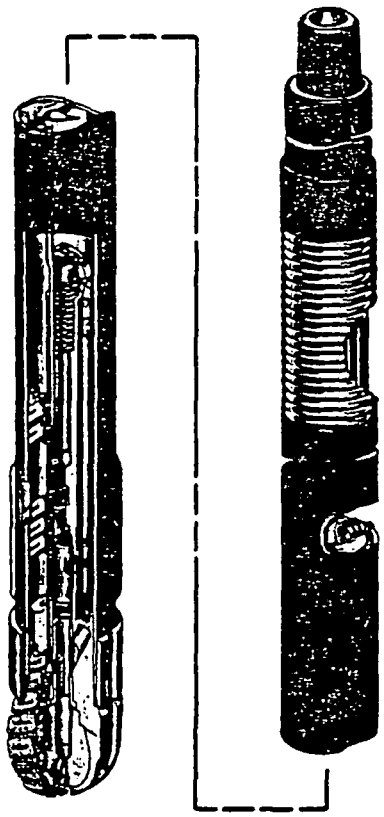

Continuous Chain Drill Bit (Prototype II)

Plans for the development of an advanced drilling system were formulated. A workshop including fifty participants from industry, universities, and government was held to provide recommendations on the development of advanced geothermal drilling systems. Concepts suggested for development include high speed motors and bits, percussion drilling systems, and jet drilling systems.

The FY 1980 program is expected to bring about the commercialization of the continuous chain-drill bit, advances in the use of manmade diamond materials for drill bits, and the evaluation of candidate technology for advanced drilling systems.

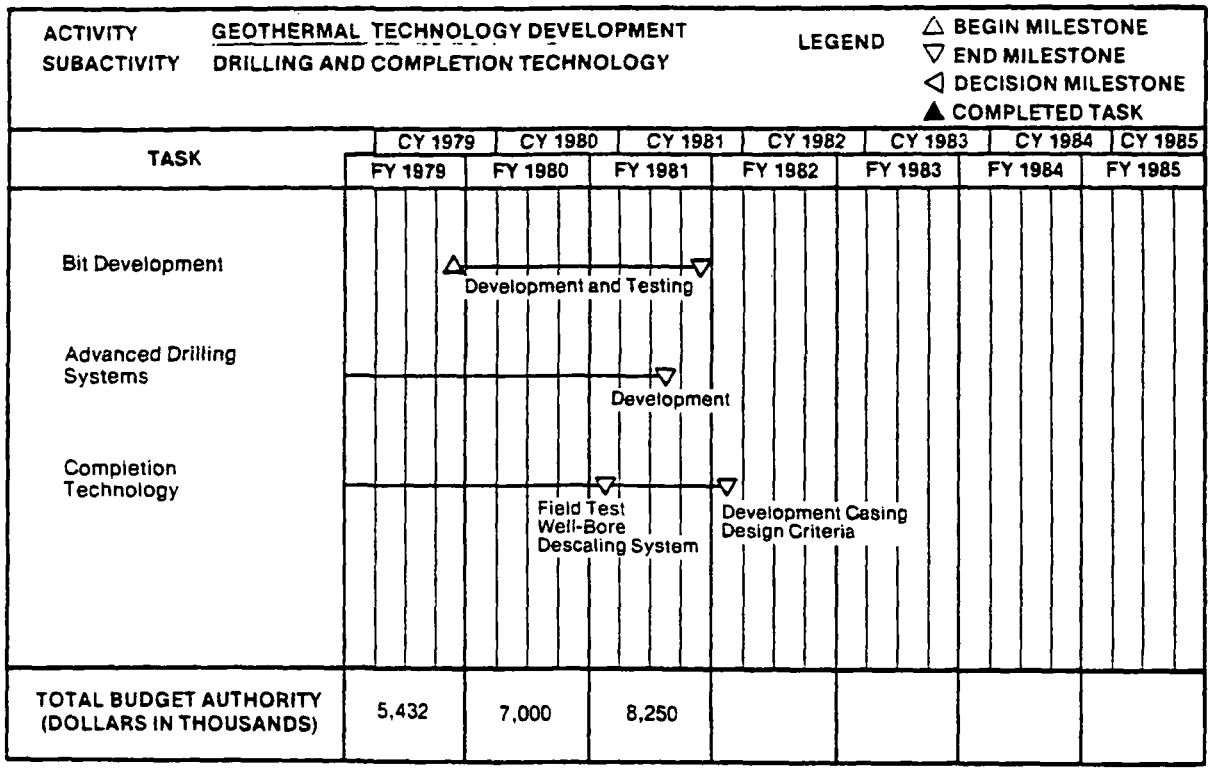

2. Energy Conversion Technology

Electricity derived from geothermal resources can serve a wide range of energy markets. The objective of the energy conversion technology program is to reduce geothermal electric generating costs. The program emphasizes conversion technology for moderate temperature resources, which have a much larger resource base than high-temperature resources but are inherently more expensive to exploit.

Binary conversion systems, which offer the greatest potential for reducing electric power generating costs, are a major focus of the program. Conversion technology seeks to improve performance and reduce costs of heat exchangers, which now account for 50 to 70 percent of binary plant costs.

Status

Major accomplishments and plans of the Conversion Technology subprogram include the following:

- The one-MW_e helical screw expander, a rugged, easily transportable wellhead generator system, was refurbished after a successful field test in Utah and made available under a cooperative agreement to the International Energy Agency (IEA) for testing at geothermal fields in Mexico, Italy, and New Zealand.

- A 500-KW_e skid-mounted binary power system employing direct contact heat exchangers has been installed at East Mesa and has undergone preliminary testing.

- A 100-KW_e transportable power system utilizing direct contact heat exchangers has been constructed and installed at a test site near El Dorado, Arkansas. Two months of preliminary shakedown and test runs have been completed. This mobile power plant is pictured on the next page.

- The preliminary design of components for the 5-MW_e ~~gravity~~ head binary cycle system was completed and major components and subsystems were ordered for assembly and installation in a test well in the Imperial Valley of California. Additional phases of the test program, including drilling of a large diameter well and final design, construction, and operation, will occur in FY 1980 through FY 1982.

- Several months of unattended continuous operation of the 60-KW_e binary plant at Raft River have provided new data on the reliability of binary system operation with low-temperature geothermal fluids.

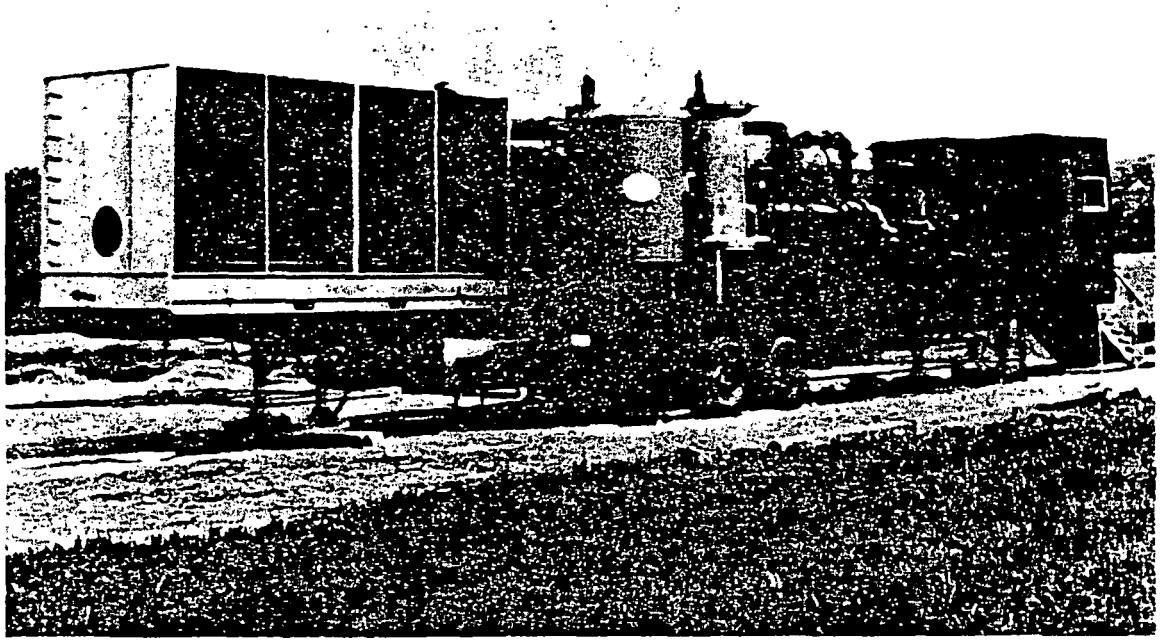

100-KW_e Mobile Power Plant

- Joint DOE/Electric Power Research Institute (EPRI) heat exchanger equipment tests have begun at the East Mesa geothermal component test facility.

- A comprehensive source book on the utilization of geothermal energy for electric power production will be published in FY 1980.

Milestones for the Energy Conversion Technology subprogram are shown on the next page.

ACTIVITY
SUBACTIVITY

GEOTHERMAL TECHNOLOGY DEVELOPMENT
ENERGY CONVERSION TECHNOLOGY

LEGEND
△ BEGIN MILESTONE
▽ END MILESTONE
◁ DECISION MILESTONE
▲ COMPLETED TASK

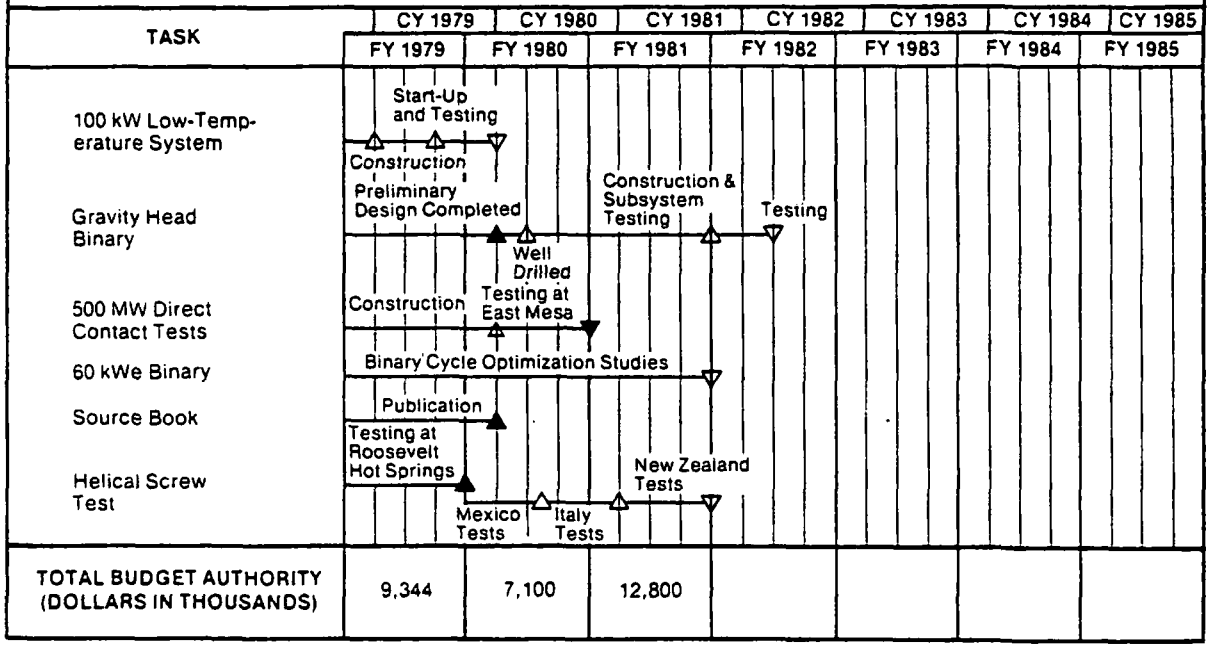

TOTAL BUDGET AUTHORITY (DOLLARS IN THOUSANDS)	9,344	7,100	12,800				

3. Reservoir Stimulation

Stimulation technology is used to increase fluid productivity of wells. Methods for stimulating geothermal wells include chemical treatment, hydraulic fracturing, and explosive fracturing. Geothermal stimulation methods can reduce the number of wells required to exploit a reservoir, thereby decreasing costs. Because of the high temperatures and the geologic conditions found in geothermal reservoirs, requirements for geothermal well stimulation technology differ from those for oil and gas wells. Under the geothermal well stimulation program, new equipment and techniques are being developed to function in the geothermal environment.

Status

An active geothermal well stimulation program was started in FY 1979 with the stimulation of wells at Raft River, Idaho. Stimulation resulted in a significant increase in production from one well and no discernable change in production from the second.

New tools and techniques for performing explosive stimulation of a well at The Geysers Geothermal Field in California have been developed. Newly developed high temperature explosives will be used in an attempt to increase fracture permeability. Explosive tests will be carried out in March 1980.

The Stimulation subprogram will carry out at least four field stimulation experiments by the end of FY 80. High-temperature equipment will be developed for use in the field experiments. The interactions between hot geothermal formations and various acids used to dissolve calcium carbonate and silica in the well bore and formation will be evaluated.

Milestones for this subprogram are shown on the next page.

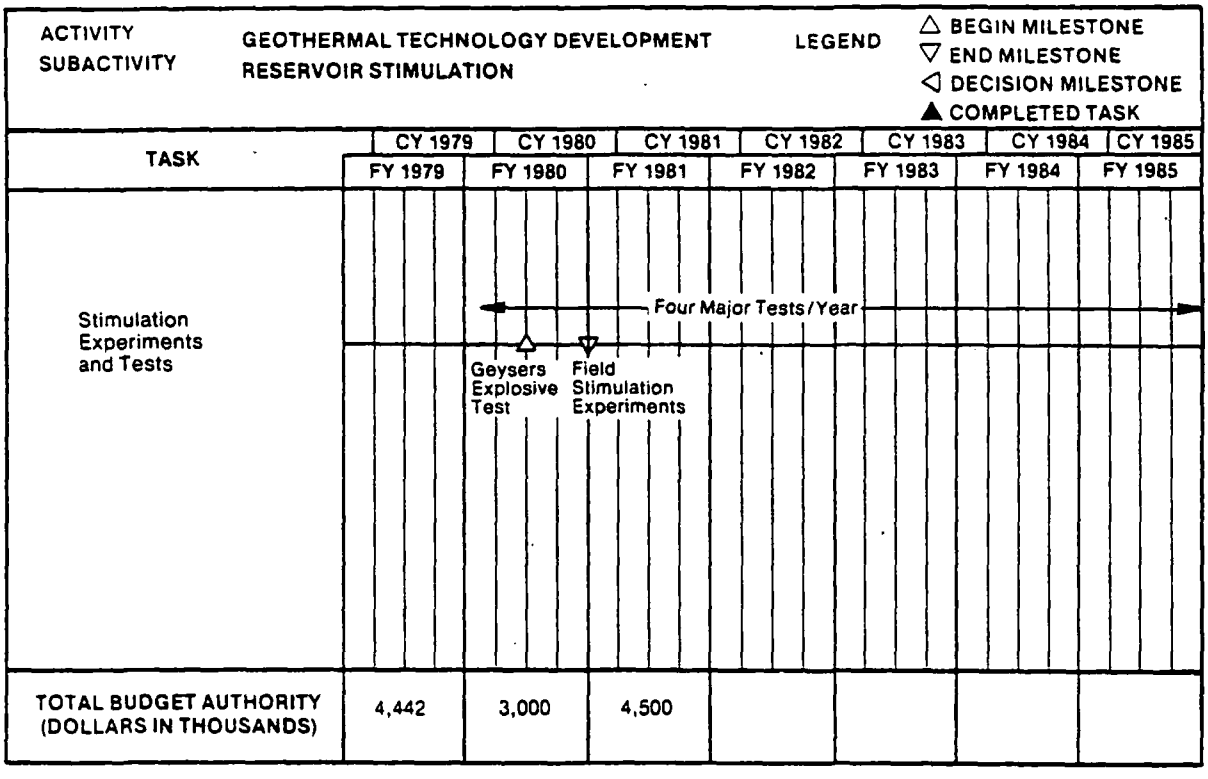

4. Geochemical Engineering and Materials

The Geochemical Engineering and Materials subprogram seeks technical solutions to problems associated with the handling and disposal of geothermal fluids. The subprogram addresses two main areas of interest: scale control and materials durability.

Materials and chemistry considerations are closely related to individual resource characteristics. To achieve overall economy in materials of construction, operation, and maintenance of geothermal systems at a wide variety of sites, durable materials resistant to localized corrosion and catastrophic failure are required.

The objective of fluid chemistry activities is to increase plant efficiency through improved fluid management techniques. Fluid disposal procedures and high-temperature chemical probes are being developed to control waste by-product removal and to optimize the potential for beneficial use of these wastes. A pilot system for controlling emission of hydrogen sulfide gas is pictured below.

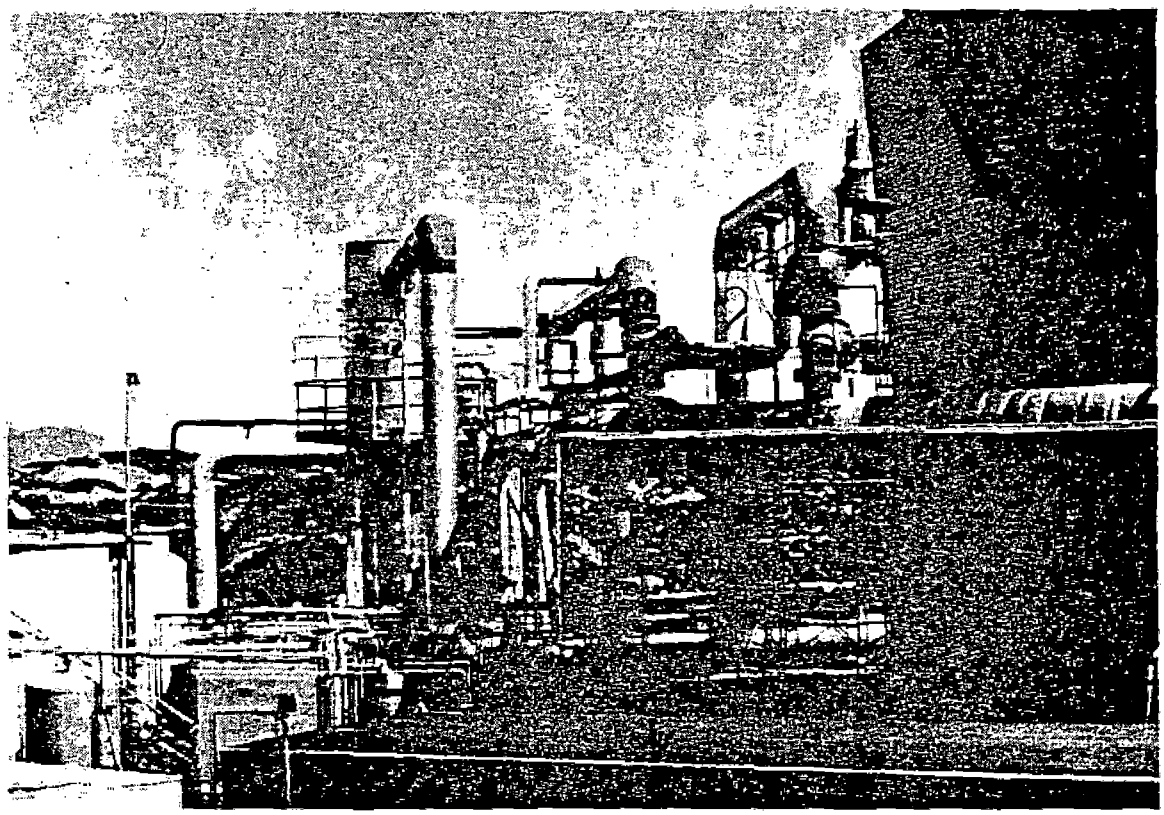

Hydrogen Sulfide Removal System at The Geysers Geothermal Field

Materials development efforts seek to advance more economical construction materials and to develop elastomers, metals, and non-metallics for use in the geothermal environment. Major subprograms are developing materials for use in logging tools, cable drill bits, and downhole pump bearings. Polymer concrete is being developed to replace expensive stainless steel and titanium for pipes and

pressure vessels. Steels that resist localized corrosion in well casing, drill pipe, and energy conversion equipment are under development.

Status

Major achievements and plans are described below:

- An analysis of available materials for use in geothermal applications has been completed. The work, presented in handbook form, will aid in the design of geothermal electric power plants. The handbook is now being updated to include materials for geothermal space heating and industrial process systems.

- Polymer concrete, high-temperature elastomers, and casing materials have been developed with 15 to 20 percent improvements in durability and corrosion resistance for geothermal environments. Polymer concrete lined pipes were tested at Niland, California, and East Mesa, California.

- The manufacture of commercial prototype polymer concrete pipe and the technology transfer of new high-temperature elastomers were initiated in September 1978. Two miles of the pipe and a non-destructive evaluation technique for prediction of drill pipe failure will be field tested in FY 1981.

- An industry cost-shared program to instrument the Magma Power Company binary plant at East Mesa, California has been initiated. DOE will provide instrumentation and data interpretation and will gain information on fluid characteristics.

- An American Society for Testing and Materials Committee (E-45) was initiated to standardize materials-related geothermal field test procedures.

- A series of high-temperature well cements has been developed and is being tested at the National

Bureau of Standards as part of an American Petroleum Institute Task Group effort for geothermal well cement standards development.

Geothermal materials work in FY 1981 will emphasize development and testing of elastomers, metals, and cements for geothermal use that are durable at high temperatures and resistant to localized corrosion, wear, fracture, and fatigue failures. Improvements in these materials are essential for the success of downhole pumps, cables, and motors, and for greater longevity of surface, well, and drilling equipment.

Efforts will continue to field test and demonstrate alternate geothermal materials in non-electric as well as electric power systems.

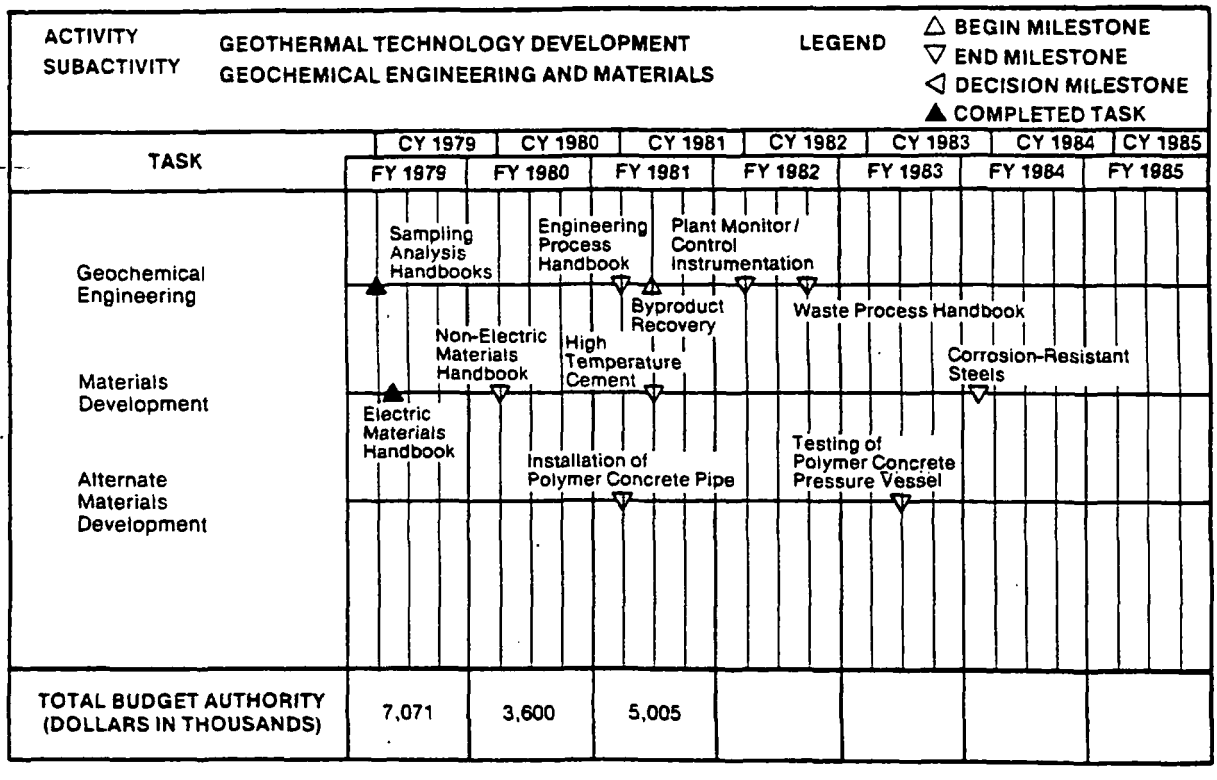

5. Geoscience Technology Development

The Geosciences subprogram, which is aimed at removing technical and economic barriers to geothermal development, includes activities in exploration technology, reservoir engineering, logging instrumentation, and log interpretation. The objectives of these components are detailed below:

- Exploration technology - to improve surface exploration equipment and techniques in order to reduce the number of dry holes drilled in the search for geothermal resources;
- Reservoir engineering - to predict reservoir volumes and productivity accurately over time;
- Logging instrumentation - to develop downhole measuring devices that can survive the geothermal environment; and
- Log interpretation - to determine the characteristics of geothermal reservoirs from borehole information.

Status

Exploration technology activities seek to overcome key technical problems identified by industry. These activities are undertaken to improve the accuracy of predrilling reservoir assessments, to reduce the number of dry holes drilled, and to reduce the cost of exploration and assessment. This effort seeks solutions to near-term problems as well as developing methods for finding "hidden resources".

The principal objective of reservoir engineering activities is to improve the capability for predicting longevity and productivity of reservoirs. This effort is systematically addressing improvements in technical areas such as well testing, rock and fluid properties, reservoir performance analysis and prediction, and economics. Research in these areas is important since the performance

of most hydrothermal reservoirs has typically been unpredictable due to unknown subsurface conditions. Case histories of producing geothermal fields are being prepared as a basis for modeling.

Logging instrumentation activities are aimed at upgrading tool capabilities from the present rating of 180°C to typical geothermal temperatures up to 275°C. Log interpretation activities seek to analyze problems in data interpretation caused by significant differences between hydrocarbon and geothermal wells. The well logging services presently available are often unsuitable for the hostile environment of geothermal wells, and data essential for reservoir engineering are difficult to acquire. Calibration facilities for industrial facilities will continue to be provided as part of this effort. Both activities work closely with industry in an effort to test and evaluate new concepts.

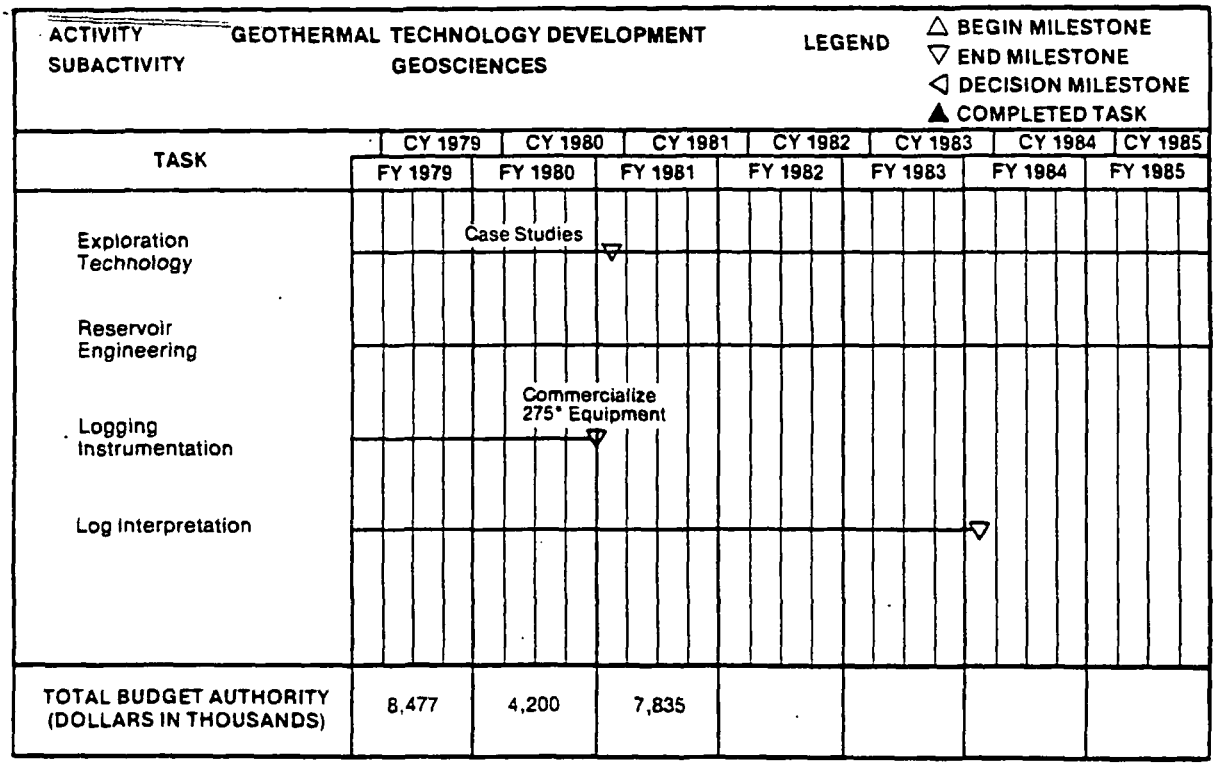

B. Hot Dry Rock

The hot dry rock (HDR) geothermal resource is defined as the heat stored in rocks that contain little or no water. The lack of sufficient water to transport heat distinguishes HDR from hydrothermal resources. HDR has an extremely large resource base.

Energy is extracted from hot dry rock by drilling two wells, fracturing the rock between the wells to provide a large heat exchange surface, then establishing a circulating fluid loop. Commercialization will depend on significant improvements and cost reductions in drilling and fracturing technology. The hot dry rock geothermal concept is depicted on the following page.

The Hot Dry Rock subprogram assesses the potential of the HDR resource and supports development of new technical approaches for extracting energy from HDR. Although HDR research began in 1972, the present HDR program was formally instituted at the beginning of FY 1979 after successful operation of a five-megawatt thermal loop at the Fenton Hill HDR site in New Mexico in 1978. General program objectives are (1) to determine the potential of the HDR resource, (2) to verify that the requisite technology for developing the resource exists, and (3) to bring about commercial exploitation of HDR before the end of the century. A major program decision point will occur in FY 1986, when a review of technical and economic feasibility will determine whether the subprogram should be continued.

Status

Since initiation of the HDR program, DOE has established a program office at Los Alamos Scientific Laboratory (LASL), prepared a draft HDR Program Plan, established the National HDR Program Development Council, and prepared the draft FY 1980 Operating Plan.

The Fenton Hill project, the largest single program element at present, is progressing on schedule. The project is a multi-phase effort. Phase I, which is nearing

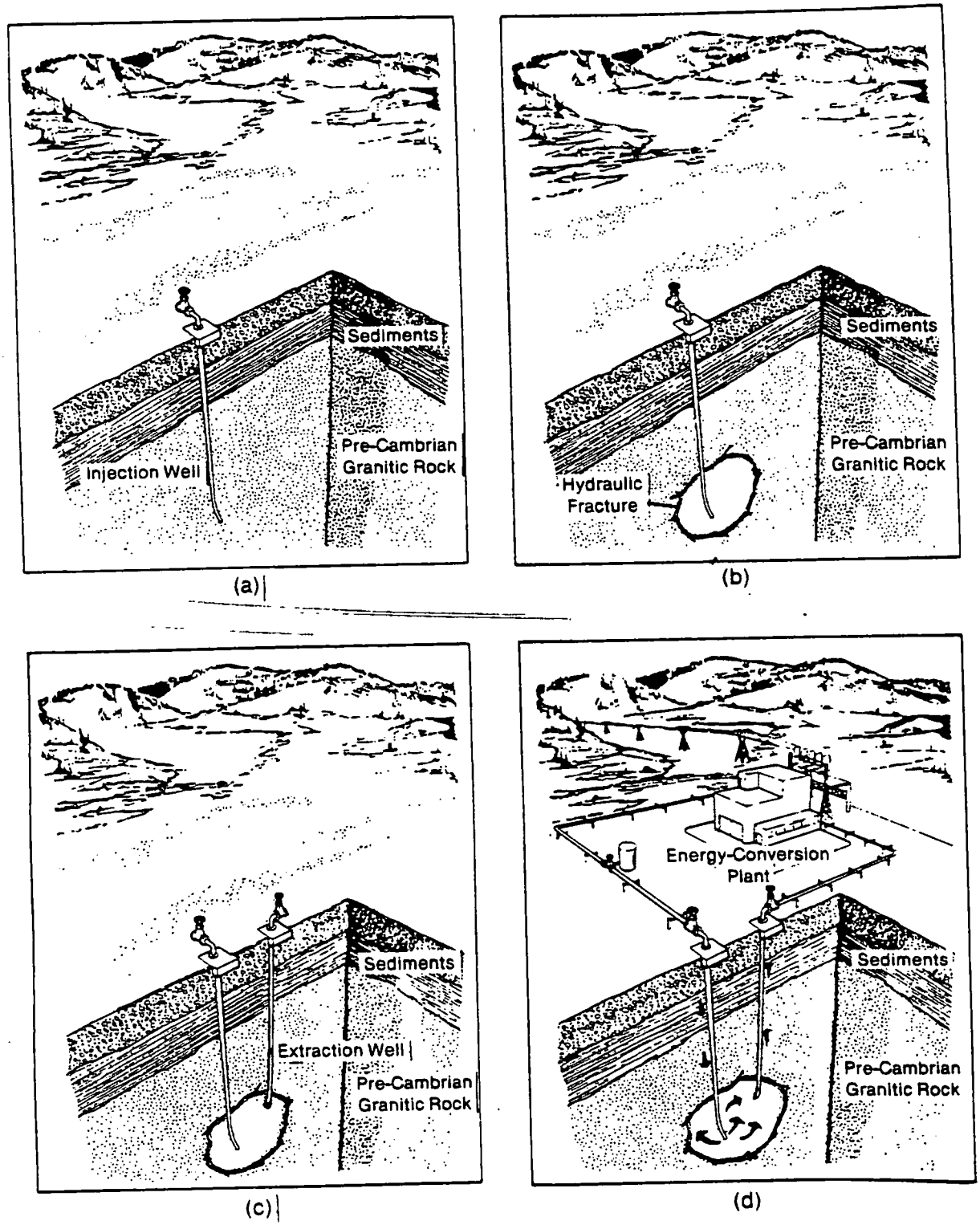

Hot Dry Rock Site Development

successful completion, is an initial feasibility investigation of LASL's HDR heat extraction technique. Phase II involves creating and testing a commercial-scale 20-50 MW_t thermal loop. In addition, one of the Phase I wells will be deepened to become a permanent downhole equipment test facility. Drilling of the new wells for the Phase II loop has begun. As a possible third phase, the Fenton Hill site could be developed for electric power generation. Although such site development is currently not part of the DOE Fenton Hill project, a local electric cooperative has shown interest in building a small power plant if the large thermal loop proves successful. Environmental surveillance at the Fenton Hill site continues to give evidence of HDR as one of the most environmentally benign energy sources.

Technology development activities associated with the Fenton Hill project have focused on development and testing of high-temperature materials, equipment, and downhole instrumentation and upgrading of commercial drilling equipment.

In addition to the Fenton Hill work, DOE is continuing regional and national activities to assess the HDR resource. In FY 1979, DOE cooperated with USGS to determine HDR resource potential and conducted geological and geophysical studies in 34 states. Sites for detailed resource investigations have been selected near Boise, Idaho and on the Delmarva Peninsula. In addition, a catalog of potential HDR sites for commercial and industrial development is being prepared.

In anticipation of HDR commercialization, a preliminary legal study has been published and a two-year industrial/economic study has been initiated.

In accordance with the program objective of proving the general availability of the HDR resources, a second HDR site in a different geologic setting will be selected by the end of FY 1981. Plans for FY 1980 include:

- Increased acquisition of resource potential data and publication of a geothermal gradient map,
- Completion of Fenton Hill Phase I system experimentation,

- Construction of a 20-50 MW thermal loop at Fenton Hill, and
- Continuation of instrumentation development and testing activities.

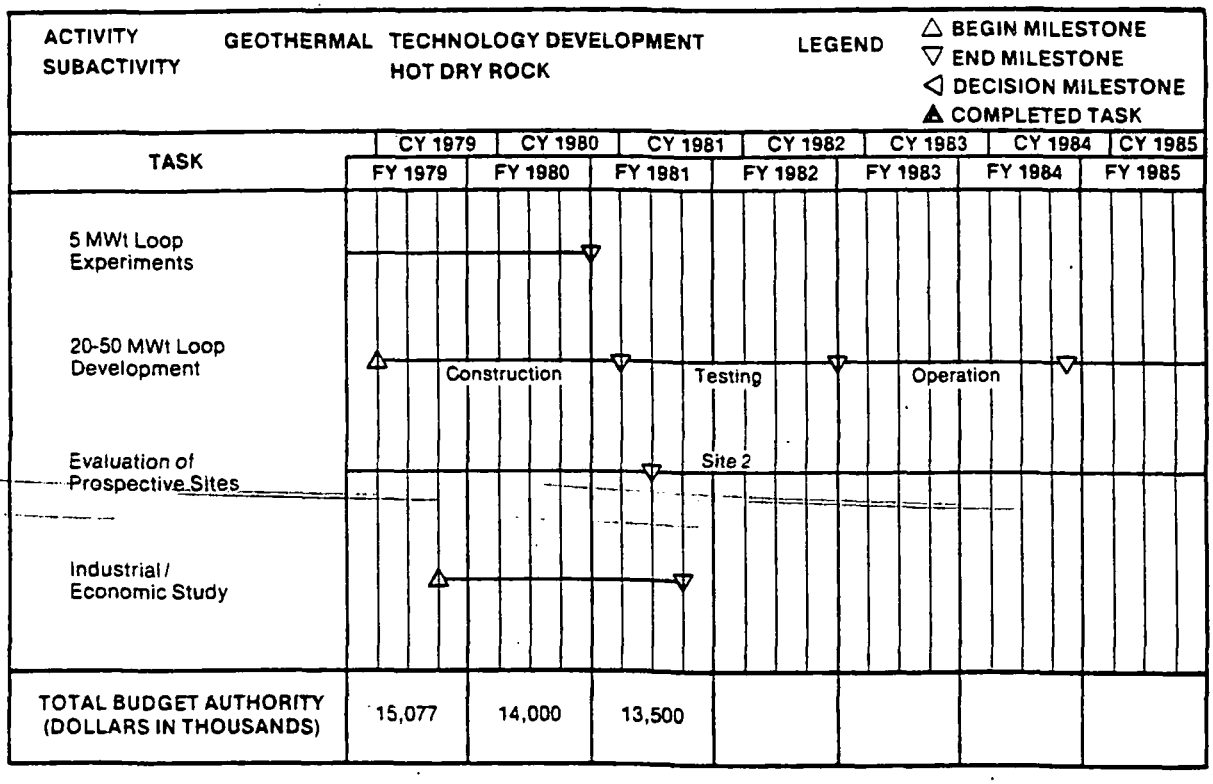

VI. INTERNATIONAL GEOTHERMAL ENERGY ACTIVITIES

Geothermal resource potential has been identified in over 20 countries. Existing worldwide installed capacity is 1978 MW_e, with planned additional capacity of 3641 MW_e.

The United States participates in international geothermal energy programs through multilateral and bilateral agreements with other nations. These agreements, which can enhance domestic commercialization, cover both exchanges of information and cooperative research and development efforts. Information exchange facilitates expansion of the geothermal data base and helps ensure that experience gained elsewhere is available to U.S. developers.

Status

In FY 1979, the United States and the Federal Republic of Germany signed an agreement providing for participation of German scientists in the Los Alamos Scientific Laboratory (LASL) HDR program. The Federal Republic of Germany will fund 25 percent of the Fenton Hill project, up to a maximum of $2.5 million per year. The agreement will be effective for an initial period of four years. In addition, a cooperative agreement under the International Energy Agency (IEA) was signed for overseas testing of a U.S. manufactured wellhead generator unit, the helical screw expander. Participating countries in this agreement are Mexico, New Zealand, and Italy.

The U.S. also has major bilateral agreements with four countries. Activities carried under these agreements are summarized below:

- The U.S. and Italy have exchanged information on drilling techniques and materials. Exchange of reservoir data has led to initial selection of wells for possible stimulation. Reservoir assessment activities have included testing of a computer model at Lardarello, Italy. In addition,

the U.S. has provided environmental monitoring equipment and cooperated in seismic studies.

- The first meeting of an executive coordinating committee for U.S.-Japan cooperation was held in 1979. Possible cooperative projects relevant to binary conversion systems and the LASL hot dry rock program were discussed.

- Cooperative investigations between the U.S. and Mexico on the geophysical and hydrological characteristics of the Cerro Prieto field continued in FY 1979. Bilinguial proceedings of the First Symposium were published. The Second Symposium was held in December 1979. Discussions are underway to extend cooperation under the bilateral agreement to other geothermal areas.

- A Memorandum of Understanding between the U.S. and New Zealand is under negotiation. Areas of cooperative study will include drilling and completion, logging instrumentation, chemistry and materials, stimulation, reservoir engineering, two-phase flow studies, and brine disposal.

Future international activities include the following:

- A conference in Paris to review recent international geothermal developments,

- Observation of stimulation activities at The Geysers by Italian scientists,

- Expansion of U.S./Italian brine technology and materials testing activities,

- Continued reservoir assessment and engineering activities by the U.S., Italy, and Mexico,

- Continued exchange of drilling and environmental information between the U.S. and Italy,

- Continued exchange of information between the U.S. and Japan, and

- Continued meetings to review progress of the IEA/Manmade Geothermal Energy Systems (MAGES) Implementing Agreements.

VII. PROGRAM MANAGEMENT

The geothermal energy programs described in this report require about $150 million annually in federal funds. These funds are expended via several hundred active DOE contracts involving projects throughout the U.S. Although DOE is designated by the Congress as the lead agency for federal geothermal energy programs, several other federal agencies have substantial geothermal responsibilities. The Department of Interior, for example, has custody of millions of acres of federal land containing geothermal resources and is responsible for leasing them as appropriate for commerical geothermal development. The leasing must be coordinated with DOE reservoir definition and technology development programs if the goals for commercial geothermal development are to be met.

The management of this multifaceted program, from long range planning and policy analysis to the testing of geothermal wells and the approval of loan guaranty applications, is itself a complex challenge. DOE's approach to this task is to concentrate policy, planning, overall budget definition and program defense activities in Washington headquarters, while assigning to DOE Operations Offices, National Laboratories and Regional Representatives the responsibility for project definition, day-to-day project management in the field, and coordination with state and local authorities.

This chapter discusses the organizational structures and their responsibilities in two sections, the first covering DOE headquarters, the other, field organizations.

A. Headquarters Organization

The Interagency Geothermal Coordinating Council (IGCC) serves as a board of directors for federal geothermal programs. This Council, chartered by the Congress (P.L. 93-410), is chaired by the DOE Assistant Secretary for Resource Applications. About 25 federal agencies are represented on the Council at the Assistant Secretary level.

The IGCC, which meets as a body four times a year, accomplishes much of its work through a staff committee and three panels. The Council reviews agency plans for geothermal programs to assure that together they constitute a coherent federal geothermal plan, submits a combined federal geothermal budget request to the President's Office of Management and Budget (OMB), and recommends appropriate changes in national policy and legislation.

In FY 1979, DOE shifted the responsibility for commercialization of hydrothermal resources from the Assistant Secretary for Energy Technology (ASET) to the Assistant Secretary for Resource Applications (ASRA). Most of the DOE geothermal energy programs remained with ASET. Early in FY 1980, as part of a major DOE reorganization, the office of ASET was abolished, and all ASET geothermal program were assigned to ASRA. Therefore, DOE geothermal programs are now conducted under the direction of ASRA, with the exception of some basic research conducted by the DOE Office of Energy Research and environmental research conducted by the Assistant Secretary for Environment.

The geothermal program staff of ASRA is responsible for intitiating the geothermal portions of the DOE annual congressional budget request; defending that request and the program itself within DOE, the Administration and the Congress; developing overall program plans; negotiating management agreements with DOE field offices and providing them with program direction and funding; and conducting periodic program reviews.

B. Field Organization

DOE field offices and some DOE National Laboratories have been assigned major responsibility for the coordination and management of substantial parts of the DOE geothermal program. The Los Alamos Scientific Laboratory (LASL), for example, has been given a lead role in the Hot Dry Rock subprogram. The DOE San Francisco Operations Office conducts the Geothermal Loan Guaranty program, and the Nevada Operations conducts drilling activities under the Geopressured Resource Definition subprogram.

In general, the relationship between each of these offices and headquarters is documented in a formal written

management agreement. Headquarters provides overall planning guidance and financial and manpower resources to the field offices and laboratories. The field offices and laboratories are responsible for project definition, contracting and subcontracting, project management, and reporting. They are accountable for achieving objectives and milestones.

The major management centers for DOE geothermal programs are listed below.

Nevada Operations Office
Idaho Operations Office
San Francisco Operations Office
Chicago Operations Office
Los Alamos Scientific Laboratory
Lawrence Berkeley Laboratory
Idaho National Engineering Laboratory
Sandia Corporation

The organizational relationships of Headquarters, a typical field office, and project contractors are displayed below.

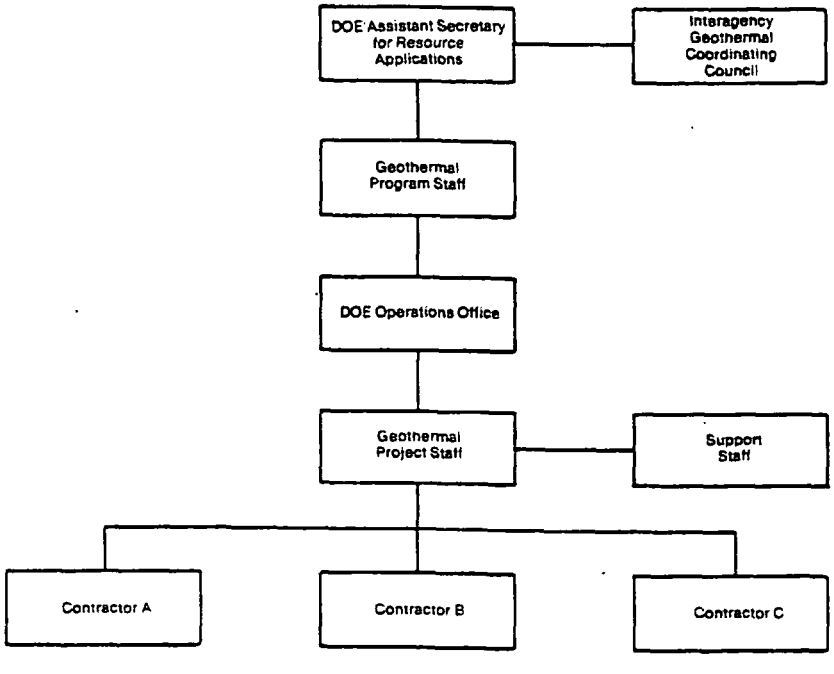

Program Management Organization

Chemical Geology, 17 (1976) 113—123

GEOCHEMISTRY OF GOLD IN ARCHEAN GRANULITE FACIES TERRAINS

G. PAOLO SIGHINOLFI and ADELAIDE M. SANTOS

Institute of Mineralogy, University of Modena, Modena (Italy)
Institute of Geosciences, Federal University of Bahia, Salvador (Brazil)

(Received June 6, 1975; accepted for publication October 13, 1975)

ABSTRACT

Sighinolfi, G.P. and Santos, A.M., 1976. Geochemistry of gold in Archean granulite facies terrains. Chem. Geol., 17: 113—123.

Gold distribution in Archean—Precambrian granulite facies terrains from Bahia state, Brazil, is investigated by means of flameless A.A. spectroscopy. The average Au content for 105 samples is 1.51 ppb, which is appreciably lower than normal values for intermediate-mafic igneous and sedimentary rocks. Gold distribution is discussed in terms of the possible effects of high-grade metamorphism and the composition of the initial material. Compositional patterns suggest that metamorphism had little influence on primary Au distribution. Alternatively, if Au was mobilized in the fluids generated by dehydration reactions, most of it would have been reprecipitated not far from the starting point. Acid-intermediate igneous and non-mature sediments predominate within the initial material of the Archean granulites.

INTRODUCTION

The purpose of the present paper is essentially two-fold: firstly to present data on Au distribution in high-grade metamorphic terrains, and in this connection to propose some tentative interpretations regarding the behaviour of Au during metamorphism; secondly, to shed new light on the question of the nature of the Archean material which, normally in the form of high-grade metamorphic rocks, is found to constitute the ancient necleii in shield areas. Light may thus be shed on the evolutionary processes of the primitive earth's crust, which are still a matter for conjecture.

Current findings support two main hypotheses regarding the behaviour of Au during regional metamorphism. The first, on account of the frequent association of Au-ore quartz veins with greenschist-facies metamorphic rocks, envisages a certain mobility of Au during metamorphism. Some differences observed in the Au content of rocks of different metamorphic grade (Moiseyenko and Neronskiy, 1968; Moiseyenko et al., 1971) are seen as confirming this view. According to the second hypothesis, Au is inert during regional metamorphism and the content, even in high-grade metamorphic

rocks, corresponds to the content in the initial rocks.

This paper presents data on Au distribution in ancient granulite rocks from Bahia state, Brazil.

NOTES ON THE GENERAL GEOLOGY AND PETROLOGY

The samples come from different areas from central-eastern Bahia. Data on the general geology and petrology of some of the areas have already been reported (Fujimori, 1968; Pedreira et al., 1969; Sighinolfi and Fujimori, 1972; Barbosa, 1973). In eastern Bahia the oldest basement formations consist of granulite facies rocks unaffected or only slightly affected by retrograde metamorphism or migmatization that appear as superimposed processes on the same formations towards W Bahia. The granulite terrains extend widely in a N–S direction and have recently been interpreted by Fyfe and Leonardos (1974) as a charnockite belt (Atlantic belt) of a low-pressure type that continues in the African Congo and Angola. Radiometric data (Cordani, 1973) on granulites give ages varying from about 2,600 to 1,000 m.y. with a maximum age frequency at about 2,000 m.y., coinciding with the Trans-Amazonian event. These ages are assumed to date different episodes of granulite facies metamorphism that have occurred in succession, after short periods of retrogradation under amphibolite facies conditions (Fyfe and Leonardos, 1974). Since true-age patterns were obscured by metamorphism, the initial material for granulites may be accepted as being of Archean age.

The great compositional and structural complexity renders any identification of the nature of the pre-metamorphic material very difficult. Indications exist that meta-sediments at least predominate (Fujimori, 1968; Sighinolfi, 1970); nevertheless geochemical studies (Sighinolfi, 1971) revealed some typical magmatic features. Mineralogically, most of the granulites consist of orthopyroxene, clinopyroxene, plagioclase and perthites. Less common are the parageneses with hornblende and/or biotite and with only one pyroxene. Most of the samples considered in this work are typical granulites with charnockite affinities. Details on parageneses different from those reported above are given in Table I.

ANALYTICAL NOTES

Gold was determined by a flameless A.A. procedure previously described by Sighinolfi and Santos (1975). Gold was extracted from HBr solution as bromoaurate with methyl isobutyl ketone (MIBK). This phase was pipetted directly into the graphite tube of the Perkin-Elmer graphite furnace model HGA-2000 coupled with a model 403 spectrophotometer. Analytical sensitivity is about 0.6–0.8 ppb Au for a 1-g sample. Two-gram samples were used for analysis. Experimental error varied between 10 and 50% depending on the absolute Au concentration.

ANALYTICAL RESULTS

Table I reports the results
cating also the respective are
present Au abundances belo
of igneous and sedimentary
ppb (the determination limit
abundances for igneous rock
ples (5.7%). The average Au
ppb samples is taken as 0.2 p
these samples is taken as zer
terrain is of the same order a
appreciably lower (more tha
This is worthy of note, since
Fujimori, 1972) and unpubli
considered show that "intern

No significant differences
may be due to the disproport
various areas and to the sprea
over, no overall relationships
sition are apparent, although
and biotite-bearing samples.

GOLD DISTRIBUTION AND HIC

The fact that Au levels in t
the same order as those in co
Table II) suggests that Au mu
phism. Nevertheless, as report
(Moiseyenko et al., 1971; Pet
during regional and contact m

The study of epithermal Au
not necessarily of igneous orig
of Au. Both thermodynamic a
ity is appreciable both in alkal
alkali chloride solutions the so
HCl molality and temperature
At high temperatures molecul
stable (Henley, 1973). Henley
mal solutions derived from m
range of the greenschist-amph
the trace Au in the country r
cates that these solutions are
mentally-determined equilibri
Thus metamorphism involvin

ANALYTICAL RESULTS

Table I reports the results of the analysis of 105 granulite samples indicating also the respective areas of provenance. More than 97% of the samples present Au abundances below 5 ppb, i.e. in the normal range for the majority of igneous and sedimentary rocks. Gold levels are as follows: lower than 0.4 ppb (the determination limit) — 27 samples (25.7%); 0.4—3.5 ppb (normal abundances for igneous rocks) — 72 samples (68.6%); above 3.5 ppb — 6 samples (5.7%). The average Au content is 1.51 ppb if the Au content of the 0.4 ppb samples is taken as 0.2 ppb, dropping to 1.46 ppb if the Au content of these samples is taken as zero. Thus the average Au content for the whole terrain is of the same order as that of acid igneous rocks (see Table II) but is appreciably lower (more than 40%) than averages for most other rock types. This is worthy of note, since published (Sighinolfi, 1970; Sighinolfi and Fujimori, 1972) and unpublished chemical data on granulites from the areas considered show that "intermediate" types predominate over the acid types.

No significant differences in the area distribution of Au are observed; this may be due to the disproportion in the number of samples analyzed from the various areas and to the spread of values observed within a single area. Moreover, no overall relationships between Au abundance and mineral rock composition are apparent, although Au is frequently concentrated in hornblende- and biotite-bearing samples.

GOLD DISTRIBUTION AND HIGH-GRADE METAMORPHISM

The fact that Au levels in the majority of the metamorphic rocks are of the same order as those in common igneous and sedimentary rocks (see Table II) suggests that Au must be relatively inert during regional metamorphism. Nevertheless, as reported in the introduction, results of some studies (Moiseyenko et al., 1971; Petrov et al., 1972) indicate that Au is mobile both during regional and contact metamorphism.

The study of epithermal Au deposits suggests that hydrothermal solutions, not necessarily of igneous origin, appear to have been active in the transport of Au. Both thermodynamic and experimental studies show that Au solubility is appreciable both in alkali chloride and alkaline bisulphide systems. In alkali chloride solutions the solubility of Au as $AuCl_2^-$ or $AuCl_4^-$ increases with HCl molality and temperature (Anderson and Burnham, 1964; Henley, 1972). At high temperatures molecular solutions with gold-chloride complexes are stable (Henley, 1973). Henley (1973) calculates the Au content of hydrothermal solutions derived from metamorphic dehydration reactions in the P—T range of the greenschist-amphibolite facies transition that have leached out all the trace Au in the country rock. The figure found (max. 0.1 ppm Au) indicates that these solutions are strongly unsaturated in relation to the experimentally-determined equilibrium solubilities at temperatures above 350—400°. Thus metamorphism involving dehydration reactions can result in Au redistri-

TABLE I

Gold content in granulite terrains

Sample		Details on mineralogy	Au (ppb)
Itabuna—Ilhéus area (SE Bahia):			
Il	1		<0.4
Il	6	garnet	<0.4
Il	7	biotite—hornblende	0.8
Il	8		2.0
Il	9		0.9
Il	10	biotite—hornblende	2.8
Il	12	biotite—hornblende	1.2
Il	14	anorthosite	0.7
Il	17	anorthosite	<0.4
Il	18		<0.4
Il	19	biotite—hornblende	<0.4
Il	24		<0.4
Il	25		3.1
Il	26		0.8
Il	27		<0.4
Il	28	garnet	1.6
Il	29		1.3
Il	30	biotite—hornblende	0.9
Il	31		1.3
Il	32	biotite—hornblende	4.2
Il	33	biotite—hornblende	1.6
Il	34		0.7
Il	36	biotite—hornblende	0.5
Il	38	amphibolite	<0.4
Il	39	biotite—hornblende	1.8
Il	40	biotite—hornblende	2.0
Il	41	biotite—hornblende	2.0
Il	42		<0.4
Il	43	garnet	1.9
Il	44		0.6
Il	45	biotite—hornblende	0.8
Il	46	biotite—hornblende	2.2
Il	47	biotite—hornblende	2.0
Il	50		0.4
Il	52		<0.4
Il	53		<0.4
Il	54	biotite—hornblende	0.5
Il	55		0.5
Il	56		2.9
Il	57		0.5
Il	58		0.6
Il	59		1.0
Il	60		1.5
Il	61		1.4
Il	62		<0.4
Il	63	garnet	8.1

TABLE I (*continued*)

Sample		Details on mineralogy
Il	64	biotite—hornblende
Il	66	
Il	67	
Il	68	
Il	70	
Il	71	
Il	72	
Il	73	
Il	76	
Il	77	
Il	78	
Il	79	amphibolite
Il	82	biotite—hornblende
Il	83	
Ita	1	biotite—hornblende
Salvador (E Bahia):		
UB	2	
UB	8	pyroxenite
UB	10	
UB	16	
P	136	biotite
Itaberaba-Seabra (central Bahia):		
RP	1	
RP	1A	
RP	2	
RP	3	
RP	3A	hornblende
RP	3B	
RP	4	
RP	5	
RP	6	
RP	7	biotite—hornblende
Itaberaba-Iaçu (central Bahia):		
RB	5	
RB	5B	
RB	53	
RB	78	
RB	253	
RB	254	biotite—hornblende
RB	266	biotite
Senhor do Bonfim (NE Bahia):		
CQ	3	
CQ	5	
Nanuque (S Bahia):		
ES	13	garnet gneiss
ES	35	biotite gneiss
Rio Pardo (S Bahia):		
NP	1	
NP	13	

TABLE I (*continued*)

Sample		Details on mineralogy	Au (ppb)
[illegible]	64	biotite—hornblende	0.8
[illegible]	66		2.3
[illegible]	67		1.4
[illegible]	68		1.4
[illegible]	70		<0.4
[illegible]	71		16.0
[illegible]	72		0.5
[illegible]	73		0.5
[illegible]	76		<0.4
[illegible]	77		2.8
[illegible]	78		16.2
[illegible]	79	amphibolite	<0.4
[illegible]	82	biotite—hornblende	1.4
[illegible]	83		0.8
Ita	1	biotite—hornblende	18.4
Salvador (E Bahia):			
UB	2		<0.4
UB	8	pyroxenite	<0.4
UB	10		<0.4
UB	16		0.6
P	136	biotite	2.3
Itaberaba-Seabra (central Bahia):			
RP	1		1.0
RP	1A		1.0
RP	2		<0.4
RP	3		0.5
RP	3A	hornblende	1.0
RP	3B		0.5
RP	4		0.6
RP	5		0.9
RP	6		2.3
RP	7	biotite—hornblende	<0.4
Itaberaba-Iacù (central Bahia):			
RB	5		0.5
RB	5B		0.5
RB	53		<0.4
RB	78		<0.4
RB	253		1.5
RB	254	biotite—hornblende	4.4
RB	266	biotite	1.7
Senhor do Bonfim (NE Bahia):			
CQ	3		1.1
CQ	5		<0.4
Nanuque (S Bahia):			
ES	13	garnet gneiss	0.8
ES	35	biotite gneiss	0.9
Rio Pardo (S Bahia):			
NP	1		1.0
NP	13		0.8

TABLE I (*continued*)

Sample	Details on mineralogy	Au (ppb)
NP 14		0.4
NP 15		0.5
Rio Salgado (S Bahia):		
NS 4		0.7
NS 5	amphibolite	<0.4
NS 7		1.2
NS 10	biotite gneiss	<0.4
NS 11	biotite—hornblende gneiss	0.4
NS 12		0.5
NS 14		0.7
Various localities:		
JP 48		1.0
GH 17		1.4
P 323		1.1
RP 8		0.8
RP 10		<0.4
P 127	garnet	3.0
P 129		<0.4
Total average (105 samples)		1.51
Standard deviation		2.87
for 27 samples (25.7%)		<0.4
for 72 samples (68.6%)		0.4—3.5
for 6 samples (5.7%)		>3.5

TABLE II

Gold abundances in common rock types

	Num sam
Bahia granulites:	105
acid (CaO+MgO 7%)	42
intermediate (CaO+MgO 7—15%)	51
mafic (CaO+MgO 15%)	8
Igneous rocks:	
total acid	
intermediate and mafic	
granite	310
rhyolite	188
intermediate plutonic	261
mafic plutonic	580
intermediate-mafic volcanic	696
oceanic island basalts	4
Sedimentary rocks:	
sandstone and siltstone	105
shale	28
carbonates	20
deep-sea sediments	28
Metamorphic rocks:	
argillite and slate	135
schists	114
gneisses	37

bution, at least within individual beds of rocks, and hence in an increased dispersion, as pointed out by Moiseyenko (1965). Since granulite assemblages are essentially determined by dehydration reactions, the low average Au content found may be due to Au depletion in migratory hydrothermal fluids possibly occurring not only at granulite facies temperatures but also during preceding stages of lower metamorphic grade. Certain factors, for example, abnormally high Au levels in some samples and generalized higher contents in correspondence of hydrated mineralogical parageneses, seem to indicate that Au was redistributed by migration in metamorphic hydrothermal fluids. Unfortunately, since such Au enrichments may be ascribed to primary features of the premetamorphic (igneous or sedimentary) material, the importance of such observations is very limited.

STARTING MATERIAL FOR THE ARCHEAN GRANULITES

Identification of the initial material of Archean granulites is hampered by two factors: firstly, our knowledge of the real constitution and, above all, the growth process of the primitive crust is very limited; secondly, the processes involved in granulite-facies metamorphism (anatexis) normally obscure most

of the primary features. This d
metamorphic grade conditions.

In any case, structural and c
material that formed the granu
ture of igneous and sedimentar
Au levels are significantly diffe
II), Au distribution may be of
material for Archean granulites
duly affected by metamorphis
cannot be classified chemically
silica sometimes used as param
types (Lambert and Heier, 196
because: (1) acid igneous and
a single group; and (2) silica m
the average composition of mo
1969, pp. 227—271), the sum

TABLE II

Gold abundances in common rock types (ppb)

	Number of samples	Ranges	Average all analyses	References
Bahia granulites:	105	0.4—18.2	1.51	this work
acid (CaO+MgO 7%)	42		0.57	this work
intermediate (CaO+MgO 7—15%)	51		1.58	this work
mafic (CaO+MgO 15%)	8		0.73	this work
Igneous rocks:				
total acid			0.72	Gottfried et al. (1972)
intermediate and mafic			2.8	Gottfried et al. (1972)
granite	310	0.1—40	1.7	Crocket (1974)
rhyolite	188	0.1—3.5	1.5	Crocket (1974)
intermediate plutonic	261	0.1—110	3.2	Crocket (1974)
mafic plutonic	580	0.3—79	4.8	Crocket (1974)
intermediate-mafic volcanic	696	0.1—48	3.6	Crocket (1974)
oceanic island basalts	4	0.29—1.1	0.50	Crocket et al. (1973)
Sedimentary rocks:				
sandstone and siltstone	105	0.3—12	3.0	Crocket (1974)
shale	28	0.66—8.6	2.5	Crocket (1974)
carbonates	20	0.8—3.9	2.0	Crocket (1974)
deep-sea sediments	28	0.21—17.3	3.4	Crocket (1974)
Metamorphic rocks:				
argillite and slate	135	0.34—10	1.0	Crocket (1974)
schists	114	0.38—9	2.2	Crocket (1974)
gneisses	37	0.2—22	3.9	Crocket (1974)

s, and hence in an increased
65). Since granulite assemblages
ctions, the low average Au
migratory hydrothermal
facies temperatures but also
grade. Certain factors, for
mples and generalized higher
alogical parageneses, seem to
n in metamorphic hydrothermal
nts may be ascribed to primary
dimentary) material, the im-

NULITES

ean granulites is hampered by
constitution and, above all, the
nited; secondly, the processes
texis) normally obscure most

of the primary features. This does not occur, as is well known, under lower metamorphic grade conditions.

In any case, structural and compositional features suggest that the Archean material that formed the granulite terrains in Bahia state consisted of a mixture of igneous and sedimentary rocks in unknown proportions. Since average Au levels are significantly different in the main igneous rock types (see Table II), Au distribution may be of a certain importance in investigating the starting material for Archean granulites, providing this distribution has not been unduly affected by metamorphism. Because of their complex nature, granulites cannot be classified chemically as in the case of igneous rocks. The total silica sometimes used as parameter to discriminate different granulite rock types (Lambert and Heier, 1968; Sighinolfi, 1970) is largely unsatisfactory, because: (1) acid igneous and detritical (quartz-rich) sediments appear within a single group, and (2) silica may be mobile during metamorphism. In view of the average composition of most igneous and sedimentary rocks (Wedepohl, 1969, pp. 227—271), the sum CaO+MgO was chosen to classify granulites

chemically, taking into account their possible starting material. In fact, both Ca and Mg are accepted as being inert elements during metamorphism, and the sum CaO+MgO increases regularly from acid to mafic igneous and affords satisfactory discrimination of the main sedimentary rock types. Thus granulites are divided (rather arbitrarily) into three groups with CaO+MgO < 7, 7—15 and > 15%, respectively. The first group comprises most of the acid igneous rocks (Nockolds, 1954), sandstones and mature sediments (pelagic clays and geosyncline shales), the second intermediate igneous and platform shales and the third mafic igneous rocks. Graywackes figure mainly in the second group. Of the samples of granulites analyzed, the "intermediate" predominates over the "acid" type, while mafics are negligible. Gold distribution in the different groups of granulites is represented in Fig.1. In calculating the average Au contents in the various groups the > 5-ppb samples were excluded so as not to unduly falsify the real figures. The results obtained (see also Table II) show that the average Au content increases markedly (from 0.57 to 1.58 ppb) from acid to intermediate granulites and seems to decrease in mafic granulites (0.73 ppb), although the latter value is hardly indicative on account of the low number of samples analyzed. The findings of many authors (Gottfried et al., 1972; Tilling et al., 1973; Crocket, 1974) would suggest that Au distribution in granulites as a whole may be regarded as a typical magmatic trend. This would at first sight seem to imply that acid-intermediate igneous rocks predominate in the initial material of Archean granulites, in accordance with the "tonalite" model recently proposed by Windley (1975).

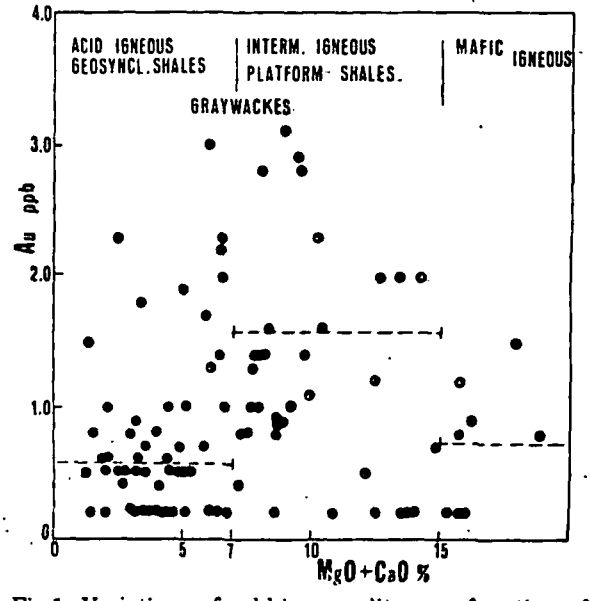

Fig.1. Variations of gold in granulites as a function of the CaO + MgO content (> 3.5-ppb Au samples not represented). Dashed lines: partial averages.

The effect that the possible s
distribution is hard to evaluate,
sedimentary rock type, and occ
(1974), for example, affirms tha
to be richer in Au than other se
sediments. On the other hand, I
elevated Au content in para-am
clay-carbonate beds, while silica
In our case, most of the higher
are quasi-systematically correla
with elevated TiO_2 contents. Th
mediate igneous rocks is quite
(Wedepohl, 1969). Of the sedin
present much higher MgO/CaO
tions have been carried out in g
reveal high Au contents probab
Since granulites with a high Mg
samples analyzed, it can be dec
graywacke type may be presen
rial of the Archean granulites.
patterns on the one hand, and,
growth of the primitive crust (
tation patterns underwent con
types) from Archean to Proter
changes (e.g. of the Na/K ratio

Finally, with reference to th
out the granulite terrains, it sh
of Au is undoubtedly a pre-me
seem to have affected Au abur
lites would therefore appear t
alternative explanation is that
without the primitive patterns
case that Au solubility in the
extremely limited (in disagree
above) or if most of the Au p
in loco or after migration ove

ACKNOWLEDGEMENTS

Financial support for this r
by Consiglio Nazionale delle

The effect that the possible sedimentary component may have had on Au distribution is hard to evaluate, for Au contents vary widely within a given sedimentary rock type, and occur in frequently contrasting patterns. Crocket (1974), for example, affirms that conglomerates and sandstones normally tend to be richer in Au than other sediments, especially carbonate rock and pelagic sediments. On the other hand, Pchelintseva and Fel'dman (1973) found an elevated Au content in para-amphibolites formed by metamorphism from clay-carbonate beds, while silica-rich meta-sediments had the lowest content. In our case, most of the higher Au contents in acid-intermediate granulites are quasi-systematically correlated with high MgO/CaO ratios and sometimes with elevated TiO_2 contents. The MgO/CaO ratio in most of the acid-intermediate igneous rocks is quite uniform and generally lower than 0.5 (Wedepohl, 1969). Of the sediments, graywackes and geosyncline shales present much higher MgO/CaO ratios (greater than unity). Few Au determinations have been carried out in graywackes, but the data available (Boyle, 1961) reveal high Au contents probably related to the mafic detrital components. Since granulites with a high MgO/CaO ratio are not infrequent among the samples analyzed, it can be deduced that a sedimentary component of a graywacke type may be present, and even abundant, within the starting material of the Archean granulites. This accounts for the observed Au distribution patterns on the one hand, and, on the other, agrees with models for the growth of the primitive crust (Engel et al., 1974) according to which sedimentation patterns underwent considerable change (from non-mature to mature types) from Archean to Proterozoic in concomitance with major chemical changes (e.g. of the Na/K ratio) in the main rock types.

Finally, with reference to the relatively low average content of Au throughout the granulite terrains, it should be pointed out that since the igneous trend of Au is undoubtedly a pre-metamorphic feature, metamorphism does not seem to have affected Au abundances. The initial Archean material for granulites would therefore appear to contain less Au than present-day material. An alternative explanation is that Au was partially mobilized by metamorphism without the primitive patterns being destroyed. This is feasible only in the case that Au solubility in the fluids deriving from dehydration reactions is extremely limited (in disagreement with the experimental results discussed above) or if most of the Au present in the leaching fluids was re-deposited in loco or after migration over short distances.

ACKNOWLEDGEMENTS

Financial support for this research was provided by Brazilian CNPq and by Consiglio Nazionale delle Ricerche (Rome).

REFERENCES

Anderson, G.M. and Burnham, C.W., 1964. Solubilities of quartz, corundum, and gold in aqueous chloride and hydroxide solutions. Geol. Soc. Am., Spec. Pap., 82: 4 (abstract).

Barbosa, P.D., 1973. Geologia das Fôlhas Ilhéus—Potiragúa. Centro de Pesquisa do Cacau, Boll. 1: 1—21.

Boyle, R.W., 1961. The geology, geochemistry and origin of the gold deposits of the Yellowknife district. Can. Geol. Surv. Mem., 310, 193 pp.

Cordani, U.G., 1973. Evoluçao geológica pré-cambriana da faixa costeira do Brasil, entre Salvador e Vitória. Livre Docência Thesis, Universidade de São Paulo, São Paulo, 98 pp.

Crocket, J.H., 1974. Gold. In: K.H. Wedepohl (Editor), Handbook of Geochemistry, II, Springer, Berlin, Ch. 79, B—D.

Crocket, J.H., Macdougall, J.D. and Harriss, R.C., 1973. Gold, palladium and irridium in marine sediments. Geochim. Cosmochim. Acta, 37: 2547—2556.

Engel, A.E.J., Itson, S.P., Engel, C.G., Stickney, D.M. and Cray, Jr., E.J., 1974. Crustal evolution and global tectonics: a petrogenic view. Geol. Soc. Am. Bull., 85: 843—858.

Fujimori, S., 1968. Granulitos e charnockitos de Salvador, Bahia. An. Acad. Brasil. Cienc., 40: 181—202.

Fyfe, W.S. and Leonardos, O.H. Jr., 1974. Ancient metamorphic-migmatite belts of the Brazilian Atlantic coast: the African connection. Rev. Bras. Geocienc., 4: 247—251.

Gottfried, D., Rowe, J.J. and Tilling, R.I., 1972. Distribution of gold in igneous rocks. U.S. Geol. Surv., Prof. Pap., 727, 42 pp.

Henley, R.W., 1972. Studies in gold transport and deposition. In: C.M.B. Henderson and D.L. Hamilton (Editors), Progress in Experimental Petrology, Nat. Environ. Res. Counc. (G.B., Publ. Ser. D, 2: 53—75.

Henley, R.W., 1973. Solubility of gold in hydrothermal chloride solutions. Chem. Geol., 11: 73—87.

Lambert, I.B. and Heier, K.S., 1968. Geochemical investigations of deep-seated rocks in the Australian shield. Lithos, 1: 30—53.

Moiseyenko, V.G., 1965. Gold metamorphism of Amur deposits. Thesis, Khabarovsk University, Khabarovsk (in Russian).

Moiseyenko, V.G. and Neronskiy, G.I., 1968. The relation of goldfields to regional metamorphism. In: Geology, Petrology, and Metallogeny of Metamorphic Complexes in the East of the U.S.S.R. Vladivostok (in Russian).

Moiseyenko, V.G., Shcheka, S.A., Fat'yanov, I.I. and Ivanov, V.S., 1971. Geochemical Features of the Gold Distribution in Rocks of The Pacific Belt. Nauka, Moscow (in Russian).

Nockolds, S.R., 1954. Average chemical compositions of some igneous rocks. Bull. Geol. Soc. Am., 65: 1007—1032.

Pchelintseva, N.F. and Fel'dman, V.I., 1973. Gold in metamorphic rocks in the Kok-chetav Uplift. Geochemistry (U.S.S.R.), 10: 1357—1365 (English translation).

Pedreira, A.J., Souto, P.G. and Azevedo, H.C.A., 1969. Metassedimentos do Grupo Rio Pardo, Bahia, Brasil. XXIII Congr. Bras. Geol., Salvador — B. Boll Esp., No.1, p. 61 (abstract).

Petrov, B.V., Krendelev, F.P., Bobrov, V.A. and Tsimbalist, V.G., 1972. Behaviour of radioactive elements and gold during metamorphism of the Patmosk highland sedimentary rocks. Geokhimiya, 8: 947—955 (in Russian).

Sighinolfi, G.P., 1970. Investigations into the deep levels of the continental crust. Petrology and chemistry of the granulite facies terrains of Bahia (Brazil). Atti Soc. Toscana Sci. Nat. Pisa, Mem. P.V., Ser.A, 77: 327—341.

Sighinolfi, G.P., 1971. Investigations into deep crustal levels: fractionating effects and geochemical trends related to high-grade metamorphism. Geochim. Cosmochim. Acta, 35: 1005—1021.

Sighinolfi, G.P. and Fujimori, S., 1972. Granadas nos granulitos de Salvador, Bahia: discussão sobre relacões entre sua
Geocienc., 2: 141—150.

Sighinolfi, G.P. and Fujimori, S., 1
granulite terrains from the Brazi
P.V., Ser. A, 81: 103—120.

Sighinolfi, G.P. and Santos, A.M., 1
ppb levels by A.A. flameless spe

Tilling, R.I., Gottfried, D. and Row
on gold mineralization. Econ. G

Wedepohl, K.H., 1969. Compositio
rocks. In: K.H. Wedepohl (Edit
Chs. 7 and 8, pp. 227—271.

Windley, B.F., 1975. A review of s
for their origin. In: The Early H
Leicester (abstract).

cussão sobre relacões entre sua variação quimica e reaçoes metamorficas. Rev. Bras. Geocienc., 2: 141—150.

Sighinolfi, G.P. and Fujimori, S., 1974. Petrology and chemistry of diopsidic rocks in granulite terrains from the Brazilian basement. Atti Soc. Toscana Sci. Nat. Pisa, Mem. P.V., Ser. A, 81: 103—120.

Sighinolfi, G.P. and Santos, A.M., 1975. Determination of gold in geological samples at ppb levels by A.A. flameless spectroscopy. Mikrochim. Acta (in press).

Tilling, R.I., Gottfried, D. and Rowe, J.J., 1973. Gold abundance in igneous rocks: bearing on gold mineralization. Econ. Geol., 68: 168—183.

Wedepohl, K.H., 1969. Composition and abundance of common igneous and sedimentary rocks. In: K.H. Wedepohl (Editor), Handbook of Geochemistry, I. Springer, Berlin, Chs. 7 and 8, pp. 227—271.

Windley, B.F., 1975. A review of some high-grade Archean regions and a tectonic model for their origin. In: The Early History of the Earth. NATO Advanced Study Institute, Leicester (abstract).

Jour. Research U.S. Geol. Survey
Vol. 2, No. 3, May-June 1974, p. 259–262

GEOCHEMICAL INDICATORS OF SUBSURFACE TEMPERATURE—PART 1, BASIC ASSUMPTIONS

By R. O. FOURNIER, D. E. WHITE, and A. H. TRUESDELL,
Menlo Park, Calif.

Abstract.—The chemical and isotopic compositions of hot-spring water and gas are used to estimate subsurface temperatures. The basic assumptions inherent in the methods are seldom stipulated. These assumptions include (1) a temperature-dependent reaction at depth, (2) a supply of the solid phase involved in the reaction to permit saturation of the constituent used for geothermometry, (3) water-rock equilibrium at depth, (4) negligible re-equilibration as the water flows to the surface, and (5) no dilution or mixing of hot and cold water. The first three assumptions are probably good for a few reactions that occur in many places. The last two assumptions probably are not valid for many hot-spring systems: information obtained is therefore for the shallower parts of those systems, or a limiting temperature (generally a minimum) is indicated.

The recent increased interest in geothermal energy has prompted widespread exploration for this resource. As expected, the areas initially receiving the most attention are those in which fumaroles and hot springs of high temperature are found. Thermal springs are numerous in the western United States. Their temperatures range from a few degrees above mean annual temperature to boiling. In general, their relative abundance decreases with increasing temperature. From an exploration point of view, the critical question is, how did a given spring attain its observed temperature? Did the warm temperature result from water circulating deeply in a region of normal or slightly above normal geothermal gradient; that is, does the temperature of the spring represent the highest subsurface temperature deep in the system? Or, did the water come from a very high temperature environment at depth and cool on the way back to the surface? We would like to use the chemical composition of the water to answer these questions. In practice, we have found that springs with high rates of discharge are most suitable for hydrogeochemical prospecting, whereas compositions of springs with low rates of discharge are very difficult to interpret.

BASIC ASSUMPTIONS

There are many basic assumptions inherent in using geochemical indicators to estimate subsurface temperatures (White, 1974). Although these assumptions may be valid in many places, it is unlikely that they will be fulfilled everywhere. The usual assumptions are:

1. Temperature-dependent reactions occur at depth.
2. All constituents involved in a temperature-dependent reaction are sufficiently abundant (that is, supply is not a limiting factor).
3. Water-rock equilibration occurs at the reservoir temperature.
4. Little or no re-equilibration or change in composition occurs at lower temperatures as the water flows from the reservoir to the surface.
5. The hot water coming from deep in the system does not mix with cooler shallow ground water.

A schematic model of a hot-spring system (fig. 1) is useful in assessing these assumptions. Critical elements of the model include a heat source of unspecified nature at the base of the system and interconnected permeability that permits convection to occur. In response to heating, water deep in the system decreases in density and is forced up and out of the system, as at A, by pressure exerted by cold, dense water. The cold water moves down and into the system at the margins along permeable structures, possibly faults or joints such as B–B′. There are many alternative possibilities, including models in which some or all of the ascending water and gas is connate, metamorphic, or even juvenile in origin. In some places the salinity of the deep water may be high enough to counteract the effects of temperature on density. Although connate and metamorphic water is probably dominant in some hot springs (White and others, 1973), isotope data indicate that most hot-spring water is predominantly meteoric in origin.

If the maximum temperature attained by the water at depth is higher than the boiling temperature appropriate for atmospheric conditions, the water will cool by boiling (adiabatically), by conduction, or by a combination of these processes as it moves toward the surface. If, on the other hand, the maximum temperature at depth is less than the boiling temperature at atmospheric conditions, the emerging water, such as at A (fig. 1) may have approximately the maximum temperature at depth or a lower temperature, depending on whether the rate of upflow of water is very fast or slow.

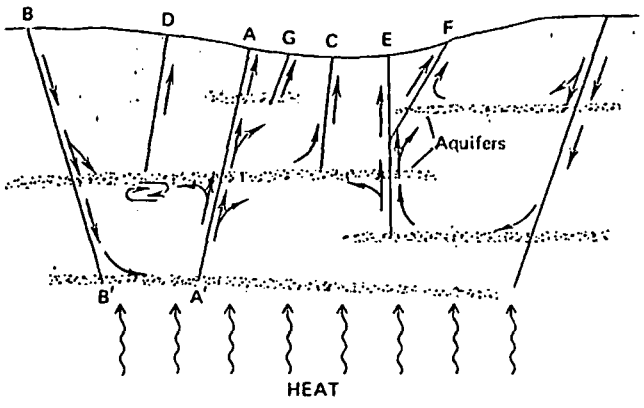

Figure 1.–Schematic model of a hot-spring system having a heat source of unspecified nature and interconnected permeability.

Solubilities

Solubilities of minerals generally change as functions of temperature and water pressure. Therefore, under some circumstances absolute quantities of dissolved constituents are useful indicators of subsurface temperature. However, the dissolving solid phase must be specified and its presence must be assumed at depth. An example is the silica geothermometer, which depends on the solubility of quartz controlling aqueous silica (Fournier and Rowe, 1966; Mahon, 1966).

In general, the solubilities of the common silicates increase with increasing temperature and pressure. As cold subsurface water is heated, it dissolves more and more silicate constituents, reaching a maximum at the hottest (and generally deepest) part of the system. Deposition of silicates may then occur as the water moves back toward the surface and cools, particularly if the cooling is adiabatic. This may result in the self-sealing of the geothermal system, as discussed by Bodvarsson (1964), Facca and Tonani (1967), and White, Muffler, and Truesdell (1971).

The common carbonates have retrograde solubilities (Holland, 1967). Other things being constant, minimum solubilities are attained at the hottest and deepest parts of the system. Generally "other things" are not constant, however. Carbonate solubilities are greatly affected by variations in pH and partial pressure of CO_2. Unfortunately, subsurface pH and P_{CO_2} are not easily estimated from the composition of hot-spring water and gas collected at the surface.

The common sulfates also have retrograde solubilities. Like the carbonates, their usefulness in geothermometry is restricted to systems in which the solid phase is present at depth. One cannot safely assume this unless sulfates have been found in cuttings or cores from holes drilled at the locality in question. In other words, there may be an inadequate supply of the "indicator" constituent in the reservoir, so that the solution at depth is unsaturated with respect to a particular phase; for example, $CaSO_4$ or $BaSO_4$.

Exchange reactions

Equilibrium constants for exchange and alteration reactions also are temperature dependent. In such reactions the ratios of dissolved constituents change with changing temperature of equilibration. Both chemical and isotopic reactions come under this category. Examples are Na:K ratios of chloride solutions equilibrated with alkali feldspars (Orville, 1963; Hemley, 1967), Na:K ratios in natural waters (Ellis, 1970; White, 1965), and Na-K-Ca relations in natural waters (Fournier and Truesdell, 1973). Again, as in the solubility method of geothermometry, the identity of the reactants and products in the high-temperature environment at depth must be assumed. If the assumed phases are not present, the geothermometer yields anomalous results (Fournier and Truesdell, 1970, 1973).

Equilibration at depth

In order to use a geochemical method of estimating subsurface temperature, one must assume equilibrium or at least an approach to equilibrium at depth for a specific "indicator" reaction. At low temperatures, this is a tenuous assumption. Metastable conditions also are likely to occur. However, the assumption of attainment of equilibrium in a high-temperature environment at depth is probably good for many reactions. This assumption is particularly good where the residence time for water in a reservoir at a relatively uniform temperature is long and there is effective mixing or homogenization of introduced water with stored water.

When an increment of water, chemically equilibrated at depth, finally does enter a channel that allows direct movement back to the surface, such as A–A′ in figure 1, the time of upward travel may be very short (minutes or hours) compared with the residence time in the reservoir. Consequently, even though the temperature of the water may decrease markedly, little chemical reaction may occur during upward flow, and the composition of the emerging water may reflect the conditions present in the deep reservoir. However, reservoirs at different depths and temperatures may be present within a given geothermal system. Hot springs located at C, E, and G in figure 1 show various possibilities for water re-equilibrating in shallow reservoirs, so that some or all of the chemical geothermometers will yield estimated subsurface temperatures lower than the maximum temperature deep in the system.

A re-equilibrated water, such as that emerging at G (fig. 1), may give a good indication of the salinity of the deep water. More commonly, deep water entering shallow reservoirs will mix with relatively dilute, shallow water, so that neither the temperature nor salinity of the deepest reservoir is indicated by the spring water that eventually emerges at the surface, as at D and F. If the residence times of both the hot- and cold-water components are long in the shallow aquifer and mixing is thorough, the composition of emerging spring water

as at D, may be indicative of the temperature of that shallow reservoir. In contrast, if the residence time in the shallow reservoir of one or both of the mixing waters is short, the composition of the emerging water (spring F) may give little or no information about that shallow reservoir. Under special circumstances, however, it may be possible to estimate the temperature and proportion of the hot-water component of a mixed water such as that emerging at F. This is discussed elsewhere (Fournier and Truesdell, 1974).

In the discussion to this point, we have assumed essentially no chemical reaction in the channels connecting different reservoirs or reservoirs with springs. Advantageous conditions that minimize reactions within channels are rapid rates of upflow, low temperature, and nonreactive wallrock. Where continued chemical reactions do occur in the channelways leading to the surface, different geochemical indicators yield different apparent temperatures, reflecting varying amounts of re-equilibration at intermediate temperatures.

Enrichment of volatiles

Tonani (1970) emphasizes the relative enrichments in spring waters and fumaroles of comparatively volatile components, particularly NH_3, B, Hg, CO_2, and sulfur compounds, that may indicate subsurface boiling. He generally assumes that steam separates from deep boiling water and that it carries other volatile constituents toward the surface. At shallow depth the steam condenses and mixes with the local ground water. Springs fed by this water are enriched in volatiles relative to chloride.

Tonani's model probably works very well for vapor-dominated systems, as described by White, Muffler, and Truesdell (1971). It has yet to be demonstrated that volatile constituents are enriched relative to chloride in neutral to alkaline hot springs above hot-water-dominated systems, even where boiling temperatures are attained at depth. Enrichment of volatile constituents in spring water may result from processes other than high-temperature boiling. Gases such as CO_2 and CH_4, if sufficiently abundant, may separate from relatively cold water deep underground and escape to the surface. If this gas later encounters shallow ground water, that ground water may become enriched in volatile constituents.

RECOMMENDED PROCEDURE

For estimating subsurface temperatures we set forth the following guidelines despite misgivings that they will be interpreted as hard-and-fast rules for always reflecting subsurface conditions. The intent is simply to suggest starting assumptions where little information is available about hydrologic conditions. As more information is obtained for a specific area, other assumptions may become more reasonable.

The recommended procedures are based upon the temperature and rate of flow of the spring water, as outlined below:

1. Boiling spring:
   (a) Small rate of flow: Assume mostly conductive cooling. Apply chemical indicators assuming little or no steam loss.
   (b) Large rate of flow: Assume adiabatic cooling. Apply chemical indicators assuming maximum steam loss.
2. Spring below boiling:
   (a) Small rate of flow: Likely to have no clear-cut interpretation. May be a water that has never been very hot, a mixed water from sources of different temperatures, or a hot water cooled entirely by conduction. Try geothermometers that assume conductive cooling; indicated temperatures are likely to be minima.
   (b) Large rate of flow: Assume no conductive cooling. Test to see if geothermometers (particularly the Na-K-Ca geothermometers (Fournier and Truesdell, 1973)) suggest chemical equilibration at the temperature (±25°C) of the water. If a higher temperature is indicated, treat as a mixed water according to the method of Fournier and Truesdell (1974).

We have not specified what large and small rates of flow are. Our intent is to distinguish between waters that cool by conduction during their ascent and those that either cool mainly by boiling or do not cool at all. This depends in part on the rate of upflow, the depth of the aquifer supplying the water, and whether a spring is isolated or is part of a larger upflowing system. For preliminary evaluation, an arbitrary cutoff at 200 l/min is suggested for a single isolated spring, and 20 l/min for single springs of larger groups.

CONCLUSIONS

Chemical analyses of hot-spring water and gas may be of great use in an exploration program for geothermal energy. Like all exploration methods, a great many assumptions must be made in order to interpret the data. We urge that these assumptions be kept in mind during the evaluation processes.

REFERENCES CITED

Bodvarsson, Gunnar, 1964, Utilization of geothermal energy for heating purposes and combining schemes involving power generation, heating, and/or by-products, *in* Geothermal Energy II: United Nations Conf., New Sources Energy, Rome 1961, Proc., v. 3, p. 429–436.

Ellis, A. J., 1970, Quantitative interpretation of chemical characteristics of hydrothermal systems, *in* United Nation Symposium on Development and Utilization of Geothermal Resources, Pisa 1970, v. 2, pt, 1: Geothermics, Spec. Issue 2, p. 516–528.

Facca, Giancarlo, and Tonani, Franco, 1967, The self-sealing geothermal field: Bull. Volcanologique, v. 30, p. 271–273.

Fournier, R. O., and Rowe, J. J., 1966, Estimation of underground temperatures from the silica content of water from hot springs and wet-steam wells: Am. Jour. Sci., v. 264, p. 685–597.

Fournier, R. O., and Truesdell, A. H., 1970, Chemical indicators of subsurface temperature applied to hot spring waters of Yellowstone

National Park, Wyoming, U.S.A., *in* United Nations Symposium on Development and Utilization of Geothermal Resources, Pisa 1970, v. 2, pt. 1: Geothermics, Spec. Issue 2, p. 529-535.

——1973, An empirical Na-K-Ca geothermometer for natural waters: Geochim. et Cosmochim Acta., v. 37, p. 1255–1276.

——1974, Geochemical indicators of subsurface temperature–Part 2, Estimation of temperature and fraction of hot water mixed with cold water: U.S. Geol.Survey Jour. Research, v. 2, no. 3, p. 263–270.

Hemley, J. J., 1967, Aqueous Na/K ratios in the system K_2O-Na_2O-Al_2O_3 SiO_2-H_2O [abs.]: Geol. Soc. America, New Orleans 1967, Ann. Mtgs., Programs with Abstracts, p. 94–95.

Holland, H. D., 1967, Gangue minerals in hydrothermal deposits, *in* Barnes, H. L., ed., Geochemistry of hydrothermal ore deposits, New York, Holt, Rinehart, and Winston, p. 382–436.

Mahon, W. A. J., 1966, Silica in hot water discharged from drill holes at Wairakei, New Zealand: New Zealand Jour. Sci., v. 9, p. 135–144.

Orville, P. M., 1963, Alkali ion exchange between vapor and feldspar phases: Am. Jour. Sci., v. 261, p. 201–237.

Tonani, F., 1970, Geochemical methods of exploration for geothermal energy, *in* United Nations Symposium on Development and Utilization of Geothermal Resources, Pisa 1970, v. 2, pt. 1: Geothermics, Spec. Issue 2, p. 492–515.

White, D. E., 1965, Saline waters of sedimentary rocks, *in* Fluids in subsurface environments–A symposium: Am. Assoc. Petroleum Geologists Mem. 4, p. 342–366.

——1974, Geochemistry applied to the discovery, evaluation, and exploitation of geothermal energy resources, *in* United Nations Symposium on Development and Utilization of Geothermal Resources, Pisa 1970: Geothermics, Spec. Issue 2. (In press.)

White, D. E., Barnes, Ivan, and O'Neil, James, 1973 Thermal and mineral waters of nonmeteoric origin, California Coast Ranges: Geol. Soc. America Bull., v. 84, no. 2, p. 547–560.

White, D. E., Muffler, L. J. P., and Truesdell, A. H., 1971, Vapor-dominated hydrothermal systems compared with hot-water systems: Econ. Geology, v. 66, p. 75–97.